Development of nanosponges from erythrocyte ghosts for removal of streptolysin-O and α haemolysin from mammalian blood

By

Vikesh Chhabria

A thesis submitted in partial fulfilment for the requirements for the degree of Doctor of Philosophy in microbial biochemistry, at the University of Central Lancashire

May 2017

Abstract

Bacteria can cause many different types of infections. Virulence factors e.g. adherence proteins, biofilm formation, endotoxins and exotoxins allow invasion by bacteria and cause infections such as respiratory, urinary, and intestinal and blood stream infections. If left untreated they can lead to a condition known as sepsis. Sepsis is a whole body inflammatory response that can be fatal. Exotoxins, such as pore forming toxins are one of the virulence factors secreted by bacteria that are responsible for causing sepsis. Current treatment and management of sepsis includes surgical drainage of fluids, blood transfusions and administration of antibiotics. Sepsis is a rapid onset with an increased mortality rate of 8% per hour. This means that prompt treatment is imperative and due to the increase in antibiotic resistance, treatment has become more difficult.

The aim of this study is to develop biomimetic nanosponges from mammalian erythrocyte ghosts, as a potential treatment for toxin related sepsis. Nanosponges were developed using ovine and leporine blood. Ovine and leporine blood were treated with hypotonic buffer to create erythrocyte ghosts and then were subjected to sonication to produce erythrocyte vesicles of non-uniform size. Vesicles were then serially extruded through a 400 nm and 100 nm polycarbonate membranes. Nanosponges were prepared by fusing poly (D, L-lactic-co-glycolic acid) (PLGA) cores with ovine erythrocyte vesicles. This developed two different types of nanosponges. One, which was coated by ovine erythrocyte membranes and the other with leporine erythrocyte membranes.

Ovine blood was chosen as a model to study sepsis as ovine erythrocytes were the most susceptible to streptolysin-O lysis. Moreover, adsorption studies *in vitro* showed that ovine nanosponges were able to adsorb streptolysin-O at 37°C as the system that contained the nanosponges had the lowest Hb release at 0.005 g/dl (± 0.005) compared to the system containing just the toxin and erythrocytes (0.23 g/dl, ±0.01). The nanosponges were also able to adsorb the streptolysin-O at 40°C, as there was no Hb release in the system containing nanosponges. Similarly, leporine blood was also chosen as a model to study sepsis treatment as leporine erythrocytes were the most susceptible to α-haemolysin lysis. However, adsorption studies *in vitro* showed that leporine nanosponges were not

able to adsorb all the toxin present in the system, as at 37°C, the concentration of Hb released, in the system containing nanosponges was 0.265 g/dl (± 0.02). At 40°C, the concentration of Hb released in the system containing the nanosponges was significantly greater compared to nanosponges incubated at 37°C. These results identify ovine nanosponges as novel therapeutic model to test adsorption of cholesterol binding toxins such as streptolysin-O.

Table of contents

List of figures

List of tables

Acknowledgements

I would primarily like to acknowledge my parents for their support in funding my education and believing in me. Moreover, I would secondly like to thank my supervisor Dr. Steve Beeton, for teaching me the field of microbiology and treating me with the utmost respect. I would also like to thank him for teaching me the ways of science in terms of research and academia. “I do not think I could have been supervised by anyone better than him”. Finally, I would like to thank him for his tolerance towards my writing.

I would like to thank the University of Central Lancashire for their excellent staff and equipment. This has provided me with a lot of support in finishing my project. I would also like to thank the technical staff for their kindness and support towards my research. Especially, Paul Knight for providing me with blood every 2nd week to conduct experiments. I would also like to specially thank William Taylor and sons for providing me with blood every month for my research.

I would like to finally, thank my peers in MB030 for their support. A few mentions Roshini, Hayley, Murassa and Ella for proof reading my work. A great thanks to Fenil Sakariya for his support. “This has been an unforgettable journey”.

List of abbreviations

Word	Abbreviations
poly (lactic acid)	**PLA**
poly(D,L-lactic-co-glycolic acid)	**PLGA**
Food and drug administration	**FDA**
poly(caprolactone)	**PCL**
magnetic resonance imaging	**MRI**
Methicillin resistant *Staphylococcus aureus*	**MRSA**
Pore forming toxins	**PFTs**
Phosphate buffered saline	**PBS**
Haemoglobin	**Hb**
Citrate phosphate dextrose	**CPD**
Storage medium	**SAGM**
4(2-Aminoethyl) benzenesulfonyl fluoride hydrochloride	**AEBSF**
1(((4Guanidinobutylamino)4methyl1oxopentan2yl)carbamoyl)cyclopropane carboxylic acid	**E-64**
Bovine serum albumin	**BSA**
Scanning electron microscope	**SEM**
Red blood cell	**RBC**
Mean corpuscular volume	**MCV**
Mean corpuscular haemoglobin	**MCH**
buffy coat and plasma	**BCP**
protease inhibitor	**PI**
Polydispersity index	**PDI**
Polyethylene glycol	**PEG**
Aminopenicillanic acid	**6APA**
Health protection agency	**HPA**
Room temperature and pressure	**RTP**
Polydispersity index	**PDI**
Protease inhibitor	**PI**
Vancomycin resistant *Enterococci*	**VRE**
Toxic shock syndrome	**TSS**
Exotoxin A gene	**SPEA**
Tumor necrosis factor alpha	**TNFα**
Interleukin one beta	**IL-1β**
Nuclear factor kapa beta	**NF-kβ**
Cholesterol bindin toxins	**CBTs**
Cholesterol standard	**S**
Cholesterol assay buffer	**CAB**
Cholesterol probe	**P**
Enzyme mix	**EM**
Cholesterol esterase	**CE**
Dye reagent	**DR**
Phospholipase D	**PLD**
Phosphotidylcholine standard	**PS**
Streptolysin-O	**SO/strep-O**

Alpha haemolysin	**α-haem**
National health service	**NHS**
Phosphatidylethanolamine	**PE**
Phosphatidylcholine	**PC**

SI unit	Abbreviations
Micromolar	**µM**
Millimolar	**mM**
Microliter	**µl**
Milliliter	**ml**
Relative centrifugal force	**xg**
Celsius	**C**
Grams per deciliter	**g/dl**
nanometres	**nm**
Millivolts	**mV**
Milligrams per milliliter	**mg/ml**
Nanograms per milliliter	**ng/ml**

Chapter 1

1 Synthesis of biomimetic nanosponges from mammalian erythrocytes

1.1 A brief history of the early stages of medicine

The birth of medicine began with the ancient Egyptians. Much of Egyptian medicine relied on magic. These doctors used a range of drugs obtained from herbs and minerals. They were either drunk with beer or wine, or at times mixed with dough to form pills. They were the creators of embalming and treated exposed wounds with honey. Egyptian surgery was limited to treating wounds and broken bones. Modern medicine came into existence from ancient Greece. They carefully observed symptoms and treated patients using herbal remedies. They believed the body was made up of four humors (pools of liquids inside the body). If a person had too much of it they became ill; this theory was known as the four humors, which became quite popular in the field of medicine (Lambert, 2016).

The Romans conquered Greece and eventually treated patients using the concept of opposites. So if a patient had a cold they were asked to eat a hot pepper. During this time, a Roman scientist suggested that tiny animals cause disease, which were carried through the air and entered the body through the nose and mouth. They also invented the concept of sanitation, as they saw people living near the swamps contracted malaria; this gave them the idea to drain the swamps. They diagnosed certain diseases by examining a patient's urine. The colour taste and smell of urine was important (Lambert, 2016). The 16^{th}-18^{th} century was an important era for science as there were many discoveries and improvements to existing theories (Table 1).

Table 1. Major discoveries made in the field of medicine and biology from the 16th-20th Century

Century	Inventor	Major discovery
16th	Girolamo Fracastoro	1546- Published a book, which suggested that infectious diseases were caused by disease seeds
16th	Andreas Vesalius	Published a book called Fabric of the human body, contained accurate diagrams of the Human body.
16th	Ambroise Pare	Invented a mixture of egg whites, rose oil and turpentine, to treat wounds
17th	Antoine Van Leeuwenhoek	Invented the Microscope and the first microbial organisms were observed
17th	Robert Hooke	Discovered the structure of a cell
17th	Santorio	He invented the medical thermometer
18th	James Lind	Discovered the treatment for scurvy (vitamin c deficiency)
19th	Rene Laennec	Invented the stethoscope
19th	John Snow	Discovered that cholera was transmitted by water
19th	Louis Pasteur	Theorised that microscopic organisms cause disease (germ theory of disease), created a vaccine for anthrax and rabies and invented Pasteurisation.
20th	Alexander Fleming	Discovered the first broad-spectrum antibiotic known as penicillin.
20th	Paul Ehrlich	Synthesized Salvarsan which was the treatment for syphilis

From the 19th century, the field of medicine has improved at an incredible rate. The discovery of antibiotics, anti-cancer drugs, asepsis, transplant surgeries and various other forms of treatment has allowed humans to survive life-threatening diseases. Yet, there are still diseases that cannot be treated, which has allowed traditional medicine to move into the new direction of using nanomedicine (Lambert, 2016).

1.2 Birth of Nanomedicine

The introduction to the field of nanomedicine began in 1959 after Richard Feynman's talk on the concepts of nanotechnology entitled "There is Plenty of Room at the Bottom" at an American Physical Society meeting at Caltech on December 29, 1959. With the development of the transmission electron microscope and field ion microscopy, he envisioned that man would one day be

able to control and manipulate things on a nanoscale level. He stated, “It would be interesting in surgery if you could swallow the surgeon. You put the mechanical surgeon into the blood vessel and it goes into the heart and looks around. It finds out which valve is the faulty one and takes a little knife and slices it out” (Feynman, 1960). After this speech, in 1991 a book titled “The Future. The Nanotechnology Revolution” was published in which the term nanomedicine was used for the first time.

This was the initial birth of nanomedicine, with the introduction of using bottom up and top down approaches to synthesize nanoparticles. The Literature during this time period on cell constituents (Bentivoglio, 1999), intra and intercellular processes, cellular communication (Mazzarello, 1999), advances in biotechnology and biochemistry aided in the production of nanoparticles. In 1960, Peter Paul Speiser developed the first nanoparticles, which was used for targeted drug therapy. Since this discovery there has be a lot of research on developing various carrier systems. At the end of the 20th century, nanoparticles were modified for the transport of DNA fragments into cells with the aid of antibodies (Krukemeyer *et al.*, 2015). Since then there has been a surge of publications in this area. The publications have increased from 10 articles in 1990 to 1200 articles in 2004, indicating an increasing interest in nanomedicine (Wagner *et al.*, 2006).

1.3 Conventional versus nanomedicine

Conventional medicine has been used to treat diseases in the past and is still being used treat diseases like cancer, infections, inflammatory disorders and neuronal disorders. Still, a significant amount of drugs receiving approvals have poor biopharmaceutical characteristics. A study stated that 40% of Food and Drug administration (FDA) approved drugs and 90% of the drugs under clinical trials are poorly soluble drugs. They suffer from low permeability, rapid clearance by the body and toxicity to the cells of the body (Kalepu and Nekkanti, 2015). This study has shown that some conventional drugs are not sufficient to achieve the desired therapeutic effect. So, drugs are now being modified into carrier systems to achieve a better pharmaceutical profile. This is where nanomedicine plays a big role. Water insoluble drugs can be encapsulated into the hydrophobic domain of carrier systems such as micelles, polymeric nanoparticles and

liposomes. This enables the drug to be carried by a system that has a hydrophilic layer, making drug delivery easily achievable. The size of these systems, provide an opportunity for targeting tumours via the enhanced permeation and retention effect. The hydrophilic coating makes them less susceptible to clearance by the immune system, leading to a longer circulation time. These carriers can also be modified with ligands or proteins that allow for therapeutic targeting. Interestingly the application of nanocarriers extends to diagnostics as these carriers have been modified with imaging contrast agents that selectively target certain cancer cells and can be visualised using techniques such as magnetic resonance imaging (MRI) (Ventola, 2012). Since this is a developing field, traditional medicine is still preferred over nanomedicine.

1.4 Introduction

1.4.1 Nanomedicine and its impact on therapeutic research

The emergence of using nanoparticles as drug delivery systems has made a difference in the field of nanomedicine. These systems have been used to treat cancer, asthma as well as bacterial infections (Hu *et al.*, 2014). Nanotherapeutic models take various different structural forms. They include nanoshells, carbon nanotubes, quantum dots, polymeric nanoparticles and lipid derived nanoparticles (Jaishree and Gupta, 2012).

Recently, there has been interest in research around lipid and polymeric systems, as therapeutic models for treating cancer and bacterial infections. The reason behind this is due to their biocompatibility and biodegradability in the human body. Several types of polymers have been used in this field such as poly (lactic acid) (PLA), poly (D, L-lactic-co-glycolic acid) (PLGA), and poly(caprolactone) (PCL). These polymers are all FDA approved for the use of developing therapeutic nanocarriers (Kumari *et al.*, 2010). Lipid systems are also used for the same application as polymeric systems. However, these systems have been chosen for their stealth function. They comprise of particular lipids, as found in the human body making detection by immune cells difficult. These systems include nanocarriers such as liposomes, nanoerythrosomes and micelles (Fang *et al.*, 2012). There have been many modifications to these systems from which a new subcategory of nanocarriers have emerged. These are biomimetic nanoparticles.

Polymeric nanoparticles are susceptible to recognition and degradation by immune cells (Kumari *et al.*, 2010). This has led to the development of biomimetic strategies, as their stealth function have the ability to bypass the immune system. Biomimetic nanotherapeutics can mimic the cells biological characteristics, as the structure of the system is designed whereby the particle has a polymeric core, coated by a lipid membrane. These particles are preferred in modern day nanomedicine as they can be fabricated with surface features that are specific for targeting cells or tissues (Meyer *et al.*, 2015). Current research has shown that biomimicry include particles such as erythrocyte membrane particles with a PLGA core (Hu *et al.*, 2011) , magnetic core (Antonelli *et al.*, 2011) and PLGA cores enveloped by a white blood cell membranes (Krishnamurthy *et al.*, 2016) .This area of nanomedicine is of particular interest as limited research has been conducted.

1.4.2 Polymeric nanoparticles and their application in research and industry

Challenges in the field of nanomedicine revolve around creating a system that is biocompatible, degradable, and non-toxic to the cells of the body, as cellular responses are critically different at the nanoscale level. Most importantly, the system needs to be stable as Tiwari *et al.* (2012) stated that unstable engineered nanomaterials may cause a haemostatic imbalance and interfere with the coagulation system, causing blood clots. This led to synthesising polymeric nanoparticles (Duncan and Vicent, 2013). These particles have revolutionised how the field of medicine is approached. Current polymeric nanotherapeutics include polymeric drugs, block co-polymeric micelles and biomimetic nanoparticles. The primary use of polymeric nanoparticles was of the non-biodegradable kind such as poly(methyl methacrylate) (Shastri, 2003). These sort of polymers were used for various applications such as wound healing, drug delivery and anti-microbial activity. it wasn't however, the best option as they lead to inflammatory and toxic reactions in the human body. This led to research in the field of biodegradable polymers (Banik *et al.*, 2016)

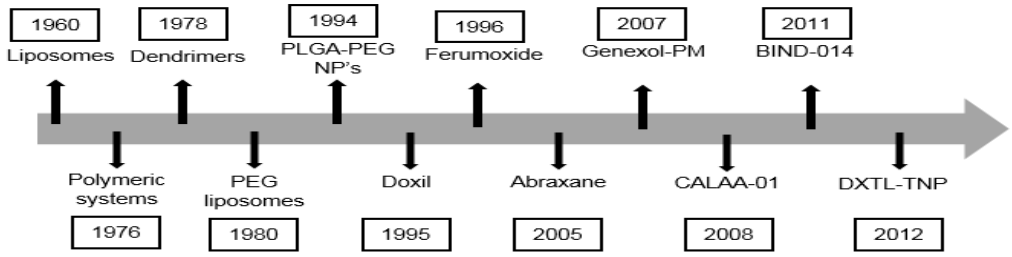

Figure 1. Timeline of nanotherapeutics. Doxil is a liposome based delivery system, was the first nanotherapeutic to be FDA approved. Genexol-PM is a paclitaxel loaded polymeric micelle and is used to treat different types of cancer (FDA approved). BIND-014 is a polymeric system used for targeted drug delivery (FDA approved). Others include PEG(polyethylene glycol) liposomes, PLGA-PEG NPs (poly (D, L-lactic-co-glycolic acid)-polyethylene glycol nanoparticles), CALAA-01 (targeted nanoparticle containing siRNA) and DXTL-TNP (docetaxel targeted polymeric nanoparticle). Adapted from Banik *et al.* (2016).

1.4.2.1 Polymers used as drug delivery systems

The polymers used for drug delivery are biodegradable polymers such as PLGA, PLA and PCL. Over the years several morphologies of biodegradable polymers have been used such as nanofibers and nanoparticles (Ahmad *et al.*, 2014). Many studies show controlled drug release profiles by polymeric nanoparticles. Cheng *et al.* (2011) indicated that cisplatin loaded PLGA nanoparticles, had a controlled drug release and were effective against ovarian cancer cells. Another study showed that docetaxel loaded nanoparticles were effective against different types of tumours and were able to release the drug in a controlled fashion (Zhao *et al.*, 2013). Based on the potential of using these particles for controlled drug release, companies such as Bind Therapeutics, Access Pharmaceuticals and Abraxis have developed polymeric nanoparticles to treat cancer. Bind Therapeutics have developed Bind-014 shown in Figure 1, which are nano particles that contain docetaxel, designed to target tumours at tissue, cellular and molecular level. There are several studies showing the use of polymers and their effects on neurodegenerative disorders and their ability to cross the blood brain barrier. For example, a paper by Kabanov and Gendelman (2007), has reported synthesis of polymeric micelles as carriers for the central nervous system. These polymers were conjugated with antibodies against a glycoprotein found in the

brain. Using a fluorescent probe, the polymeric micelle was able to deliver the drug to the target site in the brain. However, there are none that are FDA approved (Zhang *et al.*, 2014).

1.4.2.2 Polymeric nanoparticles as stimuli- responsive materials.

Targeted drug delivery is quite important in the field of nanotherapeutics as the higher the payload the more effect the drug has on the site of action. A new approach to achieve this outcome is using stimuli-responsive materials. This approach is beneficial as the polymers undergo a conformational change in response to a stimulus. This allows efficient release of the drug (Torchilin, 2014). Most frequent stimuli used are temperature, pH and magnetic field since these are easy to manipulate to achieve desired drug release. For example Li *et al.* (2009) synthesised polymeric particles, which were shown to be temperature sensitive, once in an environment with a lower temperature. This reduced environment caused breakdown of the disulphide bonds on the polymer, which allowed the drug to be released. There are several other polymeric nanoparticles that are applied in the similar way, however the only variable that changes is the stimuli (Gandhi *et al.*, 2015).

1.4.2.3 Polymeric nanoparticles as imaging agents

The development of imaging techniques such as magnetic resonance imaging (MRI) and X-rays, has benefited the field of nanomedicine. Studies have been conducted whereby polymeric nanoparticles are modified with contrasting agents, and are imaged under MRI and x-rays for diagnostic purposes. This technique has made a significant impact, as these agents can selectively target cancers and tumours, and allow for rapid diagnosis. For example Sun *et al.* (2012) has shown that PLGA nanoparticles loaded with iron oxide, have co-localised in breast cancer tissue, and could be easily imaged using MRI. Similarly, other studies on polymeric nanoparticles as imaging agents, have shown to be useful in the area of nanomedical diagnostics. Since this a developing field, there are none that are FDA approved or currently undergoing clinical trials (Srikar *et al.*, 2014).

1.4.3 Biomimetic nanoparticles, a new platform in the area of nanomedicine

The use of polymeric nanoparticles and synthetic nanoparticles has led to rapid clearance by the immune system. This was one of the factors that led to development of systems that were able to mimic the biological morphology of cells and achieve the same function as other nanoparticles would. The particulate systems can mimic structural and functional features of viruses, bacteria, erythrocytes and other biological cell membranes. They are currently used in imaging, biosensing, drug delivery and vaccine development (Carmona-Ribeiro, 2010). In order to achieve the function of biomimicry, there are several factors that need to be considered such as size, material and morphology of the particle.

Literature suggests that the closer the particle is to cell size, the greater the effect on the target cell (Meyer *et al.*, 2015). The material of the core and the coating depends on the application of the nanoparticle, for example Hu *et al.* (2011) has shown that development of a erythrocyte membrane coated nanoparticle is very effective in delivering water insoluble drugs in an animal model. Similarly, another study has shown that paramagnetic nanoparticles coated by an erythrocyte membrane makes it an effective tracer, as they can be imaged using magnetic particle imaging (Antonelli *et al.*, 2013). Morphology plays a significant role in immune recognition. For example, studies have shown that using biomimetic coatings on non-spherical particles have shown a 20 fold stronger t-cell response as compared to spherical shape particles of the same nature (Sunshine *et al.*, 2014). Therefore, to achieve the function of biomimicry these factors have shown to play a significant role.

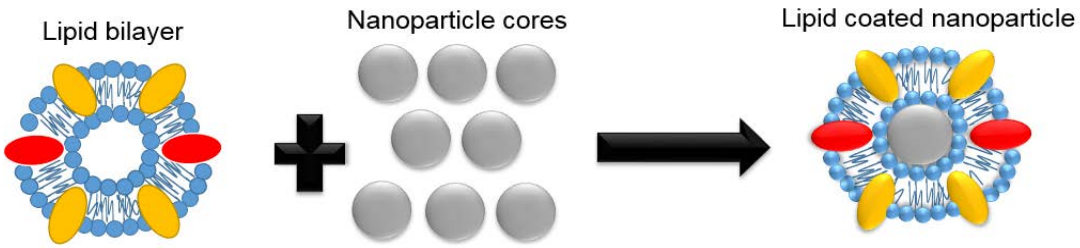

Figure 2. A diagrammatic illustration of the synthesis of biomimetic nanoparticles. Lipid bilayer isolated from biological membranes is fused with the desired nanoparticle core to formulate biomimetic nanoparticles. The phospholipids and fatty acid tails are indicated by the blue structures and the proteins are indicated by the red and yellow structures on the lipid coated nanoparticle

1.4.4 Current biomimetic nanoparticles

Current research and synthesis of biomimetic nanoparticles revolves around mimicking surface chemistry of cells, as they have shown to have benefits, when these systems are tested *in vivo*. Mimicking surface chemistry involves synthesising particles, whereby the biological substances are surrounded by highly complex membranes that comprise of lipid bilayers and cell surface proteins. Synthesis of these particles can have two approaches, the bottom-up approach and the top-down approach.

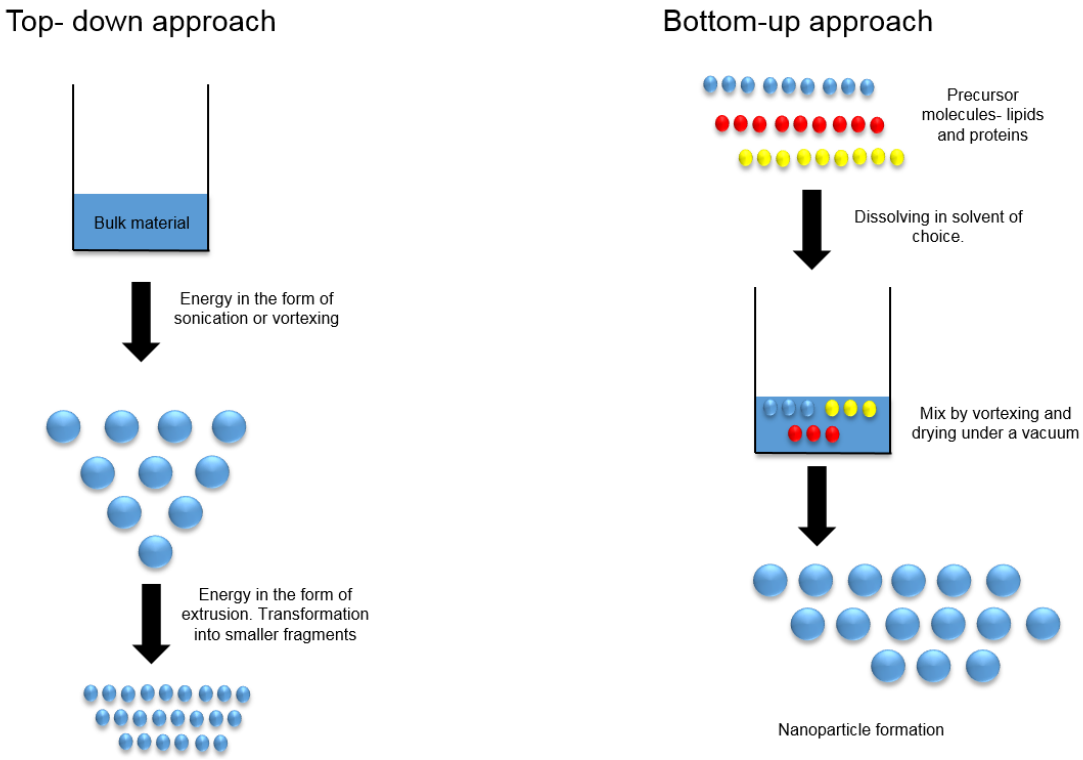

Figure 3. A diagrammatic representation of the two different approaches used to synthesize biomimetic nanoparticles. Top down approach is used to synthesise liposomes, micelles and vesicles (left). Bottom-up approach (right) is used to produce formulations of nanoparticles, which ideally use synthetic lipids and proteins. The blue sphere represents lipids, whereas the red and yellow spheres are different types of proteins.

The bottom-up approach begins with molecular components, built into a larger structure using physical and chemical techniques to mimic cells (Figure 3). This approach utilises components such as lipids and surface proteins, which are incorporated by surface functionalisation or attaching them with an adhesive

protein via a chemical interaction. The top-down approaches utilize macroscale structures and turn them into nanoscale structures. This approach is beneficial, as cell membranes are isolated from biological cells and added to particle cores. Literature suggests that a lot of research has been conducted on nanoparticles using the bottom- up approach over the last few years (Meyer *et al.*, 2015). Rather than developing particles from an artificial membrane and using synthetic lipids and proteins, several studies have been able to isolate erythrocyte membranes from purified cells and use the membrane to coat particles (Muzykantov, 2010). These studies have shown that this technique offers a clear advantage over using bottom-up approaches (Patel *et al.*, 2008).

1.4.5 The top-down approach

Development of nanoparticles such as liposomes, micelles and polymeric nanoparticles have revolutionised medicine. Nevertheless, due to their synthetic natures, they remain limited in their clinical application as they could be recognised as a foreign object by the immune system. Interestingly, there is still research that is being conducted on these particles, due to the ability to be functionalised with large number or ligands and the time required to synthesise these particles. Contrary to their advantage, they could cause a variety of health problems (Zhang, 2016). The question remains of safety of such particles. The currently used technique is to modify these particles with polyethylene glycol (PEG), which creates a hydrophilic layer around these particles. This layer allows the particle to evade the immune cells. Though, some recent studies show that the PEG layer activates the immune system and have shown to be taken up by immune cells (Wang *et al.*, 2007)

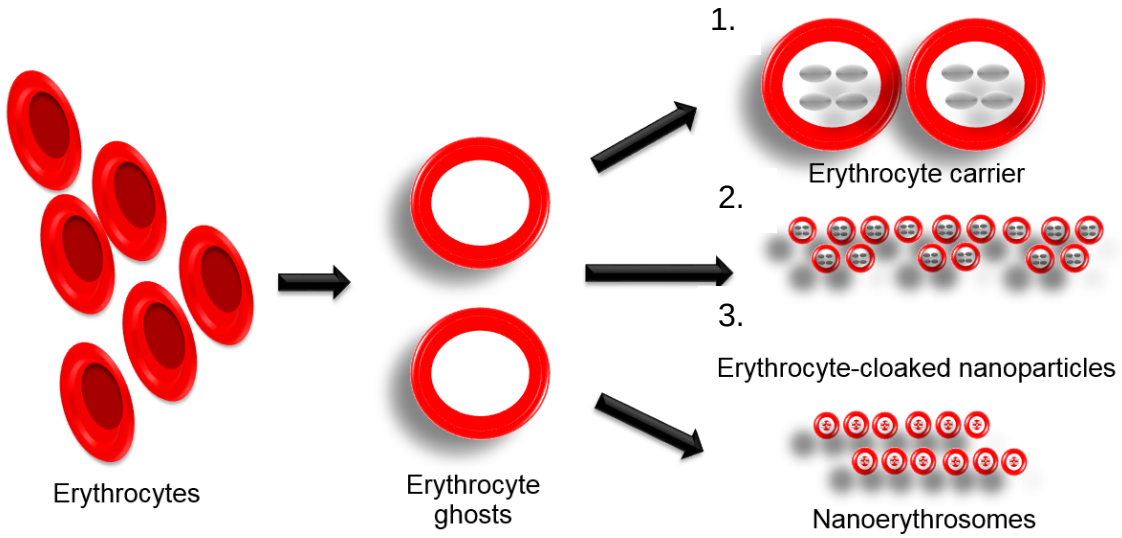

Figure 4. Diagrammatic representation of erythrocyte cloaked nanoparticles adapted from Zhang (2016). The erythrocytes are lysed to develop erythrocyte ghosts, which has been used as a coat to develop three different nanoparticles systems. (1) Erythrocyte carriers (micrometre size) which is used to coat hydrophobic drugs (represented by the grey structure, (2) Erythrocyte cloaked nanoparticles (nanometre size) are designed by coating a core structure containing the entrapped drug with the erythrocyte membrane, (3) Nanoerythrosomes (nanometre size) are erythrocyte membranes that envelop a hydrophobic drug.

The advent of using natural cell membranes as coatings for synthetic materials has shown greater promise than synthetic particles. Among these particles, using membranes derived from natural erythrocytes is of current interest. They are an interesting system to work with due to their biocompatibility and long-term circulation characteristics (Hamidi *et al.*, 2007). Another advantage of this system is that erythrocytes have the ability to re-seal. Therefore, inserting synthetic materials into the system can be easily applied. Studies published in the past have shown that erythrocytes loaded with drugs are not very effective in delivery due to the micrometre size (Patel *et al.*, 2008). This gave rise to developing nanoerythrosomes and blood cell based biomimetic carriers as shown in Figure 4.

1.4.5.1 Whole erythrocyte carrier systems

The primary use of erythrocytes in the field of nanomedicine, was the use of erythrocytes as whole carriers. These systems have shown improved pharmacokinetic properties as opposed to synthetic nanoparticles. Erythrocytes have gained a lot attention due to the properties stated earlier. Apart from immune evasion, erythrocytes can be easily fabricated using a hypotonic lysis method. This is a common strategy to prepare carrier erythrocytes (Hamidi and Tajerzadeh, 2003). Similar to synthetically derived polymeric nanoparticles and lipid nanoparticles, whole erythrocytes have been used as drug delivery vehicles (Hamidi *et al.*, 2011), as imaging agents (Brahler *et al.*, 2006) and targeted drug delivery carriers (Harisa *et al.*, 2014).

1.4.5.2 Erythrocyte ghosts

Whole erythrocytes are lysed to synthesize erythrocyte ghosts to study the components and characteristics of the erythrocyte membrane. Erythrocyte ghosts are cellular membranes formed after a hypotonic buffer is added to erythrocytes. These structures are mainly devoid of intracellular contents, and were used for membrane studies (Schwoch and Passow, 1973). Morphology of erythrocyte ghosts differ based on the method used to prepare them. The most widely used method is by hypotonic lysis of erythrocytes. There has been enormous data generated around the application and characteristics of erythrocyte ghosts.

Schwoch and Passow (1973) have reported the existence of two type of ghosts. White ghosts and resealed ghosts. White ghosts are devoid of contamination by haemoglobin (Hb) and are devoid of intracellular contents. These type of ghosts have been used in the past for membrane characteristic studies. Resealed ghosts are able to reseal by addition of a resealing buffer or if incubated on ice. The have the ability to reseal, as they regain permeability to left over Hb. These ghosts are primarily used to create nanocarriers (Figure 4).

1.4.5.3 Nanoerythrosomes

The use of any carrier system developed in this field is primarily used as a drug delivery vehicle. The use of a particle as a carrier system allows researchers to

easily investigate the pharmacokinetics of the system. These are then manipulated to suit certain pharmacological characteristics, which diversifies their application in the field. In the same way, whole carrier erythrocytes are manipulated to synthesize nanoerythrosomes (Zhang, 2016). The size of whole carrier erythrocytes could limit many properties such as targeted delivery and cell diffusion across tissue compartments becomes almost impossible (Gupta *et al.*, 2014). Moreover, due to the size being in the micrometre range the possibility of being recognized by the immune system as foreign is higher, therefore nanoerythrosomes were developed. Reduction of size from whole carrier erythrocytes can be easily performed by using techniques such as sonication or extrusion. Nanoerythrosomes have been shown to have a variety of applications such as carriers of antitumor agents (Lejeune *et al.*, 1994), antimalarial agents (Agnihotri and Jain, 2013) and they have been applied as an intra-tracheal delivery vehicle (Gupta *et al.*, 2014).

1.4.5.4 Erythrocyte membranes as a coating for synthetic particles

Nanoerythrosomes have several applications in the therapeutic field. However, due to the reduction in size, there have been limitations with drug loading and release (Zhang, 2016). This was one of the reasons that led to the creation of biomimetic nanoparticles. This field of biomimicry is where synthetically drug loaded nanoparticles are coated with an erythrocyte membrane. There are several advantages to this approach. The erythrocyte membrane coating displays “self-properties” and has shown to evade macrophage detection, which has led to a longer circulation in the blood stream (Doshi *et al.*, 2009). This is a developing area, so its use has been limited to drug delivery (Hu *et al.*, 2011).

Most of these particles are cancer targeting or are encapsulated with an anti-cancer drug. According to literature use of nanoparticles systems, has a very limited application in the field of microbiology. Most of these systems are drug carriers to target bacterial or parasitic infections (Mu *et al.*, 2016). This opens up a new avenue for research into using biomimetic particles to treat bacterial infections. A recent study has shown encapsulation of vancomycin into gelatin nanoparticles coated by an erythrocyte membrane. This system releases vancomycin upon degradation by gelatinase (Li *et al.*, 2014). Apart from this, there is limited work in this area. This study will focus on creating a biomimetic

model to treat a disease known as sepsis, which arises due to bacterial invasion and exotoxin production.

1.4.5.5 Nanosponges

The term nanosponge has several definitions, as it depends on the application of this nanoparticle. In 2012, a study stated that nanosponges are a new class of materials made of particles, which have presence of cavities. These cavities could be used to encapsulate drugs (Krishnamoorthy and Rajappan, 2012). Another study reported the use of cyclodextrin nanosponges which act by soaking up the drug to be encapsulated (Cavalli *et al.*, 2006). None of these systems however, are biomimetic. A study published by Hu *et al.* (2013), reported development of a biomimetic nanosponge that has the ability to adsorb exotoxins. This nanosponge was constructed with a polymeric core enveloped by an erythrocyte membrane. This design has shown to prolong systemic circulation in the blood stream. The erythrocyte coating enables “stealth properties” which may allow the nanoparticle to evade uptake by macrophages. Therefore, the definition for this type of nanosponge is the unique capability of the nanoparticles to adsorb exotoxins.

1.4.6 Pathogenicity- Causative agents and bacterial infections

Bacteria can cause many different types of infections (Figure *5*). They can invade and kill human cells due to many virulence factors. For example, adherence proteins, capsules, biofilm formation, endotoxins and exotoxins are all virulence factors. The infections caused by these pathogens can range from respiratory, skin, blood stream, intestinal and urinary infections (Figure *5*).

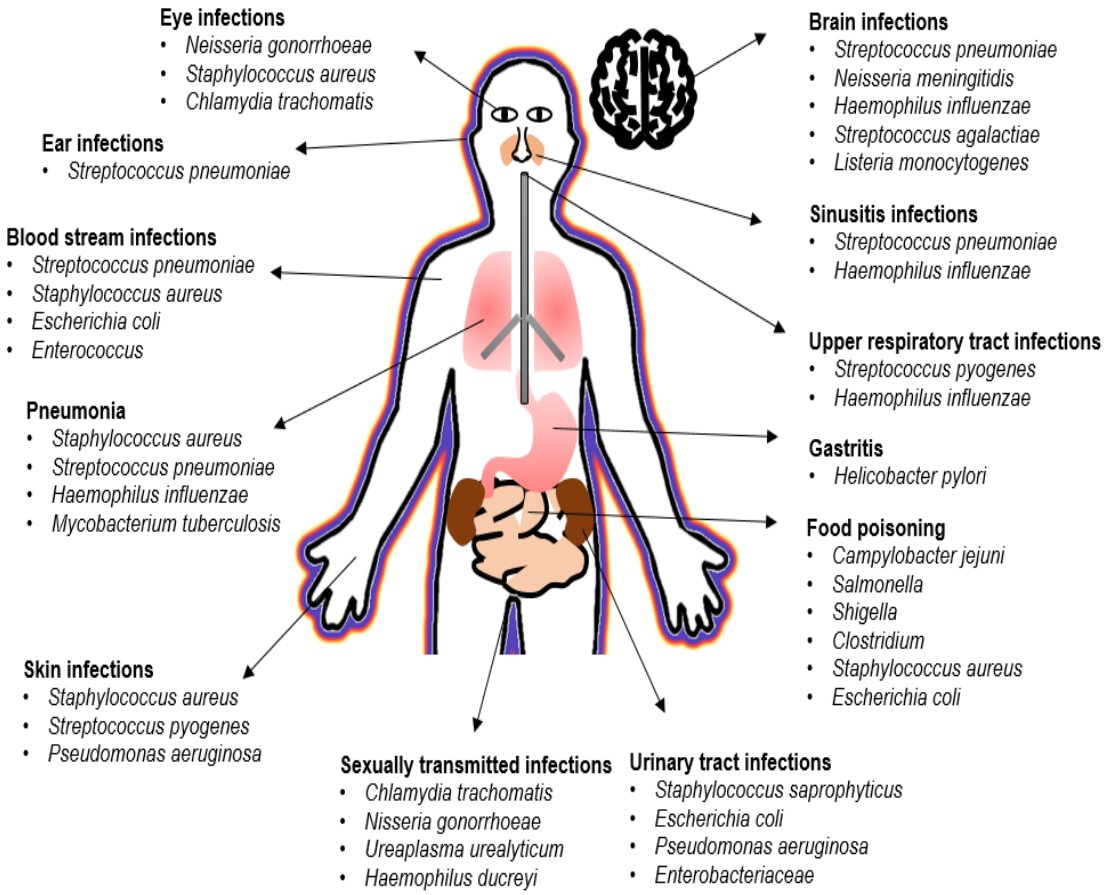

Figure 5. An overview of bacterial infections caused by different type of bacteria, adapted from Ford (2014) . The causative organism has been labelled according to its site of infection in the human body.

The only way to treat some of these infections is to synthesis a novel treatment. In 1928 Fleming discovered the first antibiotic known as benzylpenicillin (penicillin G) and observed that some bacteria were inherently resistant (Fleming, 1929). In his Nobel lecture, he noted that bacteria could develop resistance to antibiotics (French, 2010).

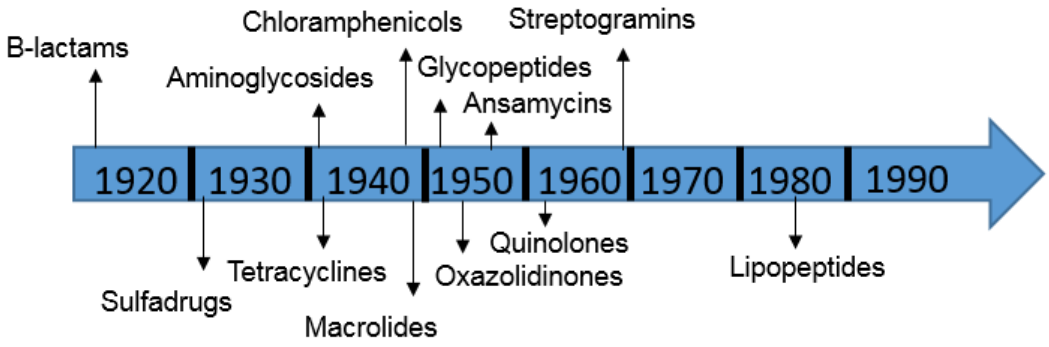

Figure 6. An antibiotic discovery timeline adapted from Lewis (2012). The timeline pinpoints the year the antibiotic was discovered.

Most resistant strains of bacteria are found in hospitals, as this environment has the maximum use of antibiotics. A few years after penicillin G was discovered. In 1935 the first bacterium that acquired penicillin resistance was discovered. This bacterium is known as *Staphylococcus aureus* (Shanson, 1981). The only way to tackle emerging strains that acquired resistance to penicillin was to discover or synthesize new antibiotics. From the 1960 to the 1980s, new antibiotics were introduced from derivatives of aminopenicillanic acid (6-APA) including broad spectrum methicillin, oxacillin and ampicillin (Figure 6). This led to the birth of multidrug resistant *Staphylococcus aureus.* Multidrug resistance is the reason as to why bacterial infections are becoming problematic and life threatening.

1.4.7 Antibiotic resistance and epidemiology of life threatening bacterial infections

The discovery of antibiotics is one of the greatest achievements in the history of medicine. They treat infections from minor to life threatening, allow surgeons to safely perform procedures and successfully allow non-infected organ transplantation. However, this treatment option is no longer the most applicable due to the rise of antibiotic resistant organisms (Watkins and Bonomo, 2016). In spite the use of antibiotics in the last 70 years, infectious diseases have had an impact on morbidity and mortality throughout the world.

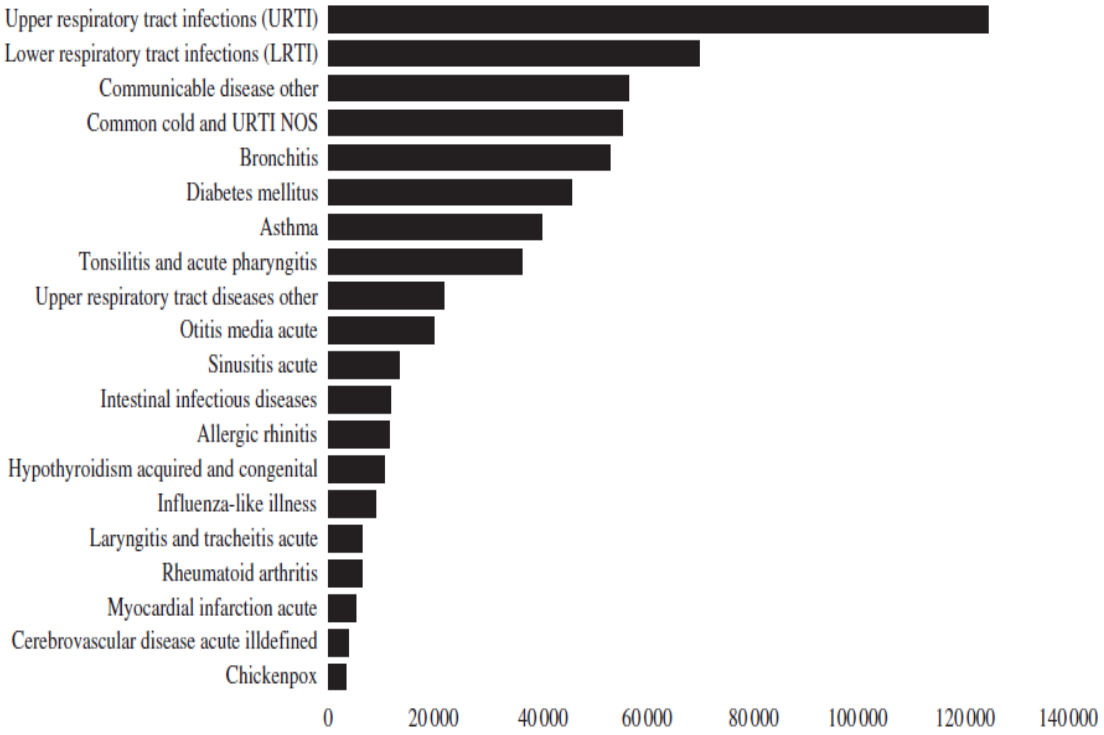

Figure 7. Epidemiological data recorded in 2003, shows the different types of bacterial infections diagnosed in the UK. The rates shown in black correspond to GP consultations per 140,000 population (Finch and Hunter, 2006).

A study conducted by the Health Protection Agency (HPA) showed that the maximum amount of patients per 100,000, were consulted for upper and lower respiratory tract infections, compared to the other diseases (Figure 7). Over 12,000 visits to the consultants were for upper respiratory tract infections with a further 8,000 for lower respiratory tract infections. The total estimated costs to the health care system for infectious diseases in England are shown in Table 2. Hospital acquired infections account for 23% of the total cost. Moreover, 50% of the total cost is towards GP consultations, These figures do show that people in England suffer from respiratory and hospital acquired infections, which cost the NHS billions of pounds (Finch and Hunter, 2006).

Table 2. The cost of treatment and management of infections in England in 2003 (Finch and Hunter, 2006)

Treatment and management	Cost £ (in billions)
GP consultations	3.52
Hospital-acquired infections	1.39
Hospital admisssions	0.89
HIV/AIDS treatment and care	0.27
Total	6.07

1.4.7.1 Multidrug resistant organisms that account for the highest mortality rates

There are many different bacterial strains that have developed resistance to specific antibiotics. But, over the years, *Staphylococcus aureus* shows high rates of infection in humans (Lowy, 1998). *Staphylococcus aureus* has the potential to cause local as well as disseminated infections, and has the potential to cause lesions near anatomical sites. Between 25% to 35% of humans carry *Staphylococcus aureus* on their skin. This is significant as any wound exposure can lead to the bacteria invading the wound and entering the blood stream (Wertheim *et al.*, 2005). This does however depend on the virulence of the strain.

Certain strains of *Staphylococcus aureus* gain antimicrobial restance through a horizontal DNA transfer mechanism. One such strain of *Staphylococcus aureus* is methicillin resistant *Staphylococcus aureus* (MRSA). Strains of MRSA were discovered soon afer methicillin was introduced. In the 1970s MRSA emerged as a major pathogen worldwide (Brumfitt and Hamilton-Miller, 1989). In both the USA and Europe 30-50% of the *Staphylococcus aureus* isolates are MRSA (French, 2010). In 2007 it was estimated that *Staphylococcus aureus* was responsible for causing 108,434 blood stream infections from which 27,711 (26%) were resistant to methicillin. In the same year it was esti~~n~~mated that 5,503 deaths were caused by MRSA infections, from which 1,096 were from the UK alone (de Kraker *et al.*, 2011). MRSA has shown to have high rates of worldwide infections and also represents a percentage of the total mortality rates in Europe. Nonetheless, these rates need to be contained and kept under control. Another bacterial strain reported in the UK has shown high rates of infection. In 2010-2011 in England,

the HPA reported a number of bacterial infections. Routine surveillance data showed increase in the number of *Streptococcus pyogenes* and *Streptococcus pneumoniae* infections (Zakikhany *et al.*, 2011). *Streptococcus* is a gram positive pathogenic bacterium, that is known to cause a range of infections such as meningitis, pneumonia and urinary tract infections. This bacterium has also showed high rates of antibiotic resitance in the UK. A study conducted by Hounsom *et al.* (2011) reported, from 686 bacteraemia episodes, which occurred in 681 patients. Drug resistant *Streptococcus* accounted for the third highest infection rate, causing 5.8% of the total infections in that year. Another study by Zakikhany *et al.* (2011) reported increased rates of *Streptococcal* infection from 2007 to 2011 contributed to high rates of infection Figure 8.

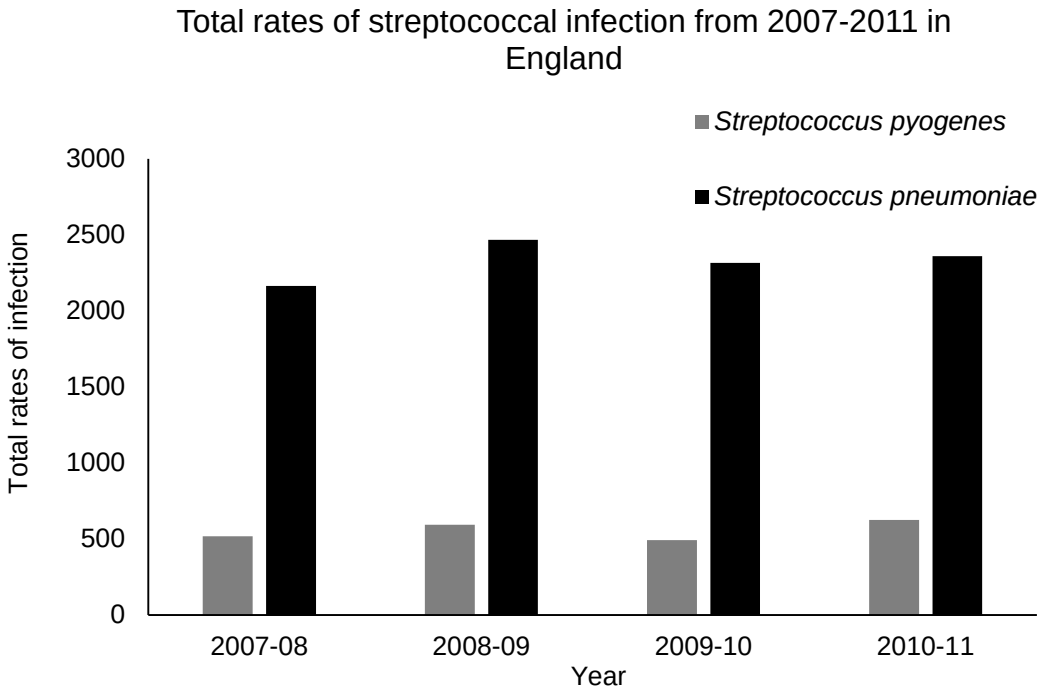

Figure 8. Epidemiology data adopted from Zakikhany *et al.* (2011) shows total rates of *Streptococcal* infections from 2007-2011, per 100,000 population

Streptococcus is of major concern as well documented research by Public Health England has shown that this group of bacteria have gained penicillin, macrolide, and tetracycline resitance. They reported in 2013 that 5% of all *Streptococcus* isolates were penicillin resistant, 7.4% were resistant to macrolides and 22% were resitant to tetracycline. (PHE, 2014). *Staphylococcus aureus* and *Streptococcus* in their non-invasive form are not harmful bacteria. However, when exposed to an open wound, due to virulence of the strain, it manages to cause an infection within the blood stream. If the bacteria was susceptible to damage

by broad spectrum antibiotics, the infection would be treatable. But, as stated above, due to the widespread of antibiotic resistance, simple infections become difficult to treat. Once in the blood stream, if infections are not treated within a few hours, they become seriously dangerous to a patients health and could lead to a condition known as sepsis (Hounsom *et al.*, 2011).

1.4.8 Sepsis and its impact on the United Kingdom

Sepsis is a whole body inflammation caused by a severe infection. This could develop into severe sepsis (organ dysfunction) or septic shock (abnormal tissue perfusion). Sepsis is a major public health problem in England.

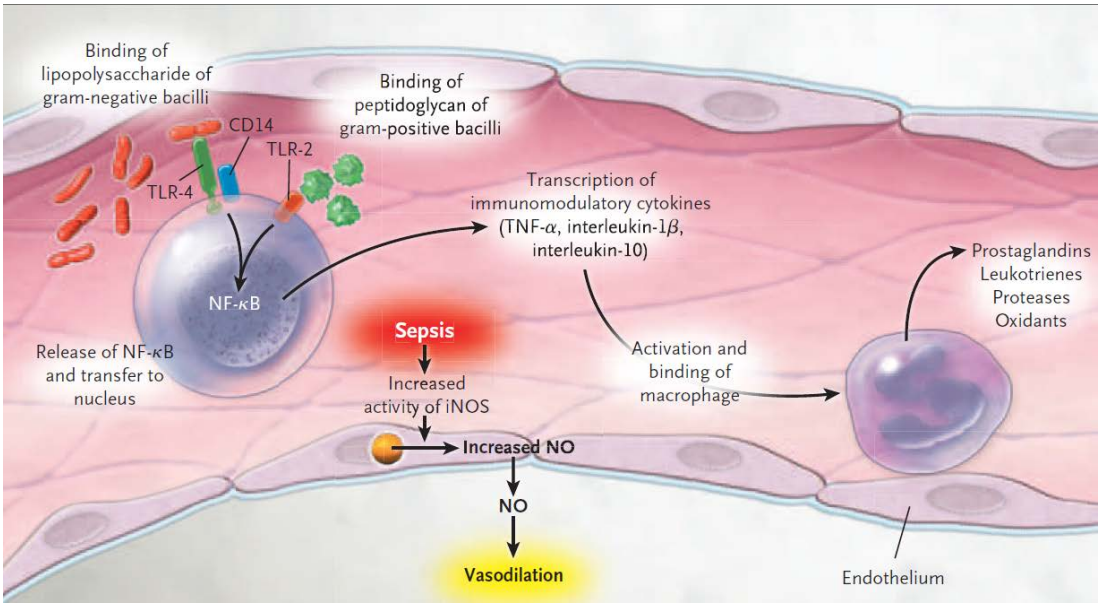

Figure 9. A diagrammatic representation of the mechanism of acquiring sepsis, adopted from (Russell 2006) .The schematic also represents, invasion of bacteria into the bloodstream of a patient which leads to leaky blood vessels, causing inflammatory mediators to leave the blood stream, leading to organ dysfunction.

The primary cell the bacteria comes into contact with are erythrocytes. This triggers inflammation by the immune cells (Figure 9). Bacteria have a variety of virulence factors such as endotoxins and exotoxins. Exotoxins are released in the blood stream of an infected patient and bind to a different types of cells including erythrocytes and cause them to lyse leading to sepsis (Peters and Cohen, 2013). Patients who acquire sepsis suffer from neurological symptoms, organ

dysfunctions, shock, organ hypo-perfusion, lactic acidosis and oliguria. From 2001-2010, 226,547 deaths were associated with sepsis in the UK, calculations showed 1 in 20 people acquired sepsis. (McPherson *et al.*, 2013)

ICD-10 codes	ICD-10 chapter	Sepsis deaths	All deaths	Percentage of sepsis-associated deaths in chapter	Percentage of all deaths in chapter that are sepsis associated
A00-B99	Infectious diseases	26296	53543	11.7	49.1
C00-D48	Neoplasms	30210	1307155	13.4	2.3
D50-D89	Diseases of the blood	1696	9610	0.8	17.6
E00-E90	Endocrine diseases	6995	69483	3.1	10.1
F00-F99	Mental and behavioural disorders	1899	150122	0.8	1.3
G00-G99	Nervous system diseases	3199	149773	1.4	2.1
H00-H59	Eye diseases	40	112	0.0	35.7
H60-H95	Ear diseases	53	206	0.0	25.7
I00-I99	Circulatory diseases	25803	1708766	11.5	1.5
J00-J99	Respiratory diseases	34581	654960	15.4	5.3
K00-K93	Digestive diseases	31550	234960	14.0	13.4
L00-L99	Skin diseases	12251	16190	5.5	75.7
M00-M99	Musculoskeletal diseases	5215	41617	2.3	12.5
N00-N99	Genitourinary diseases	40090	96988	17.8	41.3
O00-O99	Pregnancy	41	429	0.0	9.6
P00-P96	Perinatal period	372	1958	0.2	19.0
Q00-Q99	Congenital abnormalities	568	11545	0.3	4.9
R00-R99	Symptoms, signs and abnormal clinical and laboratory findings	17	109542	0.0	0.0
V01-Y98, U50.9	External causes	3849	162139	1.7	2.4
	Total	224725	4800260	100.0	4.7

ICD-10, International Classification of Diseases, 10th Revision.

Figure 10. Tabular data reports the causes of sepsis between 2001 and 2010 in the UK, adopted from (McPherson *et al.*, 2013). Labelled in red shows number of deaths reported by infectious diseases associated with sepsis.

The tabular data (Figure 10) reports the causes of sepsis along with the mortality rates between 2001 and 2010. Labelled in red is the first cause on this list and is of importance as it shows that 49.1 % of all deaths that are caused by infectious diseases are sepsis associated. This is second highest mortality rate amongst the other causes. Other well-documented research has reported deaths by infectious disease leading to sepsis. Hounsom *et al.* (2011) has reported that in 2006, 32,000 patients died due to sepsis. Another study reported that *Streptococcus* causes hig-h rates of sepsis in pregnant women (Sriskandan, 2011). Sepsis is not only affecting the UK, but has had an impact on the United States. Figure 11 shows the incidence rate of sepsis in US in 2015. Sepsis is shown to be the highest rate in 2015 at 300 cases per 100,000.

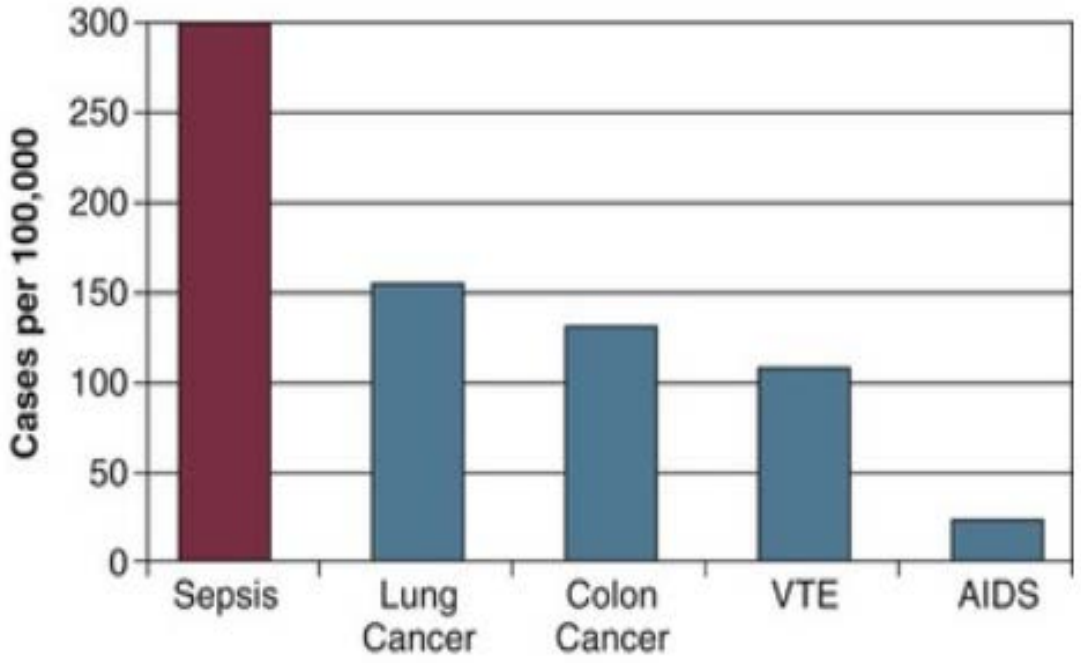

Figure 11. Epidemiology data adapted from (Trzeciak 2015) shows incidence rates of different pathologies in US in 2015, per 100,000 population.

1.4.9 Current treatment and management of sepsis

To reduce the mortality rate caused by sepsis there has to be an improvement in treatment. Current options for sepsis caused by infectious diseases include antibiotics, surgical drainage of infected fluids, blood transfusion, organ replacement and steroids. Most of these treatment strategies manage to reduce the inflammatory response, however antibiotic therapy is a selective pressure for the evolution of antibiotic resistant bacterial strains. The early treatment of patients with sepsis has shown to be an important factor in decreasing mortality rates. This concept is known as the “Golden hour”. The golden hour refers to the first 6 hours of infection. Early recognition and treatment of this condition is believed to stop the chain of events occurring at molecular and cellular levels that lead to organ dysfunction. If a patient is diagnosed with sepsis within the first 6 hours, early goal directed therapy is essential. This refers to administering antibiotics, intravenous fluids, and oxygen to the patient. Additionally, blood cultures are sampled to identify causative organism and the kidney function is monitored (Wheeler, 2015).

1.4.10 Research aims

The aim of this study is to synthesise a model biomimetic nanoparticle known as a nanosponge, using mammalian erythrocyte membranes as coatings in order to adsorb pore forming toxins (PFTs) in *vitro*. This in turn could reduce the incidence and severity of exotoxin related sepsis *in vivo*. Nanosponges are nanoparticles constructed with a polymeric core (PLGA) enveloped by, in this case, erythrocyte membranes. Each component of the nanosponge has a significant property. The erythrocyte membrane contains surface properties that allow absorption of PFTs. Its highly flexible structure could allow it to pass through narrow capillary networks (Hu *et al.*, 2013). By coating it with a mammalian erythrocyte membrane, the nanosponge is non-immunogenic even if released back into the same mammalian species.

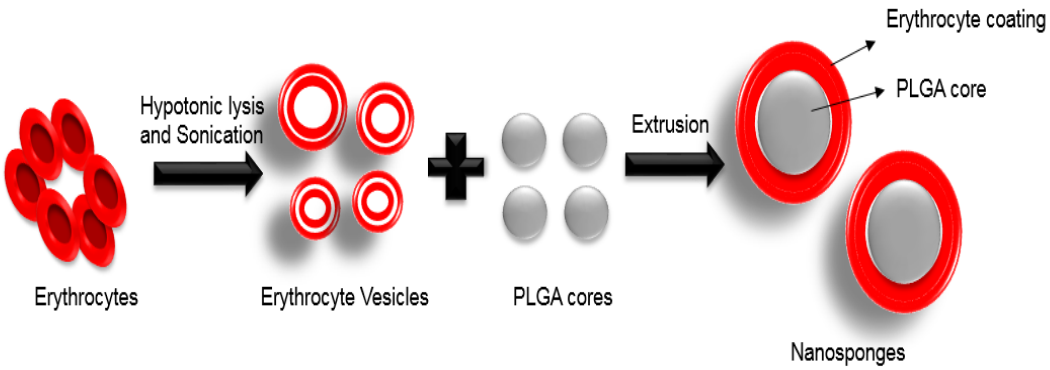

Figure 12. A diagrammatic representation of mechanisms involved to synthesize nanosponges. The extrusion allows the erythrocyte vesicles to coat the PLGA polymer, adapted from Hu *et al.* (2011)

Two different PFTs were chosen in this study, α-haemolysin released form *Staphylococcus aureus* and streptolysin-O released form *Streptococcus pyogenes*. The reason for choosing these toxins are that *Staphylococcus aureus* and *Streptococcus pyogenes* account for high rates of infection the UK, as shown in section 1.4.7. This study will test the ability of these PFTs to lyse mammalian erythrocytes. The mammalian blood that is shown to be more susceptible to damage by these PFTs, which will be the basis for a coating. One of the PFTs, streptolysin-O is specific for cholesterol present in the lipid bilayer of the erythrocyte membrane as shown in chapter 2 section 2.3.2. Therefore, the study will aim to incorporate cholesterol into the erythrocyte membranes and test the

adsorption ability of cholesterol incorporated nanosponges against streptolysin-O. This is important as phospholipids and cholesterol are significant binding sites for these PFTs. The study will also asses the loss of lipids during the synthesis of nanosponges.

1.5 Material and Methods

All chemicals were analytical grade and purchased from Fisher scientific UK Ltd (Loughborough, UK) Sigma-Aldrich Ltd (Dorset, England) Diagnostic Reagents Ltd, (Oxon, England), Electron Microscopy Sciences (Hatfield, USA) and TCS biosciences (Buckingham, UK).

1.5.1 Blood collection and storage

The method for blood collection and storage was adopted from Zehnder *et al.* (2008) and optimized to obtain accurate collection and storage conditions. Animal blood (ovine and porcine) was collected from a local abattoir (William Taylor and Sons, Bamber Bridge, Lancs, England). Murine blood was collected from the University of Central Lancashire animal laboratory (Fylde road, Preston, Lancs, UK). Leporine blood was collected purchased from TCS biosciences (Buckingham, UK). The blood was collected into a clean plastic bottle, which contained 63 ml of citrate phosphate dextrose (CPD; citrate 26.3 g/l, citric acid 3.27 g/l, glucose 25.5 g/l and sodium phosphate monobasic 2.51 g/l) as an anticoagulant. 35 ml of the blood was aliquoted into 50 ml Falcon tubes (Fisher Scientific) and centrifuged at 500x g for 10 minutes at 4°C using a Beckman Coulter (Wycombe, England) bench top centrifuge. The plasma and buffy coat was aspirated using a Pasteur pipette and stored at 4°C. This removes approximately 50% of the volume in the Falcon tube. 11.1 ml of storage medium (SAGM containing 8.77g/l sodium chloride, 0.169 g/l, 9.0 g/l glucose and 5.25 g/l mannitol) was added to each tube and stored at 4°C up to a month (Hogman *et al.*, 1983). The blood was regularly checked using light microscopy at 400X for coagulation and cellular debris. If these were found the blood was discarded.

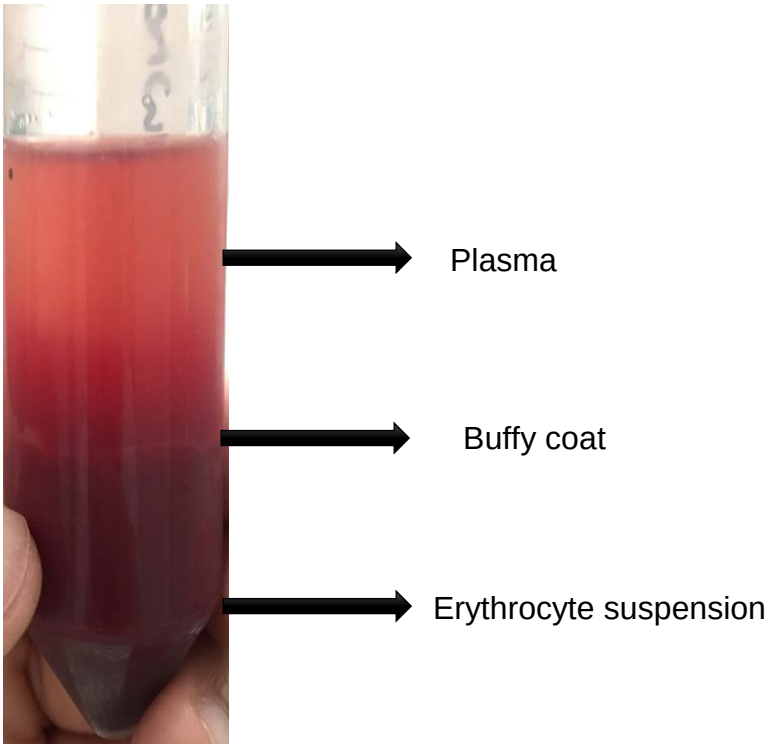

Figure 13. An image captured by a Kodak camera, shows the different compartments of blood. Centrifugation of whole blood separates it into three different compartments. The plasma at the top of the tube, buffy coat (thin white layer) and the sediment at the bottom of the tube is the erythrocyte suspension.

1.5.1.1 Lyophilization of animal red blood cells

Freeze drying of animal erythrocytes were essential for long-term storage. After the buffy coat and plasma were separated from the erythrocyte suspension. 30 ml of 166mM sodium chloride (NaCl) was added to a 15 ml erythrocyte suspension. Prior to washing both the erythrocytes and sodium chloride were cooled on ice. The suspension was then mixed by swirling the 50 ml falcon tube (Fisher Scientific) gently. The tube was then centrifuged at 500x g for 10 minutes at 4°C using a bench top centrifuge. This step washes the erythrocytes and was repeated three times. The erythrocyte suspension was separated into 5 ml aliquots, to which 5 ml of 5% (w/v) sucrose solution was added. The aliquots were sealed with parafilm and frozen overnight at -80°C. The frozen aliquots were placed in a Scanval cool safe lyophilizer overnight. The lyophilized erythrocyte suspension took on a powdered solid form, which was stored at 4°C (Han *et al.*,

2005). The erythrocyte suspension was reconstituted with 5 ml of 1X phosphate buffered saline (PBS).(Leslie *et al.*, 1995)

1.5.2 Measuring haematological parameters of animal blood

1 ml of the collected animal blood (ovine, porcine, murine and leporine) was pipetted into 1.5 ml tubes (Fisher Scientific) and kept on ice. The tube that contained animal blood was inserted into the ABX Pentra 60 c+ haemoanalyser (Horiba medical, Northampton, England). The haemoanalyser has 5 reagents ABX diluent, ABX lysebio, ABX eosinofix, ABX basolyse and ABX cleaner. The ABX diluent is an isotonic solution that diluted the animal blood cells and was used to measure haematocrit. The ABX lysebio is a mixture of 5% (w/v) ammonium salt with a 3% non-ionic based surfactant (v/v). This reagent lysed the red blood cells to determine Hb concentration. The ABX basolyse and eosinofix are reagents used for white blood cell count and was used to differentiate basophils form the other white blood cells. The ABX cleaner is a mixture of an organic buffer with proteolytic enzymes, which was used to clean the haemoanalyser after the test was conducted. After the tube was inserted, the machine took up 60 µl of the animal blood and the result was generated in 10-15 seconds on an Hp monitor (Bossche *et al.*, 2002)

1.5.3 Preparation of erythrocyte ghosts

1 ml of a cocktail of Sigma- Aldrich (Dorset, England) protease inhibitor was added prior to each wash. This comprises of 2mM 4(2-Aminoethyl) benzene sulfonyl fluoride hydrochloride (AEBSF), 0.3µM aprotinin, 130µM bestatin, 1mM ethylenediaminetetraacetic acid (EDTA), 14µM 1(((4Guanidinobutylamino)4methyl1oxopentan2yl) carbamoyl) cyclopropanecarboxylic acid (E-64) and 1µM leupeptin.

1.5.3.1 Wash 1 Removal of buffy coat and plasma

5 ml of stored porcine blood was washed three times with 7 ml of 166mM NaCl. Both the erythrocytes and NaCl were cooled on in ice. After each wash the cells were centrifuged at 500x g for 5 minutes at 4°C and the supernatant was aspirated and stored at 4°C (Dodge *et al.*, 1963)

1.5.3.2 Wash 2 Cell lysis

After the last wash, the cells are re-suspended in 166mM NaCl to form a 25% cell suspension and cooled at 0°C on ice. 1 ml of the 25% cell suspension was added to 7 ml of a hypotonic medium containing: 9.64mM NaCl, 1.20mM potassium orthophosphate (KH_2PO_4), 1mM EDTA and 3.61mM sodium phosphate dibasic (Na_2HPO_4) (pH 7.2). The solution was then re-cooled to 0°C for 20 minutes and centrifuged at 500x g for 30 minutes at 4°C. This lysis supernatant was aspirated and stored at 4°C.

1.5.3.3 Wash 3 Removal of cellular debris

The pellet was washed with 10 ml of a solution containing 9.6mM Trizma hydrochloride (Tris-HCl) and 20mM NaCl (pH 7.2). The solution was centrifuged at 500x g for 5 minutes at 4°C. The supernatant was aspirated and stored at 4°C. The sediment was then washed in a medium containing 4.8mM Tris-HCl and 10mM NaCl. The solution was centrifuged at 500x g for 5 minutes at 4°C. The supernatant was aspirated and stored at 4°C. The pellet was then washed in 100mM potassium chloride (KCl) solution and once after in distilled water (Di-H_2O). The solutions were centrifuged at 500x g for 5 minutes at 4°C. The supernatants were aspirated and stored at 4°C. At the bottom of the centrifuge tube a pink pellet is formed over a dark red agglomerate, which are the erythrocyte ghosts as shown by Figure 14 (Weed *et al.*, 1963)

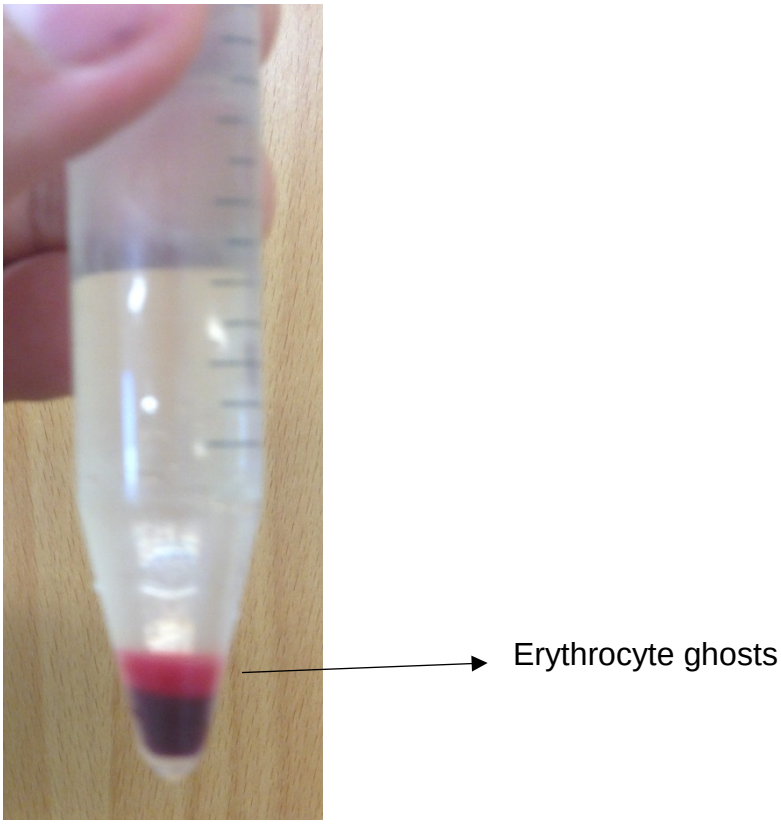

Figure 14. The pink pellet over a dark agglomerate in a 15 ml Falcon tube, is erythrocyte ghosts. These ghosts were produced after the suspension was washed with Di-H_2O

1.5.4 Preparation of erythrocyte ghost samples for light microscopy

A Pasteur pipette (Fisher Scientific) was used to deliver one drop of the erythrocyte ghost sediment onto a glass slide and a cover slip was placed on top. It was then viewed under 400X with a Nikon phase contrast microscope. The ghost suspension was compared to erythrocytes prepared using the same protocol.

1.5.5 Measuring cell size

A drop of the porcine erythrocytes was added to a glass slide using a Pasteur pipette. A cover slip was placed on top of the sample and viewed under 400X with a Nikon phase contrast microscope. The size was determined using a scale tool on the attached Nikon imaging software, which determines the diameter of the cells. This method was repeated to measure the diameter of erythrocyte ghosts.

1.5.6 Haemoglobin estimation

This haemoglobincyanide method was adopted from Bain *et al.* (2006). The reconstituted bovine Hb standard (572 mg/l) purchased from Diagnostics Reagent LTD, was diluted with distilled water according to Table 3 and allowed to stand for 20 minutes prior to use. The spectrophotometer (Jenway spectrophotometer 73 series) was zeroed using Drabkins reagent (Diagnostics Reagent LTD). 1ml of each concentration was added to a plastic cuvette and the absorbance assayed at 540nm. The experimental supernatant samples collected from the previous experiment were also estimated for Hb. These solutions were mixed before pipetting as they settle out on storage. 4 ml of Drabkins reagent was pipetted into a clean tube followed by 20 µl of the experimental samples and allowed to stand for 20 minutes. This step was repeated for all samples. 1ml of each sample was transferred to a cuvette and assayed at 540 nm.

Table 3. Bovine Hb standard diluted from a concentration of 572 mg/l to 95.3 mg/l to produce a standard curve.

Volume of Bovine Hb standard stock (ml)	Volume of distilled water (ml)	Total volume (ml)	Final concentration of standard (mg/l)
1	0	1	572.0
0.5	0.5	1	286.0
0.34	0.66	1	190.0
0.25	0.75	1	143.0
0.19	0.81	1	114.4
0.16	0.84	1	95.3

1.5.7 Measurement of protein release during porcine erythrocyte ghosting

The procedure is adopted from the Bio-Rad protein assay kit (Hertfordshire, England, UK). The Bradford reagent was prepared in a 500 ml Duran bottle (Fisher Scientific), by diluting 1 part concentrated dye reagent to 4 parts of distilled water. The reagent was filtered through Whatman No1 filter paper to remove additional particulates. Five dilutions of the Bio-Rad standard (stock: 1.41 mg/ml bovine serum albumin) were prepared according to the following table:

Table 4. Bovine serum albumin (BSA) standard diluted from a concentration of 1.41 mg/ml to 0.225 mg/ml to produce a standard curve.

Volume of Stock (ml)	Volume of diluent (ml)	Total Volume (ml)	Final concentration BSA standard (mg/ml)
1	0	1	1.41
0.5	0.5	1	0.705
0.33	0.67	1	0.465
0.25	0.75	1	0.352
0.20	0.80	1	0.282
0.16	0.84	1	0.225
0	1	1	0

100 µl of prepared standard was added to 5 ml of dye reagent and vortexed for 2 minutes. The diluted standards were left to react for 5 minutes and absorbance was assayed at 595 nm. 1 ml aliquots of the standard BSA was stored at -20°C.

1.5.7.1 Measuring protein release

The experimental supernatant samples collected from the ghosting protocol were estimated for protein content. 100 µl of the supernatants were added to 5 ml of the Bradford reagent in a falcon tube and vortexed for 2 minutes. The experimental supernatant samples were left to react for 5 minutes and the absorbance was assayed at 595 nm. (Steck, 1974).

1.5.8 Scanning electron microscopy of porcine erythrocytes and ghosts

This procedure was adopted from Mircevova (1974). 1 ml of the porcine erythrocyte suspension was added to a Falcon tube using a Pasteur pipette. 3 ml of a 3% (v/v) glutaraldehyde in 0.1M phosphate buffer (0.1 M phosphate buffer: 28 ml of 0.2M sodium phosphate monobasic added to 78 ml of 0.2M sodium phosphate dibasic, the buffer was diluted to a total volume of 200ml with Di- H_2O) (Morel *et al.*, 1971) was added (Kayden and Bessis, 1970). The solution was allowed to stand for 2 hours to allow for primary fixation, which occurred as a result of the glutaraldehyde floating on top of the porcine erythrocyte suspension as shown by Figure 15. The glutaraldehyde was then aspirated and discarded. The fixed erythrocyte suspension was washed three times with 0.1M phosphate buffer (pH 7.2)

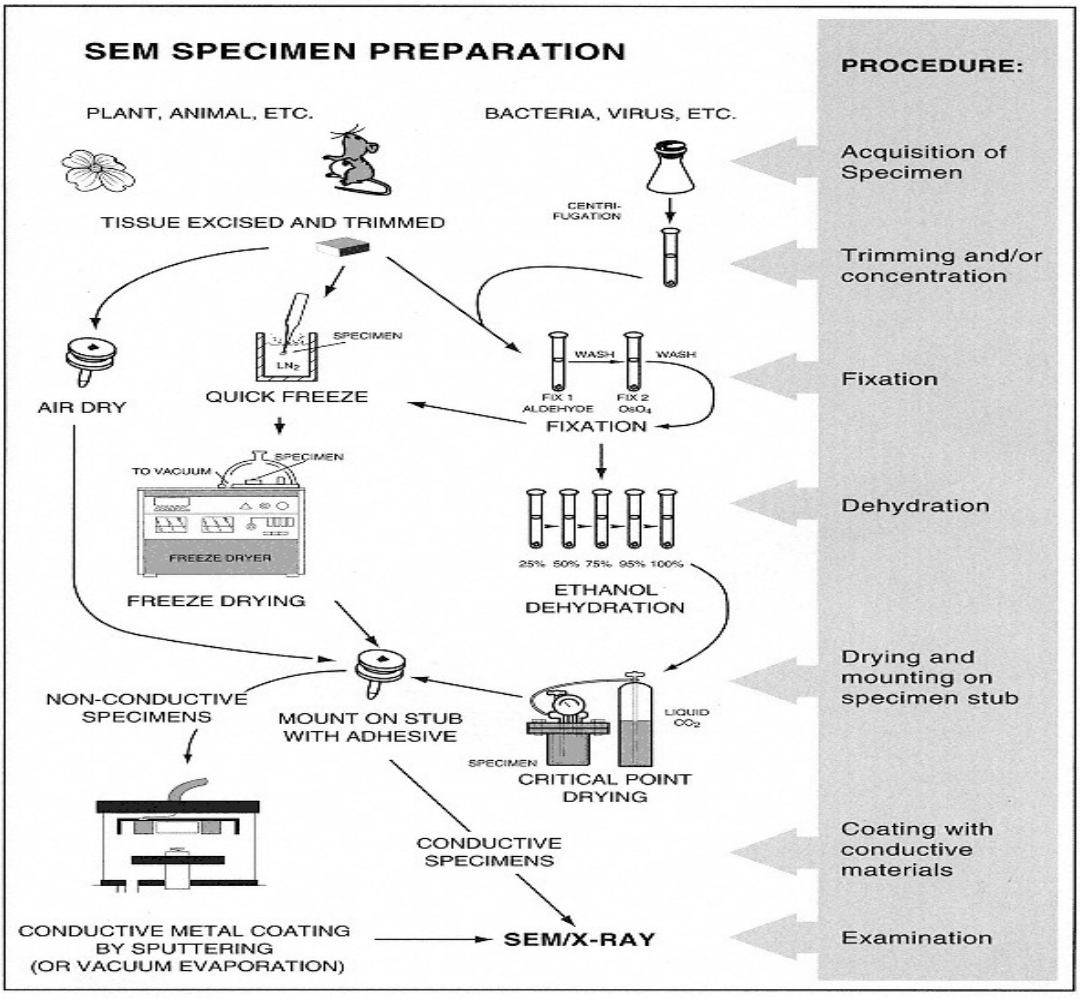

Figure 15. Diagrammatic representation of a Scanning electron microscopy specimen preparation method (Bozzola and Russell, 1999).

A 2% (w/v) aqueous osmium tetroxide was then added to the tube. The solution was allowed to stand for 2 hours to allow for secondary fixation, which occurred as a result of the osmium tetroxide floating on top of the fixed porcine erythrocyte suspension (Figure 15). The osmium tetroxide solution was aspirated and discarded in corn oil as it neutralises osmium tetroxide. The fixed pellet was then washed three times with 0.1M phosphate buffer. The erythrocyte pellet was dehydrated in a series of increasing ethanol concentrations (30%, 50%, 60%, 80%, 90%, 96% and 100% all v/v) as shown by Figure 15. Each concentration of ethanol was added using a Pasteur pipette. The pellet was dehydrated for 15 minutes in each ethanol concentration. The dehydrated pellet was kept in a desiccator containing silica gel (Fisher Scientific) overnight. The dried pellet was added to a carbon coated stub. The erythrocyte sample was viewed under a Quanta 200 scanning electron microscope (SEM – Oregon, USA) at different magnifications. The method is repeated to view porcine erythrocyte ghosts. Cell sizes were also determined using the SEM image J software (Java, California, USA).

1.5.9 Development of mammalian erythrocyte vesicles

Ovine and Leporine erythrocytes were chosen for this method, as they were found to be the most susceptible to streptolysin-O and α-haemolysin binding shown in sections 2.3.1 and 3.3.2. 3 ml of the prepared erythrocyte ghosts were added to a glass universal bottle and subjected to sonication for 20 minutes using a Ultrawave water bath sonicator (50-60 hertz) (Luk *et al.*, 2014). The sonicated erythrocyte ghosts were then serially extruded through an Avestin lipofast mini extruder (Figure 16). Prior to extrusion of the vesicles, water was passed through the extruder four times, as this allows membrane wetting, which allows the vesicles to pass through easier. 3 ml of the sonicated ghosts were extruded 13 times at 20°C, through a 400 nm and a 100 nm Avestin polycarbonate membrane, which allowed formation of erythrocyte vesicles of uniform size. A sudden decrease in resistance during extrusion shows rupturing of the membrane.

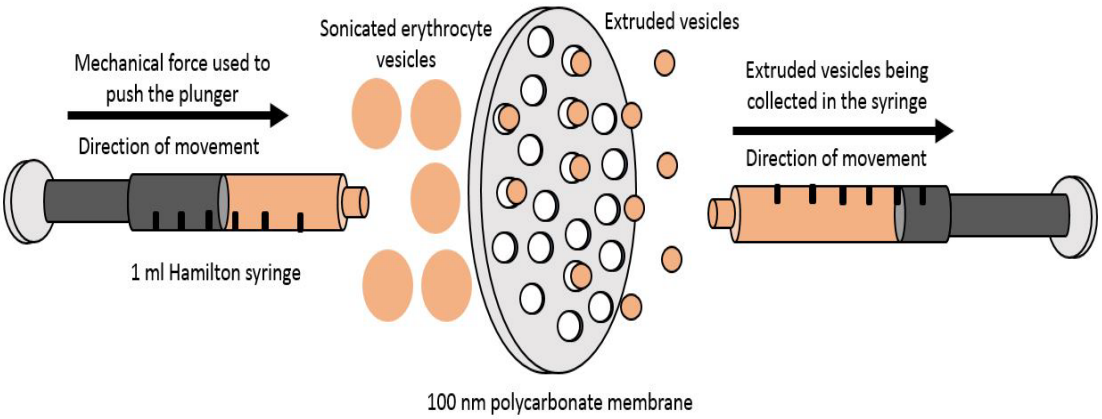

Figure 16- Mechanism of extrusion. A diagrammatic representation of sonicated vesicles being extruded through a 100 nm polycarbonate membrane. The vesicles are extruded using the mechanical force generated by the push of the syringe. This mechanical energy forces the vesicles through the 100 nm membrane synthesizing vesicles of uniform size (Chhabria and Beeton, 2016).

1.5.10 Preparation of PLGA nanoparticle core

This method was adopted from Hu *et al.* (2011) and optimized to achieve desired conditions. The PLGA cores were prepared using carboxy-terminated 50:50 PLGA polymer (Sigma-Aldrich UK). The polymer was subjected to a solvent displacement method. 15 mg of PLGA was weighed out using a thermo scientific weighing balance and dissolved in 15 ml of organic solvent acetone to make a concentration of 1mg/ml. The universal containing the PLGA polymer was sealed with parafilm and left overnight at room temperature (RTP) to dissolve. 1 ml of the PLGA polymer solution was added drop-wise to 3 ml of distilled water and stirred for 4 hours at 20°C. The prepared PLGA cores were then washed with 1x PBS in a Merck Millipore 15 ml falcon tube with a 10 kDa molecular weight cutoff, at 500 g for 20 minutes using a ALC PK120R bench top centrifuge. The PLGA cores were washed three times with isotonic PBS to filter out the organic solvent. The precipitated PLGA nanoparticles were then reconstituted in 1ml PBS.

1.5.11 Production of biomimetic nanosponges

This method was adopted from Luk *et al.* (2014) and optimized to achieve desired experimental conditions. The erythrocyte vesicles and the PLGA polymeric cores were added in equal volumes (1 ml: 1 ml) and extruded 13 times through a 100 nm polycarbonate membrane at 20°C. The mechanical force of extrusion allowed fusion of the erythrocyte vesicles with the PLGA nanoparticle, synthesizing a nanoparticle with a lipid coating and a PLGA polymeric core.

1.5.12 Characterisation of nanoparticles

The PLGA polymer and erythrocyte vesicles were characterized using Malvern Nano-zs zetasizer (Malvern, Worcestershire, England). 1 ml of the synthesized PLGA polymeric suspension was added to a polystyrene cuvette. This cuvette was inserted into the zetasizer and assayed for nanoparticle size and zeta potential. The nanosponges and erythrocyte vesicles were characterized using the same protocol (Weber *et al.*, 2000). The zetasizer was calibrated every 6 months for size and polydispersity by Malvern.

1.5.13 Storage of nanosponges

The synthesized nanosponges were stored at - 80°C for 2-3 days. For long-term storage, 1mg/ml nanosponges were lyophilized with 5% (w/v) sucrose. The nanosponges were separated into 200 µl aliquots, to which 200 µl 5% (w/v) sucrose was added. The aliquots were sealed with parafilm and frozen overnight at -80°C. The frozen aliquots were placed in a Scanval cool safe lyophilizer overnight. The lyophilized suspension took on a powdered solid form, which was stored at 4°C.

1.6 Results

1.6.1 Haematological parameters of mammalian blood

The collected animal blood (ovine, porcine, leporine and murine) were analysed for their haematological parameters using a Pentra 60c+ haemoanalyser. Specific parameters were assessed, such as red blood cell (RBC) count, Hb, and haematocrit, mean corpuscular volume (MCV) and mean corpuscular haemoglobin (MCH).

Table 5. Haematological parameters of porcine whole blood stored at 4°C for 1 day. The symbol "±" represents standard error of mean (experimental replicates =3 (n)).

Parameters	Value	Porcine Reference Range	Human Reference range
RBC count (x10^6/µl)	6.1 (±0.03)	5-8	4.1-4.5
Haemoglobin (g/dl)	12.5 (±0.06)	10-16	11.4-12.4
Haematocrit (%)	37.6 (±0.21)	32-50	42-54
Mean corpuscular volume (µm^3)	62.0	50-68	82.9-95
Mean corpuscular haemoglobin (pg)	20.5 (±0.12)	17-21	27.4-32

Haematological parameters of porcine blood (Table 5) as measured with a Pentra 60c+ haemoanalyser. The results are within the expected reference ranges (Weiss *et al.*, 2010). Human reference values are added to the table as a comparative measure to porcine blood (Hagag *et al.*, 2015).

Table 6. Haematological parameters of ovine whole blood stored at 4°C for 1 day. The symbol "±" represents standard error of mean (n=3)

Parameters	Value	Reference Range	Human Reference range
RBC count ($x10^6/\mu l$)	7.57 (±0.045)	9-15	4.1-4.5
Haemoglobin (g/dl)	10.47(±0.054)	9-15	11.4-12.4
Haematocrit (%)	24.0(±0.141)	27-45	42-54
Mean corpuscular volume (μm^3)	32.0	28-40	82.9-95
Mean corpuscular haemoglobin (pg)	13.80(±0.170)	8-12	27.4-32

60 µl of the blood was analysed to obtain the relevant haematological parameters (Table 6). The results are within the expected reference ranges (Weiss *et al.*, 2010). Human reference values are added to the table as a comparative measure to Ovine blood (Hagag *et al.*, 2015).

Table 7. Haematological parameters of murine whole blood stored at 4°C for 1 day. The symbol "±" represents standard error of mean (n=3).

Parameters	Value	Reference Range	Human Reference range
RBC count ($x10^6$/µl)	7.35 (±0.19)	5-8	4.1-4.5
Haemoglobin (g/dl)	11	10-16	11.4-12.4
Haematocrit (%)	30 (±1.15)	32-50	42-54
Mean corpuscular volume (μm^3)	56	50-68	82.9-95
Mean corpuscular haemoglobin (pg)	20.3 (±0.25)	17-21	27.4-32

The murine blood was obtained from the animal laboratory at the University of Central Lancashire. 60 µl of the blood was analysed to obtain the relevant haematological parameters (Table 7). The results are within the expected reference ranges (Weiss *et al.*, 2010). Human reference values are added to the table as a comparative measure to Ovine blood (Hagag *et al.*, 2015).

Table 8. Haematological parameters of leporine whole blood stored at 4°C for 1 day. The symbol "±" represents standard error of mean (n=3).

Parameters	Value	Reference Range	Human Reference range
RBC count (x10^6/µl)	7.1 (±0.06)	5.1-7.9	4.1-4.5
Haemoglobin (g/dl)	11.9 (±0.38)	9.8-17.4	11.4-12.4
Haematocrit (%)	44.0 (±1.53)	37-50	42-54
Mean corpuscular volume (µm^3)	61.7 (±0.67)	57.8-65.4	82.9-95
Mean corpuscular haemoglobin (pg)	22.1 (±0.87)	17.1-23.5	27.4-32

The leporine blood was purchased form TCS biosciences (Table 8). 60 µl of the blood was analysed to obtain the relevant haematological parameters. The results are within the expected reference ranges (Weiss *et al.*, 2010). Human reference values are added to the table as a comparative measure to Ovine blood (Hagag *et al.*, 2015).

1.6.2 Morphology of porcine erythrocytes and ghosts using light microscopy

Porcine erythrocyte ghosts were produced using a series of washes. To produce erythrocyte ghosts, 1 ml of the porcine erythrocyte suspension was lysed using a hypotonic buffer. The lysed erythrocytes were centrifuged, which pelleted the erythrocyte ghosts. The erythrocyte ghost pellet was reconstituted in 4 ml 166 mM PBS. This produces a suspension containing intact porcine erythrocyte ghosts. Figure 17 is a light micrograph at 400X magnification. Intact porcine erythrocytes can be seen with the edges showing crenation.

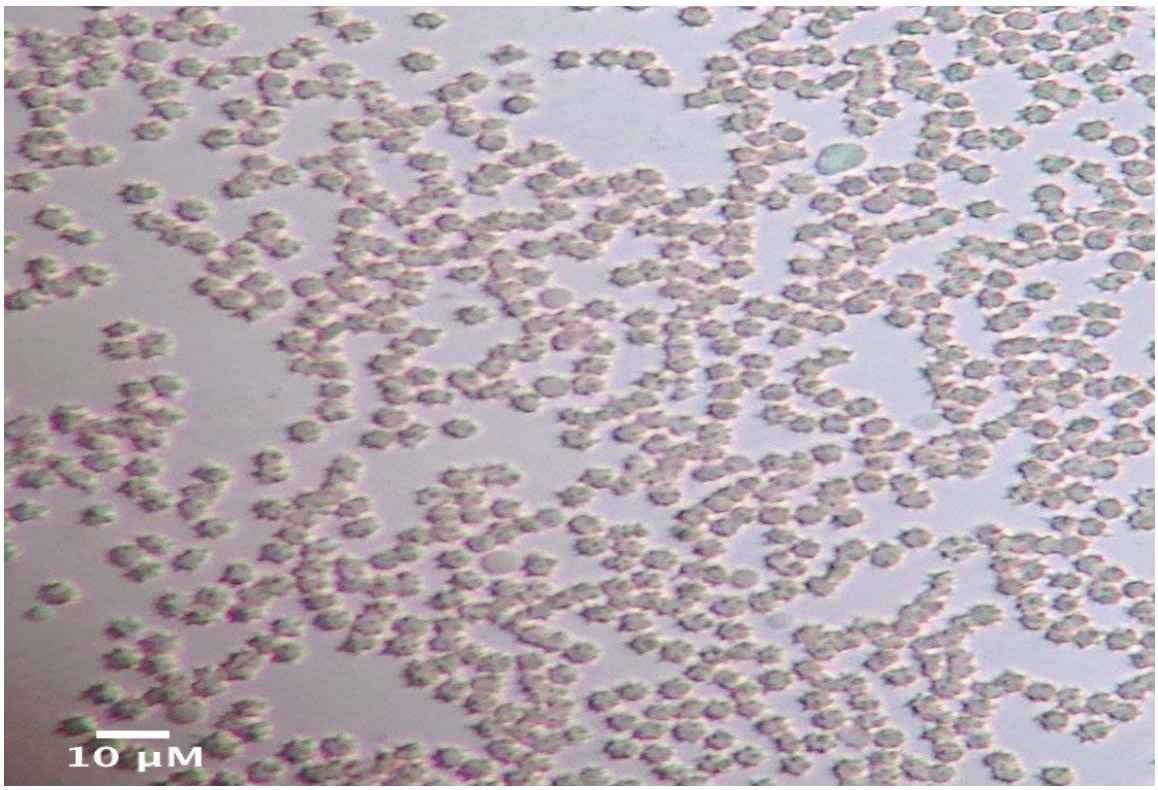

Figure 17. A light micrograph of intact porcine erythrocytes under 400X magnification, washed in 166 mM NaCl (bar represents 10 µm). The cells appear to be crenated, due to exposure to air or could be artefacts as a result of sample drying. The erythrocytes are a day old and were stored at 4°C. An anticoagulant CPD (w/v) was added to blood to prevent coagulation.

Anisocytosis (erythrocytes of unequal size) is seen among the erythrocytes, when they are measured using the image j software. Porcine erythrocytes were diluted in 166 mM NaCl (Figure 18), and therefore appear as a lower count in the field of view. After dilution, the cells have now reverted back to an intact spherical shape, without presence of crenated structures. The diluted image also shows signs of anisocytosis.

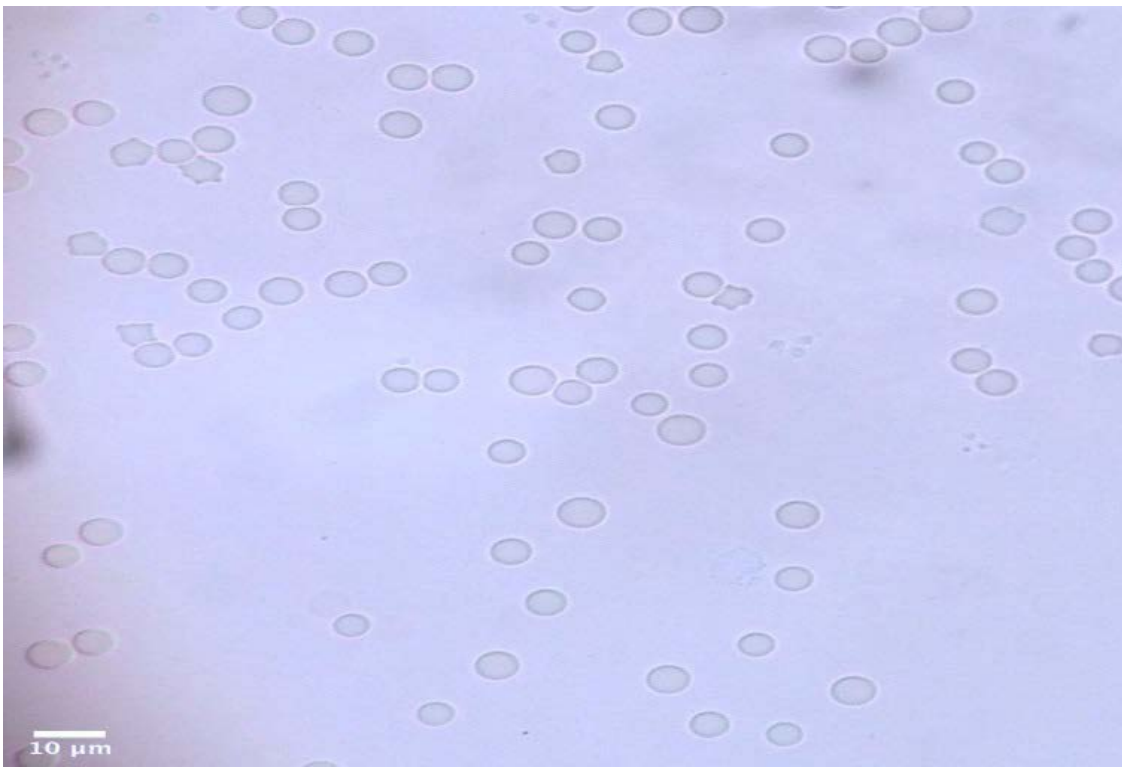

Figure 18. A light micrograph of porcine RBCs under 400X magnification (bar represents 10 µm), washed and diluted in 166 mM NaCl. The RBCs are a day old and were stored at 4°C. An anticoagulant CPD (w/v) was added to blood to prevent coagulation.

Figure 17 and Figure 18 were compared against porcine erythrocyte ghosts. The ghosts have white centres (Figure 20) and appear to be devoid of intracellular contents. The white centres could signify the release of Hb from the cytoplasm. Moreover, the ghosts appear to be smaller compared to porcine erythrocytes (Figure 19).

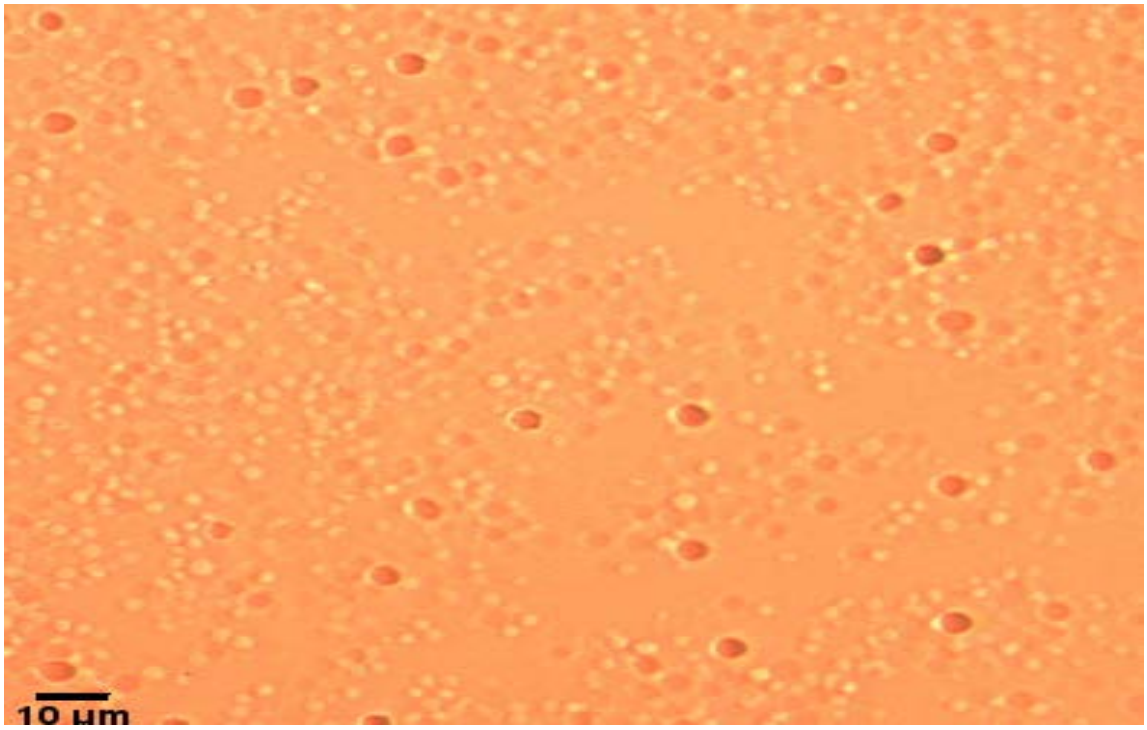

Figure 19. A light micrograph of porcine erythrocyte ghosts under 400X magnification (bar represents 10 µm) using image enhancement. The small white centres indicate ghosts, are mixed with porcine erythrocytes (large dense orange centres) and an intermediate sub-population of cells. Average diameter of the sub-population is 2.8 µm (± 0.7). The ghosts were prepared from a day old suspension of erythrocytes. The cells in the image were stored on ice.

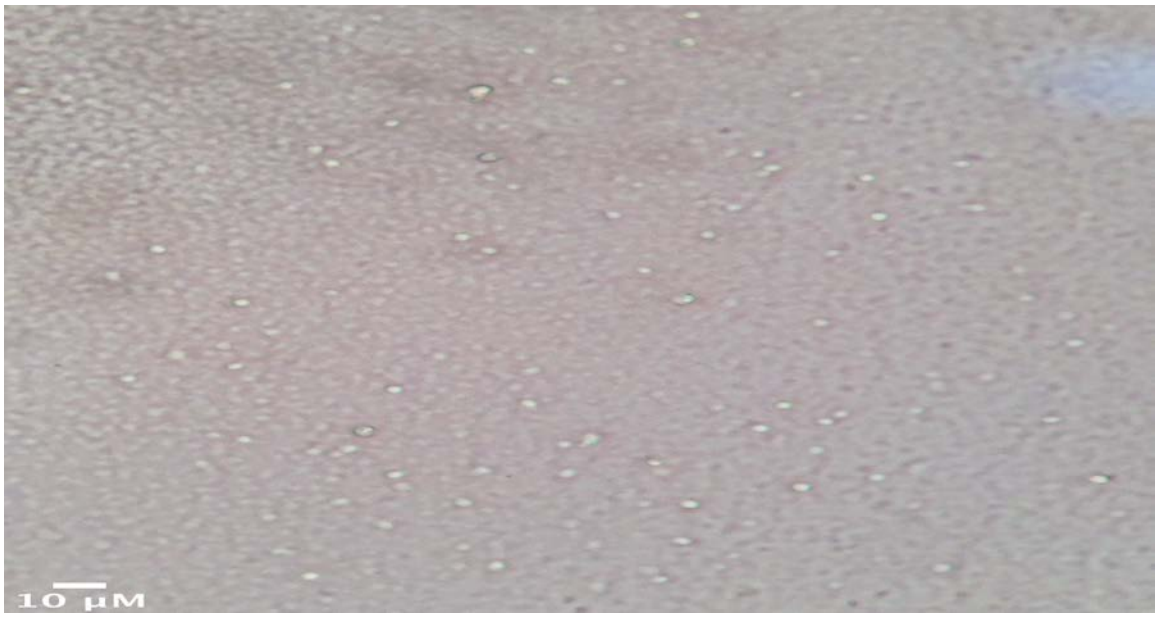

Figure 20. A light micrograph of porcine erythrocyte ghosts under 400X magnification (bar represents 10 µm), indicated by their white centres which signifies Hb release from the cytoplasm of erythrocytes. The ghosts were prepared from a day old suspension of erythrocytes. The ghosts in the image were stored on ice.

1.6.3 Morphology of porcine erythrocyte ghosts using scanning electron microscopy.

The morphology of porcine erythrocyte ghosts showed significant differences from porcine erythrocytes. The porcine erythrocytes (Figure 21 and Figure 22) and ghosts were fixed by addition of 3% glutaraldehyde and 2% osmium tetroxide. The erythrocyte ghosts were then dehydrated using increasing concentrations of ethanol. The sample was placed onto a carbon-coated stub and visualised at different magnifications to obtain the best resolution.

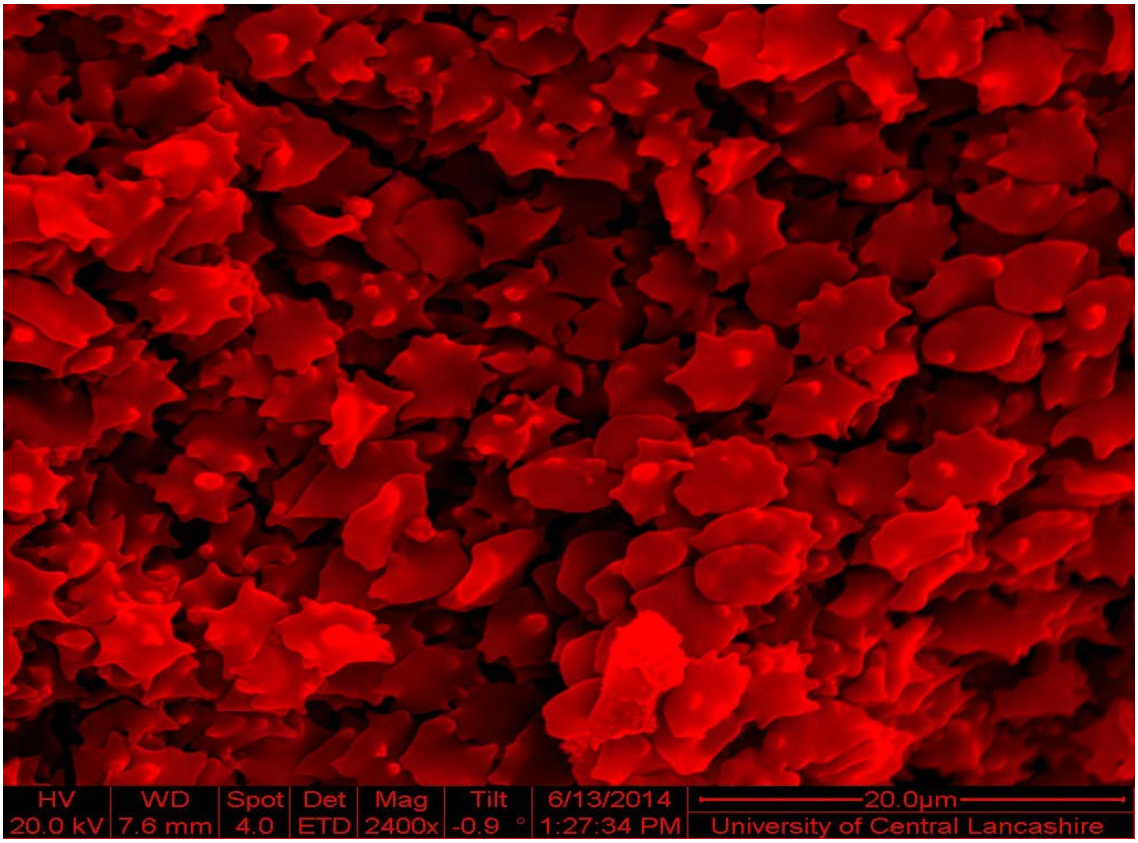

Figure 21. Digitally enhanced scanning electron micrograph of crenated porcine erythrocytes under 2400X magnification (bar represents 20 µm). Fixed in 3% glutaraldehyde (0.1M phosphate buffer) and 2% osmium tetroxide. Pseudocolour was added using image j software. The porcine erythrocytes in the image are a day old suspension stored at 4°C. An anticoagulant CPD (w/v) was added to the blood to prevent coagulation

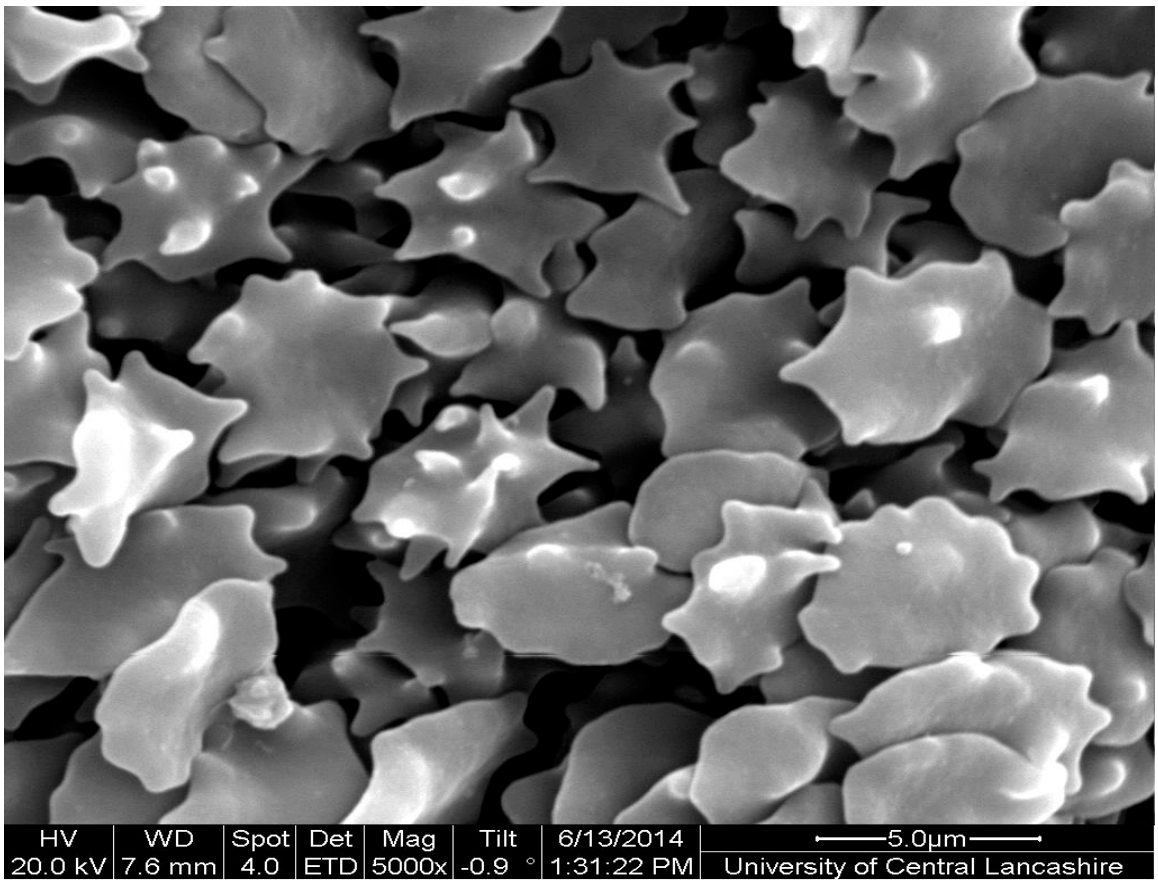

Figure 22. Scanning electron micrograph of crenated porcine erythrocytes under 5000X magnification (bar represents 5 µm). Fixed in 3% glutaraldehyde (0.1M phosphate buffer) and 2% osmium tetroxide. The porcine erythrocytes in the image are a day old suspension stored at 4°C. An anticoagulant CPD was added to the blood to prevent coagulation.

It is evident from Figure 21 that the crenations are typical structures found on these cells, though there is a variation in the number and size of the crenations. Since there are many erythrocytes in the field of view, it can be said that the sample used is a concentrated erythrocyte suspension. Figure 23 is a scanning electron micrograph of diluted porcine erythrocytes, which shows that the erythrocytes have taken on a spherical shape. Under SEM it can be seen that many are still crenated even after dilution. The crenations protrude in random directions and are different in size and number on each cell. Aggregation of cells is also present.

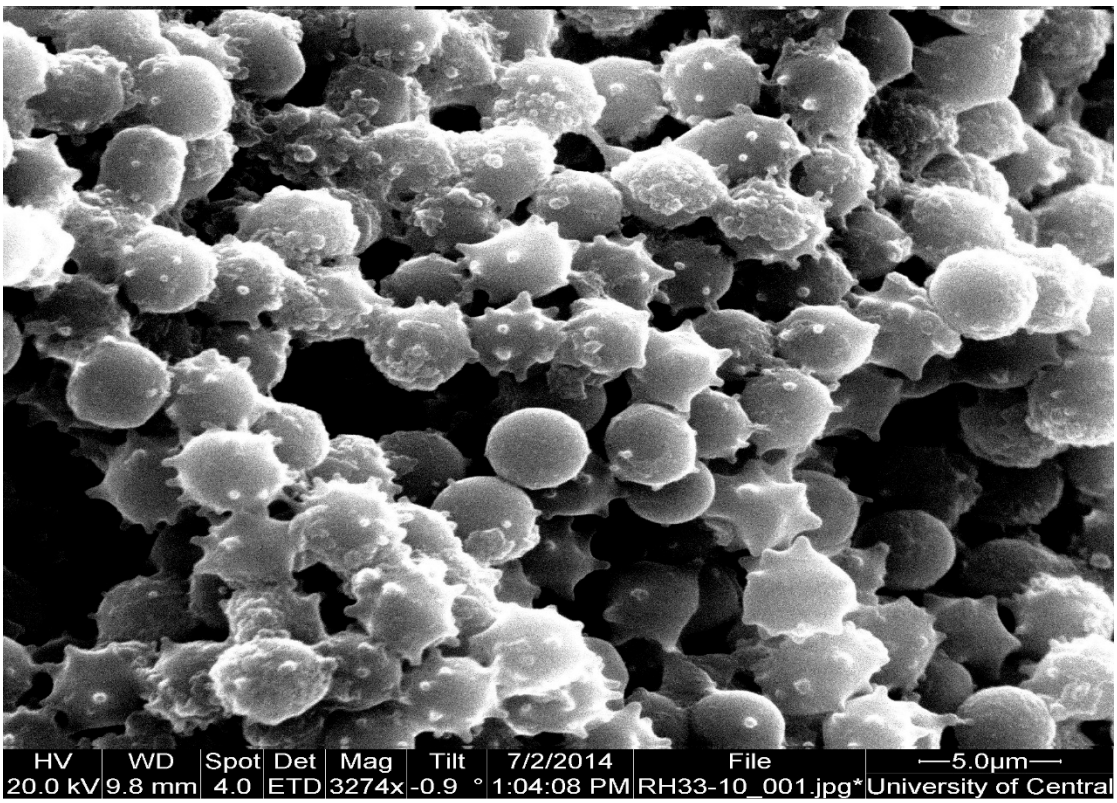

Figure 23. Scanning electron micrograph of porcine erythrocytes under 3274X magnification (bar represents 5 µm) fixed in 3% glutaraldehyde and diluted in 0.1M phosphate buffer. The porcine erythrocytes in the image are a day old suspension stored at 4°C. An anticoagulant CPD was added to the blood to prevent coagulation.

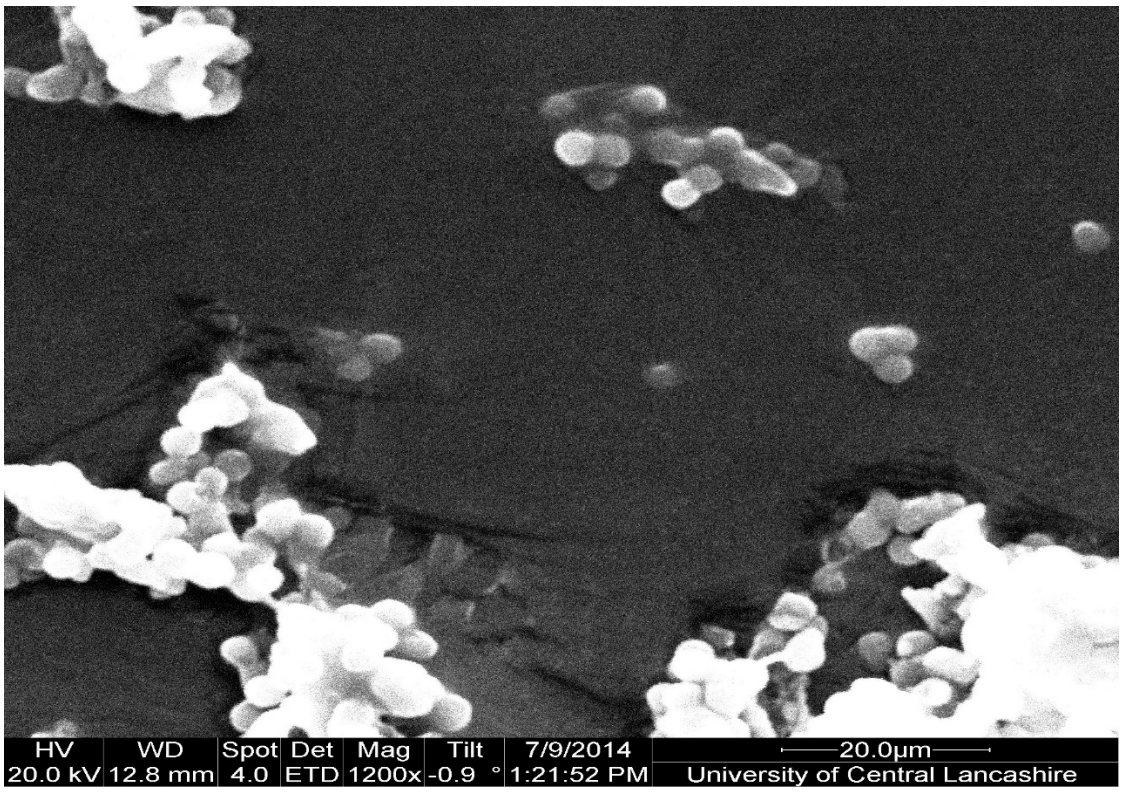

Figure 24. Scanning electron micrograph of porcine erythrocyte ghosts under 1200x magnification (bar represents 20 µm) fixed in 3% glutaraldehyde. The ghosts were prepared from a day old suspension of erythrocytes. The ghosts in the image were stored on ice.

Figure 24 and Figure 25 show porcine erythrocyte ghosts prepared using a drop preparation technique. This technique involves leaving a drop of the ghost suspension on the sample mount to dry overnight rather than using a desiccator. Additionally, this technique did not involve the need for a secondary fixation with osmium tetroxide. The ghosts have taken on a non-crenated form. Ghosts in the centre have taken on a phase dark appearance. The ghosts that are close to the borders of the image have taken on a phase white appearance. Individual ghost cells appear to be limited in number in the field of view due to presence of aggregated ghost cells. Figure 26 shows a greater magnified micrograph of porcine erythrocyte ghosts. The erythrocyte ghosts in the image appear to have taken on a spherical shape although some are smaller than the others. This could be due to the loss of Hb from the cytoplasm of porcine erythrocytes. Similar to Figure 24 and Figure 25 some also appear aggregated; this could be due to the drying protocol during fixation of the ghosts.

Figure 25. Scanning electron micrograph of porcine erythrocyte ghosts fixed under 1200X magnification (bar represents 20 µm), fixed in 3% glutaraldehyde. The ghosts were prepared from a day old suspension of erythrocytes. The ghosts in the image were stored on ice.

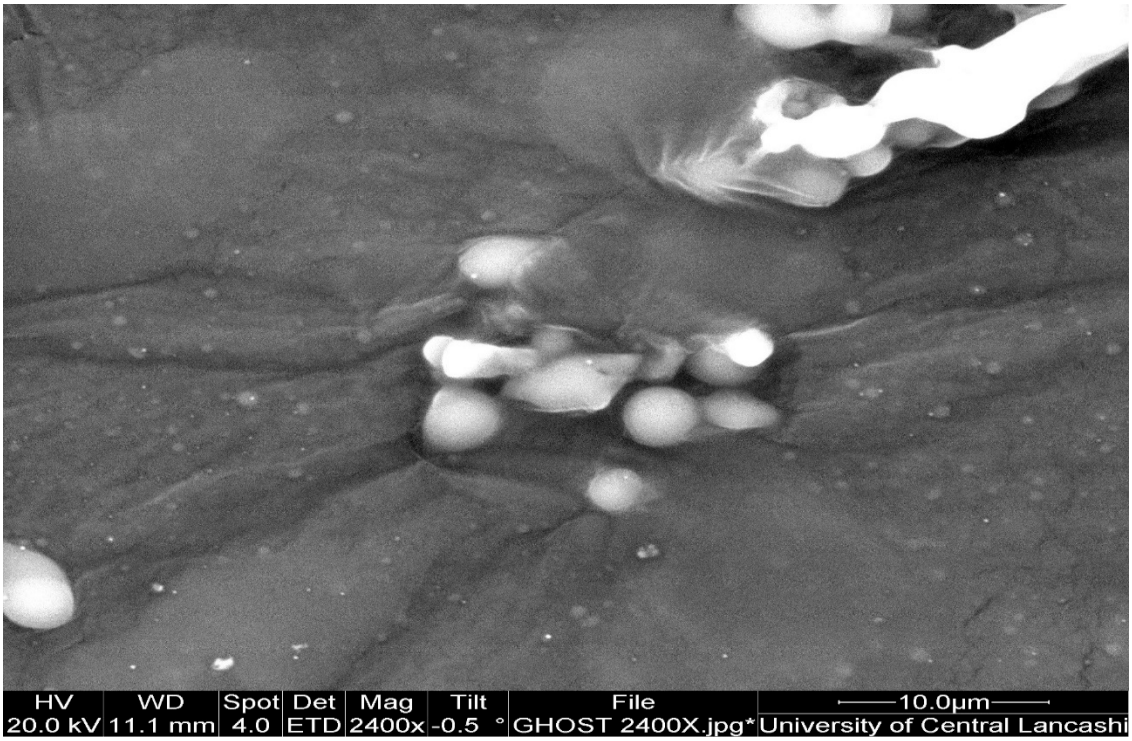

Figure 26. Scanning electron micrograph of porcine erythrocyte ghosts prepared using a drop preparation protocol, viewed under 2400X magnification (bar represents 20 µm). The ghosts were prepared from a day old suspension of erythrocytes. The ghosts in the image were stored on ice.

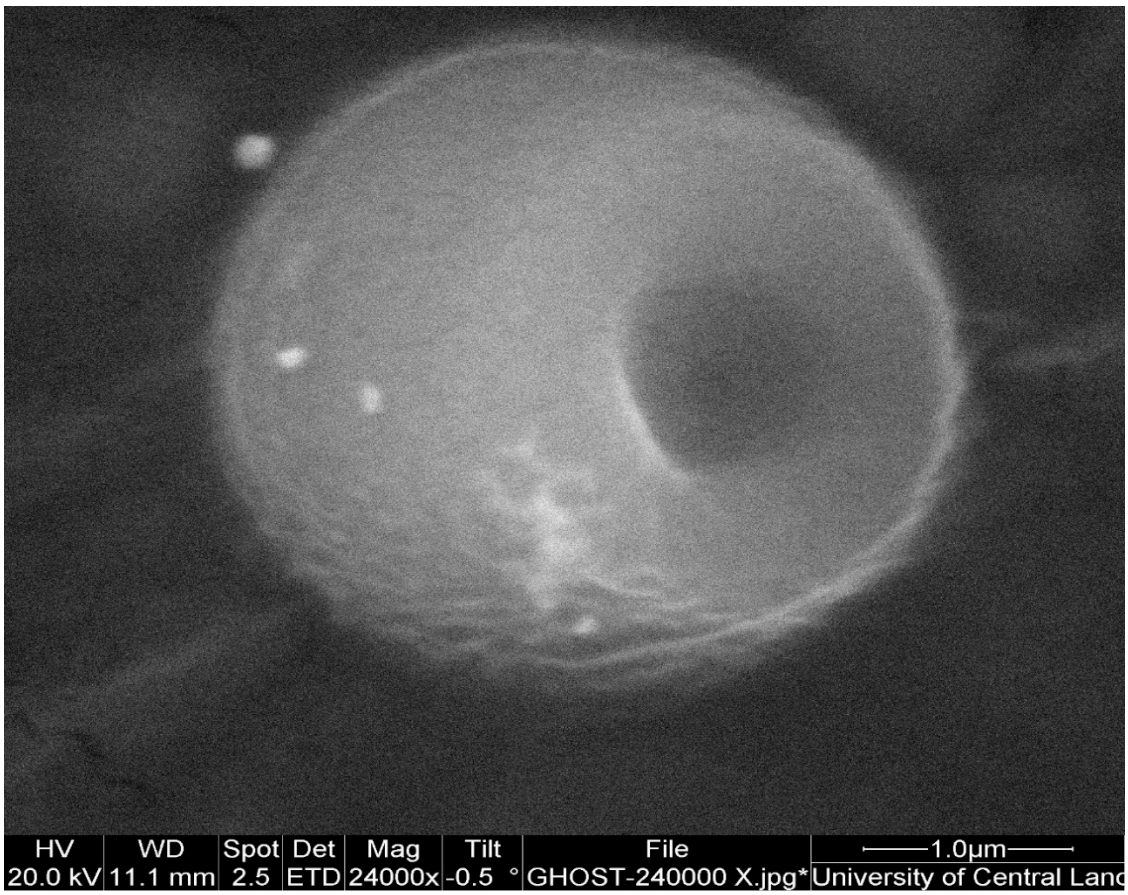

Figure 27. Scanning electron micrograph of a porcine erythrocyte ghost prepared using a drop preparation protocol, viewed under 24000X magnification (bar represents 1 µm). The ghost was prepared from a day old suspension of erythrocytes. The ghosts in the image were stored on ice.

To clearly distinguish morphological features of ghosts from erythrocytes a greater magnification was required. Figure 27 shows a micrograph with the highest magnified image of a porcine erythrocyte ghost. The image shows a spherical structure similar to the previous images. However, presence of an indent in the centre of the ghost may signify the release of Hb, which may have caused the ghost to shrink and take the form of structure with an indent in the centre. This shape could also be formed due to the process of drying

1.6.4 Measuring the diameter of porcine erythrocytes and erythrocyte ghosts

Light micrographs of porcine erythrocytes and ghosts shown in Figure 17 and Figure 20 were measured for their diameter using image j software. Figure 28 shows a significant difference between the sizes of these two types of cells. The porcine erythrocytes have a diameter of 4.11 µm (± 0.14). The ghosts have a smaller diameter of 2.3 µm (± 0.11).

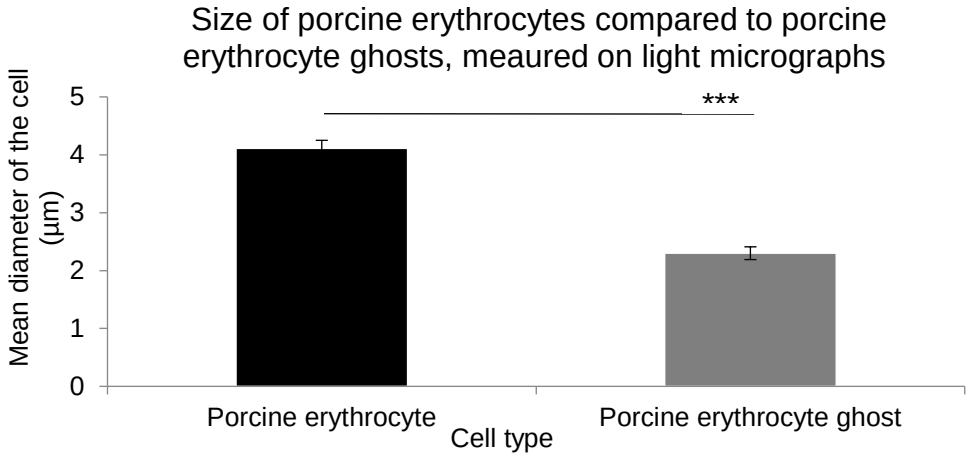

Figure 28. Size of porcine erythrocytes (control) compared to porcine erythrocyte ghost. The cells from the light micrographs (Figure 17 and Figure 20) were measured using an imaging software known as image j. "*"P≤0.05, "**"P≤0.01 and "***"P≤0.00. Error bars represent standard error of the mean (n=30).

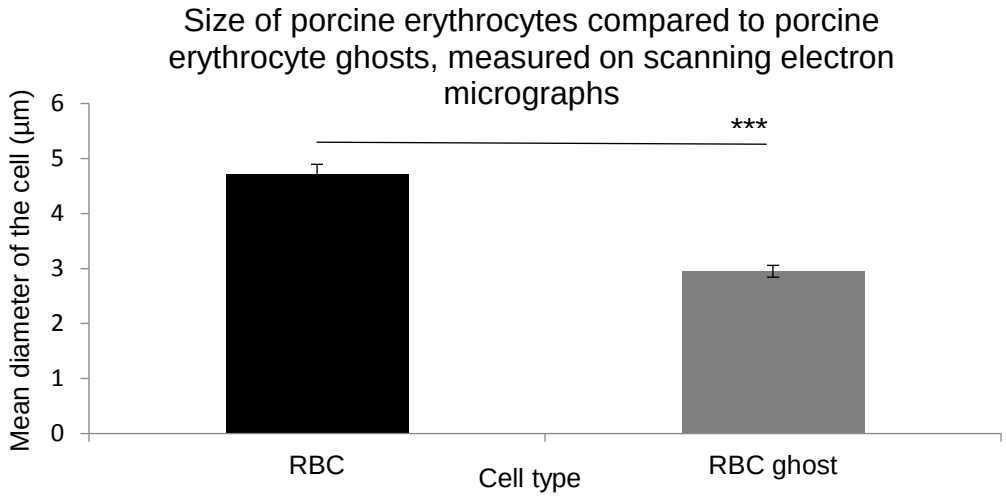

Figure 29. Size of porcine erythrocytes compared to porcine erythrocyte ghosts. The cells from the scanning electron micrographs (Figure 21 and Figure 24) were measured using image j. "*"P≤0.05, "**"P≤0.01 and "***"P≤0.001.Error bars represent standard error of the mean (n=30).

The mean cell diameter in Figure 29 was measured by a computer software known as image j. The porcine erythrocytes have a diameter of 4.71 µm (± 0.18) and the erythrocyte ghosts have a diameter of 2.95 µm (± 0.10). In both figures the erythrocyte ghosts have a smaller diameter compared to the porcine erythrocytes.

1.6.5 Haemoglobin release during synthesis of porcine erythrocyte ghosts

To synthesize erythrocyte ghosts, nine different treatments (cell washes) involved in the procedure. These treatments included a range of different isotonic solutions (the osmotic pressure in the extracellular medium is the same as the intracellular osmotic pressure) and a hypotonic solution (The osmotic pressure in the extracellular medium is greater than the intracellular osmotic pressure). After each treatment, the cells were centrifuged at 500 x g and the supernatant was aspirated with a Pasteur pipette and stored at 4°C, which was later used to measure its Hb concentration. The nine treatments were titled according to the buffer used to wash the cells. The treatments are buffy coat and plasma (BCP), NaCl, NaCl 2, NaCl 3, Lysis, Tris-NaCl 1, Tris-NaCl 2, KCl and distilled water (DH_2O).

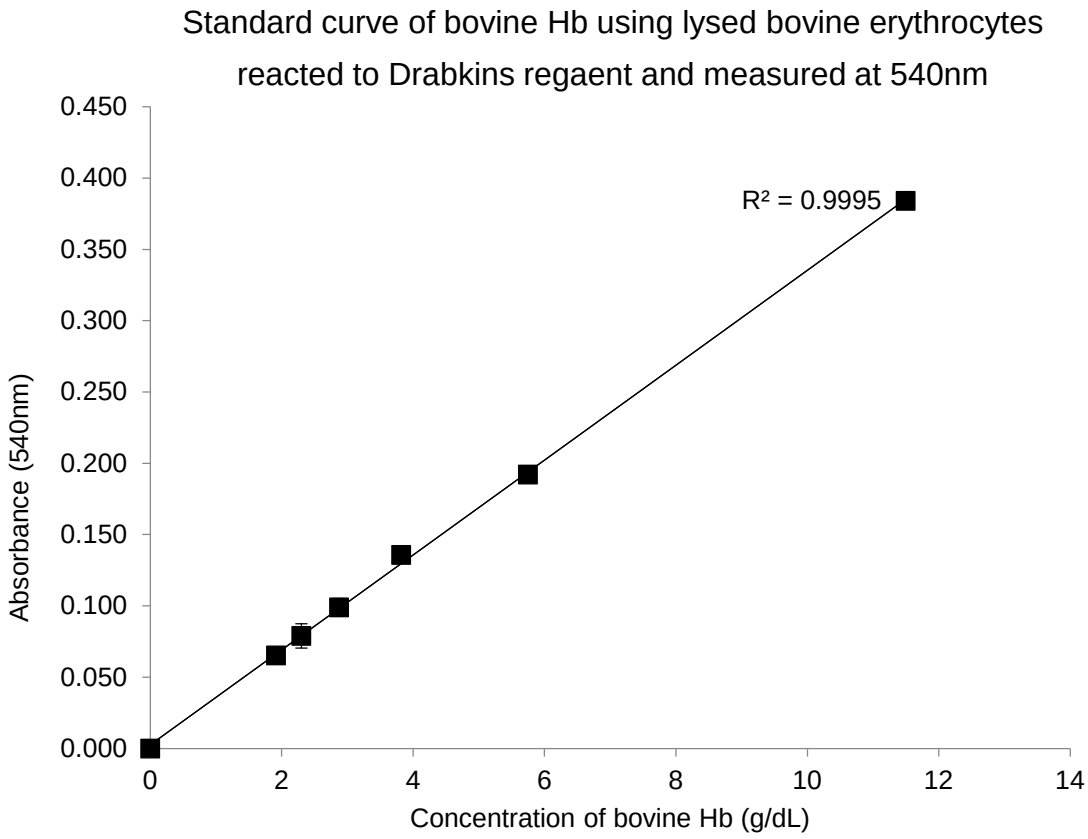

Figure 30. Standard curve of bovine Hb diluted with Drabkins reagent and read at 540 nm for absorbance. The standards were kept on ice prior to measurement. Error bars represent standard error of the mean (n=3).

Hb concentration after the nine treatments was measured using the haemoglobincyanide method. The absorbance after the nine treatments correspond to Hb concentrations on the standard curve. The standard curve in Figure 30 was measured by diluting the bovine Hb standard (572 mg/l) to the concentrations provided in

Table *3* and read for its absorbance at 540 nm. The bovine Hb standard was diluted with Drabkins reagent, therefore the standard did not require the addition of external Drabkins reagent. The R^2 value is known, as the coefficient of determination is a statistical number that shows how well the data fits the regression line. The standard curve has an R^2 value of 0.9995, which means that 99.95% of the data fits the regression line, showing a strong positive relationship.

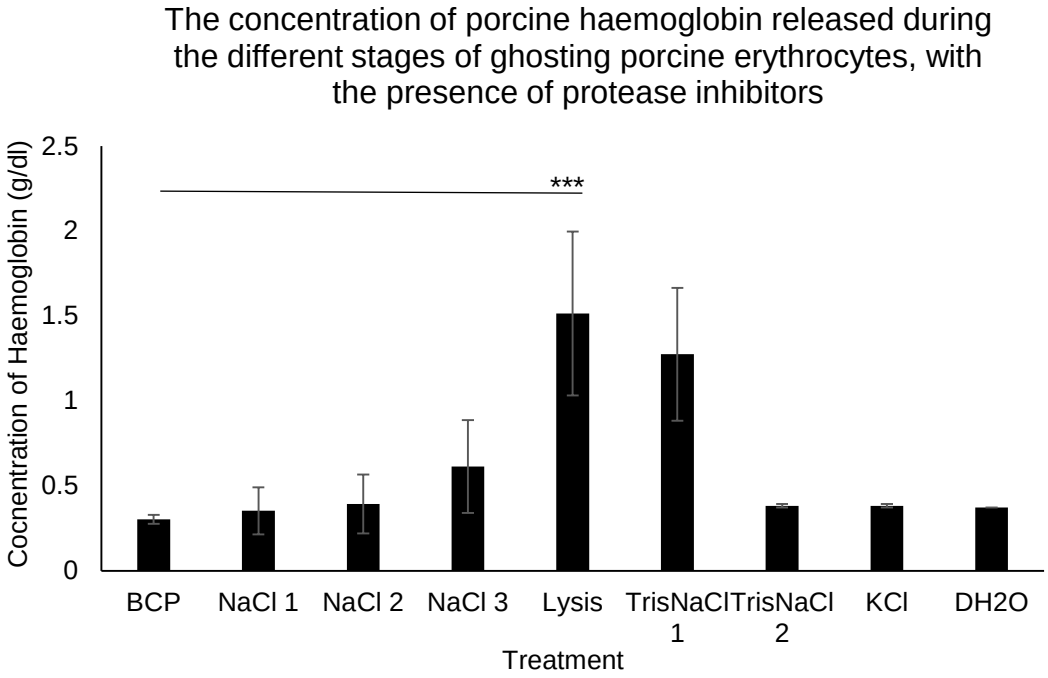

Figure 31. Concentration of Hb after each treatment, during porcine erythrocyte ghosting, with the presence of a protease inhibitor. Hb was allowed to react with Drabkins reagent and measured for absorbance at 540nm. The supernatant collected after the nine treatments were stored at 4°C prior to Hb estimation. Maximum Hb released from a 2% (v/v) porcine erythrocyte suspension was 2.5 g/dl "*"P≤0.05, "**"P≤0.01 and "***"P≤0.001. Error bars represent standard error of the mean (n=3).

Porcine erythrocyte ghosts were synthesised after a hypotonic (lysis) buffer was added to the porcine erythrocytes. The production of erythrocyte ghosts was followed by the loss of Hb from the cytoplasm of the erythrocytes. Figure 31 shows the concentration of porcine Hb released after each treatment. Hb release was tested with the presence of a protease inhibitor (PI), as Hb could be susceptible to degradation by plasma proteases. The primary treatment was BCP, which is a separation step. This involved centrifuging the whole blood. The whole blood was separated into the RBC suspension, the buffy coat (white blood cells and platelets) and plasma. The buffy coat and plasma made up the supernatant. This centrifugation step showed 0.303 g/dl (± 0.02) Hb released from porcine erythrocytes.

The supernatant on top of the erythrocyte suspension was discarded after the centrifugation step. The erythrocyte suspension was followed by three washes with 166 mM NaCl. This allowed release of unbound Hb present around the

porcine erythrocytes. There were no significant differences recorded between these treatments. The washed erythrocyte suspension was then subjected to haemolysis using a hypotonic buffer (refer to section 1.5.3). According to Figure 31, the lysis treatment had released maximum Hb at 1.51 g/dl (± 0.48). This step synthesised the porcine erythrocyte ghosts. The concentration of Hb released decreases after the lysis treatment, as the treatment is followed by isotonic washes, which allowed removal of residual Hb.

1.6.6 Protein release during porcine erythrocyte ghosting

Membrane proteins are essential in maintaining cell structure and integrity. The concentration of protein released during porcine erythrocyte ghosting was recorded. Since the production of erythrocyte ghosts involved the use of 9 different treatments, the concentration of protein released was measured after each treatment.

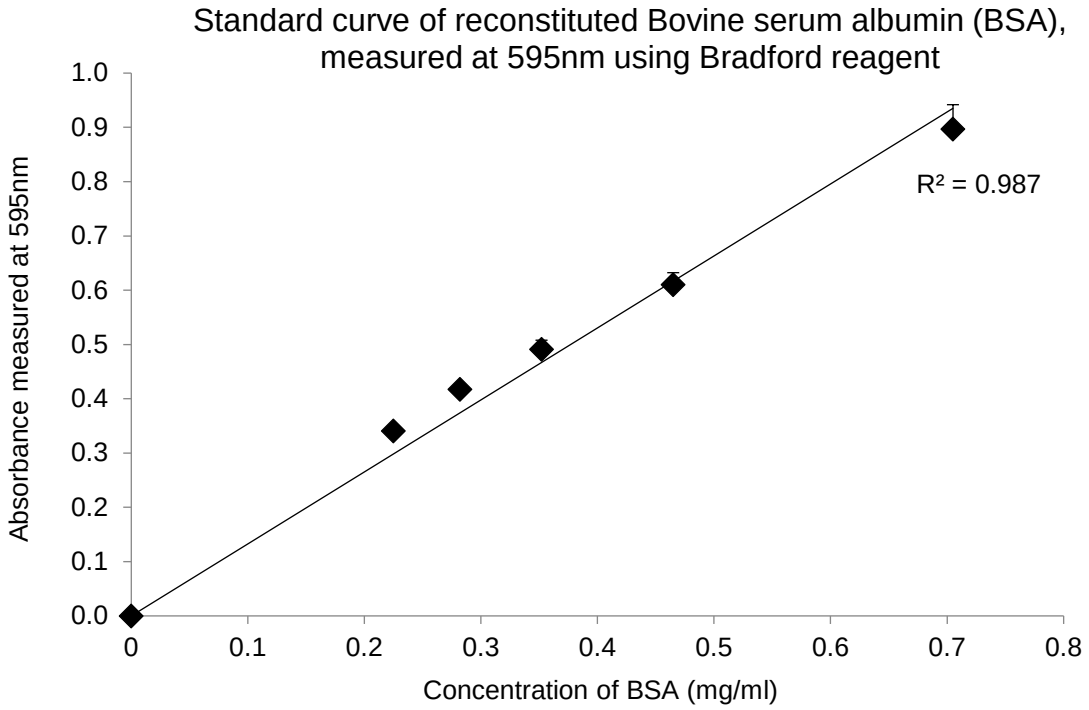

Figure 32. Standard curve of reconstituted BSA, measured at 595 nm using the Bradford reagent. The standards were kept on ice prior to measurement. Error bars represent standard error of the mean (n=3).

Figure 32 is a standard curve using reconstituted BSA. The BSA was diluted in PBS to the concentrations shown in Table 4 and was allowed to react with Bradford reagent. This solution was read for its absorbance at 595 nm. The measured absorbance after the nine treatments correspond to protein concentrations on the standard curve. The standard curve has an R^2 value of 0.986, which shows that 98.6% of the data fits the regression line.

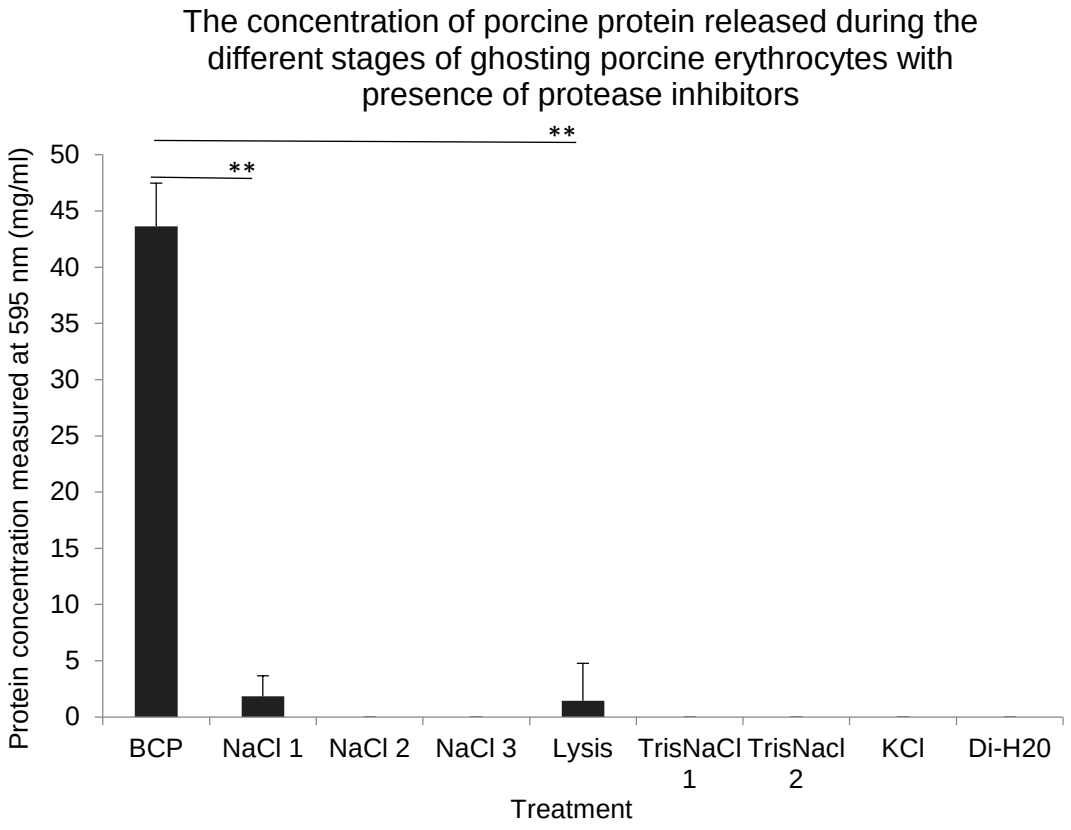

Figure 33. Concentration of protein released after each treatment, during porcine erythrocyte ghosting. The supernatant collected after nine treatments were stored at 4°C prior to protein estimation. These supernatants were allowed to react with Bradford reagent and measured for absorbance at 595 nm. Protein concentrations measured, fit into the standard curve and multiplied with appropriate dilution factors to obtain the above values."*"P≤0.05, "**"P≤0.01 and "***"P≤0.001. Error bars represent standard error of the mean (n=3).

Figure 33 shows the amount of protein released during each wash of porcine erythrocyte ghosting. Protein is mainly released in three treatments: BCP, NaCl1

and lysis. The BCP treatment contains the buffy coat (buffy coat: white blood cells) and plasma (plasma: plasma proteins and platelets) as the supernatant. The BCP treatment has the highest amount of protein present at 43.62 mg/ml (±3.82). This concentration of protein released may suggest that the proteins in this treatment could be plasma proteins (Weiss *et al.*, 2010) and unbound Hb. The second treatment NaCl 1 also has 1.83 mg/ml (±1.82) of protein present. NaCl 1 is an isotonic solution, which maintains a balance of osmotic pressure between the intracellular and extracellular compartments. Due to the balance of osmotic pressure, the proteins in NaCl1 may also be plasma proteins and not RBC membrane proteins. The NaCl 2 and NaCl 3 have no presence of protein, which signifies that all the plasma proteins have been removed after NaCl 1 treatment. The lysis treatment is a hypotonic solution; its role is to lyse the porcine RBCs. This treatment has a small amount of protein release at 1.43 mg/ml. This treatment is significant, as at this stage ghosts are produced. Therefore, there is a small amount of membrane proteins released. Not all RBCs become ghosts at this stage. Comparatively this assay may overlap with the Hb estimation assay as the values obtained by this assay could be a combination of plasma proteins, membrane proteins and Hb. For this assay a 0.70 mg/ml BSA control was used. This had an absorbance of 0.90. Moreover highest protein release was shown to be by the BCP treatment, as explained above.

1.6.7 Size of erythrocyte vesicles

Erythrocyte vesicles were synthesised using ovine erythrocyte ghosts, as described in chapter 1 section 1.5.9. Ovine blood is the more susceptible to lysis by streptolysin-O compared to the other mammalian species. Synthesizing biomimetic nanosponges utilizes a top down approach. Ovine erythrocytes were used to synthesise nanosponges using this approach. The ovine erythrocytes were lysed to produce re-sealed erythrocyte ghosts using the same method provided for porcine erythrocyte ghosts. This allowed isolation of the ovine erythrocyte membranes. The ovine erythrocyte ghosts were subjected to sonication at 20°C for varying amounts of time. This technique produced polydispersed suspensions of ovine erythrocyte vesicles of different sizes (Figure 34).

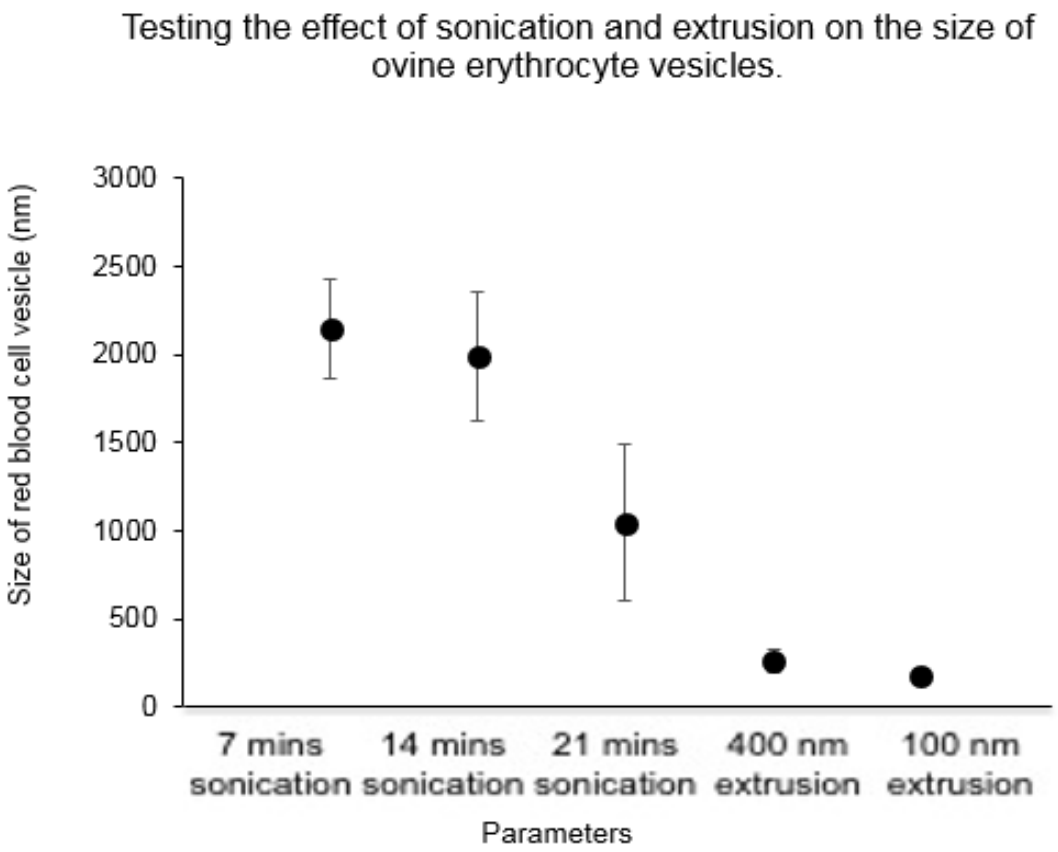

Figure 34. A graphical representation of varying sizes of ovine erythrocyte vesicles. The graph shows the effect of different sonication times and extrusion on the size of ovine erythrocyte vesicles at 20°C, measured using the Malvern zetasizer. Error bars represent standard error of mean (n=3). Refer to appendix one section 1.8.1 for distribution data.

The sonicated ovine erythrocyte vesicles are subjected to extrusion through a 400 nm and 100 nm polycarbonate membrane. This technique ensured production of a monodispersed suspension of nanosponges with a cell size of 181 nm (± 39). The zetasizer was calibrated every 6 months for size and polydispersity by Malvern. Moreover, to ensure consistency repeat measurements were conducted in batches to obtain an average size.

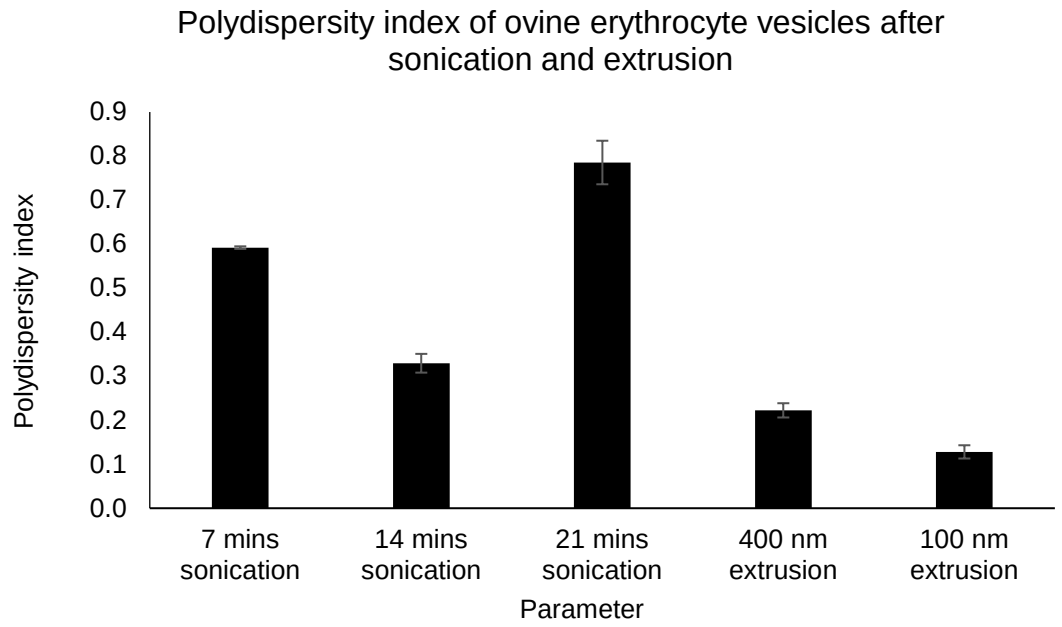

Figure 35. The polydispersity index of ovine erythrocyte vesicles after the suspensions have been subjected to varying sonication times and serial extrusion through 400 nm and 100 nm polycarbonate membranes. Sizes were measured using the Malvern zetasizer. Error bars represent standard error of mean (n=3).

Dispersity of a suspension is measured by the polydispersity index (PDI). The PDI is a measure of the distribution of the particle size in a suspension. Figure 35 shows the PDI of ovine erythrocyte vesicles after they were subjected to varying sonication times and extrusion. According to Figure 35 there is no correlation between sonication time and PDI. However, the plot does show that after sonication, polydispersed suspensions were produced. After sonication, the ovine erythrocyte vesicles were extruded through a 400 and 100 nm polycarbonate membrane. The PDI after 100 nm extrusion has decreased to 0.128 (± 0.015).

1.6.8 Size of PLGA nanoparticles and ovine nanosponges

The PLGA cores were prepared using a solvent evaporation method at room temperature. The PLGA cores were dissolved with isotonic PBS and characterised for size using a Malvern zetasizer. Figure 36, shows the average size distribution of PLGA nanoparticles measured by dynamic light scattering. Figure 36 shows two different peaks indicating two distinct sizes. Peak 1 has a

size of 75 nm (± 21) and peak 2 has a size of 303 nm (± 86). The zetasizer software has reported an average size of 243 nm (± 107 nm) with a PDI of 0.347.

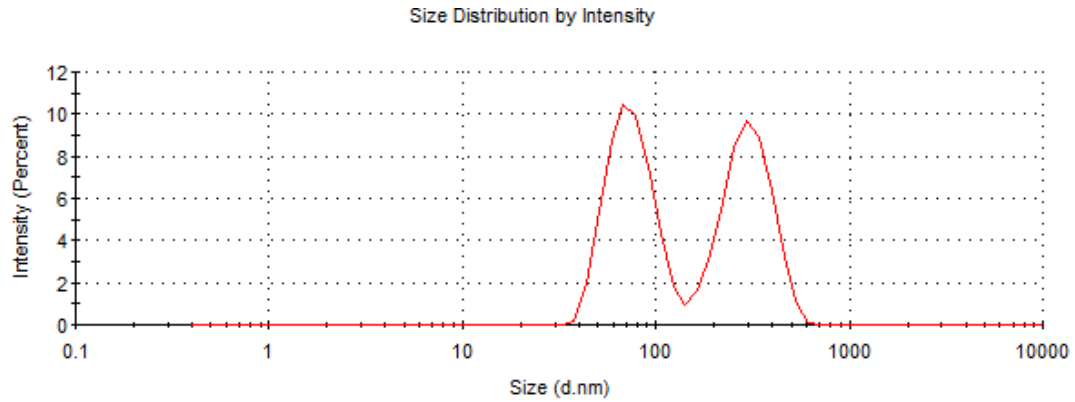

Figure 36. Size distribution graph of 1 mg/ml PLGA nanoparticles prepared using the solvent evaporation method. This plot was acquired from the Malvern zetasizer data analysis software.

The nanosponges were synthesised by extruding the ovine erythrocyte vesicles with the PLGA nanoparticles. The nanosponges were dissolved with isotonic PBS and characterised for size. Figure 37 shows the size distribution of ovine nanosponges measured using dynamic light scattering. According to Figure 37 the average size of the ovine nanosponges was 185 nm (± 50) with a PDI of 0.134.

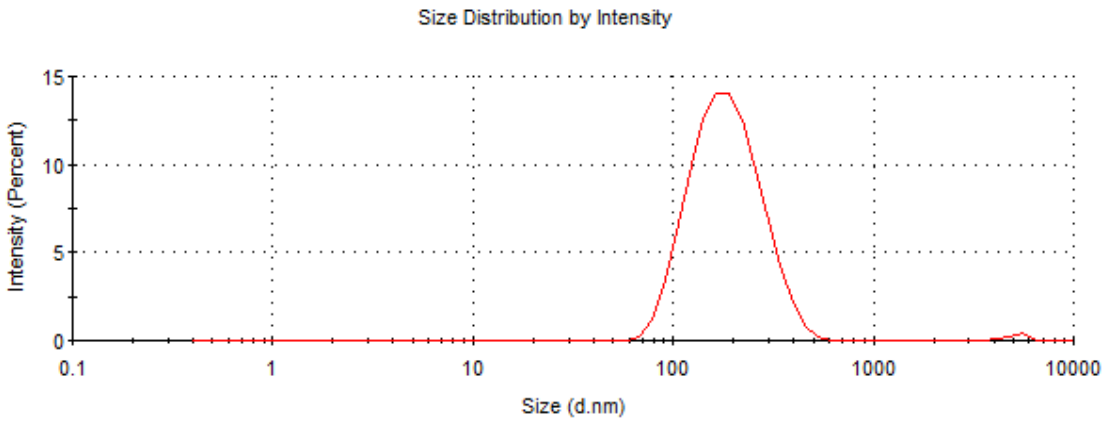

Figure 37. Size distribution graph of 1 mg/ml ovine nanosponges prepared by fusing ovine erythrocyte vesicles with PLGA nanoparticles. This plot was acquired from the Malvern zetasizer data analysis software.

1.6.9 Zeta potential of PLGA nanoparticles and nanosponges

The PLGA nanoparticle cores and the ovine nanosponges were characterised for their zeta potential. Zeta potential is a significant parameter, as it is a measure of the electrostatic charge between particles in a suspension. Figure 38 shows the zeta potential distribution of PLGA nanoparticles. According to Figure 38 the average zeta potential is -12.3 mV.

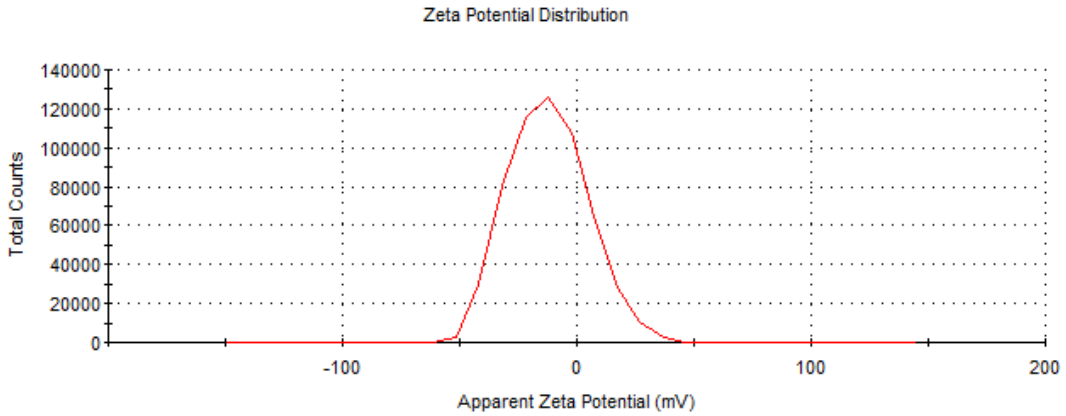

Figure 38. Zeta potential distribution graph of 1 mg/ml PLGA nanoparticles. This plot was acquired from the Malvern zetasizer data analysis software.

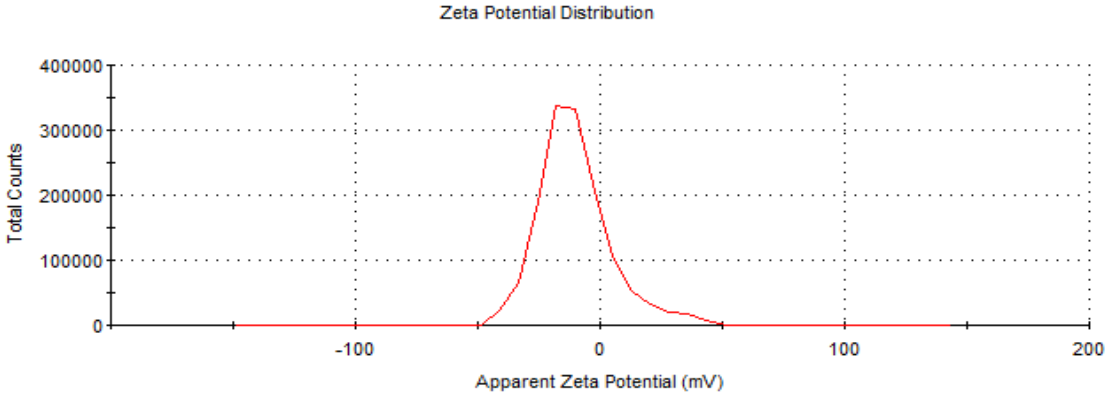

Figure 39. Zeta potential distribution graph of 1 mg/ml ovine nanosponges. This plot was acquired from the Malvern zetasizer data analysis software

Ovine nanosponges were also measured for their zeta potential. Figure 39 shows the zeta potential distribution of ovine nanosponges. According to Figure 39 the average zeta potential is -10.5 mV.

1.6.10 Size of lyophilized nanosponges after reconstitution with PBS

Ovine nanosponges were lyophilized with 5% (w/v) sucrose and stored at 4°C in the lyophilized form. The lyophilized suspensions were kept at 4°C for two different lengths of time. One of the suspensions was reconstituted with isotonic PBS after 1 week and the other suspension was reconstituted after 6 months.

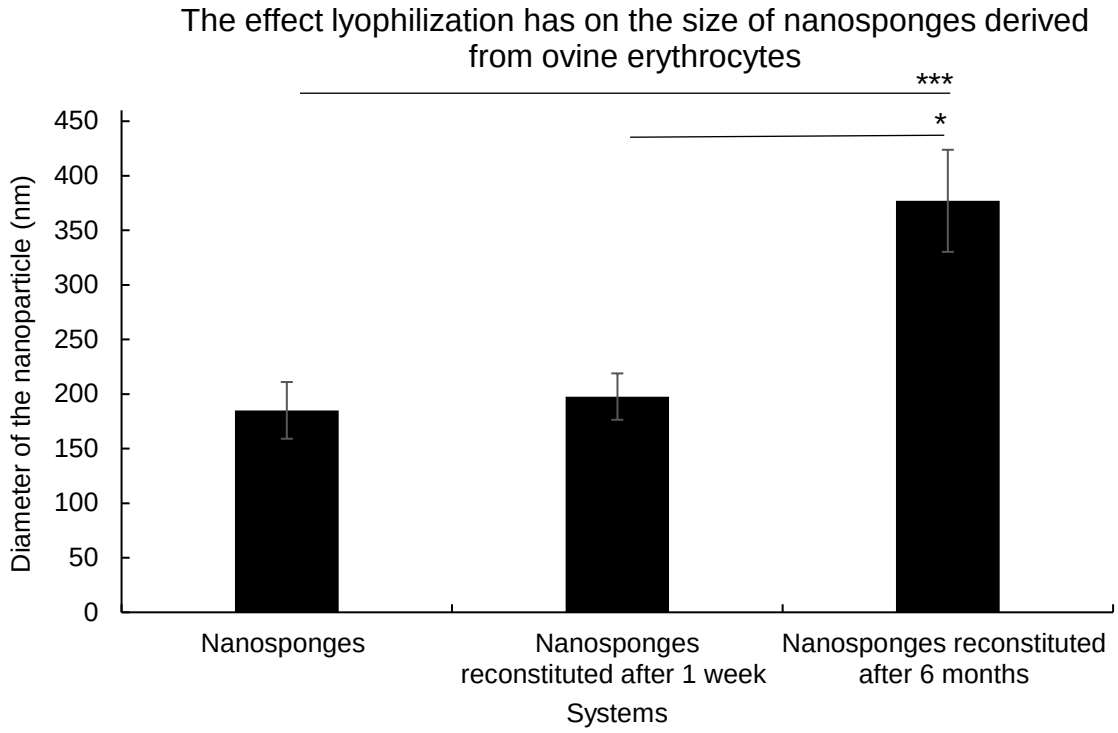

Figure 40. Average size of three nanosponge suspensions. Control nanosponges (1 day old), nanosponges lyophilized with 5% sucrose (w/v) reconstituted after 1 week and lyophilized nanosponges reconstituted after 6 months. The sizes were measured using a Malvern zetasizer. "*" P≤0.05, "**" P≤0.01 and "***" P≤0.001. Error bars represent standard error of the mean (n=3).

The control nanosponge and the reconstituted nanosponge suspensions were measured for size. Figure 40, shows the average sizes of the three nanosponge suspensions. There is a significant difference is size between the control nanosponges and the suspension reconstituted after 6 months. The lyophilized nanosponges that have been stored for 6 months have a size of 377 nm (± 46 nm) with a PDI of 0.297. There appears to be no significant difference in size between control nanosponges and nanosponges that were reconstituted after 1 week.

1.6.11 Stability studies of ovine nanosponges

Stability of ovine nanosponges was assessed by measuring the size, PDI and zeta potential of the particles at four different temperatures (4°C, 24°C, 37°C and 40°C) over one week (Figure 41). The parameters were assessed in triplicates. The suspensions were kept in a water bath at the aforementioned temperatures. Stability of the nanosponges was tested at 4°C, as it is a standard condition for storage of whole blood. Moreover hypothermic storage is based on the principle that biochemical and molecular reactions can be suppressed by a reduction in temperature (Scott *et al.*, 2005). Similarly, nanosponges were tested at 24°C as for future clinical application, as it is easier to transport batches of therapeutics at this temperature. Nanosponges were tested at 37°C and 40°C as they represent physiological conditions in humans. 37°C is the average temperature in the human body and 40°C mimics the elevated body temperature during sepsis (Lee *et al.*, 2012).

A

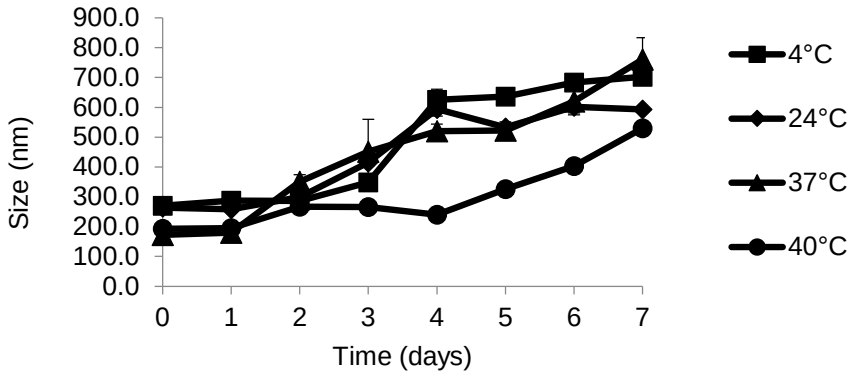

B

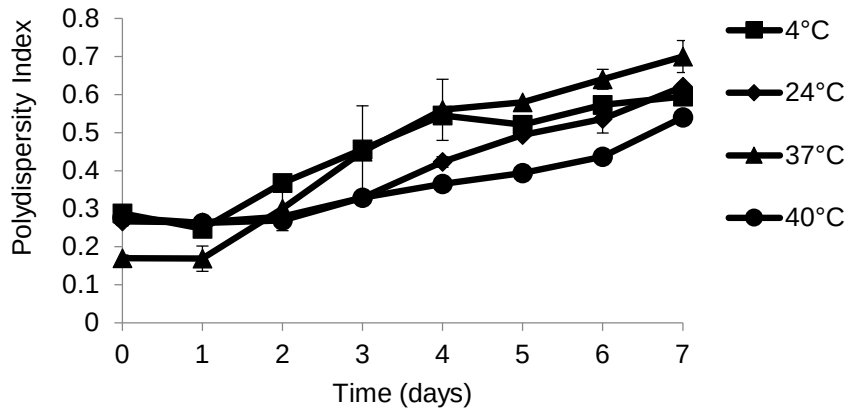

C

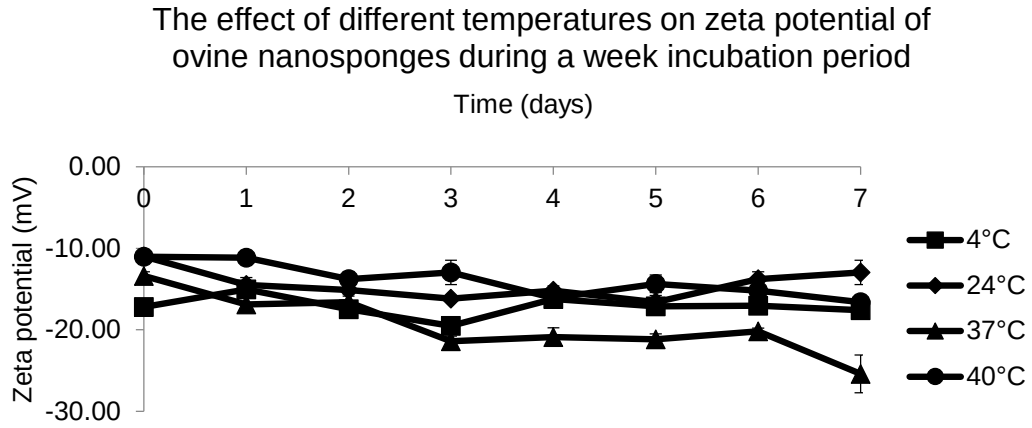

Figure 41. Nanosponge stability study. The effect of four different temperatures on the (A) size, (B) PDI and (C) zeta potential of nanosponges. The nanosponges were placed in water bath at the respective temperatures. Size was measured by a Malvern zetasizer. Error bars represent standard error of the mean (n=3).

The stability of the ovine nanosponges were assessed using size, PDI and zeta potential. According to Figure 41, size of ovine nanosponges increase over a period of 1 week. At 4°C the size increases to 702 nm (± 1.46) from 270 nm (± 3.08); at 24°C the size increases to 592 (± 4.98) from 263 (± 1.14); at 37°C the size increases to 760 nm (± 73.1) from 172.5 (± 0.27) and at 40°C the size increases to 530 nm (± 16.04) from 192 (± 3.54). Overall, this figure shows a positive correlation between size and time in days. Similarly, the PDI of ovine nanosponges has also increased, over a duration of one week at these respective temperatures. The highest PDI on day 7 was shown to be at 4°C, (0.58, ± 0.01) and the lowest was shown to be at 40°C, (0.54, ± 0.01). The zeta potential of nanosponges decreased over a period of one week. According to Figure 41C, the most significant decrease is shown at 37°C, as the nanosponges have a zeta potential of -25.4 mV (± 2.31) on day 7. Ovine nanosponges incubated at 24°C have a decreased zeta potential value at day 7 (-12.97 mV, ± 1.49). However, the decrease is not as significant as the other suspensions. Overall, Figure 41 showed that ovine nanosponges over a period of one week become unstable at the experimental temperatures.

1.6.12 Surface area to volume ratio

The surface area to volume ratio is the amount of surface area per unit volume of an object.

Table *9* shows the difference in the calculated surface area to volume ratio between porcine erythrocytes and porcine erythrocyte ghosts (Beals., 2000). The sizes obtained for the theoretical calculations were taken from Figure 28 and Figure 29. The surface area to volume ratio were measured using the equations shown below:

Surface area of a sphere = $4\pi r^2$

Volume of a sphere = $\frac{4\pi r^3}{3}$

Table 9 - The surface area to volume ratio of the porcine erythrocyte and porcine erythrocyte ghosts

Cell type	Surface area (μm^2)	Volume (μm^3)	Surface area: Volume
Measurements calculated from light microscopy			
Erythrocyte	53.03	36.36	1.45:1
Erythrocyte ghosts	16.58	6.37	2.60:1
Measurements calculated using scanning electron micrographs			
Erythrocyte	69.74	54.70	1.27:1
Erythrocyte ghosts	27.40	13.27	2.06:1

Nanosponges were designed using ovine and leporine erythrocytes. Ovine erythrocyte vesicles were synthesised by sonicating and extruding the ovine erythrocyte ghosts. The surface area to volume ratio of ovine erythrocyte vesicles was calculated using the above equations. The sizes used for the calculations were obtained from Figure 34 and Figure 37 for nanosponges.

Table 10- The surface area to volume ratio of ovine erythrocyte vesicles

Cell type	Surface area (μm^2)	Volume (μm^3)	Surface area: Volume
Vesicles after 7 mins of sonication	14.45	5.16	2.7:1
Vesicles after 14 mins of sonication	12.39	4.1	3.0:1
Vesicles after 21 mins of sonication	3.39	0.58	5.8:1
Vesicles after 400 nm extrusion	0.21	0.009	23.3:1
Vesicles after 100 nm extrusion	0.101	0.003	33.6:1

Table 11- Surface area to volume ratio of ovine erythrocytes and ovine nanosponges

Type of cell	Surface area (μm^2)	Volume (μm^3)	Surface area: Volume
Ovine erythrocyte	40.7	24.4	1.7:1
Ovine Nanosponges	0.107	0.003	32.4:1

1.6.13 Statistical analysis

Significance of recorded results was denoted by "*" symbol, was determined by a paired T-Test using SPSS 22.0 (IBM, North harbour, Portsmouth, UK)

1.7 Discussion

The overall aim of the research was to develop techniques to produce a model nanosponge constructed from biomimetic erythrocyte membranes. Secondarily the physical properties and storage characteristics were studied and finally, adsorption studies were carried out (See chapter 2 section 2.3.2). Erythrocytes are recognised as one of the oldest coating systems in the field of nanomedicine and drug delivery (Bhateria *et al.*, 2014). The application behind this approach is to use the nanosponges to adsorb PFTs. The erythrocyte membrane contains surface properties that allow adsorption of a wide range of PFTs regardless of their molecular structure (Hu *et al.*, 2013). In order to achieve synthesis of nanosponges, the primary step was to produce erythrocyte ghosts.

1.7.1 Haematological parameters of mammalian blood

Prior to synthesis of erythrocyte ghosts, blood from different types of mammalian species were collected. Quality of mammalian blood was assed using five different parameters RBC count, concentration of Hb, haematocrit (viscosity of blood), MCV (average volume of red blood cells) and MCH (average mass of Hb per RBC). Quality assessment of blood is significant as Bosman *et al.* (2008) has shown that blood stored for long periods of time before transfusion has led to aggregation between erythrocyte membranes and degradation of integral membrane protein band 4, which is essential to maintain structural integrity of the membrane. Another study suggested that stored blood led to the loss of proteins in the lipid raft regions (Kriebardis *et al.*, 2007). This ideally could lead to the loss of the lipids present in these regions, which are essential in maintaining fluidity of the membrane. The primary choice of animal blood was porcine blood due to the anatomical similarities between humans and pigs (Sullivan *et al.*, 2001). According to Table 5, the haematological parameters of porcine blood are within the reference ranges. This suggests that the blood is in good condition for experimentation. Leporine, murine and ovine were chosen as controls. However, according to studies shown in chapter 2 and chapter 3, ovine and leporine membranes form the basis for a therapeutic model as compared to porcine and murine.

1.7.2 Morphological examination of porcine erythrocyte ghosts

Previous studies have been conducted in order to study the membrane of mammalian erythrocytes (Dodge *et al.*, 1963, Schwoch and Passow, 1973, Weed *et al.*, 1963). These researchers lysed the erythrocytes with hypotonic solutions, which opened the membrane allowing the intracellular contents to leak out producing erythrocyte ghosts. These ghosts are useful in studying chemical and physiological properties of the erythrocyte membrane. Morphological examination of erythrocyte ghosts helps confirm membrane structure, shape and size. The morphology of porcine erythrocyte ghosts has been previously examined by transmission electron microscopy and scanning electron microscopy (Kostic *et al.*, 2014). Similar to the previously mentioned study, morphological differences were found between porcine erythrocytes and ghosts, under light microscopy and scanning electron microscopy.

Figure 20 shows a light micrograph of porcine erythrocyte ghosts. They are spherical in shape and smaller than porcine erythrocytes. The reduction in size could be due to the loss of Hb, water, calcium and potassium from the cytoplasm of the cell (Dodge *et al.*, 1963, Weiss *et al.*, 2010). Ideally, a hypotonic solution would completely lyse a cell surrounded by a lipid bi-layer due to the tonicity of the solution. Interestingly, erythrocytes have a property to reseal, although the reason for this phenomenon is unknown (Schwoch and Passow, 1973). This is what gives the ghost its spherical structure, as a study conducted by Gupta *et al.* (2014) shows that preparation of erythrocyte ghosts by hypotonic lysis followed by a resealing procedure produces ghosts with a spherical morphology. In comparison to the ghosts in Figure 20, porcine erythrocytes (Figure 17) appear to have crenations or formation of artefacts on the surface of the cell. These crenations were also observed in Figure 21 and Figure 22, which are scanning electron micrographs of porcine erythrocytes. These crenations are commonly known as echinocytes and are found in porcine blood. The crenated structures form as the cells were allowed to contact air or could have formed during air-

drying of the sample. The air drying process increases surface tension, which could cause the sample to form these artefacts (Price, 2002).

A scanning electron micrograph shows porcine erythrocyte ghosts, which appear to be non-crenated and have taken on a phase dark appearance (Figure 24),. Most of the porcine erythrocyte ghosts on the borders of the micrograph are aggregated. The aggregation could be caused by two factors: the use of low ionic strength buffer or the release of a protein known as spectrin. The use of low ionic strength buffers causes flocculation (the process by which particles are caused to clump together) and this is enhanced by increased centrifugation speeds and time. Porcine erythrocyte ghosts could have aggregated, as the spectrin molecules on the cytoplasmic surface of the erythrocyte ghost membranes forms a meshwork by binding to other cells, thereby reducing cell mobility (Elgsaeter and Branton, 1974). Porcine erythrocyte ghosts have shown to have an indented structure similar to those seen in human erythrocytes. This suggests that the cell takes on this morphology due to the loss of Hb or the loss of water during drying. Compared to erythrocytes in Figure 21, porcine erythrocytes take on a spherical appearance when diluted with an isotonic solution (Figure 23). This is because the erythrocyte has an influx of water from the extracellular compartment, which helps to maintain a balance in the osmotic pressure between the intracellular and extracellular compartment of the cell (Deuticke, 1968). According to the discussed images, there is a significant difference in morphology between these two cell types. However, these cell types are mainly distinguished by their cell size.

1.7.3 Testing the difference in cell size between porcine erythrocytes and ghosts

The above study showed that under hypotonic conditions the porcine erythrocyte ghosts undergo morphological changes in order to produce erythrocyte ghosts. This study provides evidence that the change in morphology is correlated with size of the erythrocyte ghosts. Johnson *et al.* (1980) showed using hypotonic lysis, that erythrocyte ghosts undergo morphological changes. These changes are correlated with the volume of Hb present in the cell. Another well-established study showed that after hypotonic lysis causes the MCV and MCH decrease with

respect to time (Tatsumi, 1981). Figure 28 shows that there is a significant difference in size between porcine erythrocytes and ghosts. Porcine erythrocytes have a diameter of 4.11 µm (± 0.14). The ghosts have a smaller diameter of 2.3 µm (± 0.11). The porcine erythrocyte diameter is within the size reference range (4-8 µm), which shows that there was no loss of intracellular contents during storage. The scanning electron micrographs further show the difference in size between the porcine erythrocytes and the porcine erythrocyte ghosts. Figure 29 shows porcine erythrocytes have a diameter of 4.71 µm (± 0.18) and the erythrocyte ghost have a diameter of 2.95 µm (± 0.10).

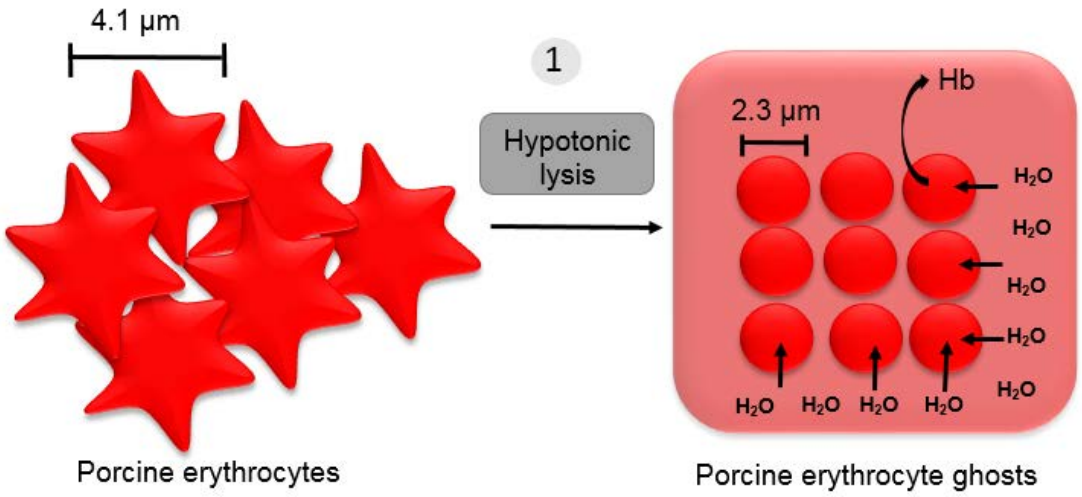

Figure 42. Diagrammatic representation of porcine erythrocyte ghosting. The morphology and size of porcine erythrocytes and ghosts were adapted from the captured scanning electron micrographs (Figure 22 and Figure 24).

This clearly shows that due to the hypotonic lysis, which caused the loss of intracellular Hb, the erythrocyte ghosts have a reduced cell size. Synthesis of nanosponges utilises a top down approach, which means from an erythrocyte to the development of nanosponges, there will be a significant reduction in cell size. Moreover reduction in size plays a very significant role, as a study conducted by Walkey *et al.* (2012) showed. From a size range (15-90 nm) of gold nanoparticles the 15 nm particles were able to adsorb maximal amount of serum proteins compared to the other sizes. The significance lies in the surface area to volume ratio. Therefore, the reduction in size is correlated with an increase in the surface area to volume ratio. It is hypothesised that the larger the surface area to volume ratio, the more area to volume there is on the nanosponge for toxin adsorption.

According to Table 9, theoretical measurements of surface area and volume do in fact show that from porcine erythrocytes to erythrocyte ghosts there is an increase in surface area to volume ratio. The average sizes taken from Figure 28 showed that the surface area to volume ratio increased from 1.45 to 2.6. Similarly, the average size taken from Figure 29 showed that the surface area to volume ratio increased from 1.27 to 2.06. The reduction in size could also make a significant impact when introduced to the blood stream of a patient suffering from sepsis. The thickness of blood vessel walls in the human body range from 1.0 mm in diameter to 0.5 µm in diameter (Burton, 1954). A study conducted by De Backer *et al.* (2002) shows that patients suffering from sepsis have a decrease in the diameter of the blood vessels, in addition to decreased perfusion in smaller blood vessels like capillaries. The reduction is size of the particle may help the particle to traverse into inaccessible vessels.

1.7.4 The relationship between the loss of haemoglobin and synthesis of erythrocyte ghosts

According to Schwoch and Passow (1973) ghost preparation requires the removal of Hb content. Estimating the release of Hb during the ghosting procedure confirms the synthesis of porcine erythrocyte ghosts, which is shown in Figure 31. The figure shows nine different treatments, which include a range of isotonic buffers and a hypotonic buffer. The experiment was carried out with presence of PI. The use of PI was significant, as it may have blocked an enzyme known as haem oxygenase-1, which is found in the plasma during stress conditions. This enzyme plays a role in the Hb degradation pathway and catalyses Hb into a compound known as biliverdin (Shibahara *et al.*, 2002).

According to Figure 31, the first treatment shows minimal Hb release, as the BCP treatment is a separation step, which involves centrifuging the whole blood. The whole blood is separated into the erythrocyte suspension, the buffy coat and plasma. The buffy coat and plasma make up the supernatant. Since the cells are not lysed during this treatment the Hb is known as free Hb, which is released during erythrocyte storage (Han *et al.*, 2010). This result suggests that the erythrocytes stored with the presence of PI achieved optimum storage as a study conducted by Seghatchian and Krailadsiri (2002) shows that systems containing

optimum storage conditions have a lower concentration of Hb released over a period of 35 days.

Maximum Hb was released during the lysis treatment. The lysis treatment uses a hypotonic solution, which caused the cells to swell and take on a spherical shape. When the haemolytic volume was reached, haemoglobin is released through tiny pores in the membrane (Schwoch and Passow, 1973). This treatment released 1.51 g/dl (±0.483) of Hb. The hypotonic solution contained EDTA and the TRIS NaCl 1 and Tris NaCl 2 contained Tris-HCl, which are used to regulate the acidity and osmolarity of the lysate, as Tris-HCl has the property to buffer solutions, keeping them in the pH range of 7.0 to 9.0 (Aitken, 2012). The Hb concentration decreases from the lysis treatment up to the distilled H_2O treatment. This decrease is due to all the solutions being isotonic after the lysis stage. This method suggests that the fate of Hb is related to the treatment used. Measurements by Hoffman (1958) showed that at the end of the lysis the Hb distribution between the cells and the medium reach an equilibrium. After this equilibrium, the erythrocyte ghosts regain their permeability to Hb and reseal. Therefore, there is a minimal amount of Hb present at the last treatment. Finally, the loss of Hb during ghosting also explains the reduction in size of erythrocyte ghosts shown from Figure 28 and Figure 29.

1.7.5 The effect of ghosting on the release of proteins from the membrane of porcine erythrocyte ghosts

Protein plays a significant role in maintaining the structural integrity of the membrane as most plasma membranes consist of approximately 50% lipid and 50% protein by weight (Cooper, 2000). Figure 33 shows the effect ghosting has on the loss of proteins during ghosting of porcine erythrocytes. Similar to the Hb assay, this assay was carried out with the presence of a protease inhibitor. The accurate analysis of protein concentration required the presence of a protease inhibitor as plasma contains an abundance of proteases, many of which are released from activated, dying or lysed neutrophils (Ayache *et al.*, 2006).

Figure 33 shows the loss of protein during porcine erythrocyte ghosting. The primary treatment, which is the BCP treatment, is a separation step, which

involves centrifuging the whole blood. The supernatant is made up of the buffy coat and plasma. The concentration of protein released during this step is 43.62 mg/ml (±3.82). This concentration of protein released may suggest that the proteins in this treatment could be plasma proteins, as the reference range for plasma proteins present in porcine blood is between 60-80 mg/ml (Weiss *et al.*, 2010). The lysis treatment has released a small amount of protein, as at this stage erythrocytes are lysed to synthesise ghosts. The result could suggest that a small amount of membrane protein has been released. According to chapter 2 section 2.3.2, this result does not hinder the process of adsorption by nanosponges.

1.7.6 Characterisation of ovine erythrocyte vesicles

In order to synthesise nanosponges, ovine erythrocyte ghosts were subjected to sonication and extrusion to produce ovine erythrocyte vesicles. A study was designed to test if varying sonication times have an effect on the size of ovine erythrocyte vesicles. Synthesised ovine erythrocyte ghosts were subjected to sonication at varying amounts of time to determine size of produced ovine erythrocyte vesicles. Figure 34 illustrates that as the time of sonication increases, the size of ovine erythrocyte vesicles decrease. This takes place as sonication uses high frequency sound waves that agitate the suspension, causing vibrations, that have the potential to break particles apart, producing particles with a decreased average size (Gupta *et al.*, 2014). However sonication does not maintain the uniformity of particle size, as shown in Figure 34. Sonication produces polydispered suspensions of ovine erythrocyte vesicles. Vesicles sonicated for 21 minutes were chosen as the standard sonication time to produce nanosponges, as it had the smallest average size.

In order to maintain uniformity, sonicated ovine erythrocyte vesicles were subjected to extrusion. The ovine erythrocyte vesicles were extruded through a 400nm and 100 nm polycarbonate membrane. Figure 34 shows a decrease in size and uniformity after sonicated vesicles are extruded through the two different membranes. Extrusion uses the principles of mechanical force, generated by a the push of a syringe as depicted in Figure 16. The generated mechanical force pushes the vesicles through the polycarbonate membranes of defined pore sizes. This technique ensures a reduction in size and synthesizes monodisperesed

suspensions, as shown in Figure 34. The reduction in size is of significant interest, as this leads to the increase in ~~size decreases~~surface area to volume ratio, shown in Table 11. The surface area to volume ratio is of considerable interest as shown in chapter 2 section 2.3, as it plays a significant role in toxin adsorbtion. Sizes obtained by sonication and extrusion from this study have also been reported by recently published studies (Hu *et al.*, 2011, Rao *et al.*, 2016).

1.7.7 Characterisation of nanosponges and PLGA nanoparticle cores

Extruded ovine erythrocyte vesicles were added to the PLGA nanoparticle cores and further extruded through a 100 nm polycarbonate membrane. The mechanical force generated during extrusion coated the PLGA core with the ovine erythrocyte membrane (Rao *et al.*, 2016). Prior to extrusion, the prepared PLGA cores were characterized for size, PDI and zeta potential. The average size of PLGA cores was 243 nm (± 71) with a PDI of 0.303 and a zeta potential of -12.3 mV (Figure 36 and Figure 38). This shows that the suspension prepared was a polydispersed suspension. The zeta potential value is a particle characteristic used to assess stability of a suspension. The electrostatic repulsion between particles prevents aggregation of the spheres (Ravi Kumar *et al.*, 2004). The negative zeta potential of PLGA may originate from the carboxylic group of PLGA as hydroxyl groups on the PLGA on molecule carry a negative charge. (Lee *et al.*, 2015).

The solvent evaporation procedure adopted from Hu *et al.* (2011), produced two distinct PLGA sizes, shown from Figure 36. Several factors could cause this to happen. The solvent evaporation procedure used in this study to produce PLGA nanoparticles required used of solvents such as acetone. Han *et al.* (2012), has shown that residual amounts of solvent present in the PLGA suspension do affect nanoparticle characteristics. Moreover, to improve PLGA nanoparticle characteristics, the technique is followed by homogenization procedures to develop highly negatively charged monodispersed nanoparticles (Hadinoto *et al.*, 2013). For example Mieszawska *et al.* (2012) prepared lipid polymeric nanoparticles using PLGA as a core for the structure. The technique used by the author to develop PLGA nanoparticles was followed by vortexing and ultra-sonication resulting in stable monodispersed formulations of PLGA nanoparticles with a zeta potential of -30 mV.

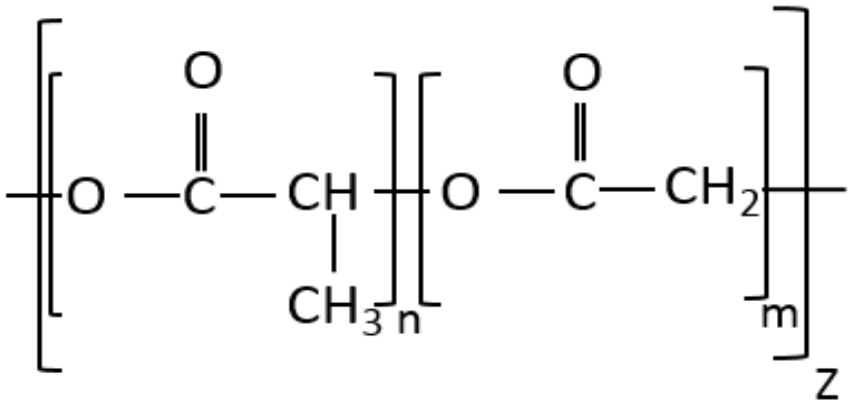

Figure 43. The chemical structure of a PLGA polymer. The structure on the left is the lactic acid group and the structure on the right is the glycolic acid group. Image adapted from Dumitru *et al.* (2015)

The nanosponges were also characterised using size, PDI and zeta potential. The size of the nanosponges was recorded as 185 nm (± 50) with a PDI of 0.134 with a zeta potential of -10.5 mV (Figure 37 and Figure 39). The size of the ovine nanosponges increase after fusion with the PLGA core compared to ovine erytrhocyte vesicles. The increase in size is due to the fusion, as a coating is formed around the PLGA core. The zeta potential of the particle reduces from -12.3 (before coating) to -10.5 mV (after coating with ovine erythrocyte vesicles). The negative charge on the erythrocyte membrane is caused by the carboxyl groups of sialic acid present on the end terminus of glycoproteins and glycolipids (Eylar *et al.*, 1962, Luk *et al.*, 2014). Moreover the reduction in zeta potential may suggest that the erythrocyte membrane has a lower concentration of carboxyl groups compared to PLGA.

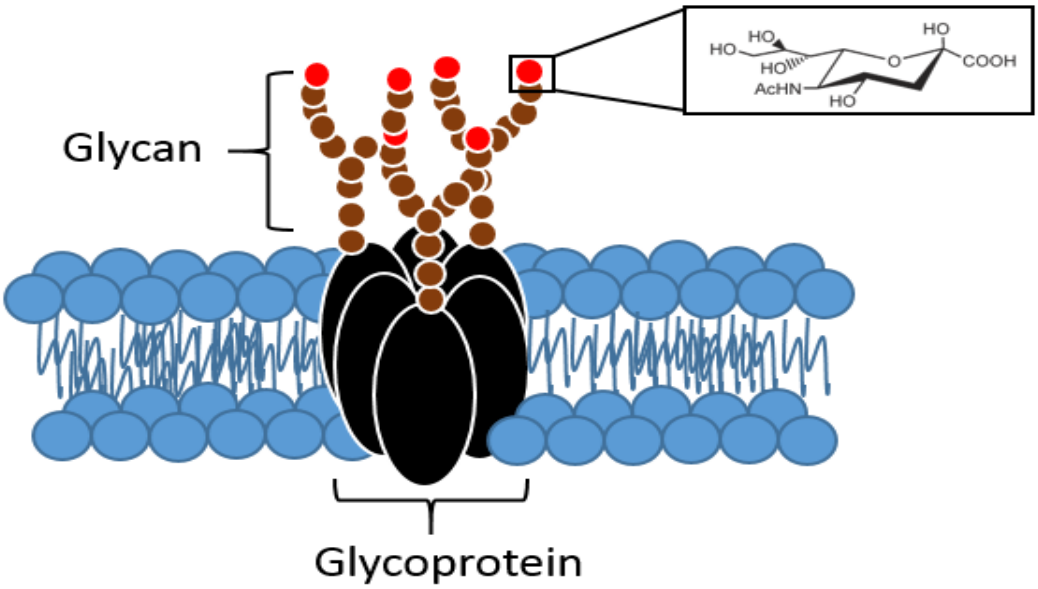

Figure 44. An illustration of an erythrocyte membrane with a glycoprotein. The glycoprotein has structures on it made out of carbohydrates known as glycans. The end terminus of the glycans have presence of sialic acid. The phospholipids and fatty acid tails are represented by the colour blue. The glycoprotein is represented by the colour black and the glycan chains are represented by the brown structure. The red represents the sialic acid residue.

A recently published study could confirm the recorded results in Figure 38 and 39 The authors showed that coating the PLGA cores with erythrocyte membranes led to a reduction in the zeta potential of the particle. This could confirm the prescence of an ovine erythrocyte coating around the prepared PLGA cores (Luk *et al.*, 2014) (Rao *et al.*, 2016). These authors have also highlighted, that using this extrusion technique results in the synthesis of nanosponges with a right side out orientation. However this could not be confirmed as scanning electron imaging led to the melting of the nanosponges, which generated unclear images. (refer to appendix section 1.8.2) Obtaining micrographs of nanosponges was tried using a lower voltage (decreased beam strength) and a lower spot size, however it still produced images similar to the micrograph shown from section 1.8.2.

1.7.8 Stability of ovine nanosponges

In the field of nanomedicine, stability is one of the critical aspects in ensuring safety and efficacy of therapeutic products. In administration of

nanosuspensions, formation of particles larger than 5 µm could lead to a blockage in the cappilaries, which could be fatal to a patient. Therefore, particle size and distribution need to be monitored. During storage and administration of nanosuspensions, the particles come into contact with different temperatures, which could cause sedimentation of particles, morphological changes and aggregation of particles. Stability studies associated with nanoparticles deserve significant attention in therapeutic product dvelopment (Wu *et al.*, 2011). Figure 41-43 are stability sudies conducted on ovine nanosponges, which test the effect of different temperatures (4°C, 24°C, 37°C and 40°C) on ovine nanosponges over the period of one week. Well established studies show that synthesising mouse blood coated PLGA nanoparticles using this extrusion method over a 2 week period produces no significant increase in size at 37°C (Rao *et al.*, 2016, Hu *et al.*, 2011, Hu *et al.*, 2013). However the recorded results here do not agree.

Figure 41-42 indicate the effect temperature has on the size and PDI of ovine nanosponges. These figures show a correlation between size or PDI and incubation time at these temperatures. Over a week of incubation, the size and PDI of the ovine nanosponges increased. Suggesting that the nanosponge suspensions are unstable at the experimental temperatures. There are a few reasons as to suggest why nanosponges increase in size over the tested time period. As shown from Figure 38-Figure 39, the zeta potential distribution curves of ovine nanosponges, indicate presence of positively charged nanosponges. Therefore, over a period of time they do have the potential to form aggregates with negatively charged nanosponges, which may lead to increased sized nanosponges (Luk *et al.*, 2014). There is a probability that some of the PLGA nanoparticle cores may not have been coated and therefore, presence of positive PLGA cores (shown by Figure 38) in the solution may cause aggregation between the particles. A study published by De and Robinson (2004) has shown, that PLGA nanoparticles aggregate into long fibres after day 2 at 24, 37 and 40°C. The author stated that this takes place, due to presence of residual organic solvent present within the PLGA nanoparticles.

In order to ensure stability of nanosponges, there are techniques used to prevent aggregation of nanoparticles. For instance, Wu *et al.* (2011) has stated that for particles that have unstable profiles, a common strategy to enhance

nanosuspension stability, is to store the suspension in a solid form. Figure 40 shows the effect of lyophilization with 5% sucrose on the size of ovine nanosponges over a period of one week to six months. This figure shows that there is no significant difference in size between the control nanosponges and the suspension reconstituted after a week. However, the suspension reconstituted after 6 months has increased in size by 192 nm (PDI 0.298). Comapritively, nanosponges stored in a lyophilized form, have shown to be more stable in size than storing the suspensions at the tested temperatures used In the stability studies. Lyophilization could be a better approach to store the ovine nanosponges because of the chemical properties of sucrose.

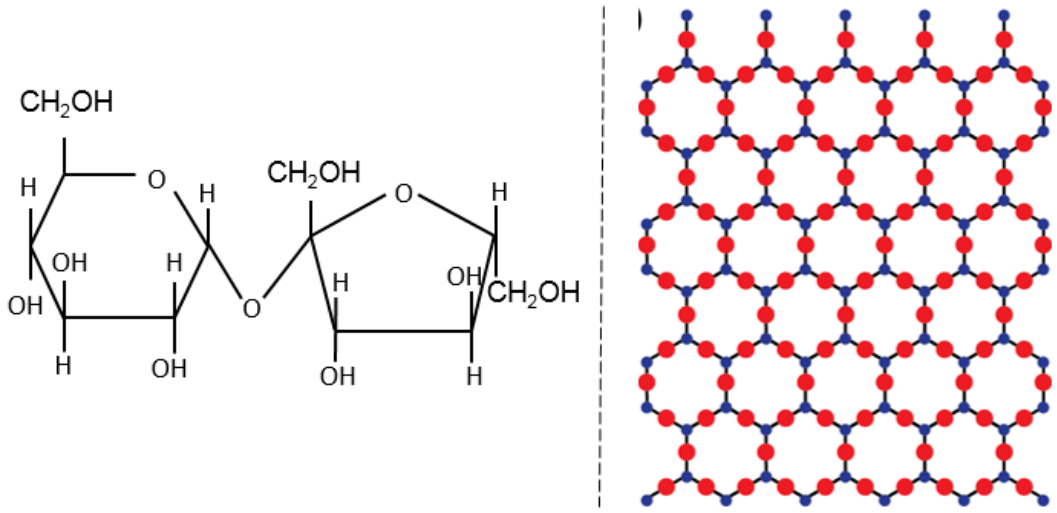

Figure 45. Diagrammatic representation of the molecular structure of sucrose. The structure of the left is the structure of sucrose, which is formed by glucose and fructose. The structure on the right is a model showing repeating units of sucrose, forming a crystalline structure (Husband, 2014).

In a sugar crystal, sucorse molecules are arranged in a pattern which extends into all three dimesions. The sucrose molecules are all linked together by intermolecular forces. When added to water, these linked sucrose molecules start seperating, as they are attracted to water molecules. During this procedure some sucrose molecules are also crystalizing by binding to other sucrose molecules. This process works on Le Chateliers principle. In terms of sucrose, the principle states that when sucrose is cooled down, in an attempt to bring the temperature up, the molecules will join together to form crystals, which release energy (Husband, 2014). This crystal formation, creates a stable glassy matrix during

lyophilization, which prevents formation of ice crystals that have the potential to break the nanosponges apart.

There are other ways to prolong stability, other than lyophilization. One way to achieve stability is through steric stabilisation. This could be accomplished by coating the nanosopnge with polyethylene glycol (PEG). PEG are long chain amphipathic copolymers that inhibit aggregation between suspensions. PEG covers nanoparticles in such a way, that the long loops extend out into the solution. Since they are hydrophillic tails they are only attracted to water and are not attracted to each other, this creates a repulsion between the nanoparticles. This is known as steric stabilisation (Stolnik *et al.*, 1994).

1.8 Appendix

1.8.1 Size distribution graphs for ovine erythrocyte vesicles, PLGA nanoparticles and nanosponges

The average size (z-average) of ovine erythrocyte vesicles that were plotted in Figure 34 and Figure 35 were recorded using a Malvern zetasizer. Below are the distribution plots of the recorded average sizes. Sonication of ovine erythrocyte ghosts produced polydispersed suspensions of ovine erythrocyte vesicles, shown in Figure 34. Moreover, showed that longer sonication times lead to a reduction in particle size.

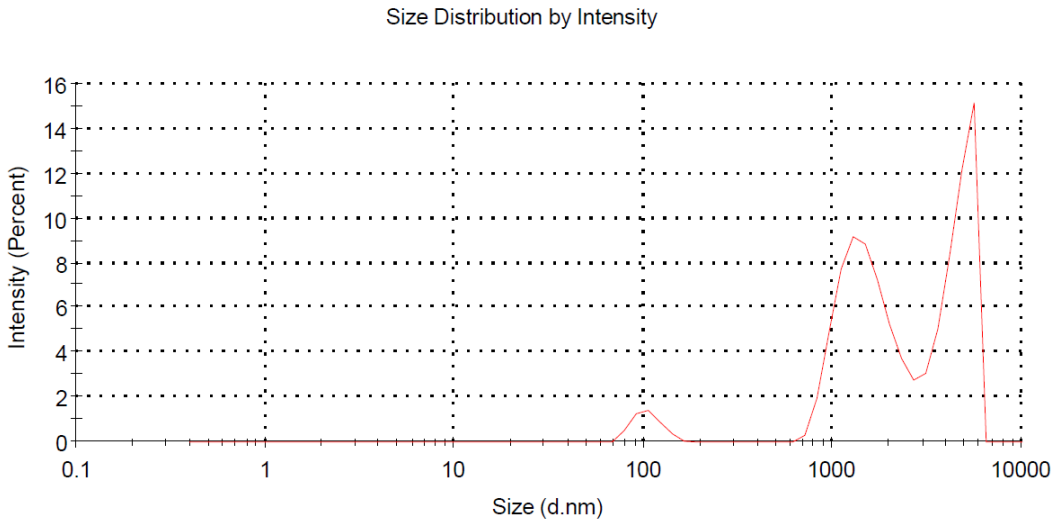

Figure 46. Size distribution plot for ovine erythrocyte vesicles, which were subjected to 7 minutes of sonication at 20°C. This plot was acquired from the Malvern zetasizer data analysis software.

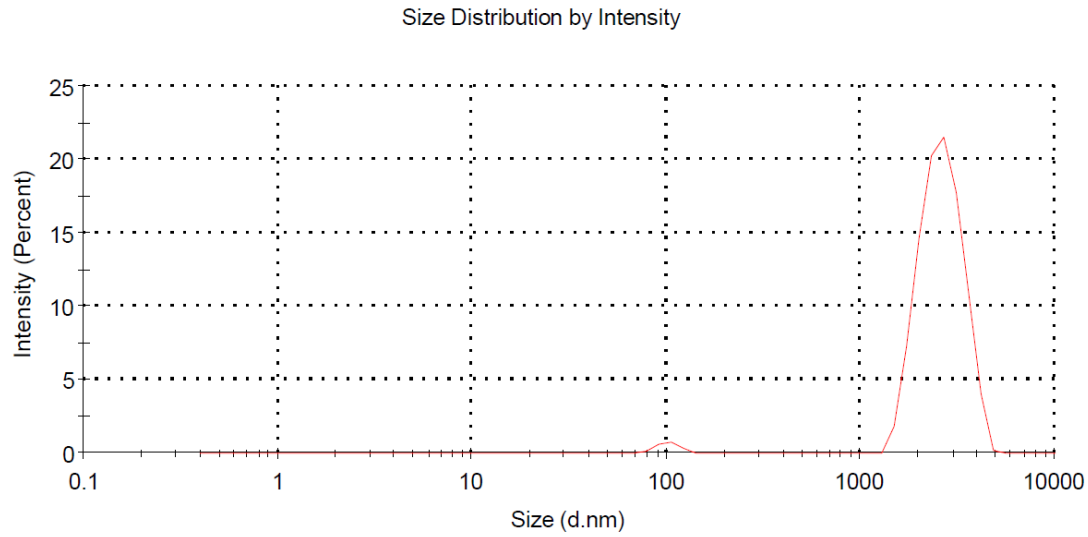

Figure 47. Size distribution plot for ovine erythrocyte vesicles, which were subjected to 14 minutes of sonication at 20°C. This plot was acquired from the Malvern zetasizer data analysis software.

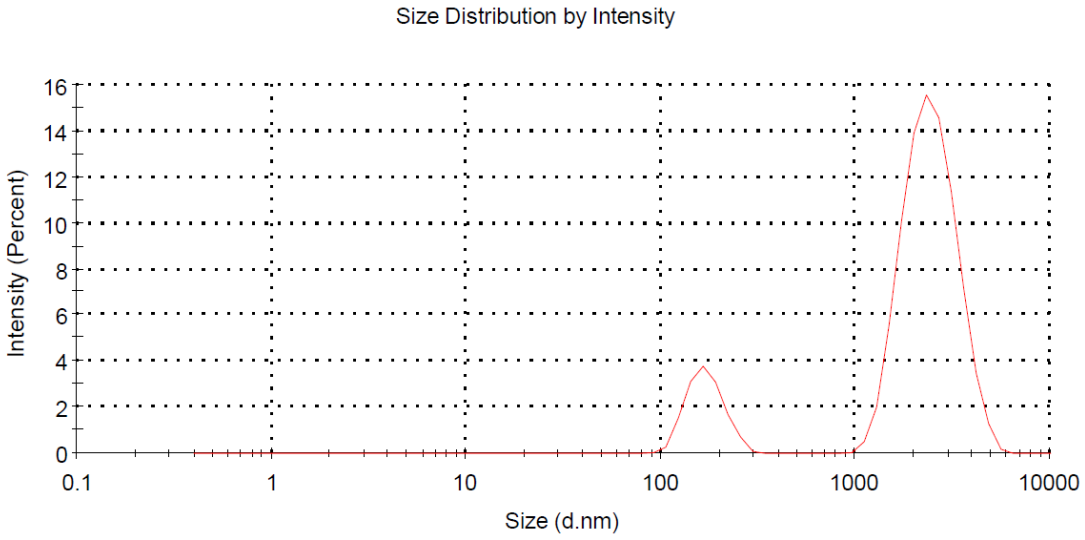

Figure 48. Size distribution plot for ovine erythrocyte vesicles, which were subjected to 21 minutes of sonication at 20°C. This plot was acquired from the Malvern zetasizer data analysis software.

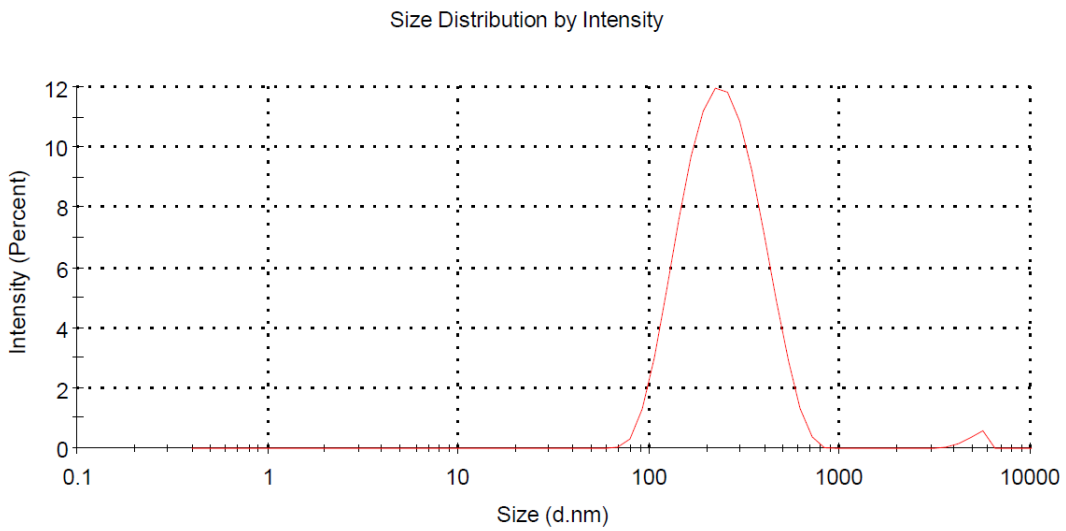

Figure 49. Size distribution plot for ovine erythrocyte vesicles, which were subjected to extrusion through a 400 nm polycarbonate membrane at 20°C. This plot was acquired from the Malvern zetasizer data analysis software.

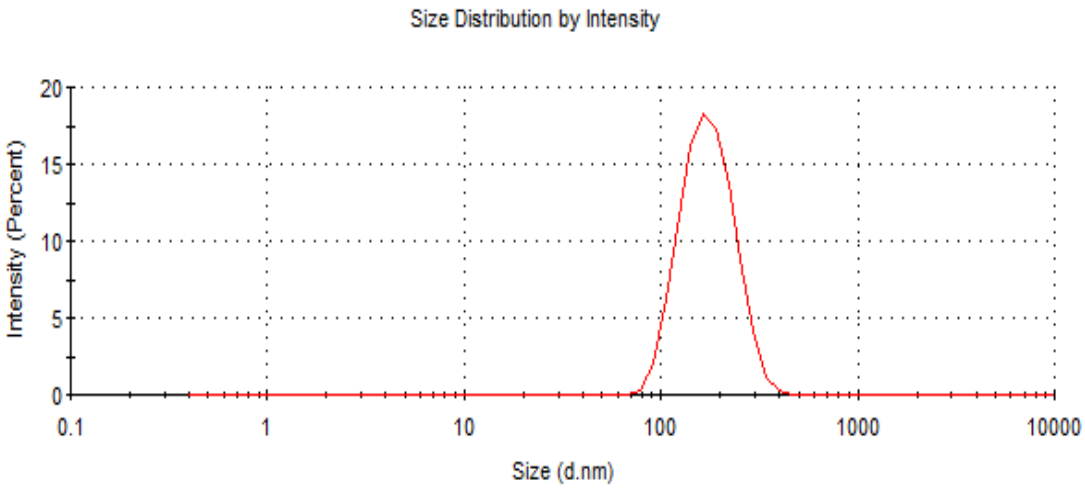

Figure 50. Size distribution plot for ovine erythrocyte vesicles, which were subjected to extrusion through a 100 nm polycarbonate membrane at 20°C. This plot was acquired from the Malvern zetasizer data analysis software.

1.8.2 Scanning electron micrographs on nanosponges

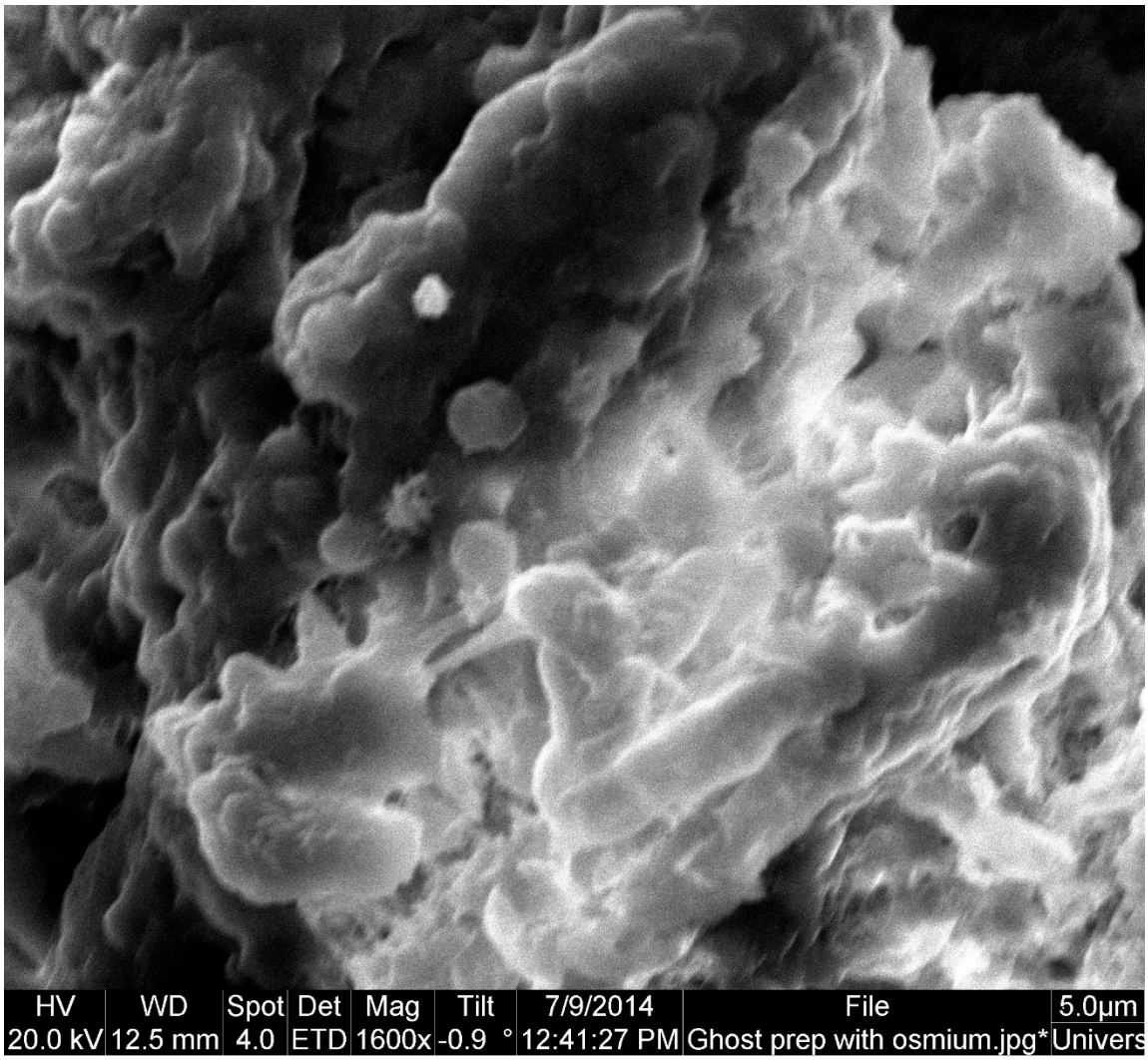

Figure 51. A scanning electron micrograph of ovine erythrocyte nanosponges. The sample was prepared by fixation with 3% glutaraldehyde and 2% osmium tetroxide. The micrograph shows melting and complete aggregation of the sample. Scale bar represents 5.0 µm.

Chapter 2

2 Streptolysin-O haemolysis and adsorption studies

2.1 Introduction

2.2 *Streptococcus*

Stevens (1995) stated that “An emerging pathogen can be one that is new, one that was known but has only recently been identified, or one that is old but has learned new tricks,”. Regardless of environmental pressures many pathogens that were discovered in the past have become major clinical problems, such as penicillin resistant *pneumococcus*, MRSA and Vancomycin resistant *enterococci* (VREs*)*. According to Stevens (1995) group A *Streptococcus* is an example of a well researched pathogen that has become more virulent over time. From 1995, British tabloids referred to *Streptococcus* as “The Flesh eating bug” to describe necrotizing infections.

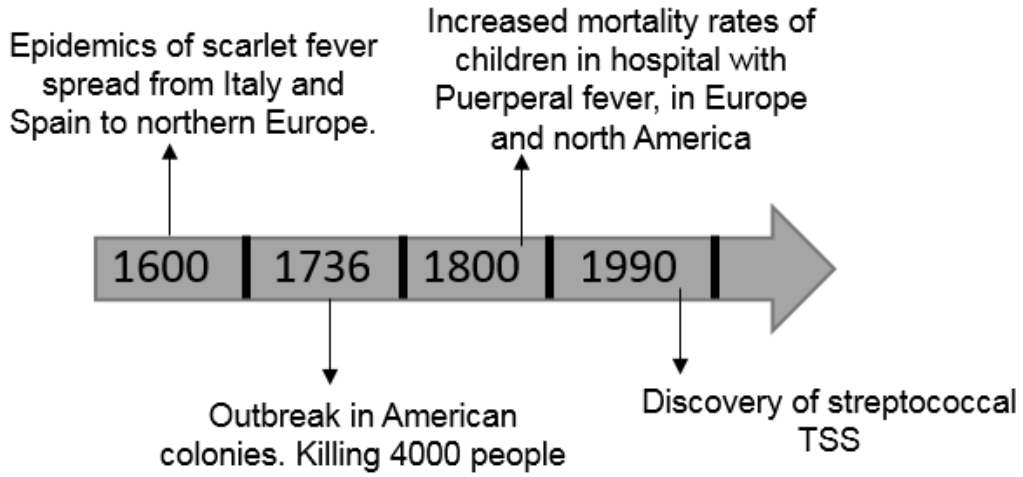

Figure 52. A timeline showing major *Streptococcal* outbreaks from the 16th century to the 20th century (Stevens, 1995, Ferretti 2016).

Group A *streptococcal* infections are currently increasing in the UK (chapter 1 section 1.4.7). The epidemiology of *streptococcal* infections is quite complex since there are more than 80 different serotypes of *Streptococcus pyogenes*. From the start of the 21st century there have been severe *streptococcal* infections, associated with shock and organ failure (Stevens, 2016).

2.1.1 Streptococcal toxic shock syndrome

Cases of severe *streptococcal* toxic shock syndrome (TSS) caused by group A *Streptococcus* have been reported since 1987. Hackett and Stevens (1992) reported a group A *streptococcal* infection outbreak in 1989, associated with renal failure, toxic shock and blood-borne bacteraemia that occurred in 20 people in outbreaks in Northern Europe and the US. Of the isolated strains of group A *Streptococcus*, 80% of these strains produce exotoxins (Stevens, 1995). Since then, similar cases have been reported in the United Kingdom. Genetic analyses has shown that strains having the speA gene (codes for exotoxin A) are more likely associated with TSS infection.

Another group A strain, known as *Streptococcus pyogenes* produces streptolysin-O; a toxin named in the 1980s, as one that belongs to the thiol-activated cytolysin group of toxins, later known as cholesterol binding toxins. Streptolysin-O was shown to be cardiocytotoxic and leukocytolytic both *in vitro* and *in vivo* (Reitz *et al.*, 1968, Bryant *et al.*, 1992). Hackett and Stevens (1992) have shown that toxic shock caused by streptolysin-O is mediated by the cytokines, tumour necrosis factor (TNFα) and interleukin (IL-1β). These cytokines have been shown to cause fever and induce shock. Signalling by these mediators occurs via transmembrane receptors known as toll-like receptors. Within the monocyte, nuclear factor-κβ (NF-κβ) is activated, which leads to the production of pro-inflammatory cytokines, TNFα and IL-1β. These mediators, including prostaglandins, leukotrienes and platelet-activating factor (Figure 53). Finally causing capillary leakage, production of adhesion molecules on the endothelial cells and neutrophils. Interaction between the neutrophils and endothelial cells causes endothelial injury through the release of neutrophil components. Neutrophils release nitric oxide, which is a vasodilator that leads to toxic shock syndrome that leads to sepsis (LaRosa, 2010).

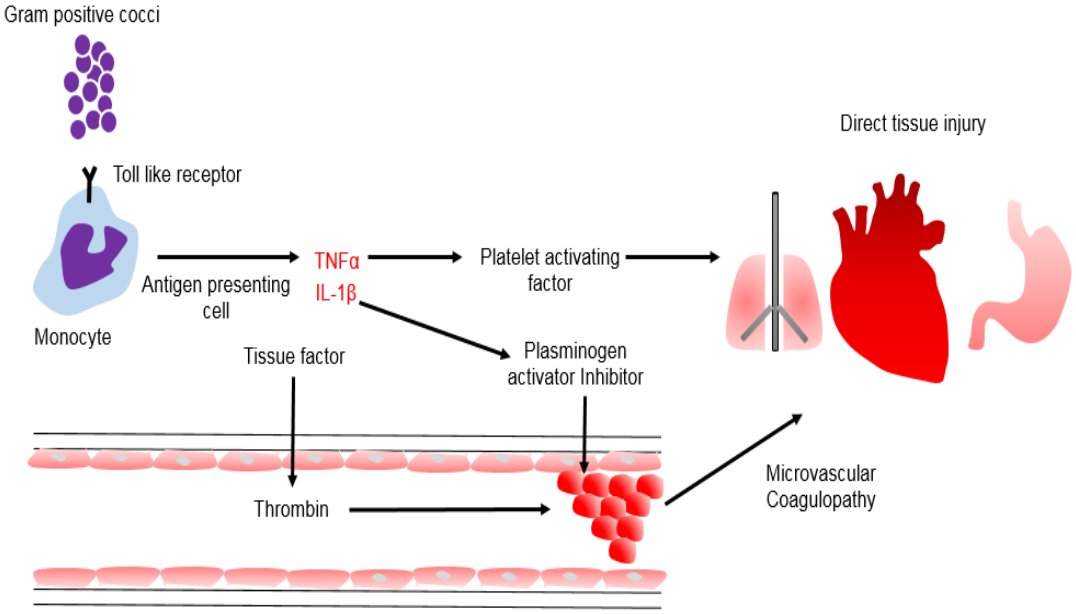

Figure 53. A diagrammatic representation of the role TNFα and IL-1β play in causing inflammation and coagulation, leading to toxic shock syndrome. The diagram was adapted from (LaRosa, 2010).

There are several symptoms that a patient could have during TSS. The initial symptom is severe pain and fever. Confusion is present in some patients. Many of the patients have clinical signs of soft tissue infection, such as swelling and erythema and 70% of these patients' progress to necrotizing fasciitis and sepsis.

2.1.2 PFTs

PFTs are produced by many pathogenic bacteria and are significant virulence factors. PFTs are the largest class of bacterial toxins form a major part of a class of pore forming proteins (Dal Peraro and van der Goot, 2016). These PFTs are highly conserved in bacteria and are an ancient family of proteins, present in all kingdoms of life. In the past, these proteins were viewed as toxins that form "pores in membranes". However, advances in the past decade have discovered the complex chemistry, and molecular mechanisms that surround pore formation in humans.

During bacterial invasion of epithelial barriers. PFTs target plasma membranes on cells. On binding, these toxins have the ability to alter the plasma membrane's permeability of their target cells, leading to leakage of intracellular contents and

ultimately cell death. These toxins are classified in two groups' α-PFTs and β-PFTs. The groups are named according to the secondary structure of the toxin, which is composed of either α-helices or β–barrels (Dal Peraro and van der Goot, 2016)**.** Different structures of these toxins have been discovered, which has led to the discovery of a range of strategies used by these proteins to traverse plasma membranes.

All currently discovered PFTs have specific targets on the plasma membrane, which are either lipids or proteins (Figure 55). The toxin exists as monomeric units when released by the bacteria. However, upon binding the monomer oligomerizes into either a α-helix or β-barrel. The α-helices family of toxins include enterotoxins of *Vibrio cholerae* and *Escherichia coli*, whereas the β-barrel family of toxins include α-haemolysin from *Staphylococcus aureus*, aerolysin from *Aeromonas hydrophila* and cholesterol-binding toxins of various other bacterial species. The α-helices family of toxins is well researched; therefore, the area of focus of this project is on toxins damaging the cellular membrane through formation of β-barrels (Gilbert, 2002).

2.1.2.1 β-barrels PFTs

The β-barrels family of toxins include the haemolysin family, aerolysin and cholesterol binding toxins. The haemolysin family of toxins are produced by *Staphylococcus aureus* and *Clostridium perfringens*. This family of toxins is described in chapter 3. The second family of toxins is the aerolysin family, which was the first discovered family in this class of toxins. Aerolysin is produced by *Aeromonas spp*. Others include α-toxin produced by *Clostridium septicum*, monalysin produced by *Pseudomonas entomophila* and parasporins produced by *Bacillus thuringiensis* (Gurcel *et al.*, 2006). Aerolysin from pathogens such as *Aeromonas hydrophila* work by disrupting epithelial barriers, which could lead to deep wound infections.

The final group of toxins under this family are cholesterol-binding toxins (CBTs). These toxins are identified in five genera of bacterium: *Streptococcus, Listeria, Clostridium, Bacillus* and *Arcanobacterium* (Alouf *et al.*, 2006) . The most prominent CBTs are streptolysin-O from *Streptococcus pyogenes*, perfringolysin from *Clostridium perfringens*, listeriolysin from *Listeria monocytogenes* and pneumolysin from *Streptococcus pneumoniae*. In general, CBTs act on the

cholesterol present in cell membranes. This chapter will mainly focus on the PFT streptolysin-O, as there is a great number of infection rates caused by *streptococcus* (Figure 8).

2.1.2.1.1 Streptolysin-O

Streptolysin-O is part of the CBTs group produced by the bacteria *Streptococcus pyogenes (*a group A *Streptococcus)*. This toxin is produced as a water-soluble monomer in the form of single chain polypeptide. It contains four domains, similar to other CBTs. There is one cysteine residue present in each molecule. Biochemical modification of this residue causes toxin inactivation (Walev *et al.*, 1995).

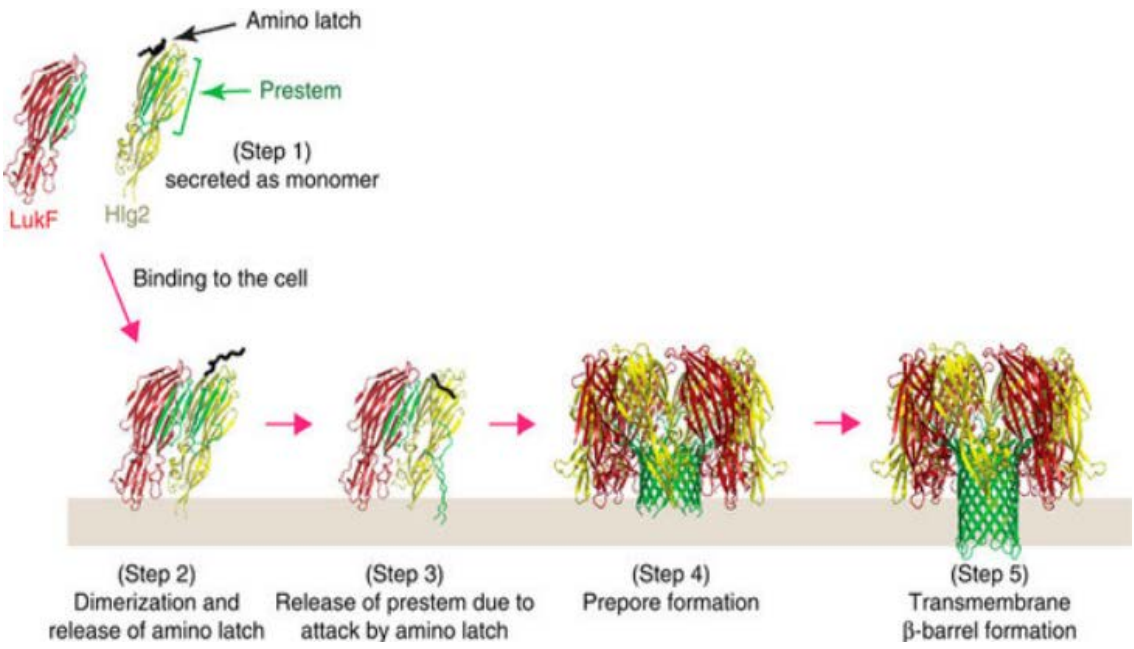

Figure 54. Molecular mechanism of pore formation. The image clearly describes pore formation in 5 steps. (Step 1) Binding, (Step 2) Dimerization, (Step 3) Release of the prestem, (Step 4) Prestem to prepore formation by the process of amino acid reorientation and (Step 5) Transmembrane pore formation (Yamashita *et al.*, 2014).

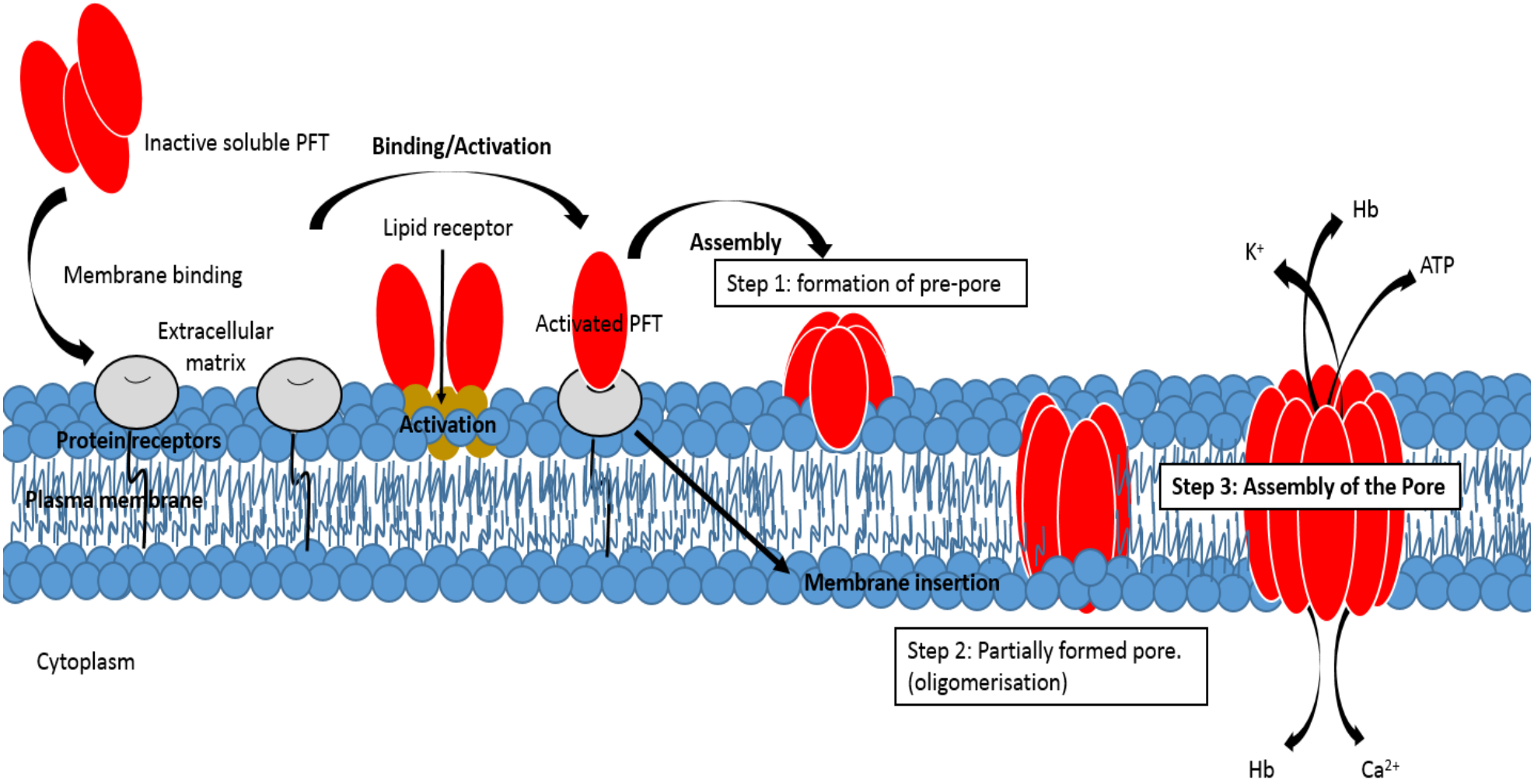

Figure 55. Diagrammatic representation of pore formation by PFTs. Diagrammatic representation of pore formation. PFTs specific for certain receptors, recognize the target site on the membrane, which are either lipids or proteins. The red colour represents alpha and beta chains of the protein structure, the blue colour represent phospholipid heads and tails and the yellow represents cholesterol in the membrane (Chhabria and Beeton, 2016).

The principal function of streptolysin-O is to disrupt host cell membranes. Streptolysin-O has four domains. Domain 4 contains an undecapeptide, which binds to cholesterol (Figure 56). After binding, between 35-50 streptolysin-O monomers oligomerize into ring-shaped pre-pores 30 nm wide, as depicted in Figure 55. Once the pre-pore is assembled, the domains undergo a conformational change from α-helices to insert β-sheets into the membrane forming a β-barrel pore in the membrane.

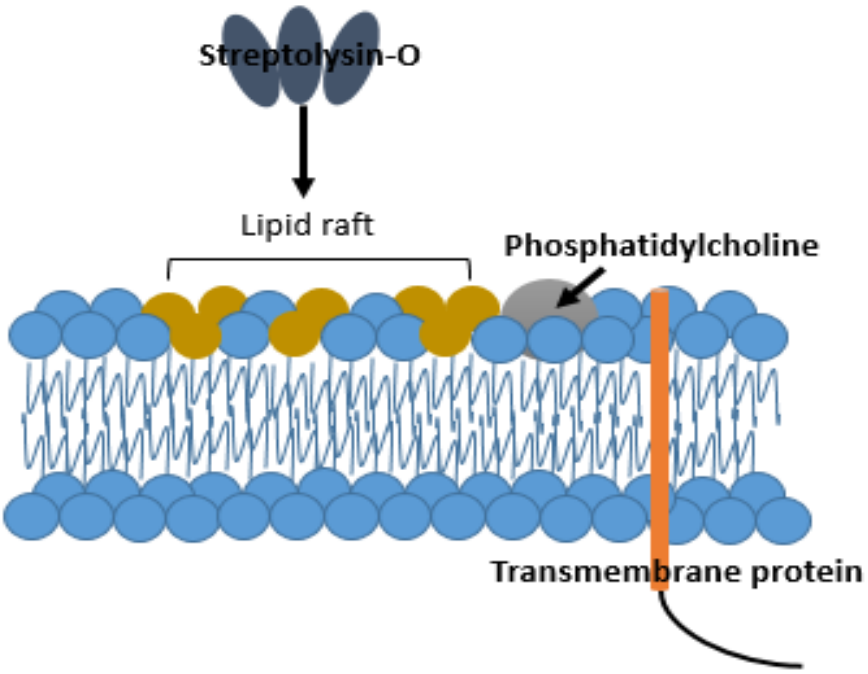

Figure 56. Diagrammatic representation of streptolysin-O (CBTs) have high affinity towards the lipid raft domain embedded in cholesterol. The dark blue represents the PFT, streptolysin-O, The yellow represents cholesterol in the membrane, the grey represents a type of phospholipid (phosphatidylcholine), the blue represents phospholipid heads and tails and the orange represents a transmembrane protein

2.2 Material and methods

All chemicals were analytical grade and purchased from Fisher scientific UK Ltd (Loughborough, UK), Sigma-Aldrich Ltd (Dorset, England), Diagnostic Reagents Ltd, (Oxon, England) and TCS biosciences (Buckingham, UK)

2.2.1 Concentration dependent haemolysis assay

The haemolysis assay is adopted form Duncan (1974) and Bernheimer (1988), and was optimized here to simulate human physiological conditions. This assay aims to test lysis of mammalian erythrocytes at different concentrations of streptolysin-O. Washed mammalian blood (ovine, porcine, murine and leporine) was diluted with PBS (137mM NaCl, 2mM KH_2PO_4, 8mM Na_2HPO_4) to make a 2% (v/v) erythrocyte suspension. 25 ml of this 2% erythrocyte suspension was incubated at 37°C in a water bath for 1 hour. At the same time, 10 ml Drabkins reagent was separately heated to 37°C for 1 hour. Streptolysin-O (0.2 mg/ml) was diluted with PBS and 0.01M L-cysteine (0.121 g added to 100 ml PBS) to make a stock of 2000 ng/ml. The stock was diluted to produce the concentrations shown in Table 12. L-cysteine was used as a reducing agent in the buffer as streptolysin-O is oxygen labile.

Table 12. Preparation of different concentrations of streptolysin-O diluted with PBS and 0.01M L-cysteine to produce the following concentrations

No	Volume of streptolysin-O Stock (µl)	Volume of PBS+L-cysteine buffer (µl)	Total volume (µl)	Final concentration of streptolysin-O (ng/ml)
1	6	44	50	250
2	12	38	50	500
3	19	31	50	750
4	25	25	50	1000
5	31	19	50	1250
6	38	12	50	1500
7	44	6	50	1750
8	50	0	50	2000

For each concentration shown in Table 12, 50 µl of streptolysin-O was added to an Eppendorf tube containing 500 µl 2% erythrocyte suspension (Figure 57). The tubes were allowed to incubate for 30 minutes at 37°C.

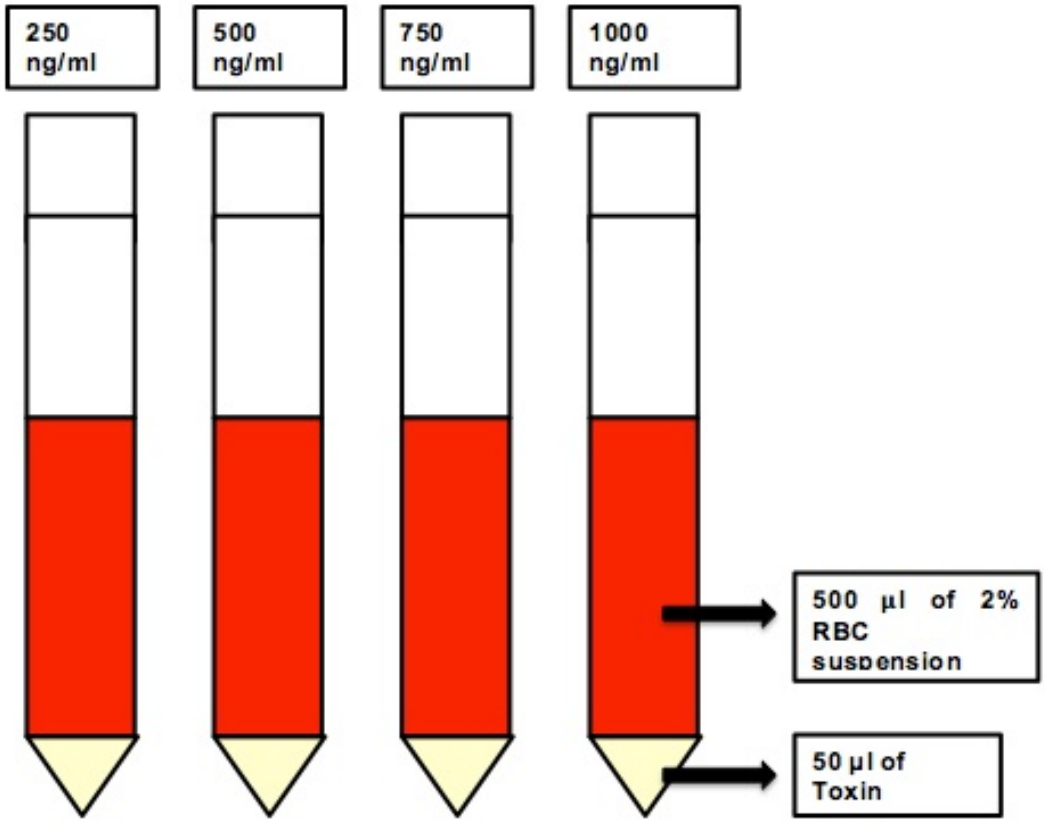

Figure 57. A diagrammatic representation of the volumes of streptolysin-O and 2% erythrocyte suspension present in the Eppendorf tubes. These solutions are then incubated at 37°C for 30 minutes.

The tubes were then centrifuged for 5 minutes at 900 x g in an Eppendorf 540R microcentrifuge at 4°C (Duncan, 1974). This temperature stopped the reaction. 20 µl of this supernatant is added to 4 ml of Drabkins reagent and was allowed to stand for 15 minutes (Bhakdi and Tranum-Jensen, 1987). The absorbance was assayed at 540 nm using a Jenway spectrophotometer

2.2.2 Time dependent haemolysis assay

The washed animal blood (ovine, porcine, murine and leporine) was diluted with PBS to make a 2% erythrocyte (v/v) suspension. The 2% erythrocyte suspension and the Drabkins reagent were incubated at 37°C in a water bath for 1 hour. 6 µl of streptolysin-O was diluted with 994 µl of PBS and 0.01 M L-cysteine to make a concentration of 1230 ng/ml (estimated physiological concentration during infection) from a 0.2 mg/ml stock solution of streptolysin-O, with a total volume of 1 ml (Alouf, 1980). The tubes were prepared according to the table below:

Table 13- Concertation of streptolysin-O and incubation time of each test sample prepared in the assay

Tube no	Incubation time for test sample (mins)	Final streptolysin-O concentration (ng/ml)
1	10	1230
2	20	1230
3	30	1230
4	40	1230
5	50	1230
6	60	1230

The ratio of toxin to blood was added according to Figure 57. Each tube that was prepared was incubated at 37°C in a water bath for a particular amount of time shown from Table 13. The tubes were then centrifuged for 5 minutes at 900 x g in a microcentrifuge at 4°C, which stopped the reaction. 20 µl of the supernatant was added to 4 ml of Drabkins reagent and was allowed to stand for 15 minutes (Bernheimer, 1974). The absorbance was assayed at 540 nm.

2.2.3 Toxin adsorption studies

This method is adopted from Hu *et al.* (2013) and optimized to achieve desired conditions. This test aimed to test nanosponges and its components as a toxin adsorbing system under different temperatures. Ovine blood was chosen for these studies as ovine erythrocytes showed maximum susceptibility towards streptolysin-O lysis compared to leporine, murine and porcine blood.

2.2.3.1 Testing the efficacy of erythrocyte ghosts as a toxin adsorbing system

Absorption of streptolysin-O by erythrocyte ghosts was tested using a novel assay. Washed ovine blood was diluted to make a 2% (v/v) erythrocyte suspension, 2% (v/v) erythrocyte ghost suspension and a 2% (v/v) mixed (ghosts and erythrocytes) RBC suspension Figure 58. The 2% erythrocyte ghost suspension was made by adding 2 parts of washed blood to 98 parts of hypotonic buffer (9.64mM NaCl, 1.20mM KH_2PO_4, 1mM EDTA and 3.61mM Na_2HPO_4). This buffer was used to lyse erythrocytes to synthesize the erythrocyte ghosts. The erythrocyte ghost pellet was washed three times with isotonic PBS and then reconstituted in it. The 2% mixed erythrocyte suspension was made by adding 1 part of the 2% erythrocyte suspension to 1 part of the 2% erythrocyte ghost suspension. 1230 ng/ml (estimated human physiological concentration) of streptolysin-O was added to the 3 suspensions and incubated in a water bath at 37°C for 30 mins. The suspensions were then centrifuged for 5 minutes at 900 x g in an Eppendorf microcentrifuge (Arlington business park, Stevenage, UK) at 4°C. The concentration of Hb was measured by adding 20 µl of the supernatant to 4 ml Drabkins reagent and the solution was allowed to stand for 15 minutes. The optical density was read at 540 nm (**Hb A**). 250 µl of the supernatant was aspirated using a Pasteur pipette from each system and added to a separate 2% erythrocyte suspension, which was incubated for 30 mins at 37°C. The tubes were then centrifuged at 4°C for 5 minutes at 900 x g. 20 µl of the supernatant is added to 4 ml of Drabkins reagent and was allowed to stand for 15 minutes. The optical density was then assayed at 540 nm (**Hb B**). The Concentration of Hb released by unbound toxin was measured by subtracting Hb A from Hb B.

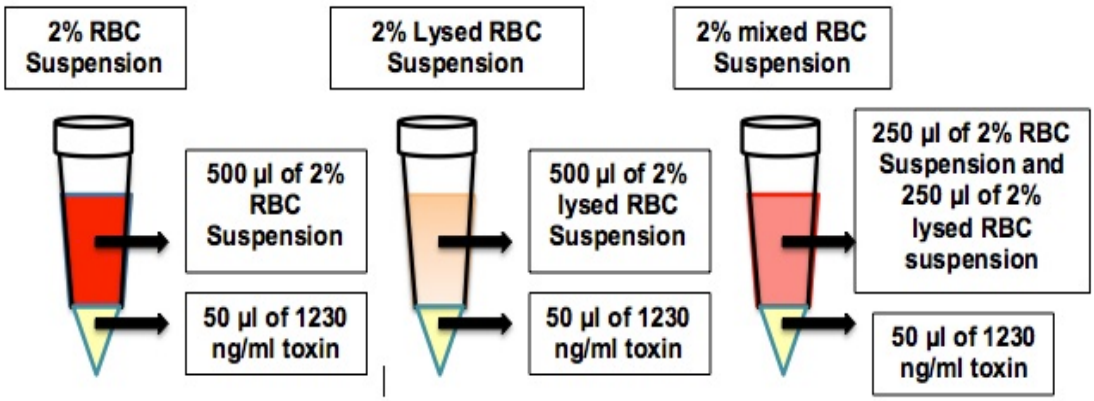

Figure 58. Diagrammatic representation of the volumes of streptolysin-O and 2% RBC suspension present in the three different solutions. The three suspensions were then incubated at 37°C in a water bath for 30 minutes.

2.2.3.2 Testing the efficacy of ovine nanosponges as a toxin adsorbing system

Toxin absorption by nanosponges were tested using a published method (Hu *et al.*, 2013). A 0.2 mg/ml solution of streptolysin-O was diluted to 1230 ng/ml (sheep physiological concentration at which 50% of the erythrocytes were lysed) by adding 6 µl of the 0.2 mg/ml stock to 994 µl of PBS and 0.01M L-cysteine. L-cysteine was added as a reducing agent, cause streptolysin-O is sensitive towards oxygen .50 µl of a 1230 ng/ml streptolysin-O solution was added to four test systems as shown in Figure 59. The total volume in the four different systems was 550 µl. The four systems were then incubated in a controlled water bath at 37°C. After 30 minutes of incubation, the four systems were then centrifuged for 5 minutes at 900 x g using a microcentrifuge at 4°C. This temperature stopped the reaction. 20 µl of this supernatant is added to 4 ml of Drabkins reagent and was allowed to stand for 15 minutes. The absorbance was assayed at 540 nm using a spectrophotometer. This assay was repeated at 40°C, which emulated the elevated body temperature during sepsis (Lee *et al.*, 2012)

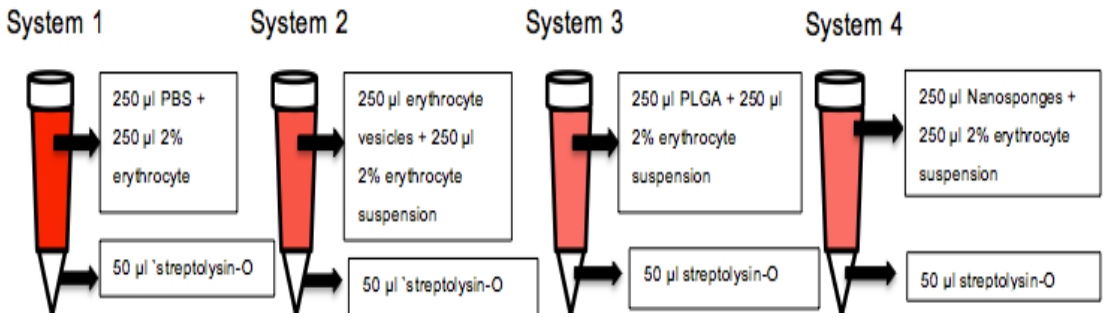

Figure 59. A diagrammatic representation of the volumes of streptolysin-O and 2% erythrocyte suspension present in the four different systems. The four different suspensions were then incubated at 37°C and 40°C in a water bath for 30 minutes.

2.2.3.3 Testing the efficacy of reconstituted ovine nanosponges as a toxin adsorbing system

Nanosponges at a concentration of 1 mg/ml were lyophilized using the lyophilization method stated in section 1.5.13. One batch of the lyophilized nanosponges were stored at 4°C for a week and the second batch was stored for 6 months at 4°C. After a week of storage, nanosponges were reconstituted with 1 ml of isotonic PBS (pH 7.2). Nanosponges were characterized for size and zeta potential, using a Nano-zs zetasizer. Nanosponges at a concentration of 1mg/ml were tested for their ability to adsorb 1230 ng/ml streptolysin-O. 50 µl of a 1230 ng/ml streptolysin-O solution was added to 4 test systems shown in Figure 59. The four systems were then incubated in a controlled water bath at 40°C. After 30 minutes of incubation, the 4 systems were then centrifuged for 5 minutes at 900 x g at 4°C. 20 µl of this supernatant was added to 4 ml of Drabkins reagent and was allowed to stand for 15 minutes. The absorbance was assayed at 540 nm using a spectrophotometer.

2.2.3.4 Ovine nanosponge dose dependent study

A stock solution of 0.2 mg/ml nanosponges was diluted with isotonic PBS (pH 7.2) to produce the concentrations shown in Table 14.

Table 14- Volume of ovine nanosponge stock solution and PBS added to prepare the following concentrations of ovine nanosponges.

No.	Volume from nanosponge stock (µl)	Volume of PBS diluent (µl)	Total volume (ml)	Final concentration of ovine nanosponges (ng/ml)
1	10	990	1	2000
2	20	980	1	4000
3	30	970	1	6000
4	40	960	1	8000
5	50	950	1	10000

A 2% ovine erythrocyte suspension was prepared along with the Drabkins reagent and was incubated at 40°C. 50 µl streptolysin-O at a concentration of 1230 ng/ml was added to 250 µl 2% erythrocyte suspension, to which 250 µl of the prepared concentrations of nanosponges were added (Table 14). The five suspensions, each containing different concentrations of nanosponges were incubated in a temperature controlled water bath at 40°C. After 30 minutes of incubation, the five suspensions were then centrifuged for 5 minutes at 900 x g at 4°C. 20 µl of this supernatant was added to 4 ml of Drabkins reagent and was allowed to stand for 15 minutes. The absorbance was assayed at 540 nm using a spectrophotometer.

2.2.3.5 Adsorption of increasing concentrations of streptolysin-O by 1mg/ml ovine nanosponges.

This method aims to test the efficacy of ovine nanosponges to adsorb increasing concentrations of streptolysin-O. A 0.2 mg/ml streptolysin-O stock solution was diluted with PBS and L-cysteine to prepare the following concentrations:

Table 15- The volume from a stock solution and diluent to prepare the following streptolysin-O concentrations

No	Volume streptolysin-O stock (µl)	Vole of PBS diluent (µl)	Total volume (µl)	Final concentration of streptolysin-O (µg/ml)
1	25	225	250	20
2	50	200	250	40
3	75	175	250	60
4	100	150	250	80
5	125	125	250	100

A 2% (v/v) ovine erythrocyte suspension was prepared along with the Drabkins reagent and was incubated at 40°C. 25 µl streptolysin-O at different concentrations (Table 15) were added to 125 µl 2% (v/v) erythrocyte suspension, to which 125 µl of the 1mg/ml ovine nanosponges were added. The five suspensions, each containing different concentrations of streptolysin-O were incubated in a temperature controlled water bath at 40°C. After 30 minutes of incubation, the five suspensions were then centrifuged for 5 minutes at 900 x g at 4°C. 20 µl of this supernatant was added to 4 ml of Drabkins reagent and was allowed to stand for 15 minutes. The absorbance was assayed at 540 nm using a spectrophotometer.

2.2.4 Cholesterol assay

The aim of this method was to quantify the concentration of cholesterol present in 2% erythrocyte suspensions from the four chosen mammalian species. This protocol makes use of a Sigma-Aldrich cholesterol quantitation kit and works by using cholesterol esterase, which hydrolyzes cholesteryl esters to cholesterol. A probe is added to the mix which, upon detection of cholesterol generates a pink colour.

2.2.4.1 Quantification of cholesterol in mammalian blood

The cholesterol quantitation kit included 25 ml cholesterol assay buffer, 0.2 ml cholesterol probe, 1 vial enzyme mix, 1 vial cholesterol esterase and 0.1 ml cholesterol standard (2 µg/µl). The assay could be used for 100 reactions. The cholesterol assay buffer was allowed to come down to room temperature before use. The enzyme mix and cholesterol esterase were reconstituted with 220 µl cholesterol assay buffer and kept on ice. 20 µl of the 2 µg/µl cholesterol standard was diluted with 140 µl cholesterol assay buffer to produce a stock of 0.25 µg/µl. A standard curve was plotted based on the reaction volumes shown in the appendix section 2.5.2. Reactants in in each well were denoted by abbreviations. Cholesterol standard (S), cholesterol assay buffer (CAB), cholesterol probe (P), enzyme mix (EM) and cholesterol esterase (CE). The total volume in each reaction well was 50 µl. Row 1 of the 96 well plate was used to measure background (appendix section 2.5.2). From rows 2-6, increasing volumes of the standard solution was added to produce a standard curve. After addition of the reactants the plate was incubated at 37°C for 30 minutes to allow the reaction to start. The reaction was measured for absorbance at 570 nm using a FLUOstar Omega UV/Vis plate reader (Allmendgruen, Ortenberg, Germany). The enzyme mix, cholesterol esterase, cholesterol probe, cholesterol and cholesterol assay buffer were aliquoted and stored at -20°C.

2.2.4.2 Sample preparation and measurement

Four mammalian blood species (ovine, murine, leporine and porcine) were measured for cholesterol using this assay. The whole blood was washed using the washing procedure describe in section 1.5.1. The erythrocyte suspension

was diluted with isotonic PBS (pH 7.2) to produce a 2% (v/v) erythrocyte suspension. The suspension was centrifuged at 900 x g using a microcentrifuge at 4°C. An extraction solution was prepared to extract cholesterol from the pelleted erythrocytes. The extraction solution contained a mix of 7 ml chloroform, 11 ml isopropanol and 0.1 ml triton x-100. 200 µl of the extraction solution was added to the pelleted erythrocytes. The tube containing the extraction solution and the erythrocytes was vortexed for 2 minutes. The tube was then centrifuged at 13000 x g for 10 minutes using a microcentrifuge, which pelleted the insoluble material. The supernatant, which contained the extracted cholesterol was pipetted into an Eppendorf tube. The Eppendorf tube containing the supernatant was placed on to a Thermo scientific heat block at 50°C, which allowed evaporation of the extraction solution. The dried cholesterol was kept in a desiccator overnight, which removed moisture from the sample. The dried cholesterol was reconstituted back to its original volume with cholesterol assay buffer. The sample was kept in a UW water bath sonicator (50-60 hertz) for 20 minutes. The sample was assayed in a 96 well plate as shown in the appendix section 2.5.2.

2.2.5 Incorporation of cholesterol into ovine nanosponges

This method was adopted form Briuglia *et al.* (2015) and optimised to synthesize the nanosponge formulations shown in Table 16. The aim of this protocol was to incorporate different concentration of cholesterol into ovine nanosponges and test the adsorption of streptolysin-O by these nanosponges. Ovine blood was washed, using the washing protocol described in section 1.5.1. 500 µl of ovine erythrocytes were lysed using a hypotonic buffer to synthesize ovine erythrocyte ghosts (section 1.5.3). The erythrocyte ghost pellet was dissolved in 200 µl extraction solution. The tube containing the erythrocyte ghost pellet and the extraction solution was vortexed for 2 minutes. The sample was centrifuged at 13000 x g using a microcentrifuge, which pelleted the insoluble material. The supernatant was transferred to another Eppendorf tube (**solution A**). 5 mg of cholesterol was dissolved in 200 µl extraction solution to yield a 25 mg/ml stock solution (**solution B**). Solution A was mixed with solution B to produced ovine nanosponges with different concentration of cholesterol, as shown from Table 16.

Table 16- Amount of solution A and B to produce ovine nanosponges with different concentrations of cholesterol.

Nanosponge formulations	Volume of solution A (µl)	Volume of solution B (µl)	Volume of Chloroform (µl)	Total volume (µl)
NS1	200	50	50	300
NS2	200	75	25	300
NS3	200	100	0	300
Control	300	0	0	300

Solution A= Ovine erythrocyte ghosts dissolved in extraction buffer
Solution B= 25 mg/ml cholesterol stock solution

The control ovine nanosponges were prepared according to the method above (section 1.5.11). NS1, NS2 and NS3 were kept in a Thermo scientific heat block at 50°C. The dried nanosponges were kept in a desiccator overnight. The dried nanosponge samples were reconstituted back to their original volume with isotonic PBS (pH 7.2). The samples were then centrifuged for 10 minutes at 13000 x g using a microcentrifuge; this allowed removal of any unincorporated cholesterol. This step was repeated three times. The samples were placed in a water bath sonicator (50-60 hertz) for 20 minutes. Each of the nanosponge formulations were then serially extruded through a 400 nm and 100 nm polycarbonate membrane, with a solution containing 0.2 mg/ml PLGA polymer. The quantitation of cholesterol was measured as shown in section 2.2.4.2 and adsorption of streptolysin-O by cholesterol incorporated nanosponges was conducted according to the method shown in section 2.2.3.2.

2.2.6 Phospholipid assay

The aim of this method was to investigate if phospholipids were lost during the synthesis of ovine nanosponges. The phospholipid quantification kit was purchased from Sigma-Aldrich. The kit provides a simple direct throughput assay for measuring choline containing phospholipids in biological samples. Using the assay, phospholipids were enzymatically hydrolysed to release choline, which was determined using choline oxidase and a hydrogen peroxide dye. Since ovine blood was used to synthesise nanosponges, the kit was used on ovine blood.

2.2.6.1 Phospholipid standard preparation

The phospholipid quantitation kit included 10 ml assay buffer (AB), 120 µl dye reagent (DR), 1 vial enzyme mix (EM), 120 µl phospholipase D (PLD) and 400 µl 2mM phosphatidylcholine standard (PS). The assay could be used for 100 reactions. The assay buffer was equilibrated to room temperature before use; all the other reactants were thawed and kept on ice. The enzyme mix was reconstituted with 120 µl assay buffer and kept on ice. The assay was conducted in a Fisher-Scientific flat-bottomed 96 well plate. 24 µl of the 2mM phosphatidylcholine standard was added to 216 µl of ultra-pure water to prepare a 200 µM standard. 0, 30, 60 and 100 µl was added to separate tubes. Ultrapure water was added to each tube to bring the final volume to 100 µl. This generated four different concentrations 0 (blank), 60, 120 and 200 µM standards. A standard curve was plotted based on the reaction volumes shown in the appendix section 2.5.2 Reactants in each well were denoted by abbreviations. The total volume in each reaction well was 88 µl. The plate was kept away from light and incubated at room temperature for 30 minutes. The reaction was measured for absorbance at 570 nm using a FLUOstar Omega UV/Vis plate reader. The enzyme mix, cholesterol esterase, cholesterol probe, cholesterol and cholesterol assay buffer were aliquoted and stored at -20°C.

2.2.6.2 Sample preparation and measurement

Synthesis of ovine nanosponges required the use of ovine blood. The ovine blood was subjected to hypotonic lysis, which produced ovine erythrocyte ghosts. The ovine erythrocyte ghosts were subjected to sonication and extrusion to synthesize ovine erythrocyte vesicles. The vesicles were extruded with the PLGA cores to synthesize ovine nanosponges. The quantification of phospholipids was estimated with each of these systems, to investigate the loss of lipids during preparation of ovine nanosponges. Ovine blood was washed using the washing procedure describe in section 1.5.1. 500 µl of the erythrocyte suspension was added to 2 ml of an extraction buffer. The extraction buffer was prepared to extract lipids from the pelleted erythrocytes. The extraction solution contained a mix of 7 ml chloroform, 11 ml isopropanol and 0.1 ml triton x-100. The tube containing the extraction solution and the erythrocytes was vortexed for 2

minutes. The tube was centrifuged at 13000 x g for 10 minutes using a microcentrifuge, which pelleted the insoluble material. The supernatant, which contained the extracted lipids, was pipetted into an Eppendorf tube. The Eppendorf tube containing the supernatant was placed on to a Thermo scientific heat block at 50°C, which allowed evaporation of the extraction solution. The dried lipid was kept in a desiccator overnight, which removed moisture from the sample. The dried lipid was reconstituted back to its original volume with assay buffer. The sample was kept in a UW water bath sonicator (50-60 hertz) for 20 minutes. The sample was assayed in a 96 well plate as shown in the appendix section 2.5.2. This protocol was repeated with ovine erythrocyte ghosts, erythrocyte vesicles and nanosponges.

2.3 Results

2.3.1 Streptolysin-O haemolysis assay

2.3.1.1 Concentration dependent assay

Streptolysin-O was assayed for release of haemoglobin against four different mammalian species. From each of these mammalian species a 2% erythrocyte suspension was prepared, to which increasing concentrations of streptolysin-O was added. The suspensions were incubated at 37°C for 30 minutes. The suspensions were then centrifuged at 4°C, which separated the whole ovine erythrocytes cells from the released Hb. The released Hb present in the supernatant was assayed for at an absorbance at 540 nm. The measured Hb was estimated using a bovine Hb standard curve shown from Figure 30. Haemolysis of the suspensions were calculated as a percentage of the total amount of Hb present in the system, since each mammalian blood species has a different amount of Hb present in their system. According to Figure 60, as the concentration of streptolysin-O increases, the concentration of Hb increases for all tested mammalian species. There was a sequential difference between the mammalian blood in terms of lysis by streptolysin-O. This was murine>ovine>porcine>leporine up to 1250 ng/ml. Above 1250 ng/ml the sequence was ovine > murine >porcine>leporine, up to 2000 ng/ml streptolysin-O. The 2000 ng/ml had the highest lysis of ovine erythrocytes at 80% release of haemoglobin (±1.40). This concentration of Hb release quantified in Figure 60 is shown qualitatively from Figure 61.

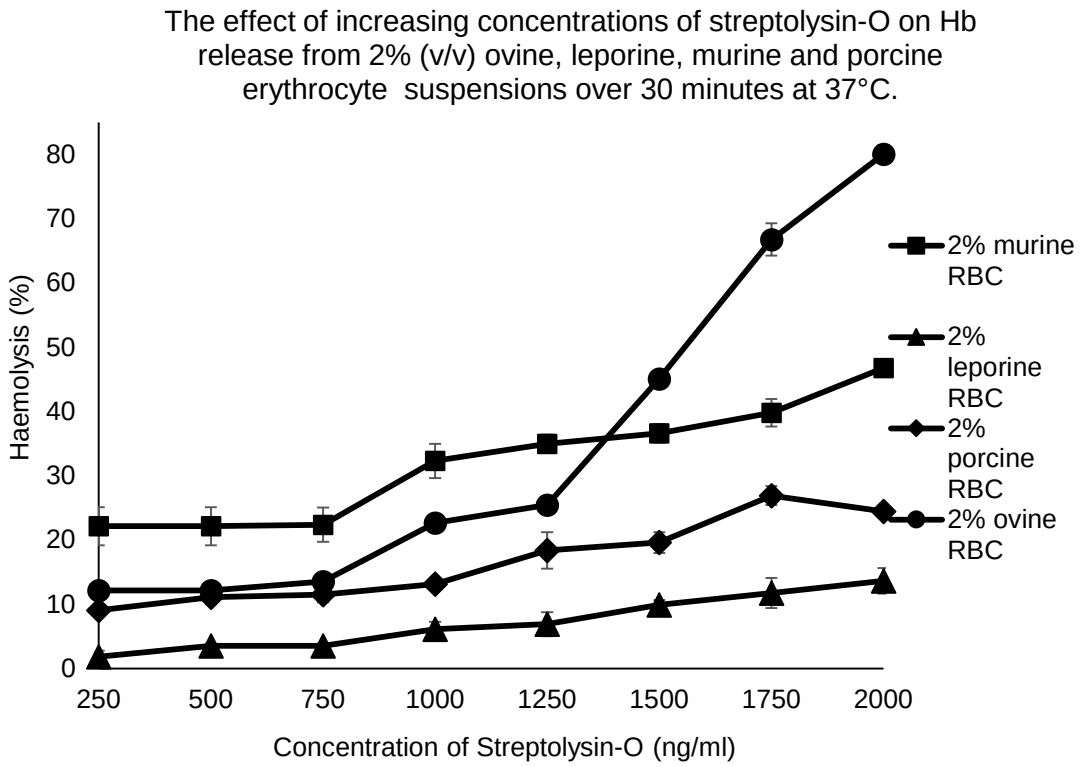

Figure 60. The effect of increasing concentration of streptolysin-O on Hb release from four different types of mammalian blood. The total Hb present in the 2% mammalian suspensions: leporine (2.67 g/dl, ± 0.07), murine (1.87 g/dl, ± 0.07), ovine (1.43 g/dl, ± 0.09) and porcine (2.47 g/dl, ± 0.32). Error bars represent SEM (n=3). R^2 values were measured for the respective mammalian blood types. Murine (R^2=0.935), leporine (R^2=0.970), porcine (R^2=0.913) and ovine (R^2=0.871). Refer to the appendix section 2.5.1, for concentration of Hb release in “g/dl”.

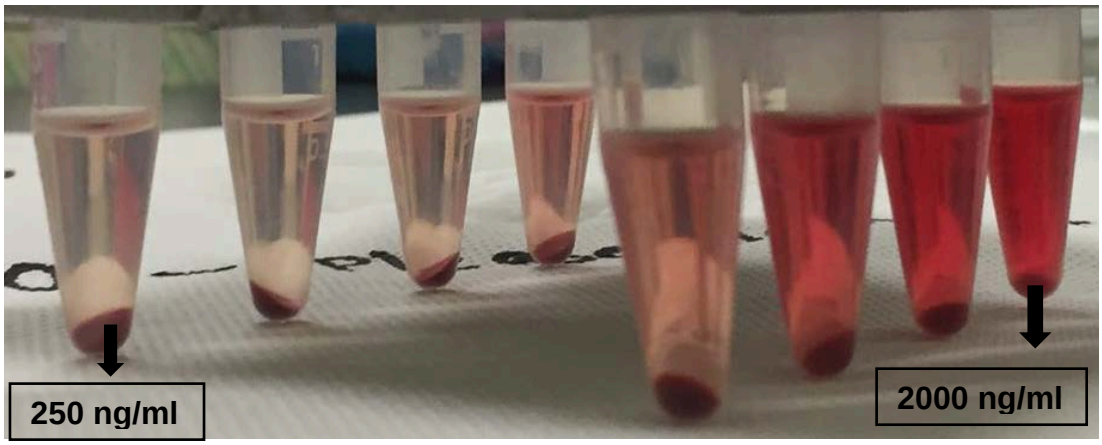

Figure 61. An image taken with a Nikon camera shows eight Eppendorf tubes, with increasing concentrations of Hb present in the supernatant. The first tube with the lowest intensity of red has a concentration of 250 ng/ml streptolysin-O, whereas the last tube has a concentration of 2000 ng/ml.

2.3.1.2 Time dependent assay

Similar to the concentration dependent assay, streptolysin-O was assayed against four different mammalian blood, with respect to time. The released Hb present in the supernatant was assayed for absorbance at 540 nm. The measured Hb was estimated using a bovine Hb standard curve shown in Figure 30. The suspensions were incubated for 60 minutes at 37°C. Haemolysis of the suspensions was calculated as a percentage of the total amount of Hb present in the system. Figure 62 shows the effect 1230 ng/ml streptolysin-O has on four different mammalian blood during 60 minutes of incubation at 37°C. After 60 minutes, ovine erythrocytes showed maximum susceptibility towards streptolysin-O haemolysis, as at 60 minutes streptolysin-O released 91.9% (±1.39) Hb as opposed to porcine and leporine Hb release. Similar to the concentration dependent haemolysis assay, murine erythrocytes were more susceptible to haemolysis by streptolysin-O, compared to leporine and porcine erythrocytes, as after 60 minutes of incubation streptolysin-O released 53.2% (±1.42) Hb.

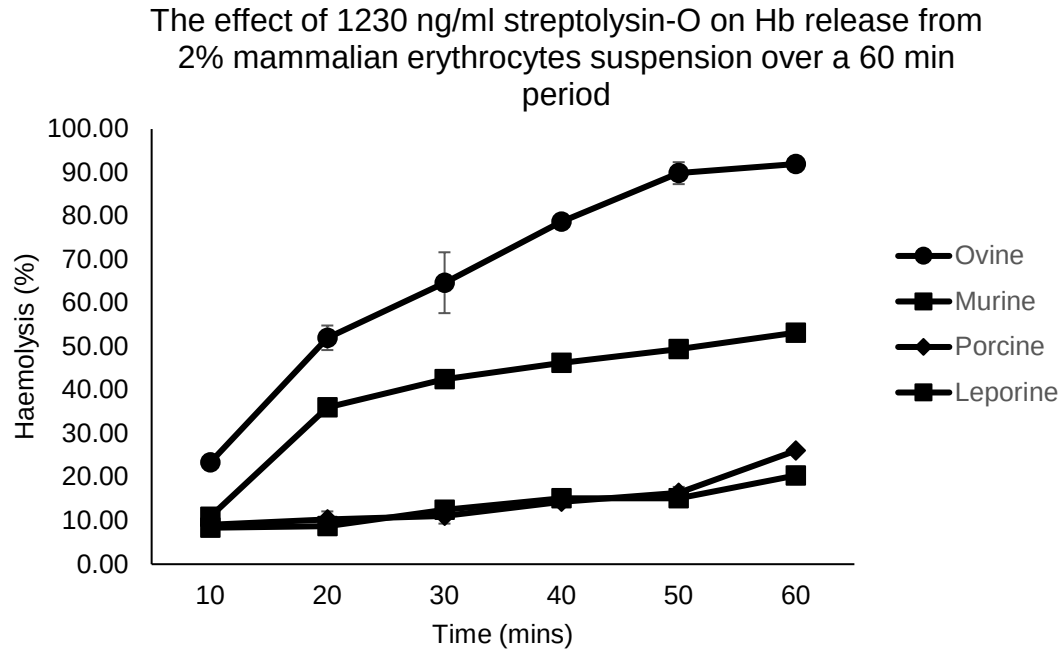

Figure 62. The effect of 1230 ng/ml (human physiological concentration) of streptolysin-O on a 2% (v/v) mammalian erythrocyte suspensions over a 60 minute time period. The Hb concentration was measured at 540 nm using Drabkins reagent. Leporine (2.67 g/dl, ± 0.07), murine (1.87 g/dl, ± 0.07), ovine (1.43 g/dl, ± 0.09) and porcine (2.47 g/dl, ± 0.32). Error bars represent SEM (n=3). R^2 values were measured for the respective mammalian blood types. Murine (R^2=0.796), leporine (R^2=0.933), porcine (R^2=0.825) and ovine (R^2=0.925)

2.3.2 Streptolysin-O adsorption assays

Streptolysin-O absorption was tested using ovine nanosponges, vesicles and PLGA. Figure 63 shows that ovine erythrocyte ghosts had the ability to absorb streptolysin-O. This test involved the addition of supernatant containing unbound toxin to a 2% erythrocyte suspension. This was shown by the degree of haemolysis. The system that contained 2% ovine RBC had the highest concentration of Hb release at 0.45 g/dl (± 0.05) compared to the system that contained 2% ghosts, which had the least Hb release at 0.30 g/dl (± 0.03). The system that contained a mixture of the ovine RBC and the ghost had nearly half the Hb release of the 2% ovine RBC system (0.36 g/dl, ± 0.03). These results

were compared to a positive control, which involved the addition of 0.1% Triton x-100 to the 3 different suspensions. This suspension has the ability to solubilize lipids, thereby releasing maximum amount of Hb from the erythrocytes and ghosts.

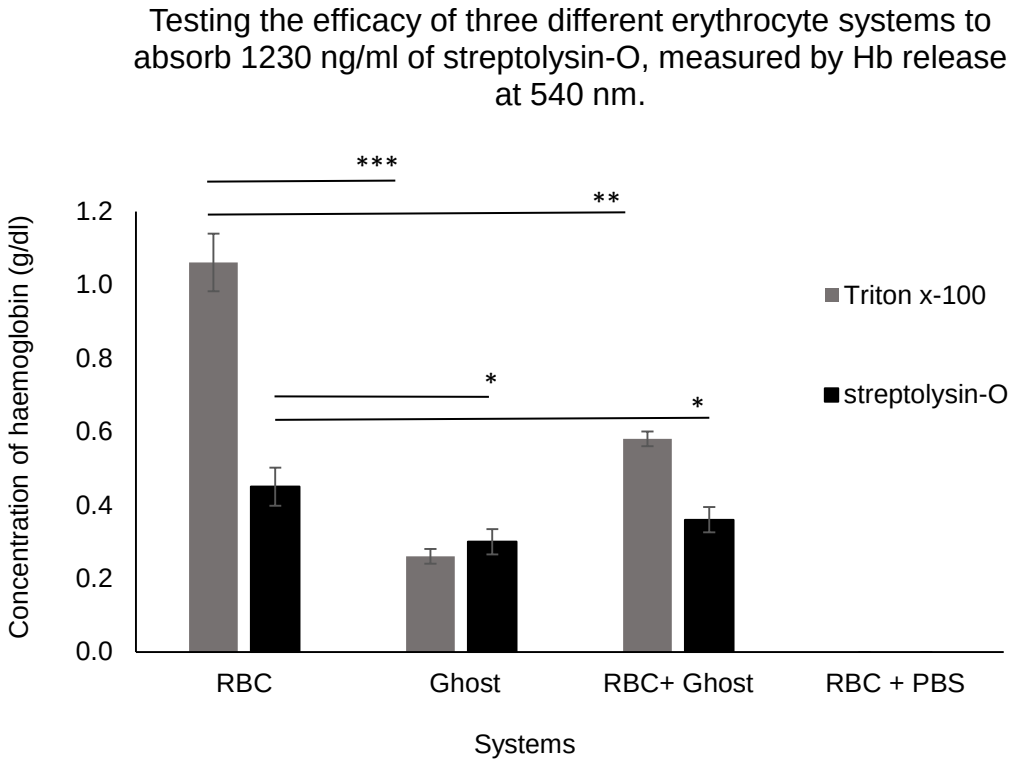

Figure 63. Testing absorption of 1230 ng/ml streptolysin-O by ovine erythrocyte ghosts. These systems were incubated at 37°C for 30 minutes. Adsorption of streptolysin-O was measured by degree of haemolysis at 540 nm. Maximum Hb released from a 2% (v/v) ovine erythrocyte suspension was 1.5 g/dl."*"P≤0.05, "**"P≤0.01 and "***"P≤0.001. The results that do not contain "*" symbol are not significant. .Error bars represent SEM (n=3).

The ovine erythrocyte ghosts were sonicated to produce ovine erythrocyte vesicles, which were extruded with the PLGA polymer to produce ovine nanosponges. Figure 64 shows the efficacy of the nanosponge and its components to absorb streptolysin-O. This was tested by adding the streptolysin-O and 2% ovine erythrocytes to systems containing the PLGA polymer, vesicles and nanosponges, which were incubated at 37°C for 30 minutes. Absorption was measured by concentration of Hb release, as shown in Figure 65.

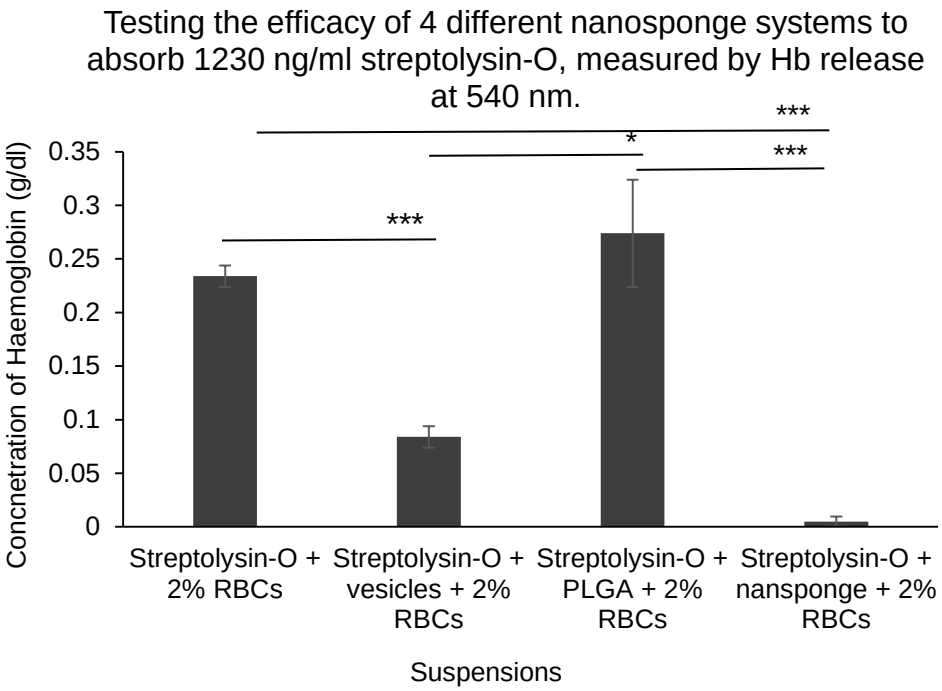

Figure 64. Testing the efficacy of ovine nanosponges and its components to adsorb 1230 ng/ml streptolysin-O, incubated at 37°C. Adsorption of streptolysin-O was measured by degree of haemolysis at 540 nm. "*"P≤0.05, "**"P≤0.01 and "***"P≤0.001. Error bars represent SEM (n=3).

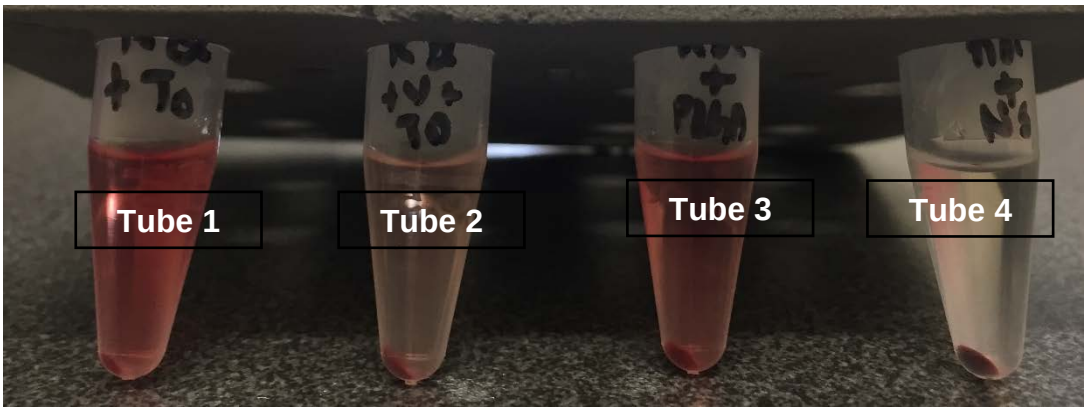

Figure 65. Testing the efficacy of the nanosponge and its components as a toxin absorption system. An image taken with a Nikon camera shows 4 Eppendorf tubes with increasing concentrations of Hb present in the supernatant after incubation at 37°C for 30 minutes and then centrifugation at 956x g. (increase in concentration of Hb is shown by the increased intensity of the red colour). Left to right: (Tube 1) 2% ovine erythrocytes+streptolysin-O+PBS, (Tube 2) 2% ovine erythrocytes+streptolysin-O+vesicles, (Tube 3) 2% ovine erythrocytes+streptolysin-O+PLGA and (Tube 4) 2% ovine erythrocytes+streptolysin-O+nanosponges.

According to Figure 64, the system that contained the nanosponges had the lowest Hb release at 0.005 g/dl (± 0.005) compared to the system containing just the toxin and erythrocytes (0.23 g/dl, ±0.01). The difference is shown by the level of significance “P≤0.001”. The system that contained the vesicles was able to absorb the toxins similar to the ovine erythrocyte ghosts in the previous test, as it had nearly half the Hb release (0.08 g/dl, ±0.01), as opposed to the system containing toxin and erythrocytes. The adsorption of streptolysin-O by ovine nanosponges was also tested at 40°C, which is the estimated human body temperature during sepsis. Figure 66, indicates the efficacy of ovine nanosponges to adsorb streptolysin-O at 40°C. There was no Hb release in the system containing nanosponges at 40 °C compared to the system incubated at 37°C (approximately 0.001 g/dl of HB released). Yet, there is a significant difference in the concentration of Hb released between the systems containing ovine erythrocyte vesicles, when incubated at 37°C and 40°C.

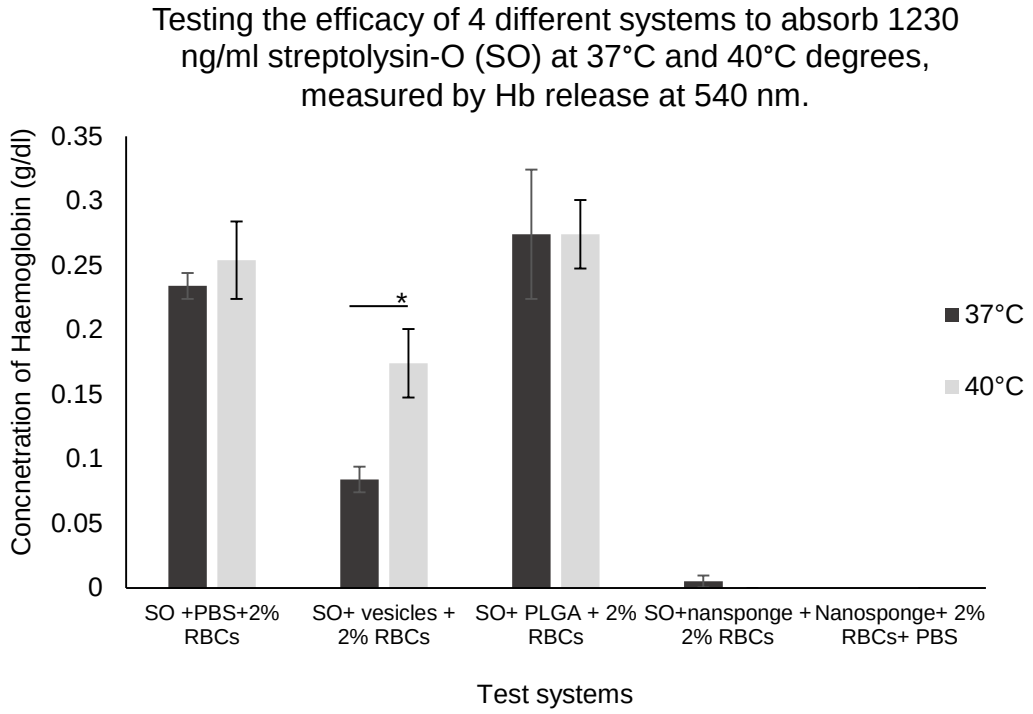

Figure 66. Testing the efficacy of ovine nanosponges and it components to adsorb 1230 ng/ml streptolysin-O, incubated at 37°C 40°C. Adsorption of streptolysin-O was measured by degree of haemolysis at 540 nm. .“*”P≤0.05, “**”P≤0.01 and “***”P≤0.001. Error bars represent SEM (n=3).

The synthesised ovine nanosponges and its components were lyophilized with 5% (w/v) sucrose and stored at 4°C for a week, as stated in section 1.5.13. The nanosponges and its components were then reconstituted with isotonic PBS (pH 7.2) and tested for their efficacy to adsorb streptolysin-O. Similar to the previous results, the system that contained the ovine nanosponges shows the least Hb release at 0.05 g/dl (± 0.04), as shown in Figure 67.

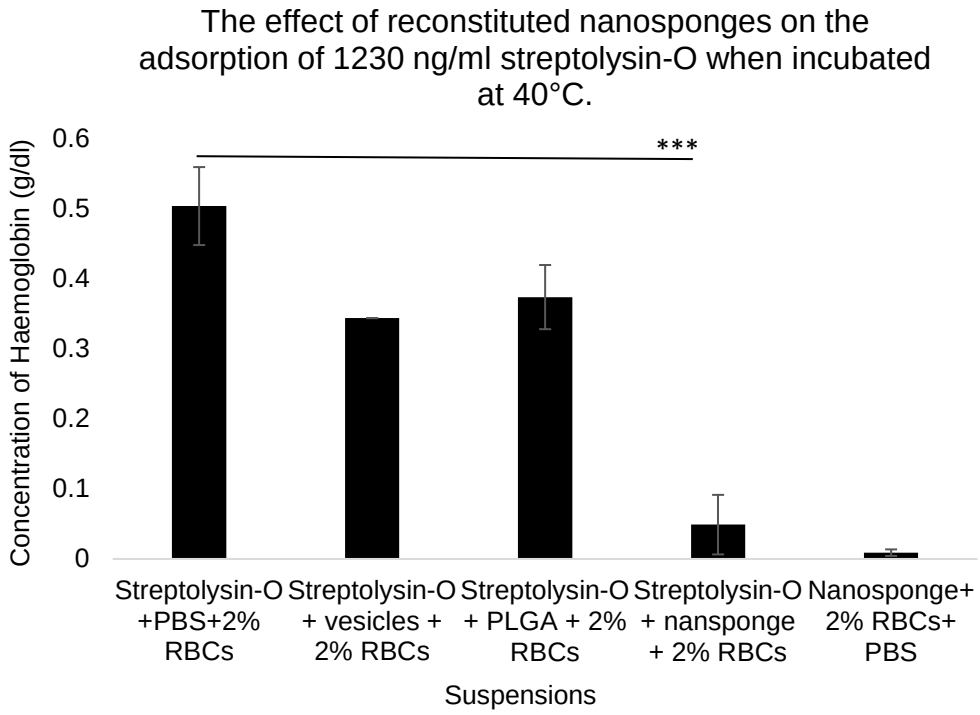

Figure 67. Testing reconstituted ovine nanosponges (1mg/ml) and its components for absorption of streptolysin-O, incubated at 40°C."*"P≤0.05, "**"P≤0.01 and "***"P≤0.001. Error bars represent SEM (n=3).

2.3.3 Nanosponge dose dependent assay

The ovine nanosponges (1mg/ml) were added in increasing concentration to systems that contained 2% ovine erythrocytes and 1230 ng/ml streptolysin-O. The suspensions were then incubated at 40°C for 30 minutes. The suspensions were then centrifuged and the supernatant was measured for concentration of Hb released. According to Figure 68, 10,000 ng/ml nanosponge absorbed 1230 ng/ml streptolysin-O, as the concentration of Hb released is minimal (0.009 g/dl, ± 0.005). Comparatively, the 2000 ng/ml nanosponge had the highest concentration of Hb released at 0.554 g/dl (± 0.03).

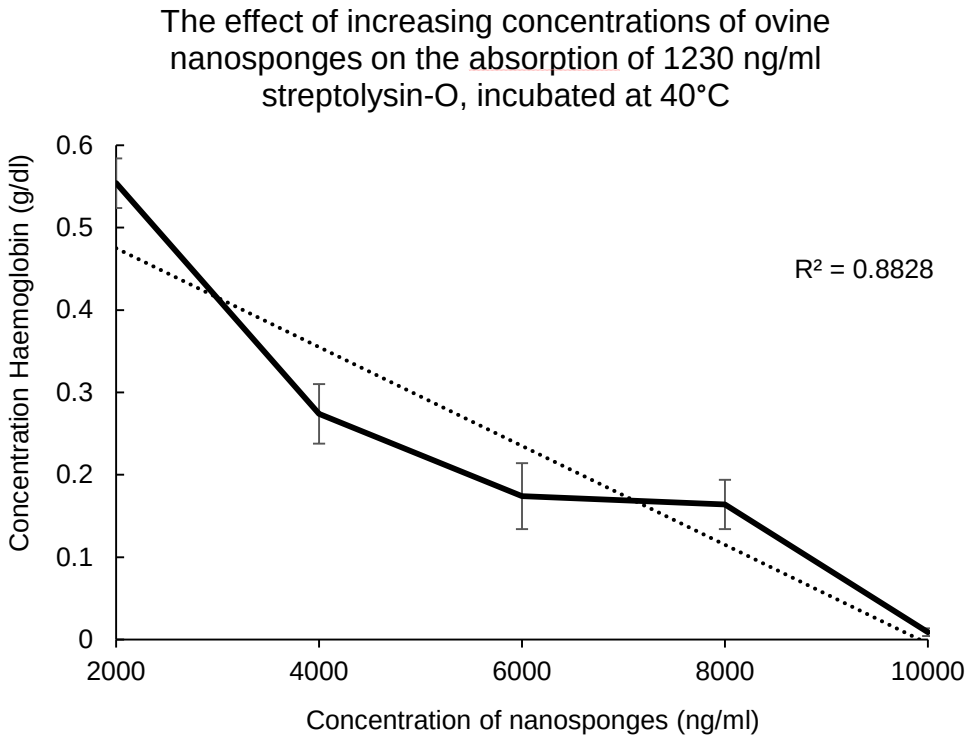

Figure 68. The effect of increasing concentrations of ovine nanosponges on adsorption of 1230 ng/ml streptolysin-O at 40°C for 30 minutes. Error bars represent SEM (n=3). R^2= 0.882

2.3.4 Cholesterol assays

2.3.4.1 Quantifying total cholesterol in 2% mammalian erythrocyte suspensions

The cholesterol quantitation kit was used to quantify the concentration of cholesterol present in 2% mammalian blood samples and ovine nanosponges. The Kit quantifies cholesterol by using a cholesterol esterase enzyme that hydrolyzes cholesteryl esters to cholesterol, and a probe that produces a pink colour. The kit was assayed for absorbance at 570 nm. The 2% mammalian erythrocyte suspensions were quantified for concentration of cholesterol by using the standard curve, shown in Figure 69.

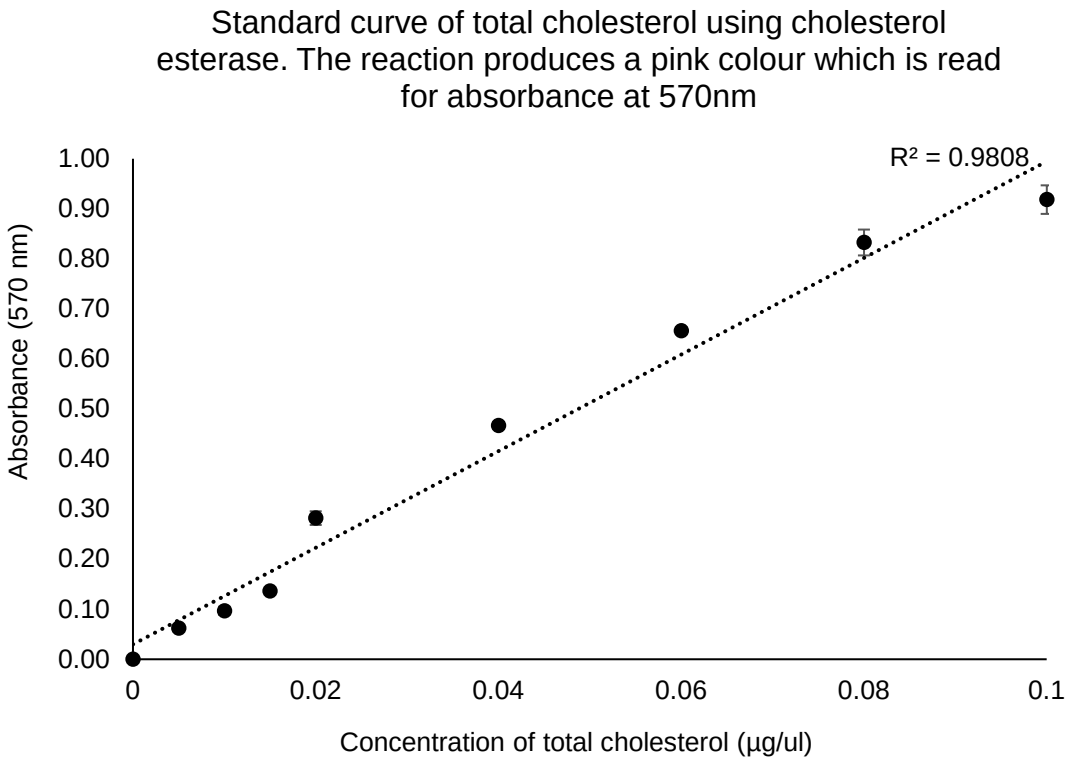

Figure 69. Standard curve of total cholesterol. The assay uses cholesterol esterase, which hydrolyzes cholesteryl esters to cholesterol. The reaction produces a pink colour, which was assayed for absorbance at 570 nm. Error bars represent SEM (n=3)

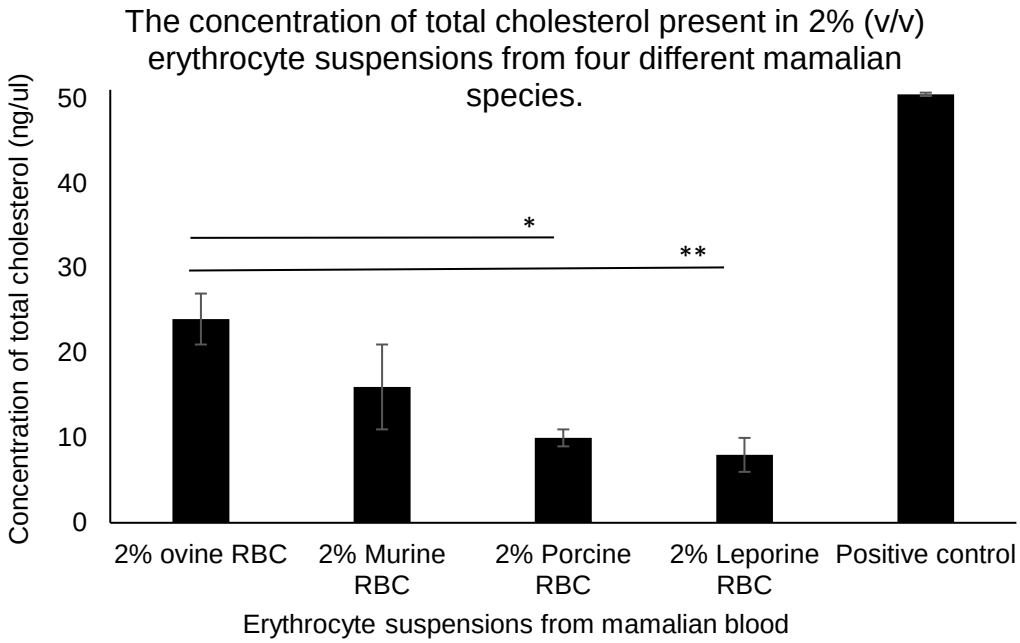

Figure 70. Estimating the concentration of total cholesterol present in 2% (v/v) erythrocyte suspensions from four different mammalian species. The reactions were incubated at 37°C for 30 minutes. The pink colour that was produced was assayed for its optical density at 570 nm. Error bars represent SEM (n=3)

The concentration of total cholesterol was estimated in four different mammalian species: ovine, murine, porcine and leporine (Figure 70). The figure shows that the 2% ovine erythrocyte suspension contains the greatest concentration of total cholesterol as opposed to the other blood types. The concentration of total cholesterol present in a 2% ovine erythrocyte suspension was 24 ng/µl (± 2.0). The lowest concentration of total cholesterol was present in a 2% leporine erythrocyte suspension, as the concentration of cholesterol was 8.0 ng/µl (2.0).

2.3.4.2 Incorporation of cholesterol into ovine nanosponges

The aim of this experiment was to test if incorporation of different concentrations of cholesterol into ovine nanosponges could have an impact on the adsorption of streptolysin-O. Three different formulations were synthesised, each having varying volumes of cholesterol; NS1 (50 µl), NS2 (75 µl), NS3 (100 µl) and NS (control). The characteristics of the three formulations were compared to the control nanosponges. They were also compared in their ability to adsorb streptolysin-O. Figure 71 shows the effect of cholesterol incorporation on size of ovine nanosponges. NS3 was formulated with a greater volume of cholesterol compared to NS1 and NS2, yet it shows a smaller size, as the size of NS3 was

271 nm (± 27.5) with a PDI of 0.378. The graph shows a strong negative correlation between the concentration of cholesterol incorporation and the size, from NS1-NS3. NS in this study was used as the control, NS being ovine nanosponges developed by the method described in chapter one section 1.5.11.

The zeta potential of these nanosponge formulations were also compared, as Figure 72 shows the zeta potential of the three different formulations. The average zeta potential of the formulations has increased compared to the control nanosponge. However, a student's T-test shows no significant difference between the formulations and the control nanosponge.

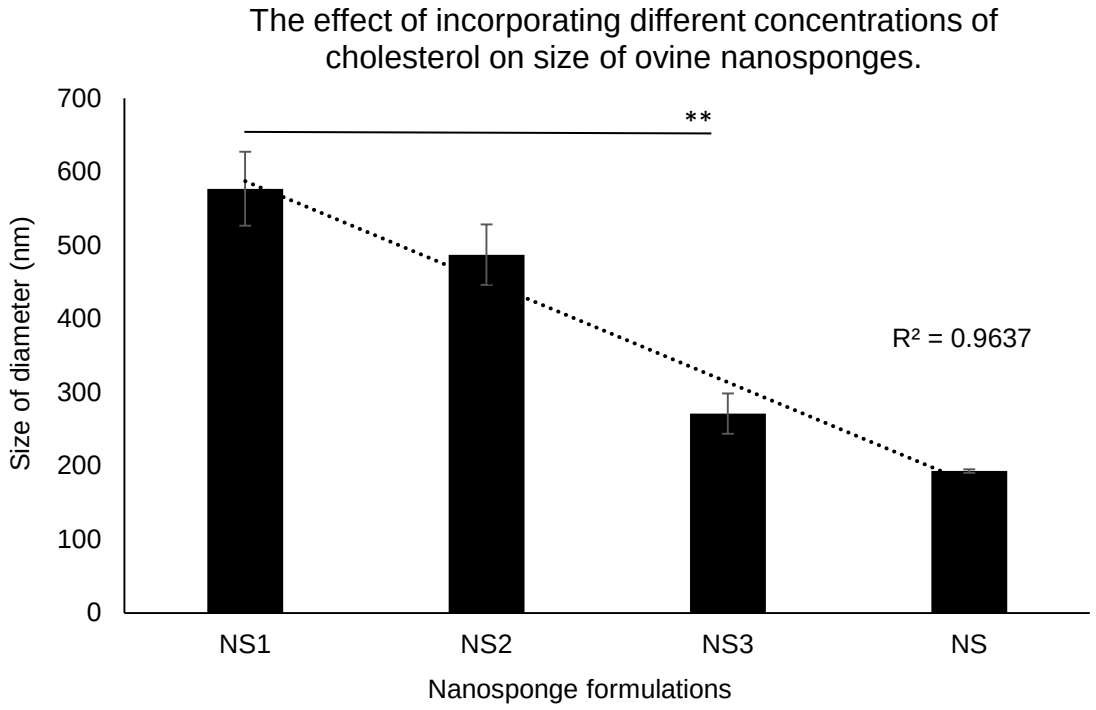

Figure 71. The effect of cholesterol incorporation on size of three different ovine nanosponge formulations. NS1 (50 µl), NS2 (75 µl), NS3 (100 µl) and NS (control). Error bars represent SEM (n=3). ."*"P≤0.05, "**"P≤0.01 and "***"P≤0.001.

According to Figure 71, the change in size of the formulations could signify the incorporation of cholesterol. However, this was further tested by quantifying the concentration of cholesterol in each of the formulations by using the Sigma-Aldrich cholesterol quantitation kit. The positive control is a known cholesterol standard, with a concentration of 45 ng/µl. Figure 73, shows the concentrations of total cholesterol present in each of the ovine nanosponge formulations. NS3 has the highest concentration of incorporated cholesterol present at 23.5 ng/µl (± 0.083) as opposed to NS2, which has the lowest concentration of incorporated cholesterol at 11.9 (± 4.1). However, a student's T-test shows that there is no significant difference in the concentration of cholesterol between NS1, NS2 and NS ($p>0.05$). Concentration of total cholesterol in NS3 ovine nanosponges show a significant difference compared to NS1.

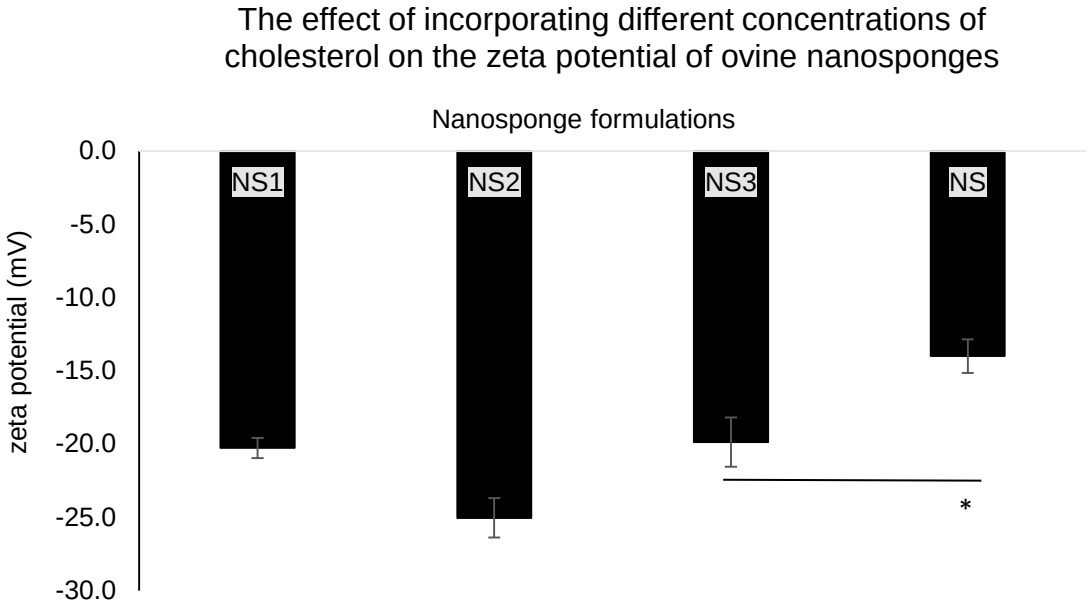

Figure 72. The effect of cholesterol incorporation on the zeta potential of three different ovine nanosponge formulations. NS1 (50 µl), NS2 (75 µl), NS3 (100 µl) and NS (control). Error bars represent SEM (n=3)

The main aim of this experiment was to test if cholesterol incorporated nanosponges had the ability to completely adsorb 0.2 mg/ml streptolysin-O at 40°C. Figure 74 shows the effect different ovine nanosponge formulations had on the adsorption of streptolysin-O. The ovine nanosponge formulations were tested for their function to adsorb streptolysin-O by the method described in section 2.2.3. 0.1% Triton x-100 was used as a positive control in this study. Figure 74 shows that NS3 has completely adsorbed 0.2 mg/ml streptolysin-O, as

the concentration of Hb released after addition of NS3 was 0 g/dl. A students T-test validates the significance of this result ($p<0.001$). NS1, NS2 and NS have also adsorbed streptolysin-O, yet there is presence of Hb release as compared to NS3. Comparatively, NS2 has adsorbed more toxin than NS1 and NS as the concentration of Hb released is 0.07 g/dl (± 0.03), which is lower than NS1 and NS.

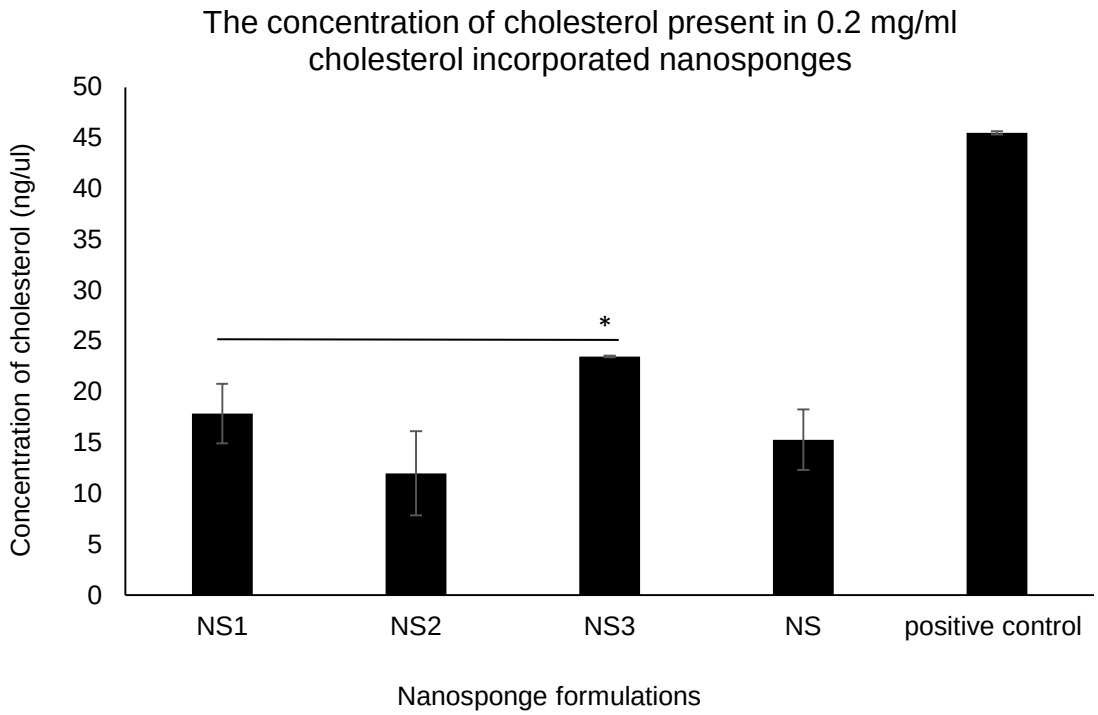

Figure 73. Quantitation of total cholesterol present in the three different formulations and the nanosponge control, using the Sigma-Aldrich cholesterol quantitation kit. NS1 (50 µl), NS2 (75 µl), NS3 (100 µl), NS (control) and a positive control (45 ng/µl). Error bars represent SEM (n=3). ."*"P≤0.05, "**"P≤0.01 and "***"P≤0.001.

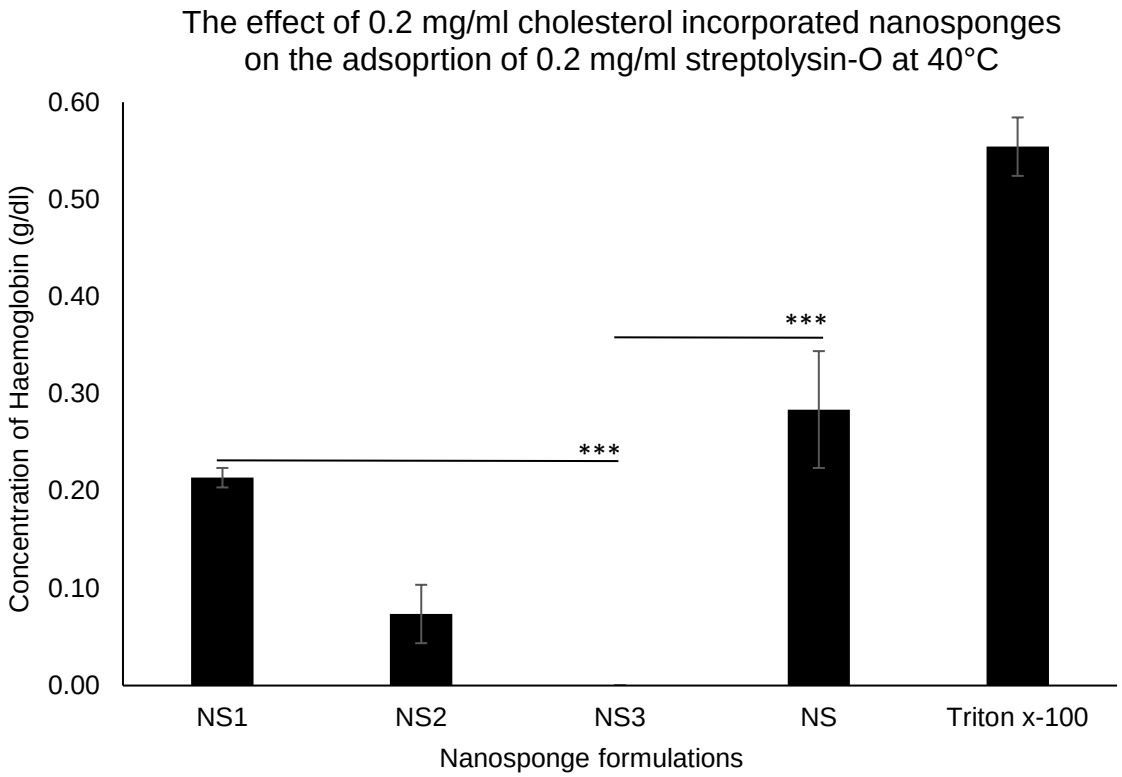

Figure 74. Adsorption of streptolysin-O by cholesterol incorporated ovine nanosponge formulations. The assay was incubated at 40°C for 30 minutes. NS1 (50 µl), NS2 (75 µl), NS3 (100 µl), NS (control) and a triton x-100 (0.1%). Error bars represent SEM (n=3). "*"P≤0.05, "**"P≤0.01 and "***"P≤0.001.

2.3.5 Phospholipid assay

Phospholipids are essential components of the erythrocyte membrane as they maintain the cytoskeletal structure. The loss of lipids during nanosponge preparation could affect PFTs adsorption and the overall structure of the nanosponge. Therefore, the aim of this experiment was to quantify the concentration of lipids at each stage of ovine nanosponge preparation. The lipids were quantified using a Sigma-Aldrich phospholipid assay. Phospholipids were enzymatically hydrolysed to release choline, which was determined using choline oxidase and a hydrogen peroxide dye. The assay was incubated at room temperature. The reaction was then read for its optical density at 570 nm. In order to synthesise ovine nanosponges, ovine erythrocytes were lysed with a hypotonic buffer to synthesize erythrocyte ghosts. The ghosts were subjected to sonication to produced erythrocyte vesicles. The erythrocyte vesicles were extruded with the PLGA core, which synthesized ovine nanosponges. At each stage. The

concentration of phospholipids were determined using a phospholipid standard curve, shown in Figure 75.

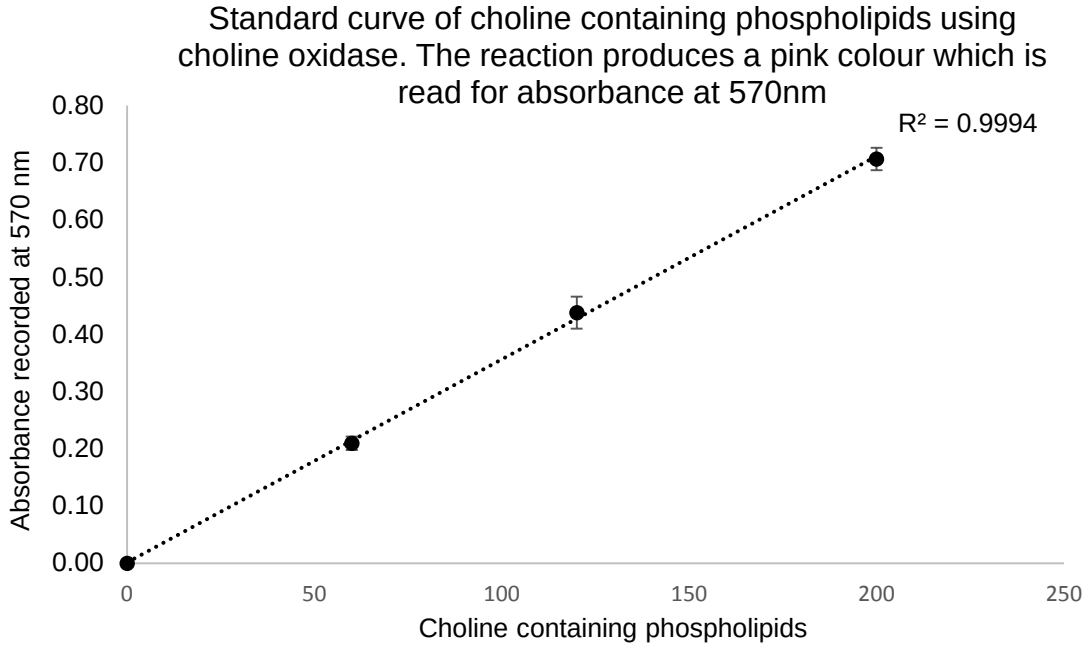

Figure 75. Standard curve of choline containing phospholipids. The reaction was assayed for optical density at 570 nm. Error bars represent SEM (n=3).

Figure 76 shows the concentrations of choline containing phospholipids at each stage of ovine nanosponge preparation. According to Figure 76, the 500 µl ovine erythrocytes have a phospholipid concentration of 314.1 µM (± 31.9). Ovine erythrocyte ghosts derived form 500 µl ovine erythrocytes, have an increased phospholipid concentration of 626.4 µM (± 179.1). Since the erythrocyte ghosts have a greater concentration of phospholipids as opposed to ovine erythrocytes. It could be suggested, that lipid extraction on ovine erythrocytes may not have extracted all the phospholipids, and that extraction of phospholipids from ovine erythrocyte ghosts is the true estimate of concentration of phospholipids present in 500 µl of ovine erythrocytes. Samples were prepared from fixed volumes of ovine erythrocytes which excluded the retentate.

From Figure 76, it is shown that from the development of erythrocyte ghosts to ovine nanosponges there is a decrease in the concentration of phospholipids, as the concentration of ovine nanosponges were 205.6 µM (± 8.9). The significance of this reduction is shown by a student's T-test ($p<0.01$), Therefore, suggesting, that phospholipids are lost during synthesis of ovine nanosponges.

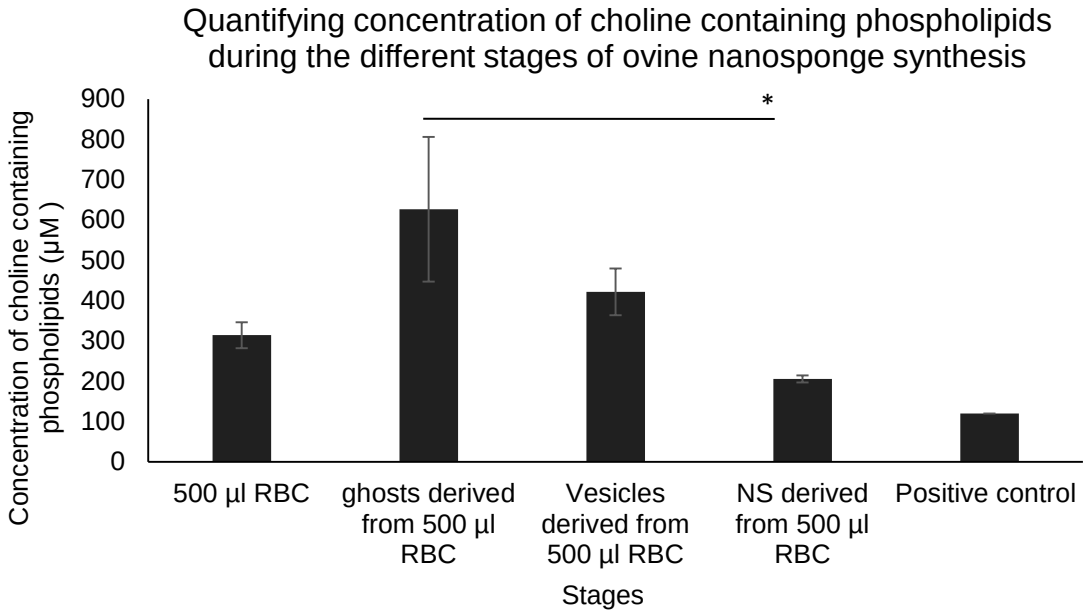

Figure 76. Concentration of choline containing phospholipids at each stage of ovine nanosponge preparation. The assay was read for optical density at 570 nm. Error bars represent SEM (n=3). The positive control is a known concertation of phospholipids (120 µM). "*"P≤0.05, "**"P≤0.01 and "***"P≤0.001.

2.4 Discussion

The overall aim of this research chapter was to test the efficacy of streptolysin-O haemolysis against ovine, porcine, leporine and murine blood. Furthermore, synthesized nanosponges constructed of a polymeric core and from mammalian blood. Ovine blood was chosen as a coating of the polymer as it was found to be more the most susceptible to streptolysin-O haemolysis. The synthesised nanosponge was then tested for its ability to adsorb streptolysin-O under different physiological and storage conditions.

2.4.1 Streptolysin-O haemolysis assay

The novel experiment investigated the degree of streptolysin-O haemolysis against ovine, porcine, leporine and murine erythrocytes. Streptolysin-O is a PFT secreted by group A *Streptococcus* and is shown to bind specifically to cholesterol on the erythrocyte membrane. Figure 60, shows that ovine erythrocytes were more susceptible to streptolysin-O haemolysis, compared to the other mammalian blood types, as 2000 ng/ml of streptolysin-O released approximately 80 % (± 1.40) ovine Hb. This is a significant result, as a previously reported study had shown that ovine erythrocytes had a higher concentration of cholesterol present in their membrane compared to the other tested blood (Nelson, 1967). At lower concentrations of streptolysin-O (250-1250 ng/ml), murine erythrocytes are more susceptible to streptolysin-O lysis, compared to ovine erythrocytes. The reason for this is unknown. Compared to the result obtained by this experiment, another study conducted by Shewell *et al.* (2014) has shown that lower concentrations of CBTs have close to 90% haemolytic activity as, 53 ng/ml pneumolysin (belongs to CBT family of PFTs) has a haemolytic activity of approximately 90% against a 1% (v/v) human erythrocytes. The author also shows that 400 ng/ml streptolysin-O has approximately 90% haemolytic activity against 1% (v/v) human erythrocytes.

The specificity of streptolysin-O for cholesterol is caused due to a hydrogen bonding interactions which are known to be weakly covalent bonds *(Ahmad et al., 2011)*. Streptolysin-O is secreted by the bacteria as a monomer containing four domains (Figure 77). Domain 1 and 3 correspond to the membrane attack complex perforin family domain found in mammalian PFTs. Domain 4 contains a

undecapeptide region (11 amino acids) which binds to cholesterol present in the membrane (Keyel *et al.*, 2013). This undecapeptide region is thought to be necessary for cytolytic activity of the toxin. The undecapeptide region contains a tryptophan residue that binds to cholesterol via a weak hydrogen interaction allowing insertion into the membrane *(Ahmad et al., 2011)*.

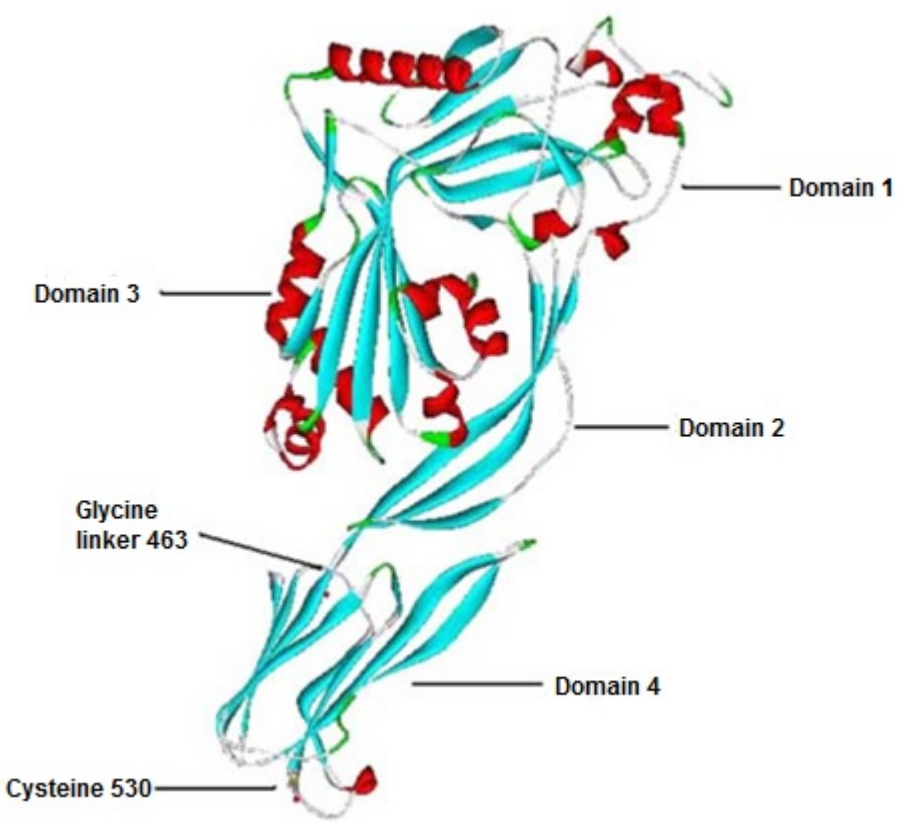

Figure 77. Structure of streptolysin-O monomer. The structure has four different domains. Upon binding to the membrane, the structure oligomerizes to form a pore (Ahmad *et al.*, 2011).

Pore forming toxins such as streptolysin-O share lineage with proteins in other organisms, which may suggest that these toxins have evolved overtime to possess virulence. For example, pore forming toxin enterolobin found from a Brazilian plant *Enterobium contortisiliquum* has significant sequence homology to aerolysin found in *Aeromonas hydrophila* (Gilbert, 2002). Another study shows a cytolytic protein in the snail B*iomphalaria glabrata* share structural features to toxins in the β-PFT family (Galinier *et al.*, 2013). These PFTs cause diseases in humans and animals. *Streptococcus* has shown to cause diseases in humans, dogs, pigs and sheep. A study conducted by Staats *et al.* (1997) showed that *Streptococcus* causes a wide range of clinical diseases in pigs, such as arthritis,

meningitis, pneumonia and sepsis. Moreover, the study has also shown that the disease can spread to humans, particularly abattoir workers. The same study shows that dogs and sheep have also contracted diseases such as pneumonia and osteomyelitis from a *streptococcal* infection.

Many infections if left untreated, either in humans or animals could lead to sepsis, as described in section 1.4.8. Early goal directed therapy is essential in management and treatment of sepsis. However, early goal directed therapy is essential in the golden hours of sepsis. Timing is important, as Figure 62 shows the effect 1230 ng/ml streptolysin-O has on 2% mammalian erythrocyte suspensions over a 60 minute period. After 60 minutes, streptolysin-O has released 91% of ovine Hb from erythrocytes (Figure 62) compared to murine, leporine and porcine erythrocytes. Murthy (2014) stated that during sepsis there is a Hb cut off value that indicates a sign of severe sepsis. In the NHS, blood transfusions are administered within the first 6 hours of sepsis only if the Hb level decreases below 7 g/dl. Kumar *et al.* (2006) showed that over the first 6 hours of sepsis, each hour of delay in initiation of effective antimicrobial therapy was associated with a decrease in survival of 7.6% (Figure 78). This highlights the correlation between time of treatment and rate of survival.

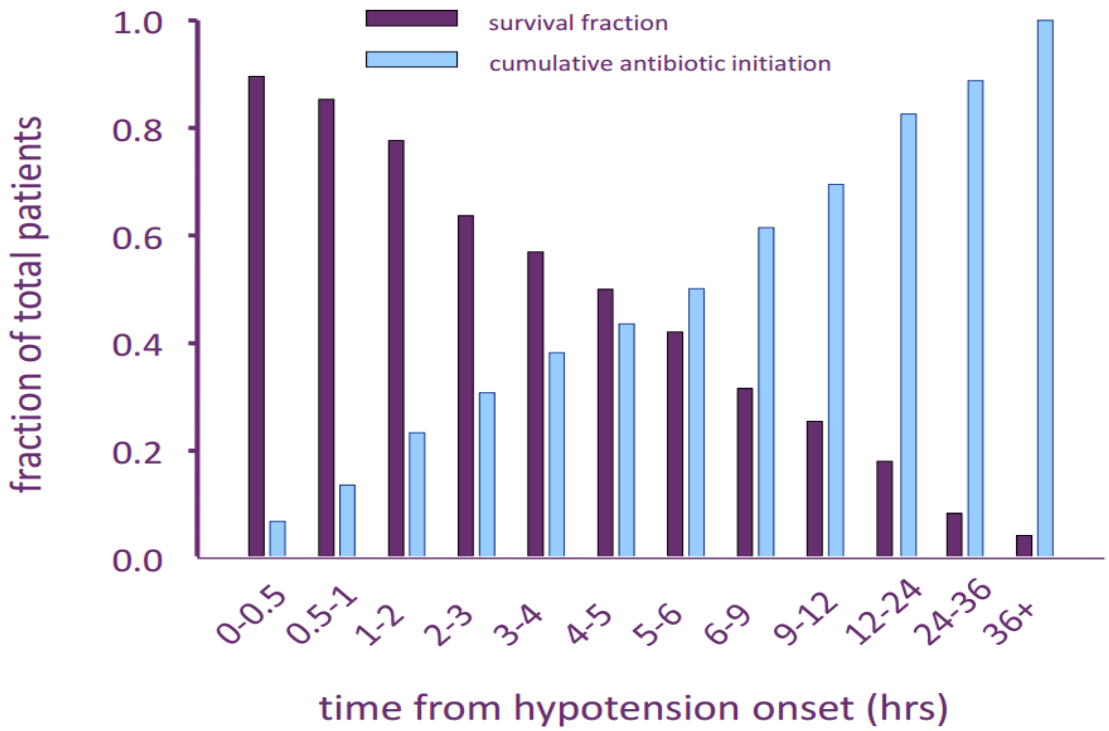

Figure 78. The effect of antimicrobial administration on fraction of total patient's survival with respect to time, following onset of septic shock-associated hypotension (Kumar *et al.*, 2006).

2.4.2 Streptolysin-O adsorption studies

Treatment options for sepsis include antibiotics, surgical drainage of infected fluids, blood transfusion, organ replacement and steroids. Most of these treatment strategies reduce the inflammatory response (Peters and Cohen). Chapter 1 introduced synthesis of a novel therapeutic model, nanosponge. This model was developed using ovine blood as an animal model. Previous studies, without nanosponges, have reported using ovine systems as a model for endotoxin derived sepsis, as the blood components are similar to that of humans and they have similar physiological parameters (Zarjou and Agarwal, 2011). Figure 60 shows that ovine erythrocytes were more susceptible to haemolysis by streptolysin-O compared to the other mammalian blood types.

Nanosponges are biomimetic nanoparticles that consist of a polymeric core, coated by an erythrocyte membrane. Streptolysin-O binds specifically to cholesterol in membranes. Therefore, the ovine nanosponges were used to test the adsorption of streptolysin-O *in vitro.* Consequently, most of the assays

developed in this chapter tested the ability of ovine nanosponges and its contents to adsorb streptolysin-O under physiological and storage conditions. To synthesize ovine nanosponges the primary step was to develop erythrocyte ghosts.

The ovine erythrocyte ghosts were tested for adsorption of streptolysin-O using a novel assay. This assay involved adding the supernatant of each of the systems into a fresh ovine erythrocyte suspension. The difference in Hb recorded before and after addition of the supernatant is what is shown in Figure 63.Figure 63 shows the 2% (v/v) ovine ghost suspension absorbed the most streptolysin-O, as the concentration of Hb released was the lowest compared to the other systems. Yet there is still Hb released after adsorption by erythrocyte ghosts, as depicted in Figure 79. This shows a new postulated mechanism behind toxin adsorption by erythrocyte ghosts *in vitro*. Erythrocyte ghosts do adsorb streptolysin-O. Miyoshi *et al.* (1997) stated that pore forming toxins like streptolysin-O, have the ability to bind reversibly. Kanbayashi *et al.* (1972) has transferred streptolysin-O, bound to leporine erythrocytes, to a fresh erythrocyte suspension, which then led to haemolysis, suggesting that there was possibility of binding reversibly (interpreted in Figure 79) . Similarly Hu *et al.* (2013) has shown that erythrocyte vesicles had the ability to adsorb α-haemolysin. These vesicles, when transferred to a murine erythrocyte suspension, were able to lyse murine erythrocytes. This may suggest that α-haemolysin also has the ability to bind reversibly to erythrocyte membranes.In comparison to the system that contains just ovine erythrocytes and the toxin, ovine erythrocyte ghosts had a lower concentration of Hb released, indicating a small concentration of unbound toxin in the supernatant. This therefore could signify that the ovine erythrocyte ghosts have the ability to adsorb the toxin.

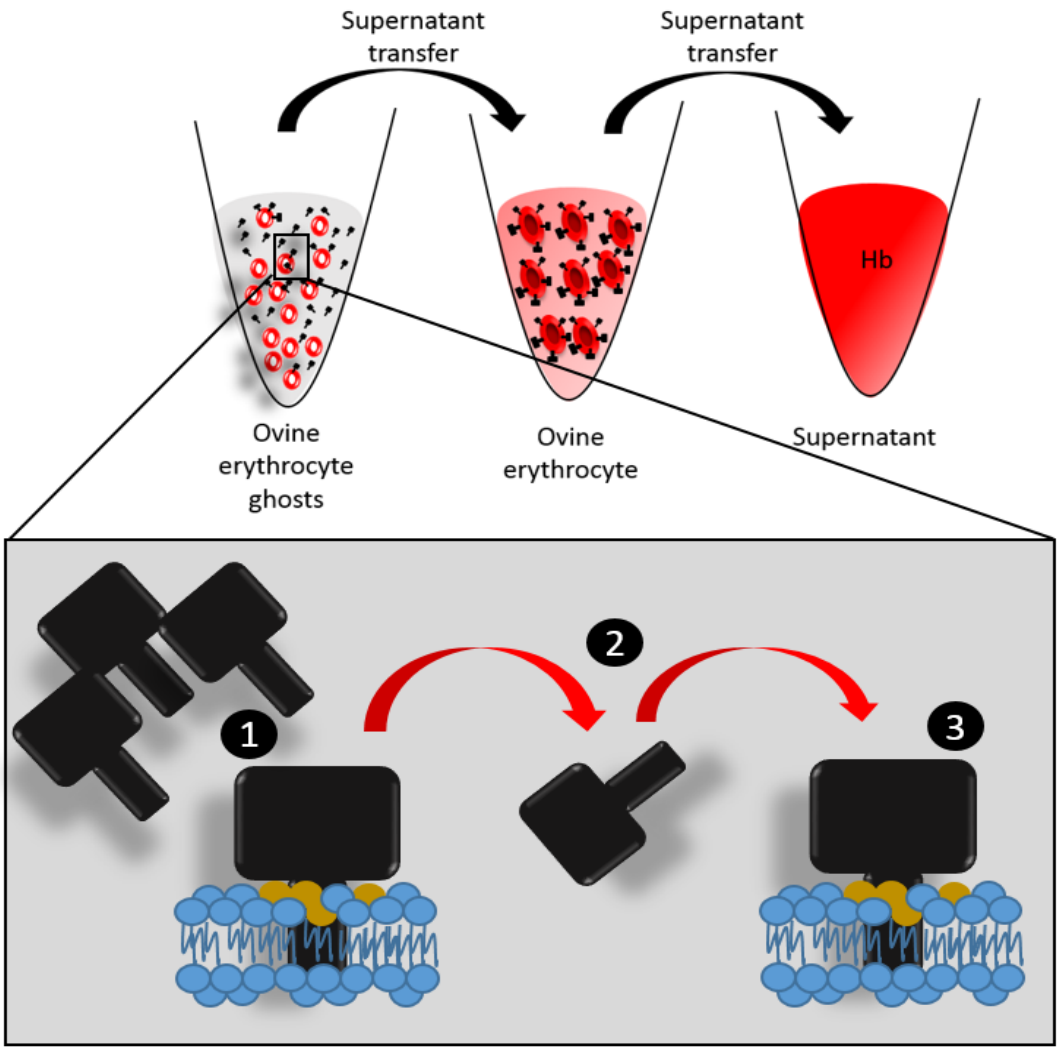

Figure 79. Diagrammatic interpretation of streptolysin-O binding to ovine erythrocyte ghosts. Supernatant containing unbound toxin from the system containing erythrocyte ghosts was transferred to a system containing whole erythrocytes. The supernatant from this system was then transferred to a separate Eppendorf tube and read assayed at 540 nm. The Eppendorf tube containing erythrocyte ghosts shows that streptolysin-O has the ability to bind reversibly to erythrocyte membranes. Step 1 involves binding of streptolysin-O to an erythrocyte membrane, step 2 involves detachment from the membrane and step 3 involves reattachment to another erythrocyte membrane.

The erythrocyte ghosts were subjected to sonication to develop erythrocyte vesicles, which were then extruded with the PLGA cores to formulate ovine nanosponges. Figure 64 showed the efficacy of the nanosponge and its components to adsorb streptolysin-O. The system that contained the nanosponges had the least Hb release compared to the system containing just the toxin and erythrocytes. The ovine erythrocyte vesicles were also able to

absorb streptolysin-O as it had nearly half the Hb release, as opposed to the system containing just toxin and erythrocytes. Conversely the system containing the PLGA had no adsorption of streptolysin-O, as it showed a greater concentration of Hb released as compared to the other systems.

When PLGA was coated by ovine erythrocyte vesicles (nanosponge), there was minimal lysis within the system. As stated above PFTs like streptolysin-O might have the ability to bind reversibly, yet there is minimal Hb released in the system containing nanosponges (Figure 65). This may suggest that PLGA plays an important role in adsorption of streptolysin-O. There are three factors that might play a role in adsorption. (1) PLGA has been used for many clinical purposes and has shown to have a better interaction with biological materials. Examples include the use of PLGA for bone tissue engineering, stabilization of spinal segments, and scaffolds for tissue engineering (Gentile *et al.*, 2014). (2) Presence of charged residues on streptolysin-O. Domain 1 and 3 of the streptolysin-O structure have a few charged polar residues, which could interact with PLGA. (3) The surface area to volume ratio of ovine nanosponges.

The surface area to volume ratio plays a significant role in adsorption, as when the size of the nanosponge decreases, the surface area to volume ratio increases (table 11). The results show that the ovine nanosponges have a greater surface area to volume as compared to ovine erythrocyte ghosts. Hu *et al.* (2013) has stated that transforming an erythrocyte to a nanosponge increases the collisional frequency with toxins by approximately 50 fold, due to the surface area to volume ratio. A study conducted by Waugh and Sarelius (1996) showed that there is a link between surface area and clearance by the immune system. They state that the loss of surface area ratio on mice erythrocytes leads to rapid clearance by the immune system. It is not clear from this study how quickly ovine nanosponges will be cleared from mammalian blood.

Patients suffering from sepsis undergo several physiological changes such as tachycardia (increased heart rate), tachypnoea (rapid breathing), prolonged hypotension (low blood pressure), acidosis (increased acidity in the blood) and hyperthermia (increased body temperature) (Lee *et al.*, 2012). Fajardo (1984) shows that there is destruction of cellular bodies under hyperthermic conditions (“lesions in the central nervous system, liver, kidney, heart, adrenal, testis, and bone marrow”). Here the adsorption of ovine nanosponges was tested at 40°C,

which is an estimation of the elevated body temperature during sepsis (Lee *et al.*, 2012). Figure 66 shows the effect ovine nanosponges and its constituents have on the adsorption of streptolysin-O at 40°C. There was no difference in the concentration of Hb released by three of the systems incubated at 37°C and 40°C. At 40°C, the system that contained the nanosponges had adsorbed the streptolysin-O as there was no Hb released compared to the system at 37°C. This may indicate the nanosponges have a better absorption efficiency at 40°C. This could be justified, as the physiological body temperature of sheep is 39°C (Piccione *et al.*, 2002). Figure 67 shows a significant difference in concentration of Hb release by the systems containing ovine erythrocyte vesicles incubated at 37°C and 40°C. The reason for this is unknown.

Chapter 1 section 1.7.8 has shown that ovine nanosponges are not stable when stored at 4°C, 24°C, 37°C and 40°C. However, when lyophilized and reconstituted, the ovine nanosponges had no significant difference in size as opposed to the control nanosponges, suggesting that the ovine nanosponges were stable when reconstituted. A study conducted by Gill (2012) stated that lyophilization of nanoerythrosomes led to an increased shelf life of the nanoparticles. Similarly, Hu *et al.* (2013) has shown that lyophilization of murine nanosponges, does not lead to the loss of function. Figure 67 shows the results of the adsorption of streptolysin-O by reconstituted ovine nanosponges and its components at 40°C. Even after lyophilization, the ovine nanosponges have retained their function of streptolysin-O adsorption, as the concentration of Hb released is minimal compared to the system containing ovine erythrocytes and streptolysin-O.

2.4.3 Nanosponge dose dependent assay

A dose response curve plays a significant role in aiding treatment of a disease and was founded by professor Alfred Joseph Clark in 1931. A dose response curve shows the maximum effect of the therapeutic agent at a certain concentration. In a clinical setting, it aids in establishing the right dose required to achieve a non-toxic, yet therapeutic effect (Aronson, 2007). Dose response curves are generated to test effects of anti-cancer therapeutics, anti-microbial testing, toxicity studies against endothelial cells etc. Therefore, this study tested the adsorption of 1230 ng/ml streptolysin-O by increasing concentration of ovine nanosponges. Figure 68, shows an inverse correlation between the concentration of nanosponges and concentration of Hb released. As the concentration of ovine nanosponges increases the concentration of Hb decreases. The dose dependent study shows that 10,000 ng/ml ovine nanosponges are required to fully adsorb 1230 ng/ml streptolysin-O.

2.4.4 Cholesterol assays

Cholesterol is a significant class of membrane lipids. It is abundant in the plasma membrane of mammalian cells. Up to 30% of the entire lipid in the membrane is composed of cholesterol. Cholesterol is a major determinant of bilayer fluidity, and plays a significant role in maintaining structural integrity of the membrane. Nonetheless, studies mentioned in section 2.4.1, show that cholesterol plays an important part in streptolysin-O haemolysis, as it is the binding site for streptolysin-O pore formation. Consequently, a cholesterol esterase colorimetric assay estimated the concentration of cholesterol present in 2% (v/v) mammalian erythrocyte suspensions chosen in this study (Figure 70). Figure 70 shows that ovine erythrocytes have the maximum concentration of cholesterol compared to the other mammalian blood types. A study conducted in 1967 shows that 27.8% of the total lipid content of ovine erythrocytes was composed of cholesterol. However, the study also shows that 29.9% of the total lipid content of leporine erythrocyte was composed of cholesterol (Nelson, 1967). The results recorded by this study do not agree with these results.

A study has reported elevated concentrations of cholesterol in erythrocyte membranes of humans, compared to the concentrations of cholesterol in 2% erythrocyte suspensions reported by this study. Tziakas *et al.* (2007) showed that human erythrocyte membranes have a range of cholesterol from 130.4-260.4 µg/mg.

Cholesterol is a significant component of lipid-based nano-formulations in the field of nanomedicine, as it maintains the rigidity of the structure. Cholesterol can improve stability of a particle by increasing packing of phospholipid molecules (Demel and De Kruyff, 1976), reduce membrane permeability to electrolyte solutes (Papahadjopoulos *et al.*, 1973) and improve vesicle resistance to aggregation (Briuglia *et al.*, 2015). Nonetheless, this study incorporated cholesterol into membranes of ovine nanosponges. The main aim of this study was to test if incorporation of cholesterol would increase adsorption of streptolysin-O. However adding external lipids such as cholesterol will have an effect on nanosponge characteristics such as the size and zeta-potential (Wang *et al.*, 2007). Figure 71 shows the effect different volumes of incorporated cholesterol have on the size of the nanosponges. Compared to the control nanosponge NS1 (577.1 ± 50.3), NS2 (487.4 ± 41.1) and NS3 (271.3 ± 27.5) all have an increased size after cholesterol incorporation. Moreover, NS1 has a greater size compared to NS3. Even though NS3 was prepared with a higher volume of cholesterol, it has the lowest size as opposed to NS1 and NS2. Briuglia *et al.* (2015) states that the highest concentration of cholesterol that can be incorporated is 50%. However, the ratio between cholesterol and lipid used to produce stable formulations is 2:1. This could suggest a reason for NS3 having the lowest size, as it could be a more stable formulation. Furthermore, the author shows that incorporation of cholesterol into liposomes, created stable particles with no significant difference in size over a period of 30 days at 37°C. Therefore indicating that incorporating cholesterol has a stabilizing effect.

As stated earlier in section 1.7.7, the zeta potential value is a particle characteristic used to assess stability of a suspension. The electrostatic repulsion between particles prevents aggregation of the spheres (Ravi Kumar *et al.*, 2004). Magarkar *et al.* (2014) shows that addition of cholesterol in lipid membranes reduces the zeta-potential. A similar result has been obtained by the study shown in Figure 72. The figure shows that there is a significant difference in the zeta-

potential between the cholesterol incorporated nanosponges (NS1, NS2 and NS3) and control nanosponges. Cholesterol incorporation reduces the zeta-potential. Magarkar *et al.* (2014) states hat sodium ions bind to carbonyl and phosphate groups of lipids, which adds to an increase in charge on phospholipid membranes. However, incorporation of cholesterol reduces sodium ion binding to phospholipid, which leads to the reduction in zeta-potential of phospholipid membranes, as the author has shown that incorporating liposomes with 60% cholesterol reduces the zeta-potential from neutral to -7 mV.

Characteristics of cholesterol incorporated nanosponges have shown a change in size and zeta-potential compared to control ovine nanosponges (Figure 71-Figure 72). In order to justify cholesterol incorporation, a cholesterol esterase enzymatic colorimetric test was conducted to quantify the concentration of cholesterol incorporated in the four different nanosponge systems, which includes the control. Figure 73 shows no significant difference in the concentration of cholesterol between NS1, NS2 and the control nanosponges. However, NS3 has a greater concentration of cholesterol as opposed to the other nanosponges. This could suggest, that 100 µl of a 25 mg/ml stock is required to incorporate cholesterol into nanosponges. However, the sample size is too small to justify the right volume and concentration required for cholesterol incorporation. A larger sample size is required to justify the optimum concentration and volume required to incorporate cholesterol in nanosponges.

Even though Figure 73 showed no significant difference in the concentration of incorporated cholesterol between NS1, NS2 and control nanosponges, when tested for their ability to adsorb 0.2 mg/ml streptolysin-O, there was a significant difference in the concentration of Hb released in these three nanosponge systems (Figure 74). NS1 shows similar adsorption to the control nanosponge, as there is no significant difference in concentration of Hb released by the two systems. NS2 has a lower concentration of Hb released compared to NS1 and the control nanosponge. NS3 has adsorbed 0.2 mg/ml streptolysin-O compared to the control nanosponge, as there was no Hb release recorded. The reason for this result is shown by Flanagan *et al.* (2009). The author states that reducing the size of the phospholipid headgroup caused an increase in cholesterol exposure on bilayer membranes, consequently leading to an increase in streptolysin-O

binding. Therefore, we suggest that rather than cholesterol being incorporated in NS2 and NS3, there could have been more exposure of cholesterol on the membrane leading to adsorption of streptolysin-O. Flanagan *et al.* (2009) has also shown that using perfringolysin (a type of CBT), several factors play a role in perfringolysin binding to cholesterol. The author states (1) that binding only occurs when the concentration of cholesterol exceeds the association capacity of phospholipids and (2) packing of lipid molecules in the bi-layer will dictate whether or no cholesterol is accessible to the toxin.

2.4.5 Phospholipid assay

Schwoch and Passow (1973) states that erythrocyte ghosts are widely used in study of composition, structure and function of the red blood cell membrane. Hanahan *et al.* (1974), Turner and Rouser (1974) and Kostic *et al.* (2014) have all studied the properties of erythrocyte ghosts and stated that, preparation of erythrocyte ghosts do not lead to the loss of lipids from the erythrocyte membrane. However, there are no studies that test the loss of lipids during nanosponge preparation. Therefore, we tested the loss of phospholipids during preparation of ovine nanosponges, by quantifying the concentration of phospholipids at each step of ovine nanosponge preparation. Figure 76, shows the concentration of phospholipids at each stage of ovine nanosponge preparation. The concentration of phospholipids decrease from the development of erythrocyte ghosts to nanosponges. Hu *et al.* (2011) has stated “an excess of blood was used to compensate for the membrane loss during RBC ghost derivation and extrusion”, which produced nanosponges. . Cho *et al.* (2013) has stated that “some sample material may be lost during extrusion during passage through the porous membrane”. This signifies, that the reduction in phospholipid concentration shown in Figure 76 is caused during extrusion.

Figure 76 also shows that ovine erythrocyte ghosts have a greater concentration of phospholipids as opposed to ovine erythrocytes. Van Deenen and De Gier (1974) has stated that in the past erythrocyte lipid extracts have been conducted on erythrocytes and erythrocyte ghosts. Furthermore, the author states using erythrocytes produces unsatisfactory results as the erythrocytes congeal into a plastic puttylike lump, during extraction. Moreover, the haem pigment is often

extracted and has catalytic effects. Therefore could produce unreliable results. For these reasons, erythrocytes ghosts have shown a greater concentration of phospholipids and have been used to estimate concentration of phospholipids in erythrocyte samples.

2.5 Appendix

2.5.1 Haemolysis assay result in grams per decilitre

Table 17- Concentration of haemoglobin released by ovine erythrocytes in grams per decilitre

Concentration of streptolysin-O (ng/ml)	Average concentration of haemoglobin (g/dl)	Standard error
250	0.174	0.010
500	0.174	0.010
750	0.194	0.017
1000	0.324	0.010
1250	0.364	0.020
1500	0.644	0
1750	0.955	0.036
2000	1.145	0.020

Table 18- Concentration of haemoglobin released by murine erythrocytes in grams per decilitre

Concentration of streptolysin-O (ng/ml)	Average concentration of haemoglobin (g/dl)	Standard error
250	0.414	0.056
500	0.414	0.056
750	0.424	0.050
1000	0.604	0.050
1250	0.654	0.026
1500	0.684	0.027
1750	0.744	0.040
2000	0.875	0.020

Table 19- Concentration of haemoglobin released by porcine erythrocytes in grams per decilitre

Concentration of streptolysin-O (ng/ml)	Average concentration of haemoglobin (g/dl)	Standard error
250	0.224	0
500	0.274	0.026
750	0.284	0.030
1000	0.324	0.020
1250	0.454	0.070
1500	0.484	0.040
1750	0.644	0.036
2000	0.604	0.020

Table 20- Concentration of haemoglobin released by leporine erythrocytes in grams per decilitre

Concentration of streptolysin-O (ng/ml)	Average concentration of haemoglobin (g/dl)	Standard error
250	0.049	0.025
500	0.094	0.010
750	0.094	0.010
1000	0.164	0.030
1250	0.187	0.049
1500	0.264	0.020
1750	0.314	0.062
2000	0.364	0.053

2.5.2 Reactants and volumes used to produce a cholesterol and phospholipid standard curve

Table 21- Reaction volumes in a 96 well plate to produce a cholesterol standard curve

	1	2	3	4	5	6
A	0 µl S 44 µl CAB 2 µl P 2 µl EM 2 µl CE	4 µl S 40 µl CAB 2 µl probe 2 µl EM 2 µl CE	8 µl S 36 µl CAB 2 µl P 2 µl EM 2 µl CE	12 µl S 32 µl CAB 2 µl probe 2 µl EM 2 µl CE	16 µl S 28 µl CAB 2 µl probe 2 µl EM 2 µl CE	20 µl S 24 µl CAB 2 µl probe 2 µl EM 2 µl CE
B	0 µl S 44 µl CAB 2 µl P 2 µl EM 2 µl CE	4 µl S 40 µl CAB 2 µl probe 2 µl EM 2 µl CE	8 µl S 36 µl CAB 2 µl P 2 µl EM 2 µl CE	8 µl S 36 µl CAB 2 µl P 2 µl EM 2 µl CE	16 µl S 28 µl CAB 2 µl probe 2 µl EM 2 µl CE	20 µl S 24 µl CAB 2 µl probe 2 µl EM 2 µl CE
C	0 µl S 44 µl CAB 2 µl P 2 µl EM 2 µl CE	4 µl S 40 µl CAB 2 µl probe 2 µl EM 2 µl CE	8 µl S 36 µl CAB 2 µl P 2 µl EM 2 µl CE	8 µl S 36 µl CAB 2 µl P 2 µl EM 2 µl CE	16 µl S 28 µl CAB 2 µl probe 2 µl EM 2 µl CE	20 µl S 24 µl CAB 2 µl probe 2 µl EM 2 µl CE

Table 22- Reaction volumes in a 96 well plate to produce a phospholipid standard curve

A	1	2	3	4
B	0 µl PS 86 µl AB 1 µl EM 1 µl DR	20 µl PS (60 µM) 6 µl AB 1 µl EM 1 µl PLD 1 µl DR	20 µl PS (120 µM) 65 µl AB 1 µl EM 1 µl PLD 1 µl DR	20 µl PS (200 µM) 65 µl AB 1 µl EM 1µl PLD 1 µl DR
C	0 µl PS 86 µl AB 1 µl EM 1 µl DR	20 µl PS (60 µM) 6 µl AB 1 µl EM 1 µl PLD 1 µl DR	20 µl PS (120 µM) 65 µl AB 1 µl EM 1 µl PLD 1 µl DR	20 µl PS (200 µM) 65 µl AB 1 µl EM 1µl PLD 1 µl DR
D	0 µl PS 86 µl AB 1 µl EM 1 µl DR	20 µl PS (60 µM) 6 µl AB 1 µl EM 1 µl PLD 1 µl DR	20 µl PS (120 µM) 65 µl AB 1 µl EM 1 µl PLD 1 µl DR	20 µl PS (200 µM) 65 µl AB 1 µl EM 1µl PLD 1 µl DR

2.5.3 Amount of nanosponges required to treat a streptolysin-O infection.

The results obtained from the nanosponge dose dependent study (Figure 68), were used to theoretically calculate the therapeutic dose required to treat a streptolysin-O infection in a human, murine, leporine and porcine system. The equation for the theoretical calculation is shown below:

Nanosponges (g) = 10000 ng/ml x total volume of blood present in the system (l)

Table 23. Estimated nanosponge dose required to treat a streptolysin-O infection in five different mammalian systems

System	Total Volume of blood (l)	Nanosponges (g)
Human	6	0.06
Murine	0.02	0.0002
Leporine	0.12	0.0012
Porcine	3	0.03
Ovine	4.2	0.04

Chapter 3

3 α-haemolysin- Haemolysis and adsorption studies

3.1 Introduction

3.1.1 Staphylococcus aureus

Staphylococcus aureus is among the most successful of human pathogens. Colonization by *Staphylococcus aureus* of the skin, mucosa and nostrils is common (Kluytmans *et al.*, 1997). *Staphylococcus aureus* is known to be the leading cause of bloodstream, lower respiratory tract, skin, and tissue infections worldwide (Tong *et al.*, 2015). Despite its prevalence, much remains to be learned about how *Staphylococcus aureus* causes disease. Although studies have been published about the genetics and microbiology of *Staphylococcus aureus* over the last few decades. There is still a lot of research to be conducted to fully understand the virulence of this microorganism.

Staphylococcus spp were first implicated in disease in 1880, when famous Scottish surgeon Alexander Ougsten linked them to abscesses and neonatal diseases (Ogston, 1984). It was later shown that *Staphylococcus spp* disease was always present in nurseries, most often causing minor skin infections (Williams, 1958). The first identified nursery outbreak took place in the United States in 1889 and subsequent outbreaks took place in the 1900s (Shinefield and Ruff, 2009). *Staphylococci spp* are common in hospitals particularly in burn or surgical units, where there are patients with deep wound infections and patients that are catheterised. These provide easy entry for the bacteria into the body of the patient. *Staphylococcus aureus* infections are mostly caused by MRSA (Shinefield and Ruff, 2009).

As discussed in section 1.4.7.1 mortality caused *Staphylococcus aureus* still remains high. The reason for death is because like *Streptococcus spp, Staphylococcus aureus* infections can lead to sepsis. If left untreated eventually it causes Toxic shock syndrome. This decreases the patient chance of survival.

3.1.2 *Staphylococcus aureus* toxic shock syndrome

TSS is an acute, life threatening intoxication, characterised by hypotension, high fever, rash and multi-organ dysfunction. This is caused by exotoxins produced by *Staphylococcus aureus.* The disease was initially described in 1978 and came to public attention in 1980 with the occurrence of a series of menstrual-associated cases (Zaghloul, 2015). However, about half the cases of TSS today occur in patients that are not menstruating. For example, a study conducted by Murphy *et al.* (2001) shows than out of 574 vascular surgical patients that developed a MRSA infection. From 574 patients 23 died in the hospital. Out of the 23 patients that died, 10 acquired TSS but died as a result of sepsis.

One of the contributing toxins behind *Staphylococcus aureus* virulence is a PFT, known as α-haemolysin. α-haemolysin is part of the family of β-barrel PFTs. This toxin is secreted in the body as a water-soluble monomer and is capable of binding and oligomerizing into a heptameric structure on the host cellular membrane (Song *et al.*, 1996). A study conducted by Adhikari *et al.* (2012) and colleagues examined a population of 100 adults at risk for *Staphylococcus aureus* sepsis, revealing that the risk of sepsis was reduced in individuals with a higher serum antibody titters to α-haemolysin and a collection of four other toxins. Another study conducted by Fritz *et al.* (2013) examined serum anti- α-haemolysin levels in 235 children, categorized into three groups. (1) *Staphylococcus aureus* colonized without evidence or history of infection, (2) primary skin/soft tissue infection and (3) invasive *Staphylococcus aureus* disease. Highest anti- α-haemolysin levels were discovered in children with an invasive *Staphylococcus aureus* disease.

Similar to streptolysin-O, α-haemolysin has been associated with inflammatory mediators that are part of inflammatory pathways in sepsis. Craven *et al.* (2009) states that α-haemolysin has been shown to induce pulmonary hypertension and inflammation in rat and rabbit models. In addition to pulmonary inflammation, α-haemolysin has been shown to induce inflammatory reactions in skin, eye and the abdomen of rats. Inflammation is induced, due to inflammatory mediators. In endothelial cells α-haemolysin induces platelet activating factor (Suttorp *et al.*, 1993). In pulmonary derived cell lines, α-haemolysin causes release of nitric

oxide and other inflammatory mediators. It has also shown to induce cell death and IL-1β secretion from human monocytes (Bhakdi *et al.*, 1989). All the above inflammatory mediators are released due to cellular/tissue injury (Figure 80). The concentrations of α-haemolysin used in this study are higher than the physiological concentration (1230 ng/ml) for a 2% leporine erythrocyte suspension. Based on Figure 80, it could be confirmed that results in this chapter show that for leporine erythrocytes lysis does take place. However since this toxin was not used against other type of cells shown from Figure 80 , lethal concentrations for other cells are not confirmed. Moreover it would defeat the purpose of this study, which is to create a nanosponge

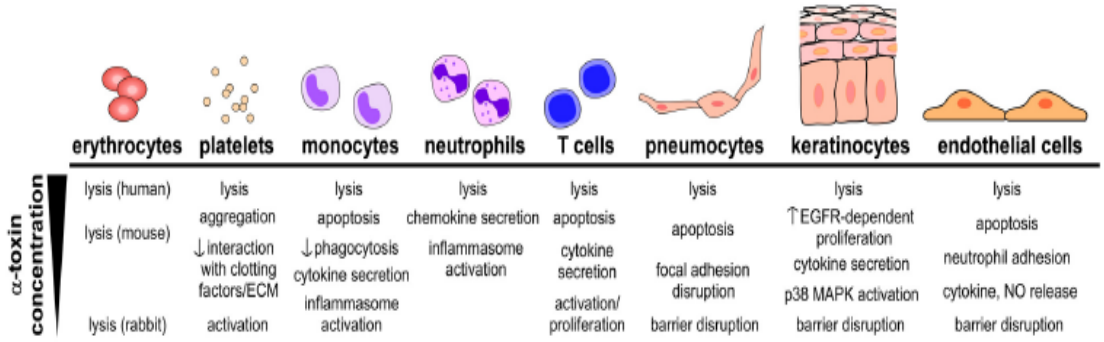

Figure 80. A diagrammatic representation of cellular responses to damage by α-haemolysin (Berube and Wardenburg, 2013).

3.1.3 α-haemolysin

In the late 1800s were the first investigation on the toxic activity of *Staphylococcal* supernatants. These studies showed that addition of the supernatant to various animal models (guinea pigs and rabbits) caused dermonecrosis, inflammation and haemolysis (Christmas-Dirckinck Holmfeld, 1888). The concept that supernatants contained *Staphylococcus* toxins came in the late 1920s following a tragedy in Bundaberg, Australia (Berube and Wardenburg, 2013). 21 children in that town were immunized for anti-diphtheria toxin. With hours 16 children experienced vomiting, high fever and unconsciousness. Within 2 days 12 children had died. The investigation stated that the culture supernatants from the vaccine was contaminated with *Staphylococcus aureus*. This led scientists to study culture supernatants of *Staphylococcus aureus,* finding out that there was presence of a toxin (Berube and Wardenburg, 2013).

After this incident, there have been many studies conducted on the activity of this toxin. This toxin was found to be potent against leporine erythrocytes and was called α-toxin (Glenny and Stevens, 1935). In the 1960s, isolation of the toxin from culture supernatants allowed for a range of biochemical tests and biological experiments to be performed. It was later found out that α-toxin caused disease by disrupting host cellular membranes. From disrupted cells oligomeric structures were found and host cells had formation of large pores in the membrane (Bernheimer and Schwartz, 1963). The molecular mechanism of pore formation became the focus of investigation for many years.

3.1.3.1 Mechanism of pore formation

α-haemolysin is secreted by *Staphylococcus aureus* as a water-soluble monomer. The α-haemolysin assembly is divided into four steps: (1) The water-soluble form approaches and binds to the membrane surface, (2) The monomers partially insert into the membrane (3) They oligomerize into a heptamer and (4) Full membrane insertion takes place and form a pore, which allows for the passage of molecules into the cell membrane (Figure 55). They finally cause the cell to swell up and burst. All β-barrel PFTs interact in the same way. These toxins are attracted to lipid bilayers made up of phosphatidylcholine, sphingomyelin and cholesterol, which are present in all mammalian cells (Bonardi *et al.*, 2012).

However, scientist believed that this toxin has to have specificity for a receptor on the erythrocyte membranes as low concentrations of this toxin caused haemolysis (Berube and Wardenburg, 2013). It was not until 2010, when ADAM 10 was defined as the target for α-haemolysin (Wilke and Wardenburg, 2010). A disintegrin and metalloprotease 10 (ADAM 10) is a proteinaceous receptor for α-haemolysin, and is found to be most abundant on leporine erythrocytes (Wilke and Wardenburg, 2010). It is a transmembrane protein on the surface of host cells. The extracellular domain of ADAM 10 is comprised of an N-terminal enzymatic domain known as disintegrin. Functioning as a sheddase ADAM 10 is responsible for cleavage of large protein present on the host cell surface.

3.2 Material and methods

3.2.1 Preparation of leporine nanosponges

Leporine nanosponges were prepared using the same protocol described in section 1.5.11. Similar to the previously used method the leporine erythrocyte vesicles and PLGA polymeric cores were added in equal volumes and extruded 13 times through a 100 nm polycarbonate membrane at 20°C. The mechanical force of extrusion allowed fusion of the erythrocyte vesicles with the PLGA nanoparticle, synthesizing a nanoparticle with a lipid coating and a PLGA polymeric core.

3.2.2 Characterisation of leporine nanosponges

The leporine nanosponges were characterized using Malvern Nano-zs zetasizer. 1 ml of the synthesized leporine nanosponge suspension was added to a polystyrene cuvette. This cuvette was inserted into the zetasizer ad assayed for nanoparticle size and zeta potential (Weber *et al.*, 2000).

3.2.3 Concentration dependent haemolysis assay

The haemolysis assay is adopted form Duncan (1974) and Bernheimer (1988), and was optimized here to simulate human physiological conditions. The aims to test the concentration of mammalian Hb released after the addition of different concentrations of α-haemolysin. Washed mammalian blood (ovine, porcine, murine and leporine) was diluted with PBS (137mM NaCl, 2mM KH_2PO_4, 8mM Na_2HPO_4) to make a 2% (v/v) erythrocyte suspension. 25 ml of this 2% erythrocyte suspension was incubated at 37°C in a water bath for 1 hour. At the same time, 10 ml Drabkins reagent was separately heated to 37°C for 1 hour. α-haemolysin (0.2 mg/ml) being an oxygen-stable PFT, was diluted with PBS to make a stock of 5000 ng/ml, and did not require the use of L-cysteine. The stock was diluted to produce the concentrations shown in Table 24.

Table 24. Preparation of different concentrations of α-haemolysin diluted with PBS to produce the following concentrations.

No	Volume of α-haemolysin stock (µl)	Volume of PBS buffer (µl)	Total volume (µl)	Final concentration of α-haemolysin
1	10	40	50	1000
2	20	30	50	2000
3	30	20	50	3000
4	40	10	50	4000
5	50	0	50	5000

For each of the concentrations shown in Table 24, 50 µl of α-haemolysin was added to an Eppendorf tube containing 500 µl 2% erythrocyte suspension. The tubes were then placed in a water bath incubator for 30 minutes at 37°C. The tubes were then centrifuged for 5 minutes at 900 x g at 4°C. 20 µl of this supernatant was added to 4 ml of Drabkins reagent and was allowed to stand for 15 minutes. The absorbance was assayed at 540 nm using a Jenway spectrophotometer

3.2.4 Time dependent haemolysis assay

This assay was design to test the correlation between time and the physiological concentration of α-haemolysin. The washed animal blood (ovine, porcine, murine and leporine) was diluted with PBS to make a 2% erythrocyte (v/v) suspension. The 2% erythrocyte suspension and the Drabkins reagent were incubated in a temperature controlled water bath at 37°C. 6 µl from a 0.2 mg/ml α-haemolysin stock was added to 994 µl PBS to produce a concentration of 1230 ng/ml, with a total volume of 1 ml. The tubes were prepared according to Table 25.

Table 25. Concentration of α-haemolysin and incubation time of each test sample prepared in the assay

No.	Incubation time for test sample (mins)	Final α-haemolysin concentration (ng/ml)
1	10	1230
2	20	1230
3	30	1230
4	40	1230
5	50	1230
6	60	1230

The volume of α-haemolysin and 2% erythrocyte suspension were added according to Figure 57. Each of the above prepared tubes were incubated at 37°C in a water bath according to the times shown in Table 25. The tubes were then centrifuged for 5 minutes at 900 x g in a microcentrifuge at 4°C. 20 µl of the supernatant was added to 4 ml of Drabkins reagent and was allowed to stand for 15 minutes. The absorbance was assayed at 540 nm.

3.2.5 Toxin adsorption studies

This method is adopted from Hu *et al.* (2013) and optimized to achieve desired conditions. This test, aims to test the efficacy of nanosponges and its components to adsorb α-haemolysin, under different temperatures. Leporine blood was chosen for this study as leporine erythrocytes showed maximum susceptibility towards α-haemolysin lysis compared to ovine, murine and porcine blood.

3.2.5.1 Testing the efficacy of leporine nanosponges as a toxin adsorbing system

Toxin absorption by nanosponges were tested using a published method (Hu *et al.*, 2013). A stock solution containing 0.2 mg/ml α-haemolysin was diluted to 1230 ng/ml, by adding 6 µl of the stock to 994 µl of PBS. 50 µl of the diluted α-haemolysin was added to each test system, as depicted in Figure 59 (for this

method streptolysin-O replaced for α-haemolysin). The 250 µl 2% (v/v) leporine erythrocyte suspension was added in last, as the addition of erythrocytes starts the reaction. However, for the system containing nanosponges, they were added in after the 2% leporine erythrocyte suspension. The total volume in the four systems were 550 µl. The four systems were then incubated in a controlled water bath at 37°C. After 30 minutes of incubation, the four systems were then centrifuged for 5 minutes at 900 x g. This allowed separation of the supernatant from the non-haemolysed components. 20 µl of this supernatant is added to 4 ml of Drabkins reagent and was allowed to stand for 15 minutes. The absorbance was assayed at 540 nm using a spectrophotometer. This assay was repeated at 40°C, which emulated the elevated body temperature during sepsis (Lee *et al.*, 2012)

3.2.5.2 Testing the efficacy of reconstituted leporine nanosponges as a toxin adsorbing system

This method aims to test the efficacy of leporine nanosponges to retain their ability to adsorb α-haemolysin, after reconstitution. Leporine nanosponges were lyophilized at a concentration of 1 mg/ml with 5% (w/v) sucrose (refer to chapter 1 section 1.5.13). The lyophilized nanosponges were stored at 4°C for a week. After a week, the leporine nanosponges were reconstituted with PBS (pH 7.2). Nanosponges were characterised for size and zeta potential. Leporine nanosponges at a concentration of 1mg/ml were tested for their ability to adsorb 1230 ng/ml streptolysin-O. 50 µl of a 1230 ng/ml streptolysin-O solution was added to 4 test systems shown in Figure 59. . The four systems were then incubated in a controlled water bath at 40°C. After 30 minutes of incubation, the four systems were then centrifuged for 5 minutes at 900 x g. 20 µl of this supernatant is added to 4 ml of Drabkins reagent and was allowed to stand for 15 minutes. The absorbance was assayed at 540 nm using a spectrophotometer.

3.3 Results

3.3.1 Characterisation of leporine nanosponges

The nanosponges were synthesized by extruding the leporine erythrocyte vesicles with the PLGA nanoparticle cores. The nanosponges were dissolved with isotonic PBS and characterised for size. Figure 81 shows the size distribution of leporine nanosponges measured using dynamic light scattering Figure 81 shows two distinct peaks. The tallest peak has a size of 571 nm and the shorter peak has a size of 114 nm. The software combined the two sizes to report an average size of 354 nm with a PDI of 0.443.

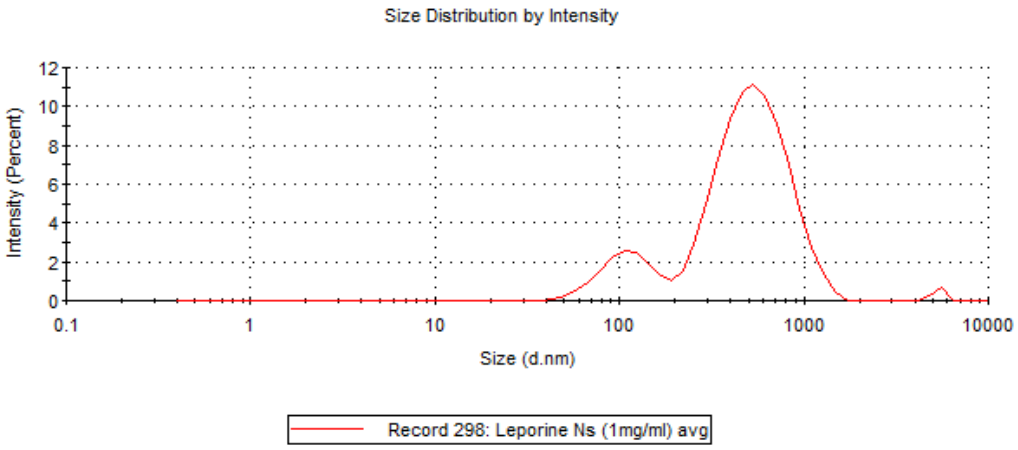

Figure 81. Size distribution graph of 1 mg/ml leporine nanosponges prepared by fusing ovine erythrocyte vesicles with PLGA nanoparticles. This plot was acquired from the Malvern zetasizer data analysis software

Leporine nanosponges were lyophilized with 5% (w/v) sucrose and stored at 4°C for a week. After a week, the lyophilized suspension was reconstituted with PBS. The reconstituted suspension was measure for size, using a zetasizer. Figure 82 shows the size distribution of reconstituted leporine nanosponges after one week of storage. Figure 82 shows two different peaks. The tallest peak has a size of 575 nm and the shorter peak has a size of 119 nm. The software combined the two sizes to report an average size of 394 nm with a PDI of 0.302.

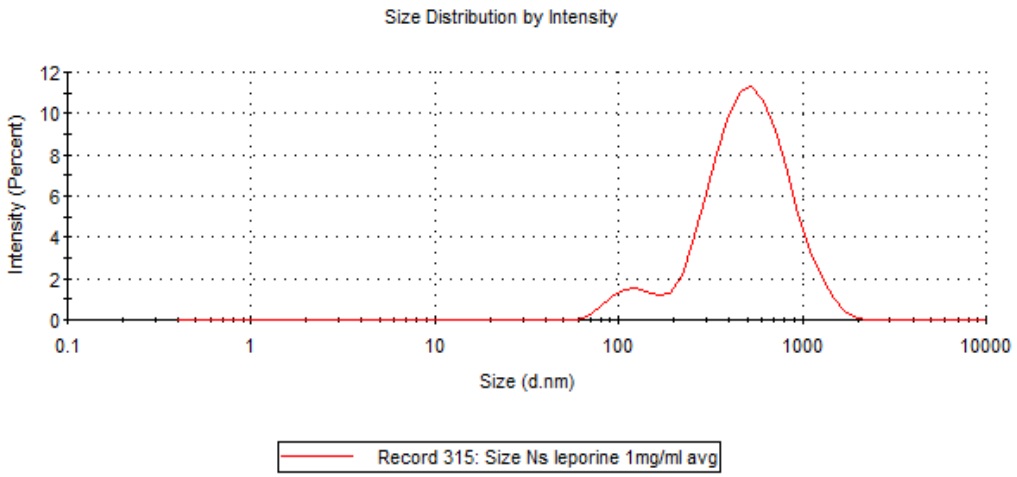

Figure 82. Size distribution graph of nanosponges lyophilized with 5% sucrose (w/v) reconstituted after 1 week, with PBS. This plot was acquired from the Malvern zetasizer data analysis software.

The leporine nanosponges were also characterised for their zeta potential. It measures the electrostatic charge between the particles in a suspension. Figure 83 shows the zeta potential distribution plot of leporine nanosponges. The average zeta potential is reported as -9.0 mV.

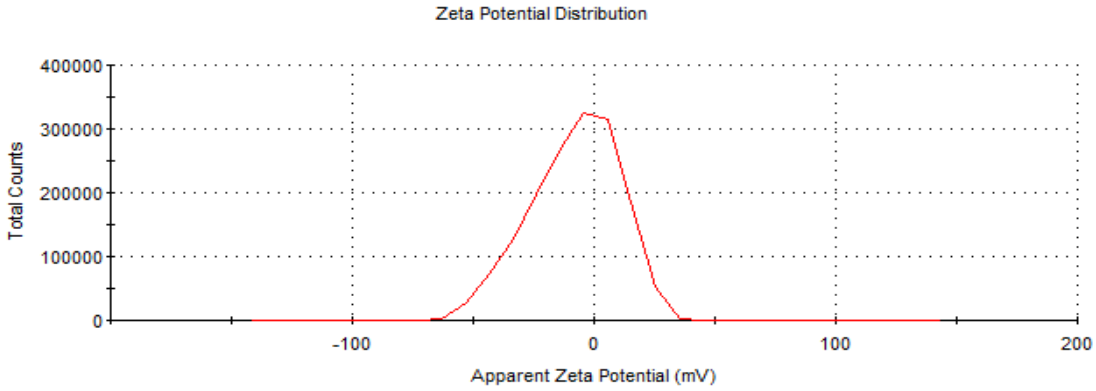

Figure 83. Zeta potential distribution graph of 1 mg/ml leporine nanosponges. This plot was acquired from the Malvern zetasizer data analysis software.

The leporine nanosponges that were lyophilized with 5% sucrose were also characterised for their zeta potential after reconstituting it with PBS. Figure 84 shows the zeta potential distribution of reconstituted nanosponges after one week of storage in a lyophilized form. According to Figure 84, the average zeta potential is -11.1 mv.

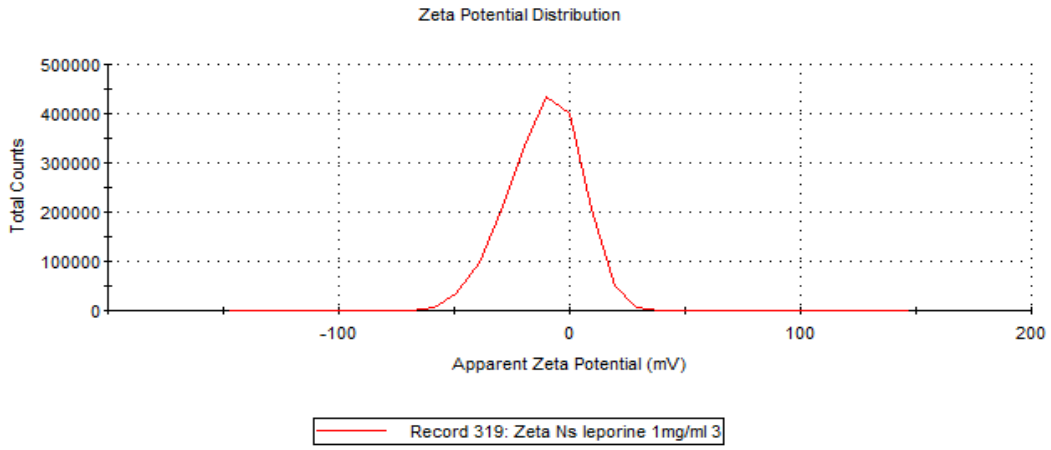

Figure 84. Leporine nanosponges were lyophilized with 5% sucrose for one week. The zeta potential distribution curve refers to the electrostatic charge recorded after reconstituting the lyophilized suspension with PBS.

3.3.2 α-haemolysin haemolysis assays

3.3.2.1 Concentration dependent assay

α-haemolysin was assayed against four different types of mammalian blood (leporine, murine, ovine and porcine). From each of these mammalian blood types a 2% (v/v) erythrocyte suspension was prepared. To which increasing concentrations of α-haemolysin were added. The suspensions were incubated at 37°C for 30 minutes. They were then centrifuged at 4°C for 5 minutes, which separated the unlysed erythrocytes from the released Hb. The released Hb was assayed for optical density at 540 nm. The measured Hb was estimated using a bovine Hb standard curve shown from Figure 30. . Haemolysis of the suspensions were calculated as a percentage of the total amount of Hb present in the system, since each mammalian blood species has a different amount of Hb present in their system. Figure 85, shows the effect of increasing concentrations of α-haemolysin on Hb release from 2% (v/v) ovine, leporine and murine erythrocyte

suspensions. Porcine data was not added to Figure 85 as it showed no concentration of Hb release, which meant that the porcine erythrocytes were unlysed and were not susceptible to haemolysis by α-haemolysin. According to Figure 85, as the concentration of α-haemolysin increases, the concentration of Hb released increases from the leporine, murine and ovine systems. Similar to streptolysin-O haemolysis assay there was a sequential difference between the mammalian blood in terms of lysis by α-haemolysin. This was leporine >murine>ovine up to 5000 ng/ml. Leporine erythrocytes released the highest concentration of Hb when incubated with 5000 ng/ml α-haemolysin, as 75% (± 1.1) of the total Hb was released by leporine erythrocytes.

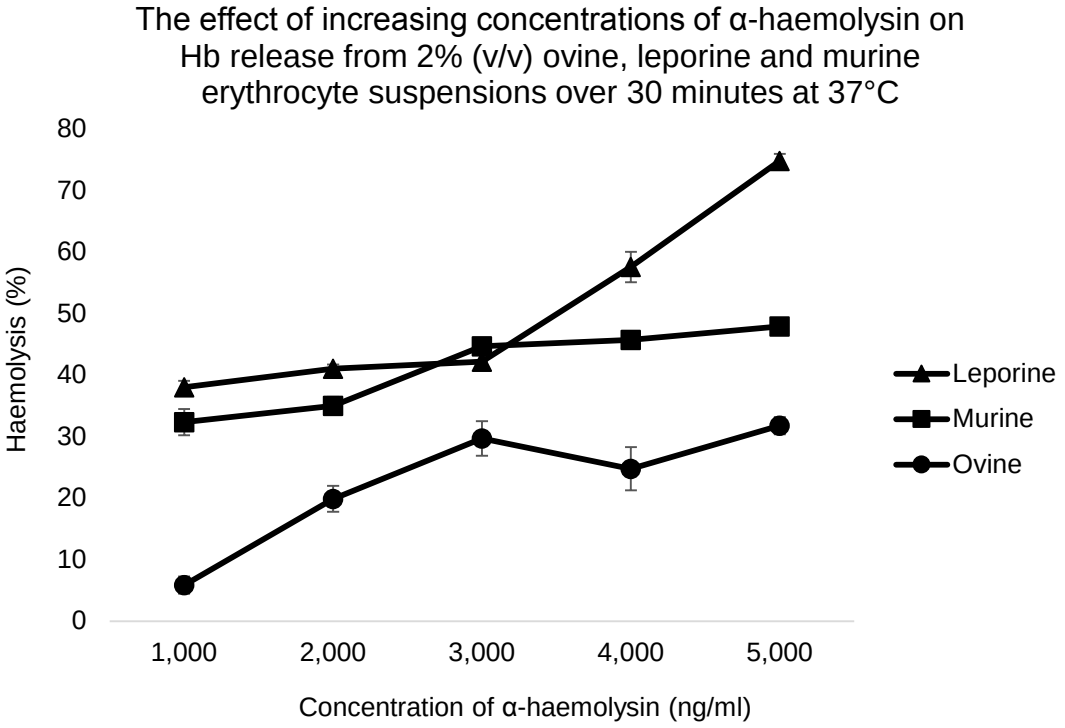

Figure 85. The effect of increasing concentration of α-haemolysin on Hb release from three different types of mammalian blood. The total Hb present in the 2% mammalian suspensions: leporine (2.67 g/dl, ± 0.07), murine (1.87 g/dl, ± 0.07) and ovine (1.43 g/dl, ± 0.09). Error bars represent SEM (n=3). R^2 values were measured for the respective mammalian blood types. Murine (R^2=0.901), leporine (R^2=0.849), porcine (R^2=0.913) and ovine (R^2=0.754).

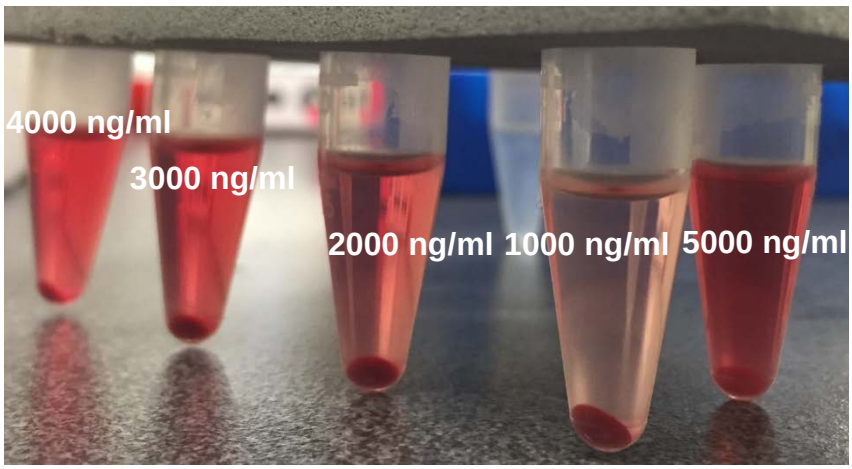

Figure 86. An image taken with a Nikon camera shows five Eppendorf tubes, with increasing concentrations of Hb present in the supernatant. The first tube with the lowest intensity of red has a concentration of 1000 ng/ml α-haemolysin, whereas the last tube has a concentration of 5000 ng/ml.

3.3.2.2 Time dependent assay

α-haemolysin was assayed against three different mammalian blood, with respect to time. According to the concentration dependent study, porcine blood did not show any signs of haemolysis against α-haemolysin. This could be as there aren't any studies indicating the presence of ADAM10 receptors on the porcine membrane. .Therefore, porcine blood was not used in this study. The suspensions were incubated for 60 minutes at 37°C. The released Hb present in the supernatant was assayed for absorbance at 540 nm. The measured Hb was estimated using a bovine Hb standard curve shown from Figure 30. Haemolysis of the suspensions was calculated as a percentage of the total amount of Hb present in the system. Figure 87 shows the effect 1230 ng/ml streptolysin-O has on three different mammalian blood during 60 minutes incubation at 37°C. After 60 minutes of incubation, leporine erythrocytes showed maximum haemolysis towards α-haemolysin. At 60 minutes α-haemolysin released 82% (± 1.35) Hb as compared to ovine and murine Hb release.

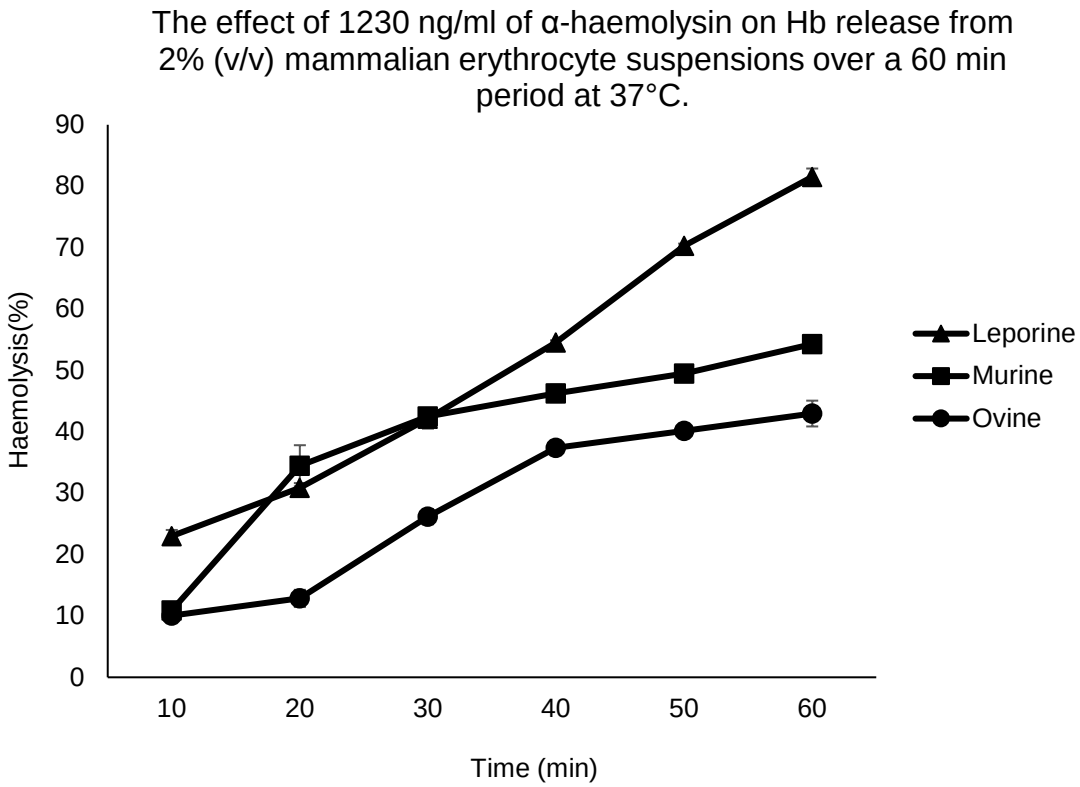

Figure 87. The effect of 1230 ng/ml (human physiological concentration) of α-haemolysin on a 2% (v/v) mammalian erythrocyte suspensions over a 60-minute time period. The Hb concentration was measured at 540 nm using Drabkins reagent. Leporine (2.67 g/dl, ± 0.07), murine (1.87 g/dl, ± 0.07) and ovine (1.43 g/dl, ± 0.09). Error bars represent SEM (n=3). R^2 values were measured for the respective mammalian blood types. leporine (R^2=0.991), Murine (R^2=0.829), and ovine (R^2=0.935)

3.3.3 α-haemolysin adsorption assays

This study tested the ability of leporine nanosponges and its components (leporine erythrocyte vesicles and PLGA core) to adsorb 1230 ng/ml α-haemolysin. This study used leporine nanosponges, because the concentration and time dependent haemolysis assays show leporine nanosponges are the most susceptible to haemolysis by α-haemolysin. Therefore, to test α-haemolysin adsorption, leporine nanosponges were developed for this study. Figure 88 shows the effect of leporine nanosponge and its components to adsorb 1230 ng/ml α-haemolysin. Adsorption was tested at 37 and 40°C, similar to the streptolysin-O adsorption assays. According to Figure 88, the system that

contained the nanosponges had the lowest Hb release at 37 and 40°C. At 37°C, the concentration of Hb released, in the system containing nanosponges was 0.265 g/dl (± 0.02). At 40°C, the concentration of Hb released in the system containing the nanosponges was significantly greater compared to nanosponges incubated at 37°C. The difference is shown by the level of significance “P≤0.05”.

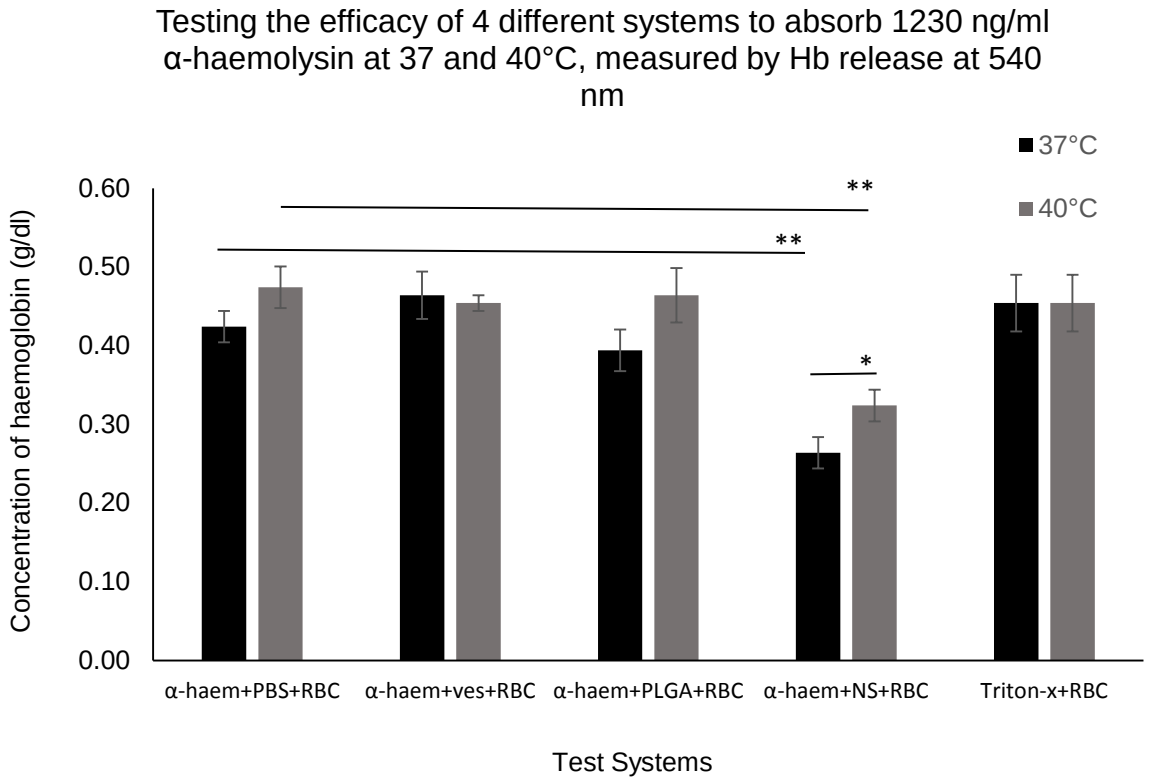

Figure 88. Testing the efficacy of leporine nanosponges and it components to adsorb 1230 ng/ml α-haemolysin, incubated at 37 and 40°C. Adsorption of α-haemolysin was measured by degree of haemolysis at 540 nm. .“*”P≤0.05, “**”P≤0.01 and “***”P≤0.001. Error bars represent SEM (n=3).

The synthesised leporine nanosponges and its components were lyophilized with 5% (w/v) sucrose and stored at 4°C for one week, as stated in section 1.5.13. The nanosponges and its components were then reconstituted with isotonic PBS (pH 7.2) and tested for their efficacy to adsorb α-haemolysin. Similar to the previous results, the system that contained the leporine nanosponges shows the least Hb release at 0.324 g/dl (± 0.02), as shown in Figure 89.

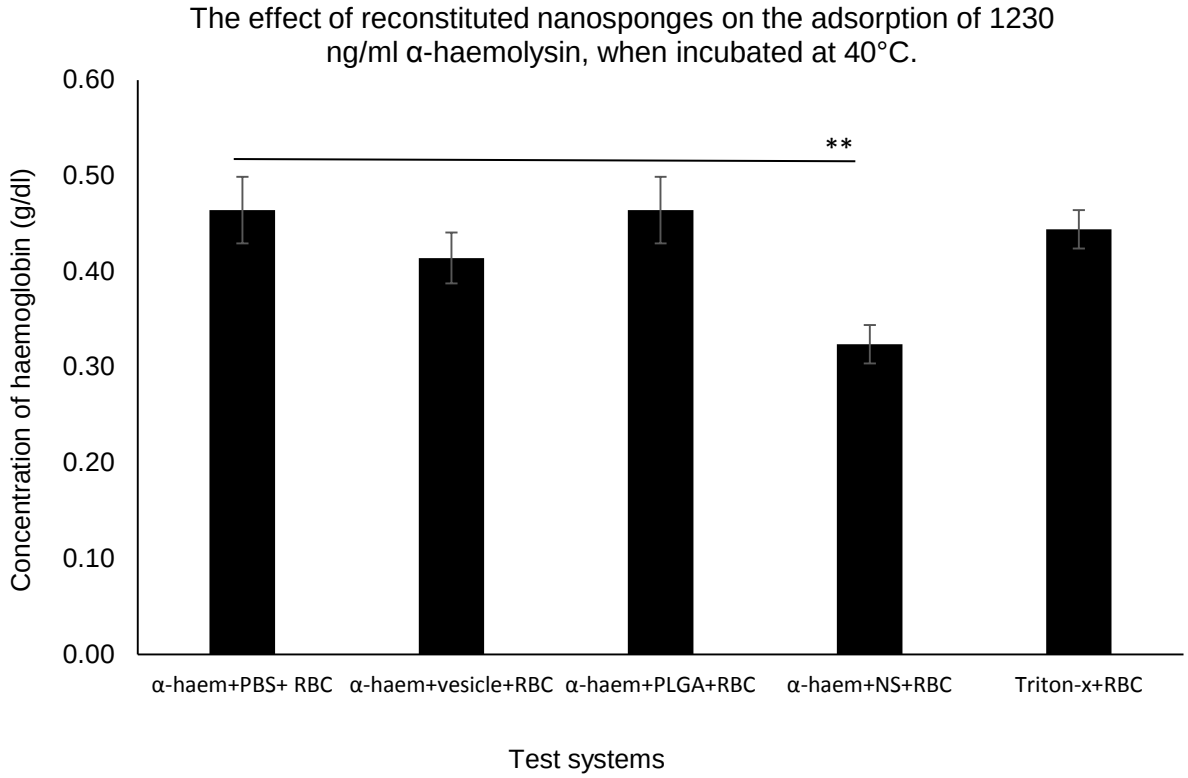

Figure 89. Testing reconstituted leporine nanosponges (1mg/ml) and its components for absorption of α-haemolysin, incubated at 40°C. "*"P≤0.05, "**"P≤0.01 and "***"P≤0.001. Error bars represent SEM (n=3).

3.4 Discussion

The overall aim of this research chapter was to test the efficacy of α-haemolysin haemolysis against ovine, porcine, leporine and murine blood. A further aim was to synthesize nanosponges from mammalian erythrocytes. Leporine blood was chosen as a coating for the polymer as it was found to be the most susceptible to α-haemolysin haemolysis. The synthesised nanosponge was then tested for its ability to adsorb α-haemolysin under different physiological and storage conditions.

3.4.1 Characterisation of leporine nanosponges

Extruded leporine erythrocyte vesicles were added to the PLGA nanoparticle cores and extruded through a 100 nm polycarbonate membrane. The mechanical force generated during extrusion coated the PLGA core with the leporine erythrocyte membrane (Rao *et al.*, 2016). The leporine nanosponge, like the ovine nanosponges were characterised for size and zeta-potential. Figure 81 shows the size distribution of 1 mg/ml leporine nanosponges. There are presence of two peaks. However, the zetasizer software has reported an average size of 354 nm with a PDI of 0.443. The extrusion method used in this research, is used to coat the PLGA polymeric cores with the erythrocyte membrane. According to Figure 81, this procedure produces a polydispersed leporine nanosponge suspension with a large size.

There are two factors that cause this to happen (1) extrusion pressure and (2) the composition of lipids on the erythrocyte membrane. Hunter and Frisken (1998) states that extrusion through 100 nm pores result in larger size vesicles. Nonetheless, extrusion is used to develop monodisperse suspension. However, the leporine nanosponge suspension is polydispersed. This could be due to the lipid composition on the membrane. Pekİner (2002) showed that leporine erythrocyte have a higher concentration of phosphatidylethanolamine (PE) rather than phosphatidylcholine (PC). This is significant as Paliwal *et al.* (2013) that PE liposomes have the tendency to form aggregates due to poor hydration of the head group. This gives them a higher affinity to adhere to cell membranes. This could be the reason as to why even after extrusion, leporine nanosponges form polydispersed suspensions.

As discussed in 1.7.8 sucrose has the potential to stabilise the nanosponges and was tested using ovine nanosponges (Wu *et al.*, 2011). Similarly, leporine nanosponges were lyophilized with sucrose and reconstituted after a week with PBS. The reconstituted leporine nanosponges were characterised for size and zeta potential. Figure 82 shows the size distribution graph of lyophilized leporine nanosponges reconstituted after a week. Similar to Figure 81, Figure 82 has two peaks and look the same if observed by eye. However, the zetasizer software has reported an average size of 394 with a PDI of 0.302. The size of leporine nanosponges have increased and PDI has decreased, compared to the size of the nanosponges reported in Figure 81. This could suggest that sucrose could have stabilized the nanosponges. However, Figure 81 shows that the size has increased and the PDI reported indicates a polydispersed suspension. These parameters show that the leporine nanosponges are unstable.

Leporine nanosponges were characterised for their zeta potential. Figure 83 shows the zeta-potential of 1mg/ml leporine nanosponges. The average zeta-potential reported was – 9.0 mv. As discussed earlier, the negative charge on the erythrocyte membrane is caused by the carboxyl groups of sialic acid present on the end terminus of glycoproteins and glycolipids (Eylar *et al.*, 1962, Luk *et al.*, 2014). Similarly, lyophilized leporine nanosponges were also characterised for their zeta potential. The average zeta-potential reported was – 11.0 mv. However, there is no significant difference between the zeta potential of leporine nanosponges and lyophilized nanosponge as the peaks do overlap.

3.4.2 α-haemolysin haemolysis assay

The novel experiment tested the effect of α-haemolysin against four different types of mammalian blood. α-haemolysin is a β-barrel PFT, and is shown to bind specifically to a protein known as ADAM 10 (Wilke and Wardenburg, 2010). Figure 85 shows the effect of increasing concentration of α-haemolysin on leporine, murine and ovine blood. Leporine erythrocytes have shown to be most susceptible to haemolysis by α-haemolysin, as 5000 ng/ml α-haemolysin has released 75% (± 1.1) of Hb present in a 2% (v/v) erythrocyte suspension. This result is significant as Berube and Wardenburg (2013) states during investigation of the Bundaberg case, culture supernatants that contained *Staphylococcus*

aureus α-haemolysin was injected into rabbits and caused lethal injury and haemolysis. Which eventually led to death. Furthermore, Cooper *et al.* (1966) and Cooper *et al.* (1964) show that leporine erythrocytes were the most sensitive to damage by α-haemolysin, compared to any other species of blood. They went on to show that 2 μg/kg of the toxin caused lethal effects in the rabbit, the lowest of any species tested in their study. In 2010, a study conducted by Wilke and Wardenburg (2010) shows that the reason α-haemolysin specific for rabbit erythrocytes is due to a protein, ADAM 10.

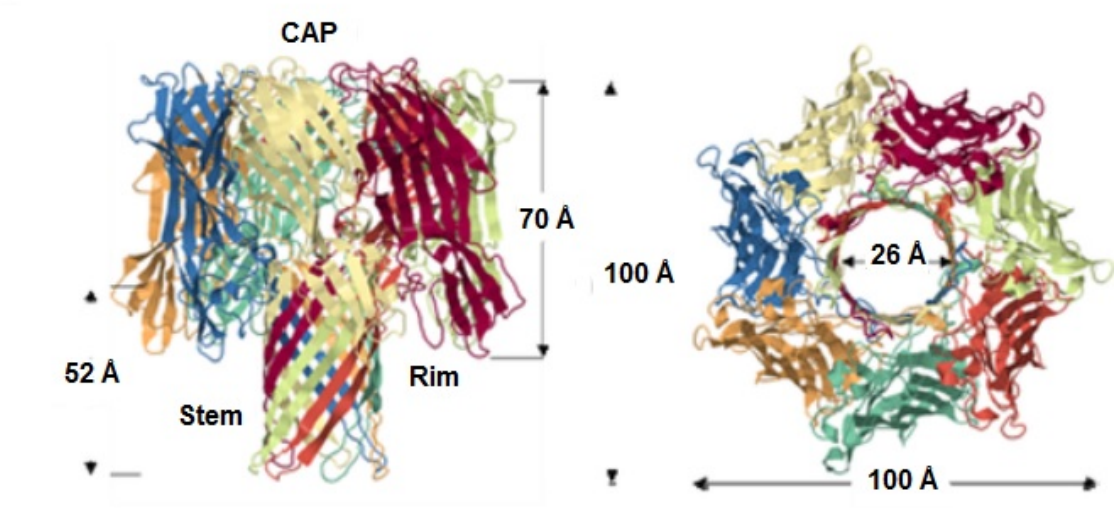

Figure 90. The molecular structure of α-haemolysin. This structure represents the form α-haemolysin take on during pore formation. The structure is made up of the cap, rim and the stem, which are essential for pore formation. The image was reproduced to depict the structure of α-haemolysin (Gurnev and Nestorovich, 2014).

The interaction between α-haemolysin and ADAM 10 cause a cascade of events that lead to inflammation and tissue injury. However, the chemistry behind the interaction is unknown. Inoshima *et al.* (2011) has suggested that the N-terminal segment of α-haemolysin undergoes a conformational shift (Figure 90) to latch on to the neighbouring protein (ADAM 10) stabilizing the heptameric pore structure. The requirement for ADAM 10 as a cellular receptor for *Staphylococcus aureus* pathogenesis was demonstrated using conditional knockout approaches in the alveolar epithelium and the mature epidermis (Inoshima *et al.*, 2011). Similarly, ADAM 10 knockout in the skin was associated with reduction in the size of *Staphylococcus aureus* skin lesions (Inoshima *et al.*, 2012)

In reference to ADAM 10 mediated cellular injury, one of the domains of ADAM 10 particularly the cytoplasmic tail of the molecule contributes to toxin-induced intracellular signalling. In context of epithelial cells that are targets of α-haemolysin, E-cadherin is a principal substrate for ADAM 10. Cleavage of this substrate results in the loss of interaction of the cadherin molecules on adjacent cells thereby injuring the epithelial tissue barrier function (Maretzky *et al.*, 2005). *In vitro* studies demonstrated that treatment of epithelial cells with sub-lytic concentrations of α-haemolysin leads to rapid up regulation of the metalloprotease activity of ADAM 10, which in turn dismantled the adherens junction through cleavage of E-cadherin (Maretzky *et al.*, 2005)

As discussed in 2.4.1 timing is significant in treatment of sepsis, as there is a correlation between time of treatment and rate of survival (Figure 78). Figure 87 shows the effect 1230 ng/ml α-haemolysin has on leporine, murine and ovine blood over a period of 60 minutes. After 60 minutes of incubation, the figure shows that leporine erythrocytes were most susceptible to haemolysis by α-haemolysin, as 1230 ng/ml α-haemolysin released 82% (± 1.35) Hb. Another study has shown that using 180 HU of α-haemolysin, has caused approximately 80% haemolysis after 12.5 minutes (Cooper *et al.*, 1964). Similarly, another study reported scanning electron images of rabbit red blood cells incubated with 1 HU of α-haemolysin. After 30 minutes, they showed scanning electron microscopy images of a disrupted RBC membrane (Klainer *et al.*, 1972).

3.4.3 α-haemolysin adsorption studies

Chapter 1 and 2 introduce synthesis of a novel therapeutic model, nanosponge. This model was developed using ovine blood. In this chapter leporine blood was chosen as a coating for the polymer, to develop nanosponges, as it was found to be the most susceptible to α-haemolysin haemolysis. Figure 88 tested the ability of leporine nanosponges and its contents to adsorb α-haemolysin at 37 and 40ºC. The system that contained the nanosponges had the least Hb release compared to the system containing just the toxin and erythrocytes. However, there is still a significant amount of Hb released in the system with the nanosponges. Several factors may cause this to happen, (1) instability of the nanosponge, (2) loss of sample during extrusion and (3) loss of ADAM 10 during extrusion. As discussed in section 3.4.1, the instability of the nanosponge could be due to the lipid

composition of the leporine membrane and the fact that extrusion leads to formation of larger sized particles. Furthermore, Cho *et al.* (2013) has stated that "some sample material may be lost during extrusion during passage through the porous membrane". Therefore, sample loss could account for the concentration of ADAM 10 being lost during extrusion. Nonetheless, there is a study that has reported the adsorption of α-haemolysin of by erythrocyte ghosts (Wilke and Wardenburg, 2010).

Figure 82, shows the improvement in polydispersity as lyophilized leporine suspension were reconstituted after a week. This shows that lyophilization could improve stability of the particle. Therefore, lyophilized leporine nanosponge and its contents were tested for their ability to adsorb 1230 ng/ml α-haemolysin at 40ºC. Similar results were obtained to the study conducted with non-lyophilized leporine nanosponges. There was no significant change in adsorption by reconstituted nanosponges at 40ºC.

Chapter 4

4 Comparative studies

This section aims to compare results obtained from prior chapters. Principally, the section will focus on the characteristics of the developed nanosponges, the haemolytic activity of streptolysin-O and α-haemolysin and the ability of the nanosponges to adsorb these PFTs at different temperatures.

4.1 Characteristics of nanosponges

Ovine and leporine nanosponges were characterised separately for their size zeta potential and PDI. However when merged together, these nanosponges show very distinct characteristics. Figure 91, shows the size distribution of ovine and leporine nanosponges. The ovine nanosponges have an average size of 185 nm (± 50) with a PDI of 0.134. Comparatively, leporine nanosponges have an average size of 354 nm with a PDI of 0.443. The figure shows that leporine nanosponges have a greater size and are polydispersed. Whereas the ovine nanosponges have a smaller, size and are monodispersed. As stated earlier the polydispersity of the leporine nanosponges, is caused either due to the lipid composition of the membrane or the extrusion pressure (refer to section 3.4.1). This result suggests that ovine nanosponges are more stable than leporine nanosponges.

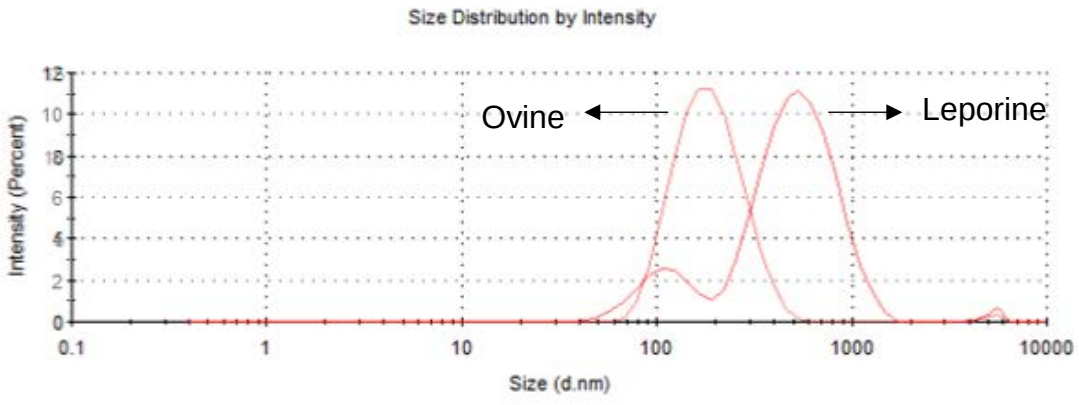

Figure 91. Size distribution graph of 1 mg/ml ovine and leporine nanosponges prepared by fusing erythrocyte vesicles with PLGA nanoparticles at RTP. This plot was acquired from the Malvern zetasizer data analysis software.

Ovine and leporine nanosponges were also characterised for their zeta potential. Figure 92 shows the zeta potential distribution of ovine and leporine nanosponges. The figure shows that ovine nanosponges have an average zeta potential is -10.5 mV. Whereas leporine nanosponges have an average, zeta potential is reported as -9.0 mV. Ovine nanosponges have a similar zeta potential compared to leporine nanosponges. The ovine nanosponge has a greater zeta potential. For this reason, it is putative that ovine nanosponges are more stable than leporine nanosponges due to the repulsion of particles.

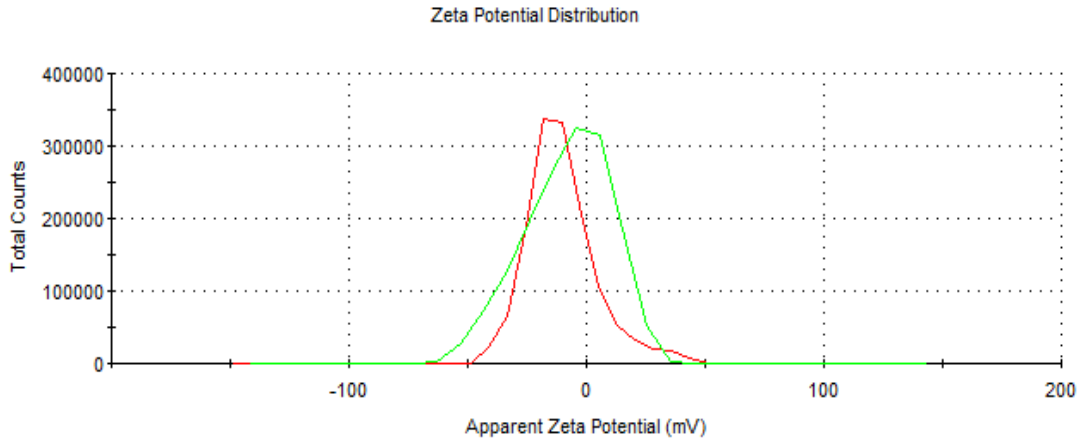

Figure 92. Zeta potential distribution graph of 1 mg/ml ovine and leporine nanosponges. This plot was acquired from the Malvern zetasizer data analysis software. The green peak represents leporine nanosponges whereas the red peak represents ovine nanosponges.

4.2 Haemolysis assay

Streptolysin-O has been assayed against four different types of mammalian blood. Similarly, α-haemolysin has also been assayed against these four types of mammalian blood. However, this section will compare the haemolytic activity of streptolysin-O with α-haemolysin for each mammalian blood type. Figure 93 shows the effect of increasing concentrations of streptolysin-O and α-haemolysin on three different mammalian blood types. Porcine blood was not included in this section, as it was only found to be susceptible to haemolysis by streptolysin-O. Figure 93A shows that ovine erythrocytes are the most susceptible to streptolysin-O haemolysis as compared to α-haemolysin haemolysis. As 2000

ng/ml, released a greater concentration of ovine Hb compared to 5000 ng/ml α-haemolysin. As stated in section 2.4.1, streptolysin-O has a high affinity towards membranes that contain a greater concentration of cholesterol.

Figure 93B shows that murine erythrocytes are susceptible to haemolysis by both streptolysin-O and α-haemolysin. However, haemolytic activity was at lower concentrations of streptolysin-O, whereas 5000 ng/ml of α-haemolysin was required to achieve similar haemolytic activity to streptolysin-O. Figure 93C shows that leporine erythrocytes are the most susceptible to haemolysis by α-haemolysin. As lower concentration of α-haemolysin, have a greater haemolytic activity compared to streptolysin-O haemolysis. As discussed section 3.4.2, α-haemolysin has high affinity towards ADAM 10, which are present on leporine erythrocytes (Wilke and Wardenburg, 2010).

The haemolysis assays were also conducted over a period of 60 minutes to test the haemolytic effect of streptolysin-O and α-haemolysin with respect to time. Figure 94 shows the effect of 1230 ng/ml streptolysin-O and α-haemolysin on 2% mammalian erythrocyte suspension over a 60 minutes period at 37°C. Figure 94A shows that over a 60-minute period ovine erythrocytes are more susceptible to streptolysin-O compared to α-haemolysin. . Figure 94B shows that over time murine erythrocytes are susceptible towards 1230 ng/ml streptolysin-O and α-haemolysin. As discussed in section 2.4.1, mice erythrocytes have cholesterol in the membrane. Wilke and Wardenburg (2010) and Inoshima *et al.* (2011) have conducted studies with mice erythrocytes and α-haemolysin , as the erythrocyte membranes are enriched with the transmembrane protein ADAM 10 in the erythrocyte membrane. Figure 94C shows that over a 60 minute period leporine erythrocytes are the most susceptible to haemolysis by α-haemolysin.

A

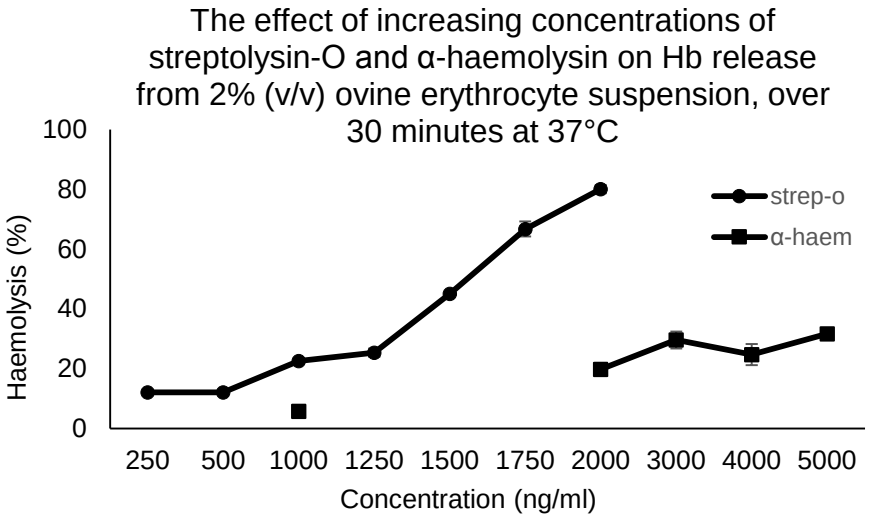

B

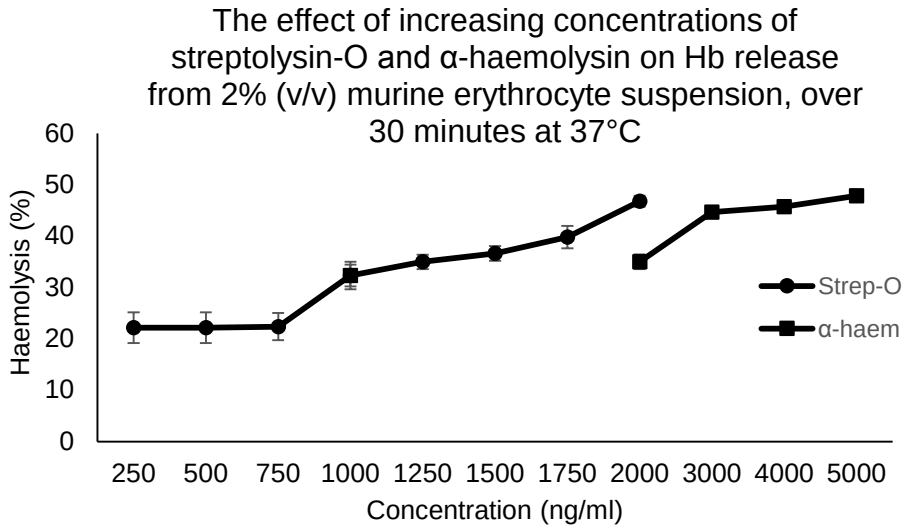

C

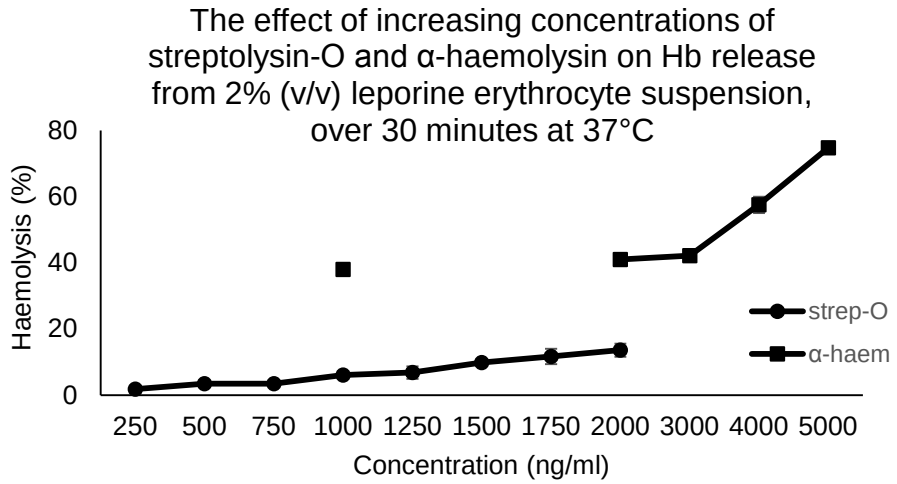

Figure 93. The effect of increasing concentration of streptolysin-O and α-haemolysin on Hb release from three different types of mammalian blood. (A) Ovine, (B) murine and (C) leporine. Error bars represent SEM (n=3).

A

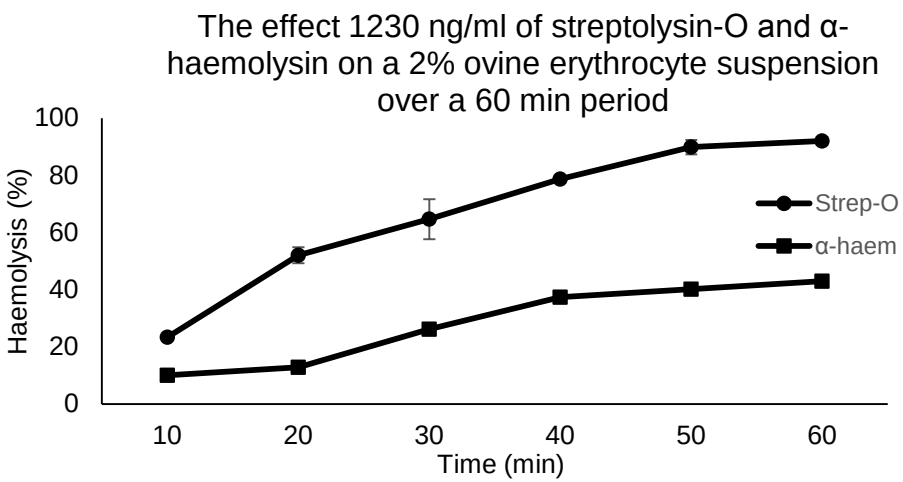

B

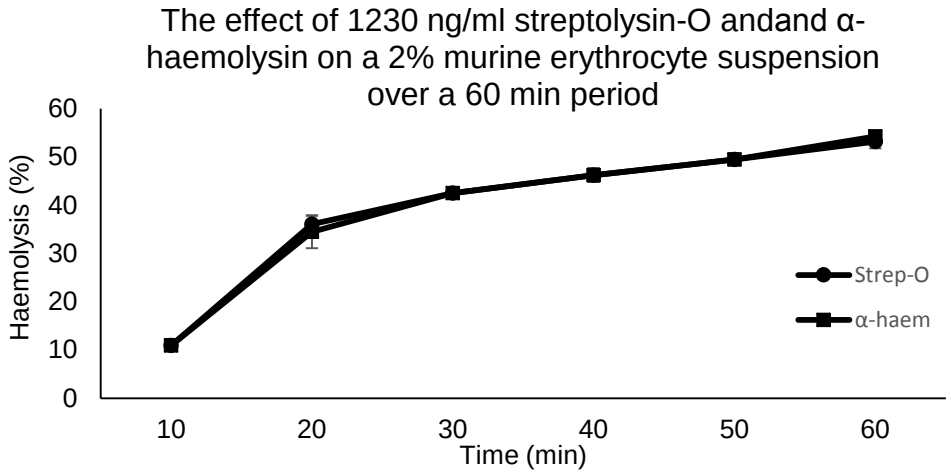

C

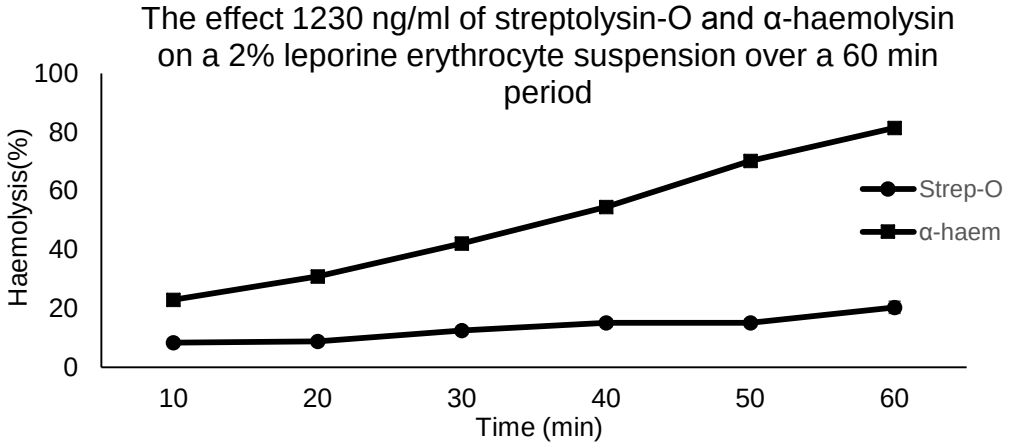

Figure 94. The effect of 1230 ng/ml of streptolysin-O and α-haemolysin on a 2% (v/v) mammalian erythrocyte suspensions over a 60-minute time period. (A) Ovine, (B) murine and (C) leporine. Error bars represent SEM (n=3).

4.3 Adsorption studies

After toxin studies, different nanosponges were developed and prepared for each toxin. Ovine nanosponges were developed to adsorb streptolysin-O and leporine nanosponges were developed to adsorb α-haemolysin. Ovine blood was found to be susceptible to haemolysis by streptolysin-O. Leporine blood was found to be susceptible to haemolysis by α-haemolysin. Previous studies compared the ability of the nanosponge at different physiological temperatures. However, this section will compare the adsorption ability of ovine nanosponges to that of leporine nanosponges. Figure 95 shows the comparison between ovine and leporine nanosponges to adsorb streptolysin-O and α-haemolysin at 37°C. Ovine nanosponges adsorbed most of the streptolysin-O as the concertation of Hb release from erythrocytes is minimal. Comparatively, leporine nanosponges have not adsorbed all the α-haemolysin as there is presence of haemolysis in the suspension. This is due to the characteristics of the prepared nanosponges. As shown is section 4.1 ovine nanosponges are more stable than leporine nanosponges.

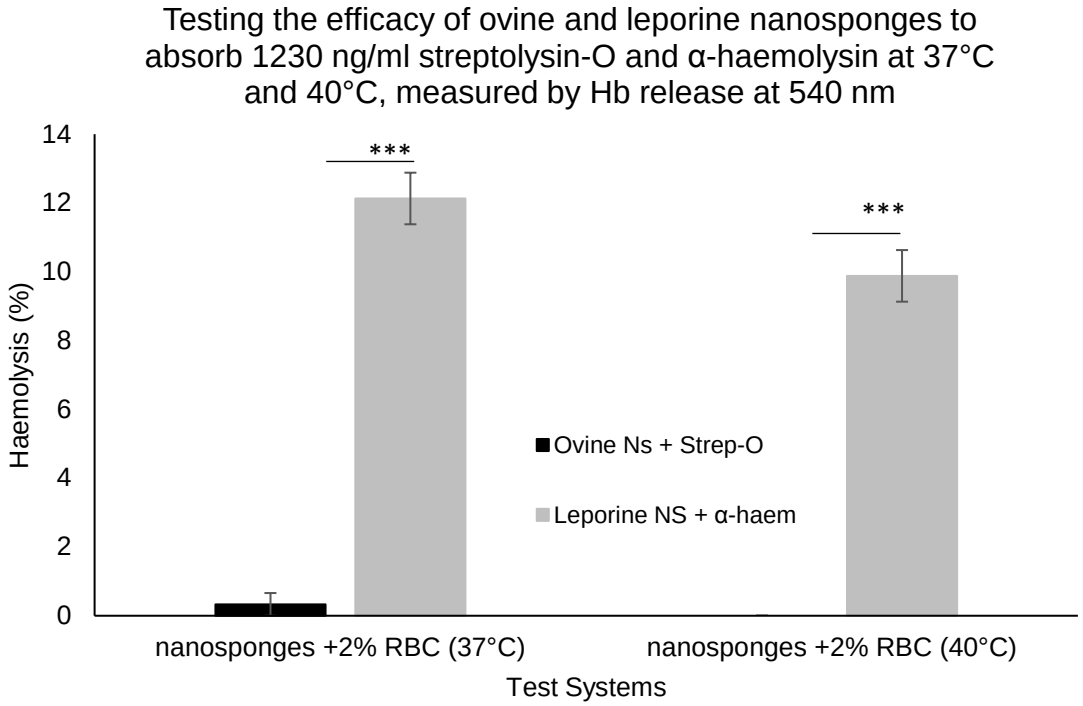

Figure 95. Testing the efficacy of ovine, leporine nanosponges to adsorb 1230 ng/ml streptolysin-O and α-haemolysin, incubated at 37°C and 40°C. Adsorption of streptolysin-O and α-haemolysin was measured by degree of haemolysis at 540 nm. .“*”P≤0.05, “**”P≤0.01 and “***”P≤0.001. Error bars represent SEM (n=3).

Ovine and leporine nanosponges were also compared for their ability to adsorb streptolysin-O and α-haemolysin at 40°C. Similar to the comparative study at 37°C, ovine nanosponges have adsorbed all the streptolysin the system as there is no presence of haemolysis. Whereas, the leporine nanosponges have shown presence of haemolysis.

Chapter 5

5 Conclusion

This thesis showed production of model ovine and leporine nanosponges that have the ability to adsorb PFTs such as streptolysin-O and α-haemolysin. However the nanosponges did face poor pharmaceutical characteristics. Nanosponges designed in this study showed increased particle aggregation with time, therefore indicating poor particle stability. Moreover structural features of vesicles and nanosponges could not be confirmed in the study due to sample melting under the SEM. Furthermore, resources to complete this study were limited. However, Luk *et al.* (2014) has shown that erythrocyte nanoparticles can be viewed under TEM using a glow discharged carbon coated grid. Moreover the authors have shown that by freeze drying the suspension with 5% sucrose, could improve long term stability of the nanosponge. These techniques could help show true vesicle and nanosponge formation and could help improve nanoparticle characteristics.

5.1 Overall thoughts and Future studies

This study did have some limitations which can be overcome in the future. Primarily this study used animal blood to produce nanosponges such as ovine and leporine. According to the study these blood types were chosen as they showed to be the most susceptible to toxin binding. Moreover, as discussed in this study they share certain physiological similarities with humans. Nonetheless, the blood parameter values differ between the animals and humans. The blood parameter values are close to the human reference ranges, however they differ due to many significant properties in blood such as size of erythrocytes, morphology of erythrocytes and viscosity of blood present in these different species. Therefore it is true by saying that in the future this study may have to be conducted by producing nanosponges with human blood or using animal blood that might be compatible in the human body.

The proof of principle of this study relied on the ability of the nanosponges to adsorb PFTs. The concept of adsorption or absorption was not tested in this study. However, we did assume that the toxin was being adsorbed on the surface of the nanosponge as the toxin is a protein (solid) and by definition adsorption is

the process by which a solid adheres to a surface. For the toxin to be absorbed rather than adsorbed it would have to be within the surface rather than on the surface. However this can be overcome. A study conducted in 2011 showed that adsorption of serum protein on gold nanoparticles could be confirmed using an optimised SDS-PAGE procedure. Moreover the author did also confirm this by using TEM (Walkey *et al.*, 2012). Another novel technique could be by using Taylor dispersion analysis, which has the ability to determine the size of proteins up till 0.5 nm(Zaman *et al.*, 2017).

The nanosponges were prepared by using extrusion. Extrusion helped coat the PLGA core with the respective erythrocyte membranes. During this process, our study showed that there is a decrease in the concentration of phospholipids. This takes place as Cho *et al.* (2013) has stated that “some sample material may be lost during extrusion during passage through the porous membrane”. The sample (retentate) either leaks during extrusion or becomes part of the porous polycarbonate membrane. To measure the concentration of the retentate would be close to impossible as one would have to completely disintegrate the extruder and the polycarbonate membrane to quantify the lost sample. Moreover if the sample leaks during extrusion it adheres to the chamber of the extruder. This would be difficult to isolate. Therefore, to overcome the loss of sample during extrusion, an increased concentration of the sample could be used, as this would overcompensate for the loss.

As stated in this study the nanosponges possess a unique property to adsorb PFTs. For example, ovine nanosponges have managed to completely adsorb streptolysin-O. The adsorption assay we used was one way of confirming PFT binding. The study showed that ovine erythrocyte vesicles had the ability to adsorb nearly half the streptolysin-O in the suspension, The PLGA cores did not adsorb any toxin and finally the nanosponges were able to adsorb all the toxin. This is because the membrane that surrounds the PLGA core has lipid or protein targets for the toxin to bind. Moreover other studies discussed in section 2.4.2 have stated that PLGA posses unique biological properties, which may allow it to act as an anchor for the toxin. Finally, this study has shown that streptolysin-O has the ability to bind to different types of mammalian erythrocytes mainly ovine and alpha haemolysin has shown specificity toward leporine erythrocytes. The reason they bind is due to specific protein and lipid targets on the membrane.

Thus indicating that PFTs in general require a target to bind. Some are specific and other non-specific and their ability to cause an infection is concentration and time dependent.

The use of cellular membranes as biomimetic therapeutic agent is a novel field of nanomedicine. Current research has shown that the field is limited to erythrocyte membranes. To take this study further, nanosponges could be produced by stable biomimetic formulations, such as platelets or white blood cell membranes for drug delivery and toxin adsorption. This biomimetic platform could also evolve into a diagnostic tool to test presence of exotoxins in bodily fluids. In conclusion, the ideal nanosponge required to treat sepsis would be one that is non-immunogenic, stable over a period of 6 months, have the ability to adsorb streptolysin-O and α-haemolysin and does not agglomerate (cause clots). The nanosponges developed by this study are therapeutic models for the treatment of sepsis in human medicine and animal veterinary medicine.

6 References

1. Adhikari, R. P., Ajao, A. O., Aman, M. J., Karauzum, H., Sarwar, J., Lydecker, A. D., Johnson, J. K., Nguyen, C., Chen, W. H. & Roghmann, M. C. 2012. Lower antibody levels to Staphylococcus aureus exotoxins are associated with sepsis in hospitalized adults with invasive S. aureus infections. J Infect Dis, 206, 915-23.

2. Agnihotri, J. & Jain, N. K. 2013. Biodegradable long circulating cellular carrier for antimalarial drug pyrimethamine. Artif Cells Nanomed Biotechnol, 41, 309-14.

3. Ahmad, A., Lutfullah, G. & Ali, R. 2011. Structural and functional features of Streptolysin O. Int J Bioinform Res Appl, 7, 427-44.

4. Ahmad, Z., Shah, A., Siddiq, M. & Kraatz, H.-B. 2014. Polymeric micelles as drug delivery vehicles. RSC Advances, 4, 17028-17038.

5. Aitken, A. 2012. 1M Tris [Online]. nhm. Available: http://www.nhm.ac.uk/content/dam/nhmwww/our-science/dpts-facilities-staff/Coreresearchlabs/tris.pdf [Accessed 2016].

6. Alouf, J. E. 1980. Streptococcal toxins (streptolysin O, streptolysin S, erythrogenic toxin). Pharmacol Ther, 11, 661-717.

7. Alouf, J. E., Billington, S. J. & Jost, B. H. 2006. CHAPTER 36 - Repertoire and general features of the family of cholesterol-dependent cytolysins. The Comprehensive Sourcebook of Bacterial Protein Toxins (Third Edition). London: Academic Press.

8. Antonelli, A., Sfara, C., Manuali, E., Bruce, I. J. & Magnani, M. 2011. Encapsulation of superparamagnetic nanoparticles into red blood cells as new carriers of MRI contrast agents. Nanomedicine, 6, 211-223.

9. Antonelli, A., Sfara, C., Rahmer, J., Gleich, B., Borgert, J. & Magnani, M. 2013. Red blood cells as carriers in magnetic particle imaging. Biomed Tech (Berl), 58, 517-25.

10. Aronson, J. K., British Journal of Clinical Pharmacology 2007. Concentration-effect and dose-response relations in clinical pharmacology. British Journal of Clinical Pharmacology, 63, 255-257.

11. Ayache, S., Panelli, M., Marincola, F. M. & Stroncek, D. F. 2006. Effects of Storage Time and Exogenous Protease Inhibitors on Plasma Protein Levels. American Journal of Clinical Pathology, 126, 174-184.

12. Bain, B. J., Lewis, S. M. & Bates, I. 2006. Chapter 3 - Basic haematological techniques. In: BATES, S. M. L. J. B. (ed.) Dacie and Lewis Practical Haematology (Tenth Edition). Philadelphia: Churchill Livingstone.

13. Banik, B. L., Fattahi, P. & Brown, J. L. 2016. Polymeric nanoparticles: the future of nanomedicine. Wiley Interdisciplinary Reviews: Nanomedicine and Nanobiotechnology, 8, 271-299.

14. Beals., S. H. 2000. sizes of organisms: the surface area:volume ratio [Online]. Available: http://www.tiem.utk.edu/~gross/bioed/bealsmodules/area_volume.htm [Accessed 18/3/15 2015].

15. Bentivoglio, M. 1999. The discovery of the Golgi apparatus. J Hist Neurosci, 8, 202-8.

16. Bernheimer, A. W. 1974. Interactions between membranes and cytolytic bacterial toxins. Biochimica et Biophysica Acta (BBA) - Reviews on Biomembranes, 344, 27-50.

17. Bernheimer, A. W. 1988. Assay of hemolytic toxins. Methods Enzymol, 165, 213-7.

18. Bernheimer, A. W. & Schwartz, L. L. 1963. Isolation and Composition of Staphylococcal Alpha Toxin. Microbiology, 30, 455-468.

19. Berube, B. J. & Wardenburg, J. 2013. Staphylococcus aureus α-Toxin: Nearly a Century of Intrigue. Toxins, 5, 1140-1166.

20. Bhakdi, S., Muhly, M., Korom, S. & Hugo, F. 1989. Release of interleukin-1 beta associated with potent cytocidal action of staphylococcal alpha-toxin on human monocytes. Infection and Immunity, 57, 3512-3519.

21. Bhakdi, S. & Tranum-Jensen, J. 1987. Damage to mammalian cells by proteins that form transmembrane pores. Reviews of Physiology, Biochemistry and Pharmacology, Volume 107. Springer Berlin Heidelberg.

22. Bhateria, M., Rachumallu, R., Singh, R. & Bhatta, R. S. 2014.

23. Erythrocytes-based synthetic delivery systems: transition from conventional to novel engineering strategies. Expert Opin Drug Deliv, 11, 1219-36.

24. Bonardi, F., Nouwen, N., Feringa, B. L. & Driessen, A. J. 2012. Protein conducting channels-mechanisms, structures and applications. Mol Biosyst, 8, 709-19.

25. Bosman, G. J. C. G. M., Lasonder, E., Luten, M., Roerdinkholder-Stoelwinder, B., Novotný, V. M. J., Bos, H. & De Grip, W. J. 2008. The proteome of red cell membranes and vesicles during storage in blood bank conditions. Transfusion, 48, 827-835.

26. Bossche, D., Devreese, K., Malfait, R., Vyvere Martine Van, D., Wauters, A., Neels, H. & Schouwer Pieter, D. 2002. Reference Intervals for a Complete Blood Count Determined on different Automated Haematology Analysers: Abx Pentra 120 Retic, Coulter Gen-S, Sysmex SE 9500, Abbott Cell Dyn 4000 and Bayer Advia 120. Clinical Chemistry and Laboratory Medicine.

27. Bozzola, J. J. & Russell, L. D. 1999. Electron Microscopy: Principles and Techniques for Biologists, Jones and Bartlett.

28. Brahler, M., Georgieva, R., Buske, N., Muller, A., Muller, S., Pinkernelle, J., Teichgraber, U., Voigt, A. & Baumler, H. 2006. Magnetite-loaded carrier erythrocytes as contrast agents for magnetic resonance imaging. Nano Lett, 6, 2505-9.

29. Briuglia, M. L., Rotella, C., Mcfarlane, A. & Lamprou, D. A. 2015. Influence of cholesterol on liposome stability and on in vitro drug release. Drug Deliv Transl Res, 5, 231-42.

30. Brumfitt, W. & Hamilton-Miller, J. 1989. Methicillin-resistant Staphylococcus aureus. N Engl J Med, 320, 1188-96.

31. Bryant, A. E., Kehoe, M. A. & Stevens, D. L. 1992. Streptococcal Pyrogenic Exotoxin A and Streptolysin O Enhance Polymorphonuclear Leukocyte Binding to Gelatin Matrixes. Journal of Infectious Diseases, 166, 165-169.

32. Burton, A. C. 1954. Relation of Structure to Function of the Tissues of the Wall of Blood Vessels. Physiological Reviews, 34, 619-642.

33. Carmona-Ribeiro, A. M. 2010. Biomimetic nanoparticles: preparation, characterization and biomedical applications. International Journal of Nanomedicine, 5, 249-259.

34. Cavalli, R., Trotta, F. & Tumiatti, W. 2006. Cyclodextrin-based Nanosponges for Drug Delivery. Journal of inclusion phenomena and macrocyclic chemistry, 56, 209-213.

35. Cheng, L., Jin, C., Lv, W., Ding, Q. & Han, X. 2011. Developing a Highly Stable PLGA-mPEG Nanoparticle Loaded with Cisplatin for Chemotherapy of Ovarian Cancer. PLoS ONE, 6, e25433.

36. Chhabria, V. & Beeton, S. 2016. Development of nanosponges from erythrocyte ghosts for removal of streptolysin-O from mammalian blood. Nanomedicine, 11, 2797-2807.

37. Cho, N.-J., Hwang, L., Solandt, J. & Frank, C. 2013. Comparison of Extruded and Sonicated Vesicles for Planar Bilayer Self-Assembly. Materials, 6, 3294.

38. Christmas-Dirckinck Holmfeld, J. D. 1888. Recherches expérimentales sur la suppuration John de Christmas-Dirckinck-Holmfeld.

39. Cooper, G. M. 2000. The Cell - A Molecular Approach 2nd Edition, Sunderland (MA): Sinauer Associates.

40. Cooper, L. Z., Madoff, M. A. & Weinstein, L. 1964. Haemolysis of rabbit erythrocytes by purified *Staphylococcal* alpha-toxin 1: Kinetics of the Lytic Reaction. Journal of Bacteriology, 87, 127-135.

41. Cooper, L. Z., Madoff, M. A. & Weinstein, L. 1966. Heat Stability and Species Range of Purified *Staphylococcal* α-Toxin. Journal of Bacteriology, 91, 1686-1692.

42. Craven, R. R., Gao, X., Allen, I. C., Gris, D., Wardenburg, J. B., Mcelvania-Tekippe, E., Ting, J. P. & Duncan, J. A. 2009. *Staphylococcus aureus* α-Hemolysin Activates the NLRP3-Inflammasome in Human and Mouse Monocytic Cells. PLoS ONE, 4, e7446.

43. Dal Peraro, M. & Van Der Goot, F. G. 2016. Pore-forming toxins: ancient, but never really out of fashion. Nat Rev Microbiol, 14, 77-92.

44. De Backer, D., Creteur, J., Preiser, J.-C., Dubois, M.-J. & Vincent, J.-L. 2002. Microvascular Blood Flow Is Altered in Patients with Sepsis. American Journal of Respiratory and Critical Care Medicine, 166, 98-104.

45. De Kraker, M. E. A., Davey, P. G., Grundmann, H. & On Behalf of The, B. S. G. 2011. Mortality and Hospital Stay Associated with Resistant <italic>Staphylococcus aureus</italic> and <italic>Escherichia coli</italic> Bacteremia: Estimating the Burden of Antibiotic Resistance in Europe. PLoS Med, 8, e1001104.

46. De, S. & Robinson, D. H. 2004. Particle size and temperature effect on the physical stability of PLGA nanospheres and microspheres containing Bodipy. AAPS PharmSciTech, 5, e53.

47. Demel, R. A. & De Kruyff, B. 1976. The function of sterols in membranes. Biochim Biophys Acta, 457, 109-32.

48. Deuticke, B. 1968. Transformation and restoration of biconcave shape of human erythrocytes induced by amphiphilic agents and changes of ionic environment. Biochimica et Biophysica Acta (BBA) - Biomembranes, 163, 494-500.

49. Dodge, J. T., Mitchell, C. & Hanahan, D. J. 1963. The preparation and chemical characteristics of hemoglobin-free ghosts of human erythrocytes. Archives of Biochemistry and Biophysics, 100, 119-130.

50. Doshi, N., Zahr, A. S., Bhaskar, S., Lahann, J. & Mitragotri, S. 2009. Red blood cell-mimicking synthetic biomaterial particles. Proc Natl Acad Sci U S A, 106, 21495-9.

51. Dumitru, A. C., Espinosa, F. M., Garcia, R., Foschi, G., Tortorella, S., Valle, F., Dallavalle, M., Zerbetto, F. & Biscarini, F. 2015. In situ nanomechanical characterization of the early stages of swelling and degradation of a biodegradable polymer. Nanoscale, 7, 5403-10.

52. Duncan, J. L. 1974. Characteristics of streptolysin O hemolysis: kinetics of hemoglobin and 86rubidium release. Infect Immun, 9, 1022-7.

53. Duncan, R. & Vicent, M. J. 2013. Polymer therapeutics-prospects for 21st century: the end of the beginning. Adv Drug Deliv Rev, 65, 60-70.

54. Elgsaeter, A. & Branton, D. 1974. Intramembrane particle aggregation in erythrocyte ghosts. I. The effects of protein removal. J Cell Biol, 63, 1018-36.

55. Eylar, E. H., Madoff, M. A., Brody, O. V. & Oncley, J. L. 1962. The contribution of sialic acid to the surface charge of the erythrocyte. J Biol Chem, 237, 1992-2000.

56. Fajardo , L. F. 1984. Pathological Effects of Hyperthermia in Normal Tissues. Cancer Research, 44, 4826s.

57. Fang, R. H., Hu, C. M. & Zhang, L. 2012. Nanoparticles disguised as red blood cells to evade the immune system. Expert Opin Biol Ther, 12, 385-9.

58. Ferretti , K. 2016. *Streptococcus pyogenes*: Basic Biology to Clinical Manifestations, Oklahoma City University of Oklahoma Health Sciences Center.

59. Feynman, R. P. 1960. There's plenty of room at the bottom. Engineering and science, 23, 22-36.

60. Finch, R. & Hunter, P. A. 2006. Antibiotic resistance--action to promote new technologies: report of an EU Intergovernmental Conference held in Birmingham, UK, 12-13 December 2005. J Antimicrob Chemother, 58 Suppl 1, i3-i22.

61. Flanagan, J. J., Tweten, R. K., Johnson, A. E. & Heuck, A. P. 2009. Cholesterol Exposure at the Membrane Surface Is Necessary and Sufficient to Trigger Perfringolysin O Binding. Biochemistry, 48, 3977-3987.

62. Fleming, A. 1929. On the Antibacterial Action of Cultures of a Penicillium, with Special Reference to their Use in the Isolation of B. influenzæ. British journal of experimental pathology, 10, 226-236.

63. Ford, M. 2014. Medical Microbiology, OUP Oxford.

64. French, G. L. 2010. The continuing crisis in antibiotic resistance. Int J Antimicrob Agents, 36 Suppl 3, S3-7.

65. Fritz, S. A., Tiemann, K. M., Hogan, P. G., Epplin, E. K., Rodriguez, M., Al-Zubeidi, D. N., Bubeck Wardenburg, J. & Hunstad, D. A. 2013. A serologic

correlate of protective immunity against community-onset Staphylococcus aureus infection. Clin Infect Dis, 56, 1554-61.

66. Galinier, R., Portela, J., Mone, Y., Allienne, J. F., Henri, H., Delbecq, S., Mitta, G., Gourbal, B. & Duval, D. 2013. Biomphalysin, a new beta pore-forming toxin involved in Biomphalaria glabrata immune defense against Schistosoma mansoni. PLoS Pathog, 9, e1003216.

67. Gandhi, A., Paul, A., Sen, S. O. & Sen, K. K. 2015. Studies on thermoresponsive polymers: Phase behaviour, drug delivery and biomedical applications. Asian Journal of Pharmaceutical Sciences, 10, 99-107.

68. Gentile, P., Chiono, V., Carmagnola, I. & Hatton, P. V. 2014. An Overview of Poly(lactic-co-glycolic) Acid (PLGA)-Based Biomaterials for Bone Tissue Engineering. International Journal of Molecular Sciences, 15, 3640-3659.

69. Gilbert, R. J. 2002. Pore-forming toxins. Cell Mol Life Sci, 59, 832-44.

70. Gill, R. 2012. Resealed erythrocytes as a potential drug carrier system. International Journal of Pharmaceutical Sciences and Research, 3, 383.

71. Glenny, A. T. & Stevens, M. F. 1935. *Staphylococcus* toxins and antitoxins. The Journal of Pathology and Bacteriology, 40, 201-210.

72. Gupta, N., Patel, B. & Ahsan, F. 2014. Nano-engineered erythrocyte ghosts as inhalational carriers for delivery of fasudil: preparation and characterization. Pharm Res, 31, 1553-65.

73. Gupta, N., Patel, B. & Ahsan, F. 2014. Nano-Engineered Erythrocyte Ghosts as Inhalational Carriers for Delivery of Fasudil: Preparation and Characterization. Pharmaceutical Research, 31, 1553-1565.

74. Gurcel, L., Lacovache, I. & Van Der Goot, F. G. 2006. CHAPTER 33 - Aerolysin and related Aeromonas toxins. The Comprehensive Sourcebook of Bacterial Protein Toxins (Third Edition). London: Academic Press.

75. Gurnev, P. & Nestorovich, E. 2014. Channel-Forming Bacterial Toxins in Biosensing and Macromolecule Delivery. Toxins, 6, 2483.

76. Hackett, S. P. & Stevens, D. L. 1992. *Streptococcal* toxic shock syndrome: synthesis of tumor necrosis factor and interleukin-1 by monocytes stimulated with pyrogenic exotoxin A and streptolysin O. J Infect Dis, 165, 879-85.

77. Hadinoto, K., Sundaresan, A. & Cheow, W. S. 2013. Lipid–polymer hybrid nanoparticles as a new generation therapeutic delivery platform: A review. European Journal of Pharmaceutics and Biopharmaceutics, 85, 427-443.

78. Hagag, A., S El-Farargy, M. & M Abo El-Enein, A. 2015. Study of Adrenal Functions using ACTH stimulation test in Egyptian children with Sickle Cell Anemia: Correlation with Iron Overload. International Journal of Hematology-Oncology and Stem Cell Research, 9, 60-66.

79. Hamidi, M., Rafiei, P., Azadi, A. & Mohammadi-Samani, S. 2011. Encapsulation of valproate-loaded hydrogel nanoparticles in intact human erythrocytes: a novel nano-cell composite for drug delivery. J Pharm Sci, 100, 1702-11.

80. Hamidi, M. & Tajerzadeh, H. 2003. Carrier erythrocytes: an overview. Drug Deliv, 10, 9-20.

81. Hamidi, M., Zarrin, A., Foroozesh, M. & Mohammadi-Samani, S. 2007. Applications of carrier erythrocytes in delivery of biopharmaceuticals. J Control Release, 118, 145-60.

82. Han, E.-J., Chung, A.-H. & Oh, I.-J. 2012. Analysis of residual solvents in poly(lactide-co-glycolide) nanoparticles. Journal of Pharmaceutical Investigation, 42, 251-256.

83. Han, V., Serrano, K. & Devine, D. V. 2010. A comparative study of common techniques used to measure haemolysis in stored red cell concentrates. Vox Sang, 98, 116-23.

84. Han, Y., Quan, G. B., Liu, X. Z., Ma, E. P., Liu, A., Jin, P. & Cao, W. 2005. Improved preservation of human red blood cells by lyophilization. Cryobiology, 51, 152-164.

85. Hanahan, D. J., Ekholm, J. E. & Luthra, M. G. 1974. Is lipid lost during preparation of erythrocyte membranes? Biochimica et Biophysica Acta (BBA) - Biomembranes, 363, 283-286.

86. Harisa, G. I., Ibrahim, M. F., Alanazi, F. & Shazly, G. A. 2014. Engineering erythrocytes as a novel carrier for the targeted delivery of the anticancer drug paclitaxel. Saudi Pharmaceutical Journal, 22, 223-230.

87. Hoffman, J. F. 1958. Physiological characteristics of human red blood cell ghosts. J Gen Physiol, 42, 9-28.

88. Hogman, C. F., Akerblom, O., Hedlund, K., Rosen, I. & Wiklund, L. 1983. Red cell suspensions in SAGM medium. Further experience of in vivo survival of red cells, clinical usefulness and plasma-saving effects. Vox Sang, 45, 217-23.

89. Hounsom, L., Grayson, K. & Melzer, M. 2011. Mortality and associated risk factors in consecutive patients admitted to a UK NHS trust with community acquired bacteraemia. Postgraduate Medical Journal, 87, 757-762.

90. Hu, C.-M. J., Fang, R. H., Copp, J., Luk, B. T. & Zhang, L. 2013. A biomimetic nanosponge that absorbs pore-forming toxins. Nat Nano, 8, 336-340.

91. Hu, C.-M. J., Zhang, L., Aryal, S., Cheung, C., Fang, R. H. & Zhang, L. 2011. Erythrocyte membrane-camouflaged polymeric nanoparticles as a biomimetic delivery platform. Proceedings of the National Academy of Sciences, 108, 10980-10985.

92. Hu, C. M., Fang, R. H., Copp, J., Luk, B. T. & Zhang, L. 2013. A biomimetic nanosponge that absorbs pore-forming toxins. Nat Nanotechnol, 8, 336-40.

93. Hu, C. M., Fang, R. H., Luk, B. T. & Zhang, L. 2014. Polymeric nanotherapeutics: clinical development and advances in stealth functionalization strategies. Nanoscale, 6, 65-75.

94. Hunter, D. G. & Frisken, B. J. 1998. Effect of Extrusion Pressure and Lipid Properties on the Size and Polydispersity of Lipid Vesicles. Biophysical Journal, 74, 2996-3002.

95. Husband, T. 2014. The sweet science of candymaking [Online]. ACS chemistry for life. Available: https://www.acs.org/content/acs/en/education/resources/highschool/chemmatters/past-issues/archive-2014-2015/candymaking.html [Accessed 14/9/16 2016].

96. Inoshima, I., Inoshima, N., Wilke, G., Powers, M., Frank, K., Wang, Y. & Wardenburg, J. B. 2011. A Staphylococcus aureus Pore-Forming Toxin Subverts the Activity of ADAM10 to Cause Lethal Infection. Nature medicine, 17, 1310-1314.

97. Inoshima, N., Wang, Y. & Wardenburg, J. B. 2012. Genetic Requirement for ADAM10 in Severe *Staphylococcus aureus* Skin Infection. The Journal of investigative dermatology, 132, 1513-1516.

98. Jaishree, V. & Gupta, P. D. 2012. Nanotechnology: A Revolution in Cancer Diagnosis. Indian J Clin Biochem, 27, 214-20.

99. Johnson, R. M., Taylor, G. & Meyer, D. B. 1980. Shape and volume changes in erythrocyte ghosts and spectrin-actin networks. J Cell Biol, 86, 371-6.

100. Kabanov, A. V. & Gendelman, H. E. 2007. Nanomedicine in the diagnosis and therapy of neurodegenerative disorders. Progress in Polymer Science, 32, 1054-1082.

101. Kalepu, S. & Nekkanti, V. 2015. Insoluble drug delivery strategies: review of recent advances and business prospects. Acta Pharmaceutica Sinica B, 5, 442-453.

102. Kanbayashi, Y., Hotta, M. & Koyama, J. 1972. Kinetic study on streptolysin O. J Biochem, 71, 227-37.

103. Kayden, H. J. & Bessis, M. 1970. Morphology of normal erythrocyte and acanthocyte using Nomarski optics and the scanning electron microscope. Blood, 35, 427-36.

104. Keyel, P., Roth, R., Yokoyama, W., Heuser, J. & Salter, R. 2013. Reduction of Streptolysin O (SLO) Pore-Forming Activity Enhances Inflammasome Activation. Toxins, 5, 1105.

105. Klainer, A. S., Chang, T. W. & Weinstein, L. 1972. Effects of purified staphylococcal alpha toxin on the ultrastructure of human and rabbit erythrocytes. Infect Immun, 5, 808-13.

106. Kluytmans, J., Van Belkum, A. & Verbrugh, H. 1997. Nasal carriage of *Staphylococcus aureus*: epidemiology, underlying mechanisms, and associated risks. Clin Microbiol Rev, 10, 505-20.

107. Kostic, I. T., Ilic, V., Dordevic, V. B., Bukara, K. M., Mojsilovic, S. B., Nedovic, V. A., Bugarski, D. S., Veljovic, D. N., Misic, D. M. & Bugarski, B. M. 2014. Erythrocyte membranes from slaughterhouse blood as potential drug vehicles: Isolation by gradual hypotonic hemolysis and biochemical and morphological characterization. Colloids Surf B Biointerfaces, 122, 250-9.

108. Kriebardis, Anastasios g., Antonelou, Marianna h., Stamoulis, Konstantinos e., Economou-Petersen, E., Margaritis, Lukas h. & Papassideri, Issidora s. 2007. Storage-dependent remodeling of the red blood cell membrane is associated with increased immunoglobulin G binding, lipid raft rearrangement, and caspase activation. Transfusion, 47, 1212-1220.

109. Krishnamoorthy, K. & Rajappan, M. 2012. Nanosponges: a novel class of drug delivery system--review. J Pharm Pharm Sci, 15, 103-11.

110. Krishnamurthy, S., Gnanasammandhan, M. K., Xie, C., Huang, K., Cui, M. Y. & Chan, J. M. 2016. Monocyte cell membrane-derived nanoghosts for targeted cancer therapy. Nanoscale, 8, 6981-6985.

111. Krukemeyer, M., Krenn, V., Huebner, F., Wagner, W. & Resch, R. 2015. History and Possible Uses of Nanomedicine Based on Nanoparticles and Nanotechnological Progress. Journal of Nanomedicine & Nanotechnology, 6, 1.

112. Kumar, A., Roberts, D., Wood, K. E., Light, B., Parrillo, J. E., Sharma, S., Suppes, R., Feinstein, D., Zanotti, S., Taiberg, L., Gurka, D., Kumar, A. & Cheang, M. 2006. Duration of hypotension before initiation of effective antimicrobial therapy is the critical determinant of survival in human septic shock. Crit Care Med, 34, 1589-96.

113. Kumari, A., Yadav, S. K. & Yadav, S. C. 2010. Biodegradable polymeric nanoparticles based drug delivery systems. Colloids and Surfaces B: Biointerfaces, 75, 1-18.

114. Lambert, T. 2016. A brief history of medicine [Online]. Local Histories. Available: http://www.localhistories.org/medicine.html [Accessed 21/7/16 2016].

115. Larosa, S. P. 2010. Sepsis [Online]. Available: http://www.clevelandclinicmeded.com/medicalpubs/diseasemanagement/infectious-disease/sepsis/ [Accessed 24/10/2016].

116. Lee, B. H., Inui, D., Suh, G. Y., Kim, J. Y., Kwon, J. Y., Park, J., Tada, K., Tanaka, K., Ietsugu, K., Uehara, K., Dote, K., Tajimi, K., Morita, K., Matsuo, K., Hoshino, K., Hosokawa, K., Lee, K. H., Lee, K. M., Takatori, M., Nishimura, M., Sanui, M., Ito, M., Egi, M., Honda, N., Okayama, N., Shime, N., Tsuruta, R., Nogami, S., Yoon, S.-H., Fujitani, S., Koh, S. O., Takeda, S., Saito, S., Hong, S. J., Yamamoto, T., Yokoyama, T., Yamaguchi, T., Nishiyama, T., Igarashi, T., Kakihana, Y. & Koh, Y. 2012. Association of body temperature and antipyretic treatments with mortality of critically ill patients with and without sepsis: multi-centered prospective observational study. Critical Care, 16, 1-13.

117. Lee, B. H., Inui, D., Suh, G. Y., Kim, J. Y., Kwon, J. Y., Park, J., Tada, K., Tanaka, K., Ietsugu, K., Uehara, K., Dote, K., Tajimi, K., Morita, K., Matsuo, K., Hoshino, K., Hosokawa, K., Lee, K. H., Lee, K. M., Takatori, M., Nishimura, M., Sanui, M., Ito, M., Egi, M., Honda, N., Okayama, N., Shime, N., Tsuruta, R., Nogami, S., Yoon, S. H., Fujitani, S., Koh, S. O., Takeda, S., Saito, S., Hong, S. J., Yamamoto, T., Yokoyama, T., Yamaguchi, T., Nishiyama, T., Igarashi, T., Kakihana, Y. & Koh, Y. 2012. Association of body temperature and antipyretic treatments with mortality of critically ill patients with and without sepsis: multi-centered prospective observational study. Crit Care, 16, R33.

118. Lee, S. S., Lee, Y. B. & Oh, I. J. 2015. Cellular uptake of poly(dl-lactide-co-glycolide) nanoparticles: effects of drugs and surface characteristics of nanoparticles. Journal of Pharmaceutical Investigation, 45, 659-667.

119. Lejeune, A., Moorjani, M., Gicquaud, C., Lacroix, J., Poyet, P. & Gaudreault, R. 1994. Nanoerythrosome, a new derivative of erythrocyte ghost: preparation and antineoplastic potential as drug carrier for daunorubicin. Anticancer Res, 14, 915-9.

120. Leslie, S. B., Israeli, E., Lighthart, B., Crowe, J. H. & Crowe, L. M. 1995. Trehalose and sucrose protect both membranes and proteins in intact bacteria during drying. Appl Environ Microbiol, 61, 3592-7.

121. Lewis, K. 2012. Antibiotics: Recover the lost art of drug discovery. Nature, 485, 439-40.

122. Li, L., Jiang, X. & Zhuo, R. 2009. Synthesis and characterization of thermoresponsive polymers containing reduction-sensitive disulfide linkage. Journal of Polymer Science, Part A: Polymer Chemistry, 47, 5989-5997.

123. Li, L. L., Xu, J. H., Qi, G. B., Zhao, X., Yu, F. & Wang, H. 2014. Core-shell supramolecular gelatin nanoparticles for adaptive and "on-demand" antibiotic delivery. ACS Nano, 8, 4975-83.

124. Lowy, F. D. 1998. Staphylococcus aureus infections. N Engl J Med, 339, 520-32.

125. Luk, B. T., Jack Hu, C.-M., Fang, R. H., Dehaini, D., Carpenter, C., Gao, W. & Zhang, L. 2014. Interfacial interactions between natural RBC membranes and synthetic polymeric nanoparticles. Nanoscale, 6, 2730-2737.

126. Magarkar, A., Dhawan, V., Kallinteri, P., Viitala, T., Elmowafy, M., Róg, T. & Bunker, A. 2014. Cholesterol level affects surface charge of lipid membranes in saline solution. Scientific Reports, 4, 5005.

127. Maretzky, T., Reiss, K., Ludwig, A., Buchholz, J., Scholz, F., Proksch, E., De Strooper, B., Hartmann, D. & Saftig, P. 2005. ADAM10 mediates E-cadherin shedding and regulates epithelial cell-cell adhesion, migration, and beta-catenin translocation. Proc Natl Acad Sci U S A, 102, 9182-7.

128. Mazzarello, P. 1999. A unifying concept: the history of cell theory. Nat Cell Biol, 1, E13-E15.

129. Mcpherson, D., Griffiths, C., Williams, M., Baker, A., Klodawski, E., Jacobson, B. & Donaldson, L. 2013. Sepsis-associated mortality in England: an analysis of multiple cause of death data from 2001 to 2010. BMJ Open, 3.

130. Meyer, R. A., Sunshine, J. C. & Green, J. J. 2015. Biomimetic particles as therapeutics. Trends Biotechnol, 33, 514-24.

131. Mieszawska, A. J., Gianella, A., Cormode, D. P., Zhao, Y., Meijerink, A., Langer, R., Farokhzad, O. C., Fayad, Z. A. & Mulder, W. J. 2012. Engineering of lipid-coated PLGA nanoparticles with a tunable payload of diagnostically active nanocrystals for medical imaging. Chem Commun (Camb), 48, 5835-7.

132. Mircevova, L. 1974. Scanning electron microscopy of erythrocyte ghosts prepared with and without ATP addition. Blut, 29, 108-14.

133. Miyoshi, S., Sasahara, K., Akamatsu, S., Rahman, M. M., Katsu, T., Tomochika, K. & Shinoda, S. 1997. Purification and characterization of a hemolysin produced by Vibrio mimicus. Infect Immun, 65, 1830-5.

134. Morel, F. M. M., Baker, R. F. & Wayland, H. 1971.Quantitation of human red blood cell fixation by glutaraldehyde. The Journal of Cell Biology, 48, 91-100.

135. Mu, H., Tang, J., Liu, Q., Sun, C., Wang, T. & Duan, J. 2016. Potent Antibacterial Nanoparticles against Biofilm and Intracellular Bacteria. Scientific Reports, 6, 18877.

136. Murphy, G. J., Pararajasingam, R., Nasim, A., Dennis, M. J. & Sayers, R. D. 2001. Methicillin-resistant *Staphylococcus aureus* infection in vascular surgical patients. Annals of The Royal College of Surgeons of England, 83, 158-163.

137. Murthy, T. 2014. Blood transfusion practices in sepsis. Indian Journal of Anaesthesia, 58, 643-646.

138. Muzykantov, V. R. 2010. Drug delivery by red blood cells: vascular carriers designed by mother nature. Expert Opin Drug Deliv, 7, 403-27.

139. Nelson, G. J. 1967. Composition of neutral lipids from erythrocytes of common mammals. J Lipid Res, 8, 374-9.

140. Ogston, A. 1984. Classics in infectious diseases. "On abscesses". Alexander Ogston (1844-1929). Rev Infect Dis, 6, 122-8.

141. Paliwal, S., Paliwal, R. & Vyas, S. P. 2013. CHAPTER 3 pH-sensitive Liposomes in Drug Delivery. Smart Materials for Drug Delivery: Volume 1. The Royal Society of Chemistry.

142. Papahadjopoulos, D., Jacobson, K., Nir, S. & Isac, I. 1973. Phase transitions in phospholipid vesicles Fluorescence polarization and permeability measurements concerning the effect of temperature and cholesterol. Biochimica et Biophysica Acta (BBA) - Biomembranes, 311, 330-348.

143. Patel, P. D., Dand, N., Hirlekar, R. S. & Kadam, V. J. 2008. Drug loaded erythrocytes: as novel drug delivery system. Curr Pharm Des, 14, 63-70.

144. Pekİner, B. D. 2002. Fatty acid composition of red blood cell membrane phophatidylethanolamine and phosphatidylcholine in rat, rabbit, human and dog J. Fac. Pharm, 31, 13.

145. Peters, J. & Cohen, J. Sepsis. Medicine, 41, 667-669.

146. Peters, J. & Cohen, J. 2013. Sepsis. Medicine, 41, 667-669.

147. Phe. 2014. English surveillance programme for antimicrobial utilisation and resistance [Online]. Public Health England. Available: https://www.gov.uk/government/uploads/system/uploads/attachment_data/file/362374/ESPAUR_Report_2014__3_.pdf [Accessed 14/8/16 2016].

148. Piccione, G., Caola, G. & Refinetti, R. 2002. Maturation of the daily body temperature rhythm in sheep and horse. Journal of Thermal Biology, 27, 333-336.

149. Price, B. 2002. Electron Microscopy, Second Edition, John J. Bozzola and Lonnie D. Russell. Jones and Bartlett Publishers, Inc., Sudbury, MA, 1999, 670 pages (hardback, $56.25). ISBN 0-7637-0192-0. Microscopy and Microanalysis, 8, 365-366.

150. Rao, L., Xu, J. H., Cai, B., Liu, H., Li, M., Jia, Y., Xiao, L., Guo, S. S., Liu, W. & Zhao, X. Z. 2016. Synthetic nanoparticles camouflaged with biomimetic erythrocyte membranes for reduced reticuloendothelial system uptake. Nanotechnology, 27, 085106.

151. Ravi Kumar, M. N. V., Bakowsky, U. & Lehr, C. M. 2004. Preparation and characterization of cationic PLGA nanospheres as DNA carriers. Biomaterials, 25, 1771-1777.

152. Reitz, B. A., Prager, D. J. & Feigen, G. A. 1968.An analysis of the toxic actions of purified streptolysin-o on the isolated heart and separate cardiac tissues of the guinea pig. The Journal of Experimental Medicine, 128, 1401-1424.

153. Russell , J. A. 2006. Management of Sepsis. New England Journal of Medicine, 355, 1699-1713.

154. Schwoch, G. & Passow, H. 1973. Preparation and properties of human erythrocyte ghosts. Mol Cell Biochem, 2, 197-218.

155. Scott, K. L., Lecak, J. & Acker, J. P. 2005. Biopreservation of Red Blood Cells: Past, Present, and Future. Transfusion Medicine Reviews, 19, 127-142.

156. Seghatchian, J. & Krailadsiri, P. 2002. Red cell storage lesion assessed by the levels of potassium, haemoglobin and Annexin V in supernatants. Transfus Apher Sci, 26, 139-43.

157. Shanson, D. C. 1981. Antibiotic-resistant *Staphylococcus aureus*. J Hosp Infect, 2, 11-36.

158. Shastri, V. P. 2003. Non-degradable biocompatible polymers in medicine: past, present and future. Curr Pharm Biotechnol, 4, 331-7.

159. Shewell, L. K., Harvey, R. M., Higgins, M. A., Day, C. J., Hartley-Tassell, L. E., Chen, A. Y., Gillen, C. M., James, D. B. A., Alonzo, F., Torres, V. J., Walker, M. J., Paton, A. W., Paton, J. C. & Jennings, M. P. 2014. The cholesterol-dependent cytolysins pneumolysin and streptolysin O require binding to red blood cell glycans for hemolytic activity. Proceedings of the National Academy of Sciences, 111, E5312-E5320.

160. Shibahara, S., Kitamuro, T. & Takahashi, K. 2002. Heme degradation and human disease: diversity is the soul of life. Antioxid Redox Signal, 4, 593-602.

161. Shinefield, H. R. & Ruff, N. L. 2009. Staphylococcal infections: a historical perspective. Infect Dis Clin North Am, 23, 1-15.

162. Song, L., Hobaugh, M. R., Shustak, C., Cheley, S., Bayley, H. & Gouaux, J. E. 1996. Structure of *staphylococcal* alpha-hemolysin, a heptameric transmembrane pore. Science, 274, 1859-66.

163. Srikar, R., Upendran, A. & Kannan, R. 2014. Polymeric nanoparticles for molecular imaging. Wiley Interdisciplinary Reviews: Nanomedicine and Nanobiotechnology, 6, 245-267.

164. Sriskandan, S. 2011. Severe peripartum sepsis. J R Coll Physicians Edinb, 41, 339-46.

165. Staats, J. J., Feder, I., Okwumabua, O. & Chengappa, M. M. 1997. Streptococcus Suis: Past and Present. Veterinary Research Communications, 21, 381-407.

166. Steck, T. L. 1974. The organization of proteins in the human red blood cell membrane: A Review. The Journal of Cell Biology, 62, 1-19.

167. Stevens, B. A. 2016. Severe Group A *Streptococcal* Infections., Oklahoma City, University of Oklahoma Health Sciences Center.

168. Stevens, D. L. 1995. *Streptococcal* toxic-shock syndrome: spectrum of disease, pathogenesis, and new concepts in treatment. Emerging Infectious Diseases, 1, 69-78.

169. Stolnik, S., Dunn, S. E., Garnett, M. C., Davies, M. C., Coombes, A. G., Taylor, D. C., Irving, M. P., Purkiss, S. C., Tadros, T. F., Davis, S. S. & Et Al. 1994. Surface modification of poly(lactide-co-glycolide) nanospheres by biodegradable poly(lactide)-poly(ethylene glycol) copolymers. Pharm Res, 11, 1800-8.

170. Sullivan, T. P., Eaglstein, W. H., Davis, S. C. & Mertz, P. 2001.The pig as a model for human wound healing. Wound Repair and Regeneration, 9, 66-76.

171. Sun, Y., Zheng, Y., Ran, H., Zhou, Y., Shen, H., Chen, Y., Chen, H., Krupka, T. M., Li, A., Li, P., Wang, Z. & Wang, Z. 2012. Superparamagnetic PLGA-iron oxide microcapsules for dual-modality US/MR imaging and high intensity focused US breast cancer ablation. Biomaterials, 33, 5854-5864.

172. Sunshine, J. C., Perica, K., Schneck, J. P. & Green, J. J. 2014. Particle shape dependence of CD8+ T cell activation by artificial antigen presenting cells. Biomaterials, 35, 269-77.

173. Suttorp, N., Fuhrmann, M., Tannert-Otto, S., Grimminger, F. & Bhadki, S. 1993. Pore-forming bacterial toxins potently induce release of nitric oxide in porcine endothelial cells. J Exp Med, 178, 337-41.

174. Tatsumi, N. 1981. The size of erythrocyte ghosts. Biochimica et Biophysica Acta (BBA) - Biomembranes, 641, 276-280.

175. Tiwari, G., Tiwari, R., Sriwastawa, B., Bhati, L., Pandey, S., Pandey, P. & Bannerjee, S. K. 2012. Drug delivery systems: An updated review. International Journal of Pharmaceutical Investigation, 2, 2-11.

176. Tong, S. Y., Davis, J. S., Eichenberger, E., Holland, T. L. & Fowler, V. G. 2015. Staphylococcus aureus infections: epidemiology, pathophysiology, clinical manifestations, and management. Clinical microbiology reviews, 28, 603-661.

177. Torchilin, V. P. 2014. Multifunctional, stimuli-sensitive nanoparticulate systems for drug delivery. Nat Rev Drug Discov, 13, 813-827.

178. Trzeciak , R. P. D. a. J. E. P. 2015. Septic Shock [Online]. Available: http://clinicalgate.com/septic-shock/ [Accessed 25/4/17 2017].

179. Turner, J. D. & Rouser, G. 1974. Removal of lipid from intact erythrocytes and ghosts by aqueous solutions and its relevance to membrane structure. Lipids, 9, 49.

180. Tziakas, D. N., Kaski, J. C., Chalikias, G. K., Romero, C., Fredericks, S., Tentes, I. K., Kortsaris, A. X., Hatseras, D. I. & Holt, D. W. 2007. Total Cholesterol Content of Erythrocyte Membranes Is Increased in Patients With Acute Coronary Syndrome: A New Marker of Clinical Instability? Journal of the American College of Cardiology, 49, 2081-2089.

181. Van Deenen, L. L. M. & De Gier, J. 1974. Chapter 4 - Lipids of the Red Cell Membrane A2 - Surgenor, Douglas MacN. The Red Blood Cell (Second Edition). Academic Press.

182. Ventola, C. L. 2012. The nanomedicine revolution: part 1: emerging concepts. P t, 37, 512-25.

183. Wagner, V., Dullaart, A., Bock, A.-K. & Zweck, A. 2006. The emerging nanomedicine landscape. Nat Biotech, 24, 1211-1217.

184. Walev, I., Palmer, M., Valeva, A., Weller, U. & Bhakdi, S. 1995. Binding, oligomerization, and pore formation by streptolysin O in erythrocytes and fibroblast membranes: detection of nonlytic polymers. Infection and Immunity, 63, 1188-1194.

185. Walkey, C. D., Olsen, J. B., Guo, H., Emili, A. & Chan, W. C. W. 2012. Nanoparticle Size and Surface Chemistry Determine Serum Protein Adsorption and Macrophage Uptake. Journal of the American Chemical Society, 134, 2139-2147.

186. Wang, H., Zhao, P., Su, W., Wang, S., Liao, Z., Niu, R. & Chang, J. 2010. PLGA/polymeric liposome for targeted drug and gene co-delivery. Biomaterials, 31, 8741-8.

187. Wang, X., Ishida, T. & Kiwada, H. 2007. Anti-PEG IgM elicited by injection of liposomes is involved in the enhanced blood clearance of a subsequent dose of PEGylated liposomes. J Control Release, 119, 236-44.

188. Wang, Y.-S., Liu, L.-R., Jiang, Q. & Zhang, Q.-Q. 2007. Self-aggregated nanoparticles of cholesterol-modified chitosan conjugate as a novel carrier of epirubicin. European Polymer Journal, 43, 43-51.

189. Watkins, R. R. & Bonomo, R. A. 2016. Overview: Global and Local Impact of Antibiotic Resistance. Infectious Disease Clinics, 30, 313-322.

190. Waugh, R. E. & Sarelius, I. H. 1996. Effects of lost surface area on red blood cells and red blood cell survival in mice. American Journal of Physiology - Cell Physiology, 271, C1847.

191. Weber, C., Coester, C., Kreuter, J. & Langer, K. 2000. Desolvation process and surface characterisation of protein nanoparticles. International Journal of Pharmaceutics, 194, 91-102.

192. Weed, R. I., Reed, C. F. & Berg, G. 1963. Is hemoglobin an essential structural component of human erythrocyte membranes? J Clin Invest, 42, 581-8.

193. Weed, R. I., Reed, C. F. & Berg, G. 1963. Is haemoglobin an essential structural component of human erythrocyte membranes. The Journal of Clinical Investigation, 42, 581-588.

194. Weiss, D. J., Wardrop, K. J. & Schalm, O. W. 2010. Schalm's veterinary hematology, Ames, Iowa, Wiley-Blackwell.

195. Wertheim, H. F., Melles, D. C., Vos, M. C., Van Leeuwen, W., Van Belkum, A., Verbrugh, H. A. & Nouwen, J. L. 2005. The role of nasal carriage in Staphylococcus aureus infections. Lancet Infect Dis, 5, 751-62.

196. Wheeler, D. S. 2015. Is the “golden age” of the “golden hour” in sepsis over? Critical Care, 19, 1-3.

197. Wilke, G. A. & Wardenburg, J. 2010. Role of a disintegrin and metalloprotease 10 in *Staphylococcus aureus* alpha-hemolysin-mediated cellular injury. Proc Natl Acad Sci U S A, 107, 13473-8.

198. Williams, R. E. O. 1958. Investigations of *Staphylococcal* infection acquired in Great Britain's hospitals. Public Health Reports, 73, 961-970.

199. Wu, L., Zhang, J. & Watanabe, W. 2011. Physical and chemical stability of drug nanoparticles. Advanced Drug Delivery Reviews, 63, 456-469.

200. Yamashita, D., Sugawara, T., Takeshita, M., Kaneko, J., Kamio, Y., Tanaka, I., Tanaka, Y. & Yao, M. 2014. Molecular basis of transmembrane beta-barrel formation of staphylococcal pore-forming toxins. Nature Communications, 5, 4897.

201. Zaghloul, M. Z. 2015. *Staphylococcus aureus* Toxic Shock Syndrome. Tropical Medicine & Surgery, 2015.

202. Zakikhany, K., Degail, M. A., Lamagni, T., Waight, P., Guy, R., Zhao, H., Efstratiou, A., Pebody, R., George, R. & Ramsay, M. 2011. Increase in invasive Streptococcus pyogenes and Streptococcus pneumoniae infections in England, December 2010 to January 2011. Euro Surveill, 16.

203. Zaman, H., Bright, A. G., Adams, K., Goodall, D. M. & Forbes, R. T. 2017. Characterisation of aggregates of cyclodextrin-drug complexes using Taylor Dispersion Analysis. International Journal of Pharmaceutics, 522, 98-109.

204. Zarjou, A. & Agarwal, A. 2011. Sepsis and Acute Kidney Injury. Journal of the American Society of Nephrology, 22, 999-1006.

205. Zehnder, L., Schulzki, T., Goede, J. S., Hayes, J. & Reinhart, W. H. 2008. Erythrocyte storage in hypertonic (SAGM) or isotonic (PAGGSM) conservation medium: influence on cell properties. Vox Sanguinis, 95, 280-287.

206. Zhang, C., Wan, X., Zheng, X., Shao, X., Liu, Q., Zhang, Q. & Qian, Y. 2014. Dual-functional nanoparticles targeting amyloid plaques in the brains of Alzheimer's disease mice. Biomaterials, 35, 456-65.

207. Zhang, H. 2016. Erythrocytes in nanomedicine: an optimal blend of natural and synthetic materials. Biomaterials Science, 4, 1024-1031.

208. Zhao, S., Tan, S., Guo, Y., Huang, J., Chu, M., Liu, H. & Zhang, Z. 2013. pH-sensitive docetaxel-loaded D-alpha-tocopheryl polyethylene glycol succinate-poly(beta-amino ester) copolymer nanoparticles for overcoming multidrug resistance. Biomacromolecules, 14, 2636-46.